

Spring 1-1-2013

Effects of Snow Loads on the Behavior and Risk of Structures with Open Web Steel Joist Roofs

Derek Lorne Kozak

University of Colorado at Boulder, derek.kozak@colorado.edu

Follow this and additional works at: https://scholar.colorado.edu/cven_gradetds



Part of the [Civil Engineering Commons](#)

Recommended Citation

Kozak, Derek Lorne, "Effects of Snow Loads on the Behavior and Risk of Structures with Open Web Steel Joist Roofs" (2013). *Civil Engineering Graduate Theses & Dissertations*. 319.

https://scholar.colorado.edu/cven_gradetds/319

This Thesis is brought to you for free and open access by Civil, Environmental, and Architectural Engineering at CU Scholar. It has been accepted for inclusion in Civil Engineering Graduate Theses & Dissertations by an authorized administrator of CU Scholar. For more information, please contact cuscholaradmin@colorado.edu.

EFFECTS OF SNOW LOADS ON THE BEHAVIOR AND RISK OF STRUCTURES WITH
OPEN WEB STEEL JOIST ROOFS

by

DEREK LORNE KOZAK

B.Eng., McGill University, 2011

A thesis submitted to the

Faculty of the Graduate School of the

University of Colorado in partial fulfillment

Of the requirement for the degree of

Master of Science

Department of Civil, Environmental, and Architectural Engineering

2013

This thesis entitled:

Effects of Snow Loads on the Behavior and Risk of Structures with Open Web Steel Joist Roofs

written by Derek Lorne Kozak

has been approved for the Department of Civil, Environmental, and Architectural Engineering

(Abbie Liel)

(Ross Corotis)

(James Harris)

Date _____

The final copy of this thesis has been examined by the signatories, and we find that both the content and the form meet acceptable presentation standards of scholarly work in the above mentioned discipline

ABSTRACT

Kozak, Derek Lorne (M.S., Structural Engineering, Department of Civil, Environmental, and Architectural Engineering)

Effects of Snow Loads on the Behavior and Risk of Structures with Open Web Steel Joist Roofs

Thesis directed by Assistant Professor Abbie B. Liel

Roof collapses of any nature have severe impacts on building owners in the form of financial losses, and on building occupants in the form of physical harm. It has been observed recently that lightweight steel roofs subjected to snow loads account for a large number of roof collapses every year in the United States. The combination of the impacts and potential risk associated with lightweight steel roofs makes it important to properly understand their behavior under snow loads. This study focuses on a specific type of lightweight steel roof: open web steel joist supported roofs. Open web steel joist roofs with different design characteristics are analyzed in order to form a better understanding of how these types of roofs behave under uniform and drifted snow loads as well as their associated risks.

The first part of the study explains the nonlinear model created to analyze open web steel joist structures. The wide array of capabilities offered by *OpenSees* allows the model to employ nonlinear fiber elements as the elements within the open web steel joists. The software is also capable of exerting both uniform and drifted snow loads onto the roof of the building. Pre- and post-processing of the code using MATLAB is also discussed.

The second part explores the behavior of open web steel joist structures of varying design characteristics, such as joist span, joist spacing, and joist length, under both uniform and drifted

snow loads. The failure method and failure load trends are observed and presented to associate specific building properties with specific failure characteristics.

The third section investigates the risk associated with each building studied. Monte Carlo simulations are used to determine the annual probability of occurrence and reliability indices for structural and serviceability failure of buildings with various characteristics under varying loads. Trends are identified between building risk and specific characteristics.

The final part explores the effects of construction errors on open web steel joist buildings. Both the risk and behavior of open web steel joist roofs containing common construction errors are investigated. Construction errors included weak welds, misplaced joists, and joists installed out-of-plumb.

ACKNOWLEDGEMENTS

I would like to acknowledge and thank my advisor, Professor Abbie Liel, for the help, support, and guidance she has provided me with throughout this project. I am extremely grateful and honored for having the opportunity to work with her in this project. I would also like to acknowledge the other members of my committee; Jim Harris, and Professor Ross Corotis for their advice and guidance through various parts of this project.

I would like to acknowledge the National Science Foundation for sponsoring this project. Support for this work was provided by the National Science Foundation Grant No. 0926680.

Numerous people helped along the course of this project that should be recognized. Prof. George Hearn should be acknowledged and thanked for aiding in my knowledge of open web steel joists and other steel structures. The Structural Engineers Association of Colorado's snow load committee, specifically Dick Cunningham, Michael DePaolo, and Jeannette Torrents, must also be acknowledged for their continued support and guidance of all research involving snow loads in Colorado.

Finally, I would like to thank my friends and family. I was helped throughout my research with guidance and moral support by many other graduate students in the University of Colorado's Civil, Environmental, and Architectural Engineering department. I would like to thank all my office-mates and other graduate students for their help and support. Many members of my family must also be recognized and thanked for their continuous support in everything and anything I choose to do.

CONTENTS

1	INTRODUCTION.....	1
1.1	Motivation.....	1
1.2	Objectives.....	1
1.3	Organization.....	2
2	MODELING OF OPEN WEB STEEL JOIST STRUCTURES.....	4
2.1	Overview.....	4
2.2	Open Web Steel Joist Roof Structures.....	4
2.2.1	Joists Components and Connections.....	4
2.2.2	Columns and Girders.....	8
2.2.3	Bridging.....	9
2.3	Overview of OpenSees Model.....	11
2.4	Materials.....	13
2.4.1	Typical Steel Material.....	13
2.4.2	Steel Buckling Materials.....	15
2.5	Element Properties.....	20
2.5.1	Nonlinear Elements.....	21
2.5.2	Elastic Elements for Columns, Girders and Lateral Bridging.....	34
2.5.3	Zero-Length Elements for Welded and Bolted Connections.....	36
2.6	Displacement Controlled “Pushdown” Analysis.....	48

2.6.1	Loading.....	49
2.6.2	Pushdown Analysis Details.....	55
2.6.3	Convergence Algorithm	57
2.6.4	Parallel Processing	58
2.6.5	Output.....	60
2.7	Validation of the Model	64
3	RESPONSE OF OPEN WEB STEEL JOIST STRUCTURES UNDER SNOW LOADS... 67	
3.1	Introduction	67
3.2	Open Web Steel Joists.....	69
3.2.1	Design, Regulation and Uses of Open Web Steel Joists.....	69
3.2.2	Components of Open Web Steel Joists	71
3.2.3	OWSJ Roof Systems	73
3.3	Buildings Considered in This Study.....	74
3.3.1	Basic Building.....	74
3.3.2	Building Variations	77
3.4	Nonlinear Models of OWSJ Supported Roof Buildings	80
3.4.1	Properties of Nonlinear Models	80
3.4.2	Pushdown Analysis	84
3.4.3	Specific Features of Analysis under Drifted Snow Loads	86
3.4.4	Model Validation.....	87

3.5	Response of OWSJ Supported Roofs to Snow Loads.....	88
3.5.1	Overview	88
3.5.2	Observed Failure Mechanisms in Modeled OWSJs.....	90
3.5.3	Uniform Snow Load Pushdown Results	93
3.5.4	Drifted Snow Load Pushdown Results	102
3.6	Conclusions	106
3.7	Failure Methods.....	107
3.7.1	Buckling of a Web Member	108
3.7.2	Connection Failure	109
3.7.3	Flexural Failure of a Chord Section	112
3.7.4	Local Buckling of a Chord Element.....	113
3.7.5	Shear Failure of a Chord Section	115
4	RELIABILITY ANALYSIS OF OPEN WEB STEEL JOIST ROOF STRUCTURES UNDER SNOW LOADS	118
4.1	Introduction	118
4.2	OWSJ Supported Roof Structures.....	122
4.2.1	Configuration and Design	122
4.2.2	Representative Buildings Considered in Assessment	124
4.2.3	Nonlinear Response under Snow Loads.....	130
4.3	Roof Structures Supported by Wide Flange Steel Sections	136

4.3.1	Configuration, Design and Representative Buildings	136
4.3.2	Response of Wide Flange Section Steel Sections	138
4.4	Structural Reliability Assessment under Snow Loads	138
4.4.1	Reliability Assessment Methods and Metrics	138
4.4.2	Reliability Assessment for OWSJ Supported Roof Structures	143
4.4.3	Reliability Assessment for Wide Flange Roof Structures.....	146
4.5	Discussion	148
4.5.1	Overview	148
4.5.2	Variation of Design Ground Snow Loads.....	149
4.5.3	Variation of Joist Span	150
4.5.4	Variation of Girder Span.....	151
4.5.5	Variation of Joist Spacing	153
4.5.6	Variation of Joist Depth	155
4.5.7	Variation of Design Dead-to-Snow Load Ratios	156
4.5.8	Variation of Parapet Height.....	158
4.6	Conclusions	160
5	EFFECT OF CONSTRUCTION ERRORS ON THE RISKS OF SNOW-INDUCED FAILURE OF ROOFS SUPPORTED BY OPEN WEB STEEL JOISTS.....	162
5.1	Abstract	162
5.2	Introduction	162

5.3	Open Web Steel Joists.....	164
5.3.1	Uses of OWSJs.....	164
5.3.2	Components of OWSJs	165
5.3.3	OWSJ Design for Denver, CO	166
5.4	Construction Errors	168
5.4.1	Possible Construction Errors.....	168
5.4.2	Construction Errors Considered in this Study.....	171
5.5	Numerical Model of OWSJs	171
5.5.1	Properties of Nonlinear Models	171
5.5.2	Implementation of Construction Errors.....	173
5.5.3	Pushdown Analysis	174
5.5.4	Pushdown Analysis Results	175
5.6	Reliability Analysis.....	178
5.6.1	Methodology	178
5.6.2	Reliability Results	179
5.7	Conclusions	182
6	CONCLUSIONS.....	183
6.1	Summary	183
6.2	Future Work	185
	LIST OF REFERENCES.....	187

APPENDIX A.....	194
APPENDIX B.....	198

LIST OF TABLES

Table 2.1: Acceptable reliability (maximum annual probability of failure) and associated reliability indexes (β) for load conditions that do not include earthquake (ASCE 2010).	64
Table 3.1: Buildings subjected to uniform snow loads (i.e. having no parapet).....	78
Table 3.2: Buildings subjected to drifted snow loads.....	79
Table 3.3: Summary of pushdown results for OWSJ supported roofs	90
Table 3.4: Failure modes for OWSJ supported roofs	92
Table 4.1: Buildings subjected to uniform snow loads.....	129
Table 4.2: Buildings subjected to drifted snow loads.....	130
Table 4.3: Re-designed roof structures with W-section steel beams subjected to uniform snow loads	137
Table 4.4: Re-designed roof structures with W-section steel beams subjected to drifted snow loads	137
Table 4.5: Definition of limit states of interest.....	139
Table 4.6: Random variables considered in reliability assessment of OWSJ and W-section roof structures (loading)	140
Table 4.7: Random variables considered in reliability assessment of OWSJ and W-section roof structures (resistance).....	140
Table 4.8: Reliability assessments for OWSJ supported roof structures under uniform snow loads	144
Table 4.9: Reliability assessments for OWSJ supported roof structures under drifted snow loads	144
Table 4.10: Trends observed from reliability indices of OWSJ buildings, where \uparrow signifies increase, \downarrow signifies decrease, -- signifies no significant change.....	145

Table 4.11: Reliability assessments for W-section supported roof structures under uniform snow loads 147

Table 4.12: Reliability assessments for W-section 147

Table 4.13: Trends observed from reliability indices of W-sections, where ↑ signifies increase, ↓ signifies decrease, -- signifies no significant change 148

Table 5.1: List of buildings under investigation designed for Denver, CO (25 psf of design ground snow load) 173

Table 5.2: Results of reliability analysis 180

LIST OF FIGURES

Figure 2.1: Configuration of elements within an OWSJ.....	5
Figure 2.2: Cross-section of an angle	6
Figure 2.3: Crimping of an angle web member (Yost <i>et al.</i> 2006).....	8
Figure 2.4: OWSJ structure, including columns and girders	9
Figure 2.5: Illustration of a) horizontal bridging and b) diagonal bridging.....	11
Figure 2.6: Dodd-Restrepo steel model (Dodd & Restrepo-Posada 1995).....	14
Figure 2.7: Stress-strain relationship of grade 50 steel.....	15
Figure 2.8: Steel material modified for buckling.....	17
Figure 2.9: In-plane and out-of-plane buckling given the cross-section of an OWSJ.....	18
Figure 2.10: A single frame element with ends coupled to fiber cross-sections (Perea & Leon 2008)	21
Figure 2.11: Location of nodes and zero-length elements in a joist.....	23
Figure 2.12: A closer look at the positions of nodes and zero-length elements in a joist.....	23
Figure 2.13: Global and local coordinate systems	25
Figure 2.14: Typical upper (top) chord section	26
Figure 2.15: Upper (top) chord section around panel points	27
Figure 2.16: Typical lower (bottom) chord section	28
Figure 2.17: Lower (bottom) chord section around panel points.....	29
Figure 2.18: End rod section.....	30
Figure 2.19: Uncrimped, rotated angle web member section	33
Figure 2.20: Crimped, rotated web member angle section	33
Figure 2.21: Rod web member section	34
Figure 2.22: ZLE connections between web members and chords	37

Figure 2.23: Welding of single angle web members to chords (Yost *et al.* 2006) 40

Figure 2.24: Crimped single angle web connection to chord, a) side view, b) view looking down chord, c) weld position..... 40

Figure 2.25: Rod Web or end rod connection to chord, a) side view, b) view looking down chord, c) weld position..... 41

Figure 2.26: Force-displacement relationships for a web-chord connection 43

Figure 2.27: Moment-rotation relationships for a web-chord connection 43

Figure 2.28: Comparison between a) double web angle connection (Green *et al.* 2005) and b) OWSJ-girder connection (SJI 2005)..... 44

Figure 2.29: Moment-rotation relationship for a column-joist connection..... 46

Figure 2.30: Approximate force-displacement relationships for a column-joist connection in response to shear and axial (normal) forces..... 48

Figure 2.31: Uniform load pattern on a 1 bay x 1 bay structure 51

Figure 2.32: Heights and lengths in snow drift as described by ASCE 7-10..... 53

Figure 2.33: Increasing drifted load with no base load pattern (case 1) on a 1 bay x 1 bay structure..... 54

Figure 2.34: Increasing drifted load (red) with a constant base load pattern (blue) (case 2) on a 1 bay x 1 bay structure 54

Figure 2.35: Increasing drifted load and base load pattern (case 3) on a 1 bay x 1 bay structure 55

Figure 2.36: Positions of the node of interest, represented by a star, to use in a pushdown analysis 56

Figure 2.37: Procedure followed by processors..... 59

Figure 2.38: Pushdown curve 60

Figure 2.39: Monte Carlo simulation process.....	63
Figure 2.40: Details of joists used for validation (Yost <i>et al.</i> 2004).....	65
Figure 2.41: Comparison of Yost <i>et al.</i> (2004)'s experimental results to the <i>OpenSees</i> model ...	66
Figure 3.1: Examples of OWSJ roofs (Geis 2011)	71
Figure 3.2: Arrangement of the components within an OWSJ.....	72
Figure 3.3: a) 3D view of a portion of the basic building, b) plan view of a portion of the basic building with girders in yellow, joists in red, bridging in black and columns in blue.....	75
Figure 3.4: Illustration of a nonlinear beam-column element discretized into fiber sections.....	81
Figure 3.5: Nonlinear steel materials for chords and web members.....	82
Figure 3.6: Crimped and uncrimped sections defined for web members, shown from the perspective of a cross-section of an OWSJ.....	83
Figure 3.7: Pushdown curves for roofs with varying design ground snow loads.....	85
Figure 3.8: Comparison of model results with experimental results from Yost <i>et al.</i> 2004.....	88
Figure 3.9: Bending moment diagram in the top chord at the end of a joist, positive values on the plot indicate negative bending (<i>i.e.</i> tension at the top)	93
Figure 3.10: Normalized pushdown curves for roofs with varying design ground snow loads ...	94
Figure 3.11: Pushdown curves for roofs with varying joist spans.....	95
Figure 3.12: Normalized pushdown curves for roofs with varying joist spans	95
Figure 3.13: Pushdown curves for roofs with varying girder spans	96
Figure 3.14: Normalized pushdown curves for roofs with varying girder spans.....	97
Figure 3.15: Pushdown curves for roofs with varying joist spacing.....	98
Figure 3.16: Normalized pushdown curves for roofs with varying joist spacing.....	98
Figure 3.17: Pushdown curves for roofs with varying joist depth.....	99

Figure 3.18: Normalized pushdown curves for roofs with varying joist depth	100
Figure 3.19: Pushdown curves for roofs with varying design dead-to-snow load ratios.....	101
Figure 3.20: Normalized pushdown curves for roofs with varying design dead-to-snow load ratios.....	101
Figure 3.21: Pushdown curves for roofs with varying parapet heights for the assumed wind direction shown.....	103
Figure 3.22: Normalized pushdown curves for roofs with varying parapet heights for the assumed wind direction shown	103
Figure 3.23: Pushdown curves for buildings with varying parapet heights; wind is acting orthogonal to the joists.....	105
Figure 3.24: Normalized pushdown curves for buildings with varying parapet heights; wind is acting orthogonal to the joists.....	105
Figure 3.25: Example of a failure due to web buckling, showing stresses in the critical web member of Bldg. U4. Plot shows stress in fibers in web member against the downward displacement of the control node during the analysis.....	109
Figure 3.26: Example of modeled force-displacement relationships describing the connection between the web and the top and bottom chords for the critical web member in Bldg. U15. Plot shows the force capacity of the connection under different displacements of the control node	110
Figure 3.27: Example of an axial force progression through a welded connection between the critical web member and bottom chord of Bldg. U15 leading to loss of load carrying capacity. Plot shows the axial stress in the connection against the downward displacement of the control node	111

Figure 3.28: Example of a flexural failure in a top chord section of Bldg. BD1. Plot shows the stress progression of the fibers in a top chord against the maximum downward deflection in the roof.....	113
Figure 3.29: Example of local buckling of a top chord element in Bldg. U7. Plot shows the stress in the fibers of the chord section against the downward displacement of the control node	115
Figure 3.30: Bending moment diagram for the top chord of a Bldg. U1 OWSJ at failure.....	117
Figure 4.1: Illustration of distributions of loading and resistance impacting computation of structural reliability	120
Figure 4.2: Arrangement of the components within an OWSJ (Adapted from Geis 2011).....	123
Figure 4.3: Plan view of the basic building with girders in yellow, joists in red, and bridging in black, a 3D view of a portion of the building accompanying.....	125
Figure 4.4: Pushdown curves for roofs under a uniform snow load with varying a) design ground snow load (including examples of limit states), b) joist span, c) girder span, d) joist spacing, e) joist depth, and f) design dead-to-snow load ratio.....	134
Figure 4.5: Pushdown curves for roofs under a drifted snow load with varying a) parapet height with wind assumed to act parallel to joists, & b) parapet height with wind assumed to act orthogonal to joists.....	136
Figure 4.6: Distribution of annual maximum ground snow loads for various sites in Colorado (Map from Google).....	140
Figure 4.7: Trends in OWSJ and W-section reliability indices with varying design ground snow loads	150
Figure 4.8: Trends in OWSJ and W-section reliability indices with varying joist spans	151

Figure 4.9: Trends in OWSJ and W-section reliability indices with varying girder spans	153
Figure 4.10: Trends in OWSJ and W-section reliability indices with varying joist spacing.....	154
Figure 4.11: Trends in OWSJ and W-section reliability indices with varying joist depths.....	156
Figure 4.12: Trends in OWSJ and W-section reliability indices with varying design dead-to-snow load ratios.....	157
Figure 4.13: Trends in OWSJ and W-section reliability indices with varying parapet heights and wind blowing parallel to the joists (→)	159
Figure 4.14: Trends in OWSJ and W-section reliability indices with varying parapet heights and wind blowing orthogonal to the joists (↓).....	160
Figure 5.1: Arrangement of the components within an OWSJ.....	166
Figure 5.2: Plan view of the structure showing the location of OWSJs (red) and girders (black)	167
Figure 5.3: Pushdown results for buildings 1-5	176
Figure 5.4: Pushdown results for buildings 6-10	177
Figure 5.5: Probability density function for the ground snow load of Denver, Colorado	179

1 INTRODUCTION

1.1 Motivation

The failure of a roof due to snow loads can lead to severe consequences for both building owners and occupants. Building owners are typically affected financially through costly repairs, replacement of merchandise, and loss of income due to the building being non-occupiable. Building occupants may suffer consequences in the form of injuries or death. A 2010 study demonstrated that these snow-induced roof failures are quite common, accounting for over 40% of the structural failures for that year (Bolduc 2011). There has also been evidence to suggest that lightweight steel roofs are more susceptible to snow-induced failure than other types of roofs (Bennett 1988, Holický 2007, Sadovský & Páleš 2008, Geis 2011, Geis *et al.* 2011).

Open web steel joists (OWSJs) are prefabricated structural elements which fit under the lightweight steel member category. These structural elements are generally used in design for the exact purpose of being able to resist relatively large loads while still maintaining a relatively small self-weight (Fisher *et al.* 2002, Yost *et al.* 2004, Buckley *et al.* 2008). The idea that lightweight steel structures such as OWSJs are particularly susceptible to consequential snow-induced failures highlights the necessity to fully understand the behavior of OWSJs under snow loads.

1.2 Objectives

This study seeks to provide information on the behavior and performance of structures with open web steel joist roofs. A nonlinear model created in *OpenSees* is used to describe the behavior of an OWSJ roof structure with varying roof snow loads applied. These roof loads include drifted snow loads due to this type of loading being the most damaging in past studies (O'Rourke & Auren 1997). The risk accompanying the structures is also assessed through the

use of Monte Carlo simulations and various historical snow data for sites around Colorado, provided by the Structural Engineers Association of Colorado. The effects of common construction errors on the risk and behavior of OWSJ roof structures is also investigated.

1.3 Organization

Chapter 2 provides an overview of the nonlinear *OpenSees* model used to analyze the OWSJ roof structures. Utilizing fiber elements to capture the nonlinear behavior of the OWSJ members allows the analysis to accurately determine the behavior of the structure under various snow loads. The model is also validated against experimental results in this chapter.

Chapter 3 discusses the behavior of OWSJ roof structures with varying roof characteristics. This chapter observes the changes in load and deflection capacities, as well as changes in failure modes as roof characteristics vary. Specific trends in building behavior are identified and related to roof characteristics in order to provide a better understanding of the effects certain roof characteristics have on OWSJ roof structures.

Chapter 4 uses the results from the analyses of roofs with varying characteristics to identify the reliability of the structures with respect to structural failure and serviceability. The reliability of the structures is determined through Monte Carlo simulations and considers variations in the annual maximum ground snow load for specific sites, as well as variations in the ground-to-roof snow load conversion factor. These reliability assessments are compared to W-Section beam alternatives under the same loads and recommended target values found in the ASCE 7-10 commentary.

Chapter 5 studies the effects of construction errors on the behavior, probability of structural failure, and probability of serviceability failure in OWSJ roof structures. This chapter studies buildings which have flaws in them such as weak welds, misplacement of joists within

the structure, or installing OWSJs out-of-plumb. The behavior and risks assessed for the flawed buildings are compared to error-free buildings in order to determine the change in risk and behavior each construction error causes.

2 MODELING OF OPEN WEB STEEL JOIST STRUCTURES

2.1 Overview

The first step towards accurately modeling an open web steel joist (OWSJ) roof structure is to understand the structure, elements and connections in OWSJs. The first section of this chapter describes a typical OWSJ roofed structure and all the separate elements that comprise an OWSJ roof structure. Subsequent chapters will define the specific features and design characteristics of the joists of interest.

All the joists considered are assumed to be designed according to Steel Joist Institute (SJI) standards. The SJI is the governing body for OWSJ design in the United States requiring joist manufacturers to conform to SJI standards in order to be certified. The SJI also provides guidelines for the bridging and connections to use in OWSJ structures.

2.2 Open Web Steel Joist Roof Structures

2.2.1 Joists Components and Connections

As shown in Figure 2.1, the joists themselves are composed of 4 different elements: the upper (top) chord, the lower (bottom) chord, and the web; some manufacturers have a special standard for the end web member. These elements are arranged in a configuration which allows them to resist loads specified in load tables provided from the SJI (Fisher *et al.* 2002, Yost *et al.* 2004). The points at which the web members meet the chords (known as panel points) are spaced at different lengths between each other and some manufacturers define the joist's geometry with only four lengths for these panel point-to-panel point spacings: the distance to the first panel point from the end of the joist (ERtoPP in Figure 2.1), the distance between the first panel point and the second panel point on the upper chord (extUCpan in Figure 2.1), the distance between the first and second panel point on the lower chord (extLCpan in Figure 2.1), and the distance

between all other panel points along both the upper and lower chords, neglecting the intersection of vertical web members (intpanel in Figure 2.1). These four distances, along with the depth of the joist (D_j in Figure 2.1), specifies the arrangement of the joist. In addition, some joists include vertical web members, which are typically found in OWSJs that have angle sections as web members.

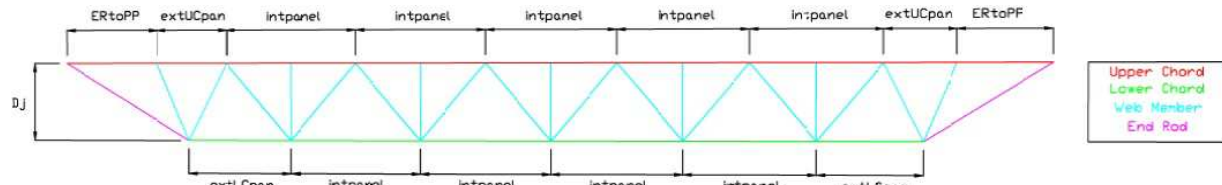


Figure 2.1: Configuration of elements within an OWSJ

Both the upper (top) and lower (bottom) chords in open-web steel joists are continuous members along the span of the joist. This means that these elements are not usually spliced at any point along the span, including the panel points. The chords used in OWSJs are typically two back-to-back angle sections which have a space between them large enough to fit the end rod (Buckley *et al.* 2008). The two angle sections, which can vary in leg sizes (b in Figure 2.2) between 1.25 and 3 in. and have thicknesses (t in Figure 2.2) between 0.109 and 0.281 in., are not connected to each other at any places aside from panel points where welded web members or end rods act as the connection between the two. Neither the upper nor lower chords are likely to buckle globally. The lower chord is typically under tension when the joist is subjected to uniformly distributed gravity loads. Upper chord buckling out of the plane of the joist is neglected due to its attachment to the roof or ceiling that restrains movement and global buckling. Upper chord buckling may occur in the plane of the joist between panel points, however the inclusion of vertical web members generally prevents this from occurring.

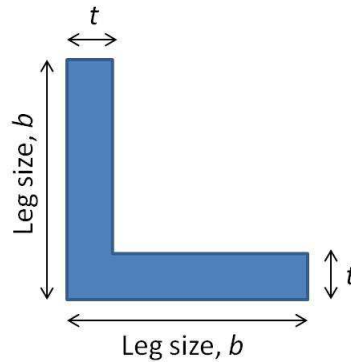


Figure 2.2: Cross-section of an angle

The web members can be a variety of sections, the two most common being rods and angles. A rod web member is typically a single long rod that is bent to meet the configuration of the OWSJ that is used. However, sometimes individual rods are installed for each web member so that different rod sizes can be used along the length of the joist; in particular, larger rods, which can reach a diameter of 1.0625 in., may be used in positions which require greater strength and smaller rods in positions where less strength is required (Buckley *et al.* 2008). This technique increases the efficiency of the joist design by resisting the required loads while providing the minimal amount of steel, maximizing the joist's strength to weight ratio. Angle section webs always utilize this technique and can specify angle sections as big as L8.00x8.00x1.125 in high strength-demand positions and sections as small as L1.00x1.00x0.109 in low strength-demand positions. Typically, the largest and strongest web member is the first web member in compression from each end which experiences the largest compression stresses under a uniform gravity loading of the joist. This member is often referred to as the critical web member. Web members may be under tension or compression depending on their position and orientation within the OWSJ (Buckley *et al.* 2008).

The final element type within an OWSJ is the end rod. As the name suggests, it is a rod section, varying in size between diameters of 0.5 to 1.0625 in., which is used to connect the ends of the upper and lower chords to each other (Buckley *et al.* 2008). These members may also be in compression when the joist is subjected to wind uplift loads so buckling must be considered.

Through observations of local buildings, and reports from case studies and experiments, the author determined that the web members and end rods are connected to the chords by welds which can be taken as semi-rigid connections (Yost *et al.* 2004). Although the connections are fabricated as welds, the study found that companies who follow Steel Joist Institute (SJI) Guidelines, such as Vulcraft and Canam Steel, actually design the joists to be pinned at these connections (Yost *et al.* 2004, Canam 2005). This pinned assumption in design covers the worst-case scenario from the perspective of serviceability because it under-estimates joist stiffness. This assumption is further justified because in the case of rigid connections, the members around the connections will eventually yield and, when this happens, have an effect similar to a pin.

If web members are angles, the angles need to be crimped at their ends in order to fit in the space between the two angles of the chords (see Figure 2.3). The crimped section of an angle section has a different centroid than the uncrimped section of the same angle. This different centroid location means that as compression or tension loads are applied at the ends of the web members (the crimped sections) the axis of loading does not match the centroid throughout the entire member causing an internal moment which can accelerate the buckling of the web member (Buckley *et al.* 2008). In fact this is very troubling considering that often times the failure mechanism of these joists is the buckling of a web member (most likely the critical web member, hence the name) (Yost *et al.* 2004).

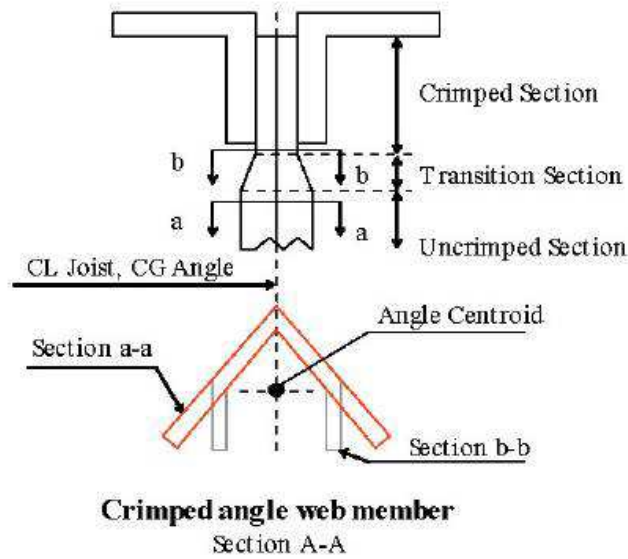


Figure 2.3: Crimping of an angle web member (Yost *et al.* 2006)

2.2.2 Columns and Girders

Columns and girders support the open-web steel joists, providing a load path for the roof loads to the ground, as shown in Figure 2.4. The columns may be either steel W-sections or HSS-sections. Such members are designed for AISC specifications, not SJI. These sections must have sufficient strength to pass all design requirements such as compression, bending, and shear. Similarly, the girders are designed by AISC specifications. There are a wide variety of sections used for girders in buildings; for this study, only W-sections will be considered. Another common type of girder used is an open web steel joist girder which is similar to an OWSJ and also has its designed governed by the SJI (2005). Open web steel joist girders are not considered in this study.

The joists are connected directly to the girders by sitting on top of them at specific points along the girder corresponding to the designated joist spacing, as illustrated in Figure 2.4. The SJI joist catalogues states that the joists should be attached to the columns or girders through the

use of two ½” ASTM A307 bolts or more commonly through the use of two 1 in. long 0.125 in. fillet welds (SJI 2005). In this study, it is assumed that all joist to girder connections are bolted either directly to the girder, or to a plate welded to the top of a column.

This project is not extremely interested in how the girders and columns connect to each other, so it is assumed that rigid connections are provided. This assumption for the connection is justified through observations of girders being welded on top of columns in various local buildings.

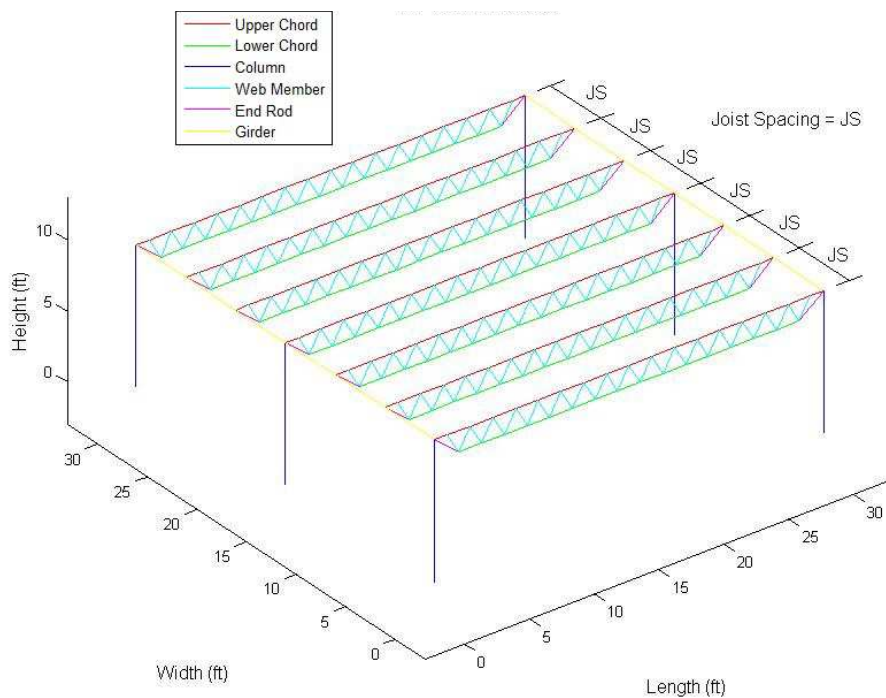


Figure 2.4: OWSJ structure, including columns and girders

2.2.3 Bridging

The final type of elements commonly seen in OWSJ structures is bridging, which connect the joists to each other within the span (i.e. not the girders). These bridging members are designed to resist lateral loads such as winds acting orthogonal to the joists. The bridging is typically included for safety during the construction process. Once the deck is attached to the top

of the OWSJs the lateral forces are generally resisted through the roof or floor deck itself. This study does not consider the decking on the OWSJs which leads to the bridging being necessary to resist any lateral loads in the decking's absence. According to the SJI bridging specifications there are two types of bridging: horizontal bridging and diagonal bridging. The bridging guide also goes on to provide the SJI bridging tables, which are used by every joist manufacturing company in the country (see Appendix A), and dictate the appropriate bridging member sections, and spacing between bridging depending on the joist depth, type, and section number (Vulcraft 2007).

Horizontal bridging (Figure 2.5a) uses angle sections as the bridging members, and as indicated by the name, these members are oriented horizontally. The angles used as horizontal bridging are all angles of equal leg size, the leg size spans from 1 in. to 2.5 in. and the thickness of the legs vary between 0.109375 in. and 0.15625 in. The bridging members are welded to the chords and are continuous throughout the entire width (perpendicular to the joists) of the structure. In the roofs considered in this study, the bridging members are attached to both the upper and lower chords at the same position along the joist. This means that bridging along the upper chord will be directly above the bridging along the lower chord, facilitating modeling. In reality, the bridging can be staggered between the upper and lower chord, so long as it conforms to the SJI's bridging guidelines (Vulcraft 2007).

Diagonal bridging (Figure 2.5b) also uses angles as the bridging member sections but, unlike horizontal bridging, the diagonal bridging members are not continuous throughout the width of the structure. Instead, the length of each member is only enough to reach from the upper chord of one joist to the lower chord of the adjacent joist. This arrangement provides an X-shape from the crossing bridging members. Diagonal bridging members use angle sections of equal leg

size whose leg size spans from 1 in. to 3.5 in. with leg thicknesses between 0.109375 in. and 0.25 in. In reality, these bridging members are either bolted or welded to both of the chords to which they are connected, as the SJI requires them to be attached by “positive mechanical means” (Vulcraft 2007). Where the X intersects, the bridging members are bolted to each other. In this project, the positive mechanical means used to connect this type of bridging is assumed to be welds (Vulcraft 2007).

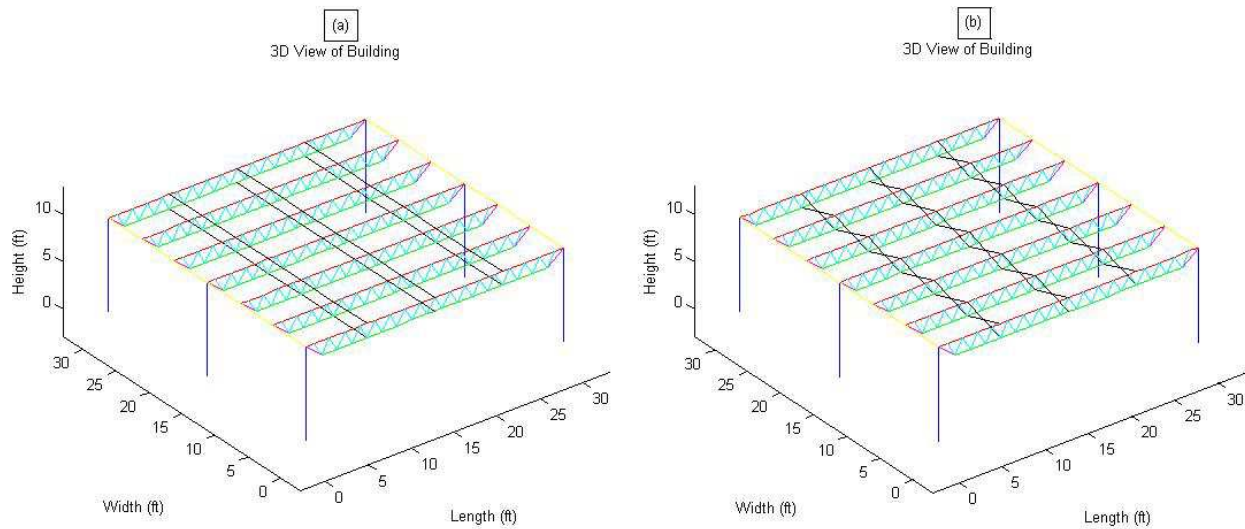


Figure 2.5: Illustration of a) horizontal bridging and b) diagonal bridging

2.3 Overview of OpenSees Model

The *OpenSees* model used to analyze OWSJ supported structures is a nonlinear model which takes into account a variety of failure modes. *OpenSees* is chosen to run the analyses due to its ability to accurately represent nonlinear elements in buildings as well as its ability to analyze 3D models under a static analysis. *OpenSees* is also very compatible with MATLAB for pre- and post-processing calculations. This allows joist and building variables to be input into a series of MATLAB scripts which will produce a tcl¹ file which is run by *OpenSees*. These MATLAB scripts and input variables allow for fast, simple changes to be made to buildings and

¹ tcl is the programming language used by the *OpenSees* program.

joists accounting for a wide variety of building and joist geometries. Another major reason for the use of *OpenSees* is its prevalent use within the University of Colorado at Boulder's Structural Engineering Department; this eased the troubleshooting process by being able to confer with colleagues.

The nonlinear model gains its nonlinear properties through the geometric and material nonlinearities of its elements, as well as through the nonlinear behavior of the connections within the structure. The geometric and material nonlinearities of elements are accounted for through the use of fiber section elements which have the ability to define specific section geometries through the placement of its fibers which are assigned specific material properties (Perea & Leon 2008). The bolted and welded connections are represented by zero-length spring elements which provide specific force-displacement and moment-rotation relationships based on published models.

The nonlinearities in the members and connections account for the possible failure modes of the model. The nonlinear material model allows for the failure of the material to occur under certain stress-strain conditions. The material also accounts for the buckling of the web members; this is explained in more depth in a later section. The geometric properties of the members determined through the fiber positions allow for the members to accurately predict their overall behavior. The geometric and material properties also combine to account for failures such as flexural failure or local buckling. The models of the connections account for the fracture of the welds under specific forces or moments allowing the model to predict connection failure.

The methods used to create the OWSJ elements and models used in the *OpenSees* model, as well as the analysis procedure are described in the following sections. The nonlinear model is also validated against experimental results in the final section of this chapter.

2.4 Materials

2.4.1 Typical Steel Material

Due to the same steel material being used multiple times when describing the elements in *OpenSees*, the material will be defined here first, then referenced in a later section. The data used to create the constitutive model for steel in *OpenSees* was based on a model from Dodd & Restrepo-Posada (1995). Figure 2.6 illustrates the model, some limitations of this model can be observed by noting that it does not distinguish the differences in tension and compression behavior. The Doss-Restrepo steel material is chosen despite it being a rebar model due to its capability of experiencing yielding, a yield plateau, strain hardening, and finally, failure of the material at a specific point. The following parameter values are assumed in defining the steel material: (1) the Young's modulus is $E = 29000$ ksi; (2) the actual yield strength is 1.1 times the yield strength provided from the grade of the steel based on ASCE 41-06 values for Grade 50 steel; (3) the point where strain hardening is initiated has a strain, ϵ_{sh} , of 10 times the yield strain (Bruneau *et al.* 1998) and a stress of $(1+\epsilon_{sh})$ times the yield stress; (4) the point of ultimate stress is at a strain of 10 times ϵ_{sh} and a stress of 1.49 times the yield strength provided from the steel grade (ASCE 41-06). The failure, which represents the fracture of the steel, of the model is assumed to be immediately after the ultimate stress point due to post-ultimate behavior being highly dependent on the shape of the section. This assumption is consistent with the Dodd-Restrepo model's recommendation that "the ultimate coordinates mark the end of the useful region of stress-strain curve" (1995).

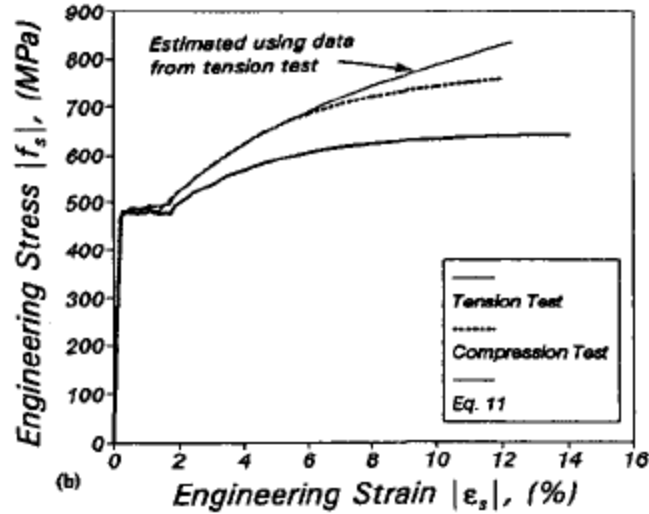


Figure 2.6: Dodd-Restrepo steel model (Dodd & Restrepo-Posada 1995)

In order to use the data provided in the previous paragraph in the context of *OpenSees*, a uniaxial material is defined in *OpenSees* which is either similar to this curve, or could be modified to represent this curve. The command *uniaxialMaterial ElasticMultiLinear* was chosen over the pre-programmed Dodd-Restrepo steel model because it has the capability of representing a customized multi-linear curve and it can provide a failure point for the material by reducing its allowable stress to zero after failure so the analysis can continue. The pre-programmed Dodd-Restrepo model allows for failure, but the analysis stops once failure occurs, rather than tracking the post-peak response. As shown in Figure 2.7, the steel model used is discretized into 8 segments defined using the multilinear command. Also, the *ElasticMultiLinear* command states that once the final indicated stress-strain point is specified it will compute any strain beyond that point to be along the slope of the last specified segment (PEER 2013b). In order to ensure that failure/fracture occurs in the material, two additional segments are added; the first brings the curve down to a stress of 0 psf with an increase of 0.1 [ft/ft] strain from the ultimate stress point; the next point continues to have 0 psf stress at a slightly larger strain ensuring no strength resistance for any strain larger than 0.1 [ft/ft] past the failure strain. The

multi-linear stress-strain curve is shown in Figure 2.7 where the selected points for a grade 50 steel are labeled as (strain [unitless or ft/ft], stress [psf]). It should be noted that although Figure 2.7 shows the curve for positive stress and strain (tension) only, this curve describes the negative stress and strain (compression) as well by reflecting the curve across both the stress and strain axes.

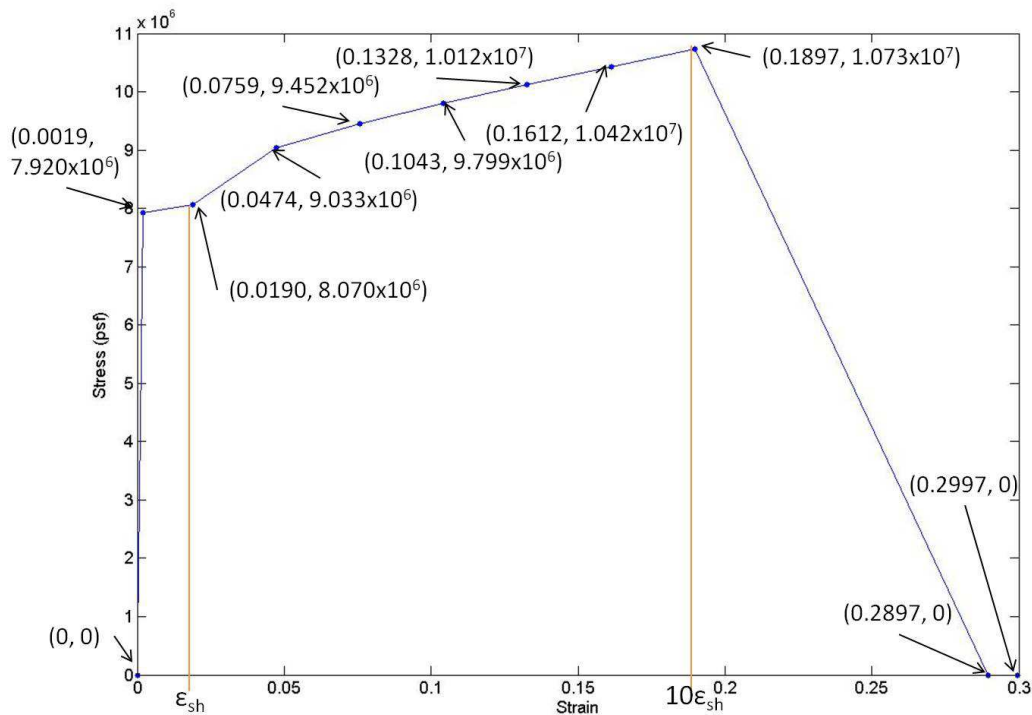


Figure 2.7: Stress-strain relationship of grade 50 steel

2.4.2 Steel Buckling Materials

One of the most common failure mechanisms for open-web steel joists to experience is the buckling of one of the web members (Yost *et al.* 2004, Buckley *et al.* 2008). However, the *OpenSees* model implemented as described does not account for the buckling of members, so it is necessary to consider buckling behavior of the web members in an alternative approach. The adopted method implements the buckling directly by modifying the material properties used for

web members. The modified material defines the particular strain at which buckling occurs, ϵ_b , and changes the steel material so that the behavior of the material after the buckling strain gradually decreases in strength down to 0 psf stress (Elnashai & Elghazouli 1993, Perea & Leon 2008).

In order to determine the buckling strain value, ϵ_b , equations taken from the AISC Steel Construction Manual (2011) are used to determine the stresses required for flexural and flexural-torsional buckling modes, accounting for the geometry of the members and the configuration of each element in the joist. For these calculations it is assumed that the welds which connect the web members and end rods to the chords are semi-rigid and produce an effective length factor, k , of 0.70 in the elements (Yost *et al.* 2004). Taking the smaller of the two buckling stresses, and assuming the equations provided by the AISC (2011) are elastic, the buckling strain is determined by dividing the governing buckling stress by the Young's modulus of steel. This strain, ϵ_b , is then used in the *ElasticMultiLinear OpenSees* command to create a buckling steel model which initially follows the Dodd-Restrepo model shown above until the buckling strain is reached. Following recommendations from Elnashai & Elghazouli (1993), the point where the material's stress-strain curve becomes 0 corresponds to a strain of $5\epsilon_b$. Another segment is added to the model which keeps the stress-strain relationship at a stress of 0 psf for strains larger than $5\epsilon_b$, much like the last segment in the typical steel material model. It's important to note that these changes are done for only the compression (negative stress and strain) part of the stress-strain curve because buckling only effects compression as seen in Figure 2.8.

There are multiple equations taken from the AISC (2011) in order to determine the buckling strain, which depend on the shape of the element being compressed. The following section describes the equations and calculations relevant for angle sections so that the results can

be used to determine the angle steel buckling material respectively. Buckling of the rod members used for the end web members is neglected due to those members being in tension for all the applied loads in this study.

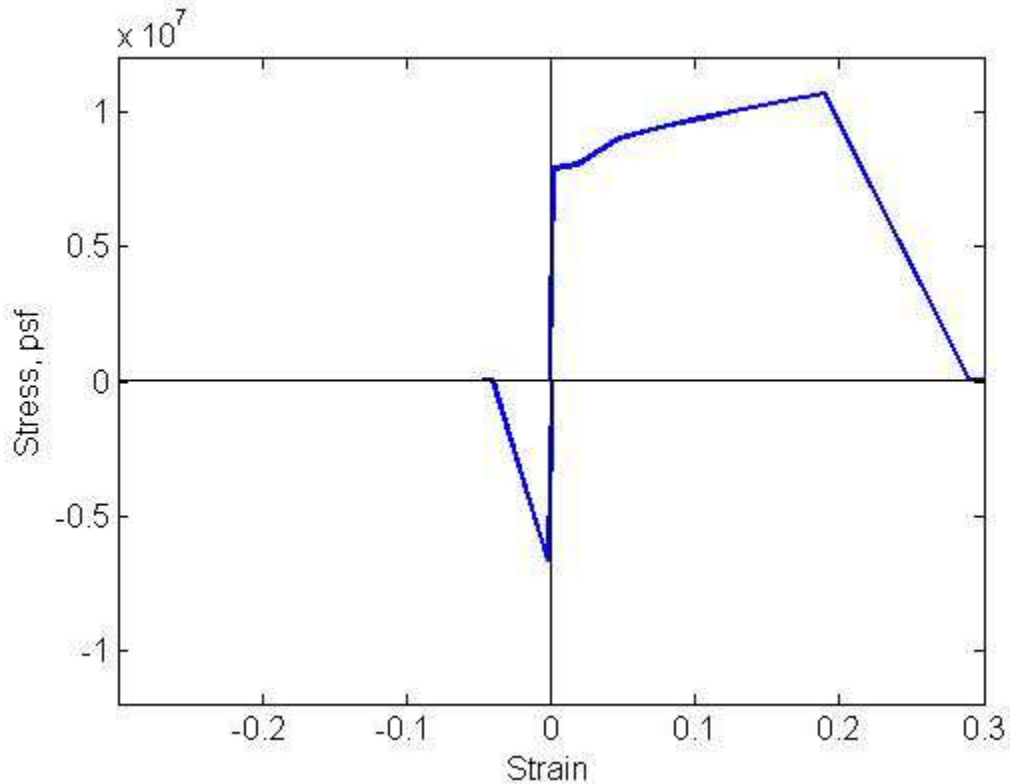


Figure 2.8: Steel material modified for buckling

2.4.2.1 Angle Buckling

The flexural buckling stress is determined by assuming that the entire length of the member multiplied by the effective length factor is the effective length for buckling (*i.e.* $kL = 0.7L$). It should also be noted that there are two flexural buckling stresses due to the angle sections being asymmetric with respect to bending in the two directions. One of the flexural buckling stresses represents buckling about the local z-axis (out of the plane of the joist as seen in Figure 2.9) and the other represents buckling about the local y-axis (in the plane of the joist as seen in Figure 2.9). This designation of directions allows the moments of inertia (I_y & I_z) and

radii of gyration (r_y & r_z) to be defined appropriately depending on their direction. It should be noted that, when angled web members with crimped ends are used, the moments of inertia and radii of gyration are determined as one value for the entire member despite the change in shape (which will be discussed further in a later section). This value is computed by first assuming that there is a 2 in. transition zone between crimped and uncrimped sections at each end as well as a 0.5 in. extension of the crimped section past its confinement at the edge of the chords. Using these assumptions the uncrimped length can be computed as $L_{uncrimped} = L - (5 \text{ in.}) - [\text{length of web confined by upper and lower chords}]$. The moments of inertia and radii of gyration in the crimped-ended angles are computed as a weighted average between the crimped and uncrimped sections depending on the length of each section.

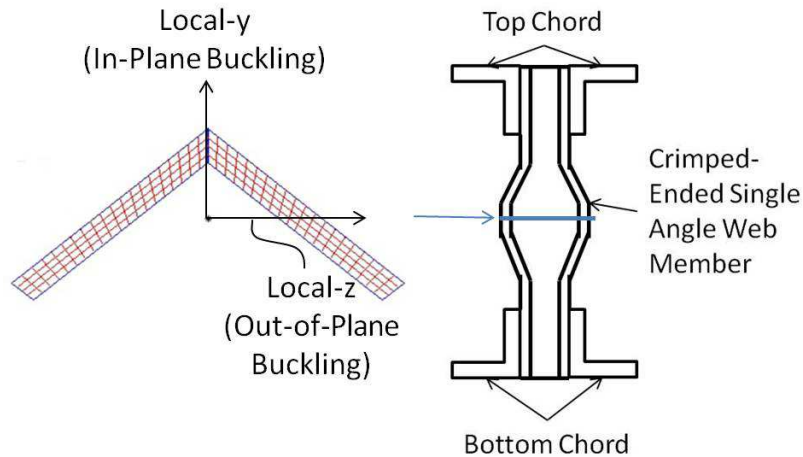


Figure 2.9: In-plane and out-of-plane buckling given the cross-section of an OWSJ

The value for Q must then be found, and the following equations are used where b is the length of the smaller angle leg and t is the thickness of the legs (AISC 2011 Eqns. E7-10, E7-11, & E7-12):

$$\text{if } \frac{b}{t} \leq 0.45 \sqrt{\frac{E}{F_y}}, \text{ then } Q = 1.0 \quad (2.1)$$

$$\text{if } 0.45 \sqrt{\frac{E}{F_y}} < \frac{b}{t} \leq 0.91 \sqrt{\frac{E}{F_y}}, \text{ then } Q = 1.34 - 0.76 \left(\frac{b}{t}\right) \sqrt{\frac{F_y}{E}} \quad (2.2)$$

$$\text{if } \frac{b}{t} > 0.91 \sqrt{\frac{E}{F_y}}, \text{ then } Q = \frac{0.53E}{F_y \left(\frac{b}{t}\right)^2} \quad (2.3)$$

The flexural Euler buckling stresses in both buckling directions is found through ASCE (2011) Eqn. E3-4:

$$F_{efi} = \frac{\pi^2 E}{\left(\frac{kl}{r_i}\right)^2} \text{ where } i = y \text{ or } z \quad (2.4)$$

The flexural Euler buckling loads, F_{efi} , and the Q values allow for the flexural buckling stress to be determined in both directions through the following equations (AISC 2011 Eqns. E7-2 & E7-3):

$$\text{if } \frac{kl}{r_i} \leq 4.71 \sqrt{\frac{E}{QF_y}}, \text{ then } F_{crfi} = Q \left[0.658 \frac{QF_y}{F_{efi}} \right] F_y, \text{ else } F_{crfi} = 0.877 F_{efi} \quad (2.5)$$

This value is computed in the two directions, as denoted by the symbol i which can be either y or z , and later combined with the flexural torsional values to define the stress strain properties.

Flexural-torsional buckling of angle sections is only applicable if the member is non-slender. In order to fulfill this requirement b/t must be less than or equal to $0.91 \sqrt{E/F_y}$. If this condition is satisfied, a handful of variables must be computed in order to complete the flexural-torsional buckling calculations. First, the gross area, A_g , warping constant, C_w , coordinates of the shear center with respect to the centroid, x_o & y_o , the moments of inertia, I_x & I_y , polar moment of inertia, J , and the radii of gyration, r_x & r_y , for the section are determined. Second, a length of analysis is determined which describes the length of the member which will be experiencing torsion. In this analysis it was assumed that the length for analysis would be the uncrimped length plus half of the transition length on each side, giving $L_{ana} = L_{uncrimped} + (2 \text{ in.})$. More

variables and Euler buckling loads which require more complicated equations are also needed in the analysis; they are as follows (AISC 2011 Eqns. E4-7, E4-8, E4-9, & E4-11):

$$\bar{r}_o^2 = x_o^2 + y_o^2 + \frac{I_x + I_y}{A_g} \quad (2.6)$$

$$H = 1 - \frac{x_o^2 + y_o^2}{\bar{r}_o^2} \quad (2.7)$$

$$F_{ezt} = \frac{\pi^2 E}{\left(\frac{L_{ana}}{r_z}\right)^2} \quad (2.8)$$

$$F_{ext} = \left(\frac{\pi^2 E C_w}{(L_{ana})^2} + GJ\right) \frac{1}{A_g \bar{r}_o^2} \quad (2.9)$$

Using these variables, the flexural-torsional buckling load is calculated as follows from AISC (2011) Eqn. E4-2:

$$F_{ef-t} = \left(\frac{F_{ezt} - F_{ext}}{2H}\right) \left[1 - \sqrt{1 - \frac{4F_{ezt}F_{ext}H}{(F_{ezt} + F_{ext})^2}}\right] \quad (2.10)$$

This flexural-torsional Euler buckling stress allows the flexural-torsional buckling stress to be calculated by using the same equations used to determine the rod's flexural-torsional buckling stress (AISC 2011 Eqn. E3-2 & E3-3):

$$\text{if } \frac{kL}{r} \leq 4.71 \sqrt{\frac{E}{F_y}}, \text{ then } F_{crf-t} = \left[0.658^{F_{ef-t}}\right] F_y, \text{ else } F_{crf-t} = 0.877 F_{ef-t} \quad (2.11)$$

The minimum value of F_{crfy} , F_{crfz} , and F_{crf-t} is then used to determine the overall buckling stress of the angle section member.

2.5 Element Properties

This section describes the elements required to model the OWSJ structure so that they may easily be implemented into the *OpenSees* software platform. Since the previous section already discussed what these elements are, how they are connected to each other, and what

materials are implemented in each element, the rest of the description generally includes the type of element and geometric transformation of the element.

2.5.1 *Nonlinear Elements*

The first type of element is the nonlinear element, which is used in order to take into account both material and section nonlinearities represented in the different constituent elements of the OWSJ. Material nonlinearities are dealt with by using the appropriate steel material described above, and the section nonlinearities are taken into account through the use of fiber sections. Fiber section nonlinear elements predict the behavior of an element by dividing the element into multiple two-end frame elements with a specific cross-sectional arrangement of fibers, each of which have specific material properties which are defined above, at each end (Figure 2.10). The appropriate stress and strain values for each fiber are calculated under the given loads, the behavior across the frame element is determined using finite element interpolation functions which satisfy compatibility and equilibrium of the element (Perea & Leon 2008).

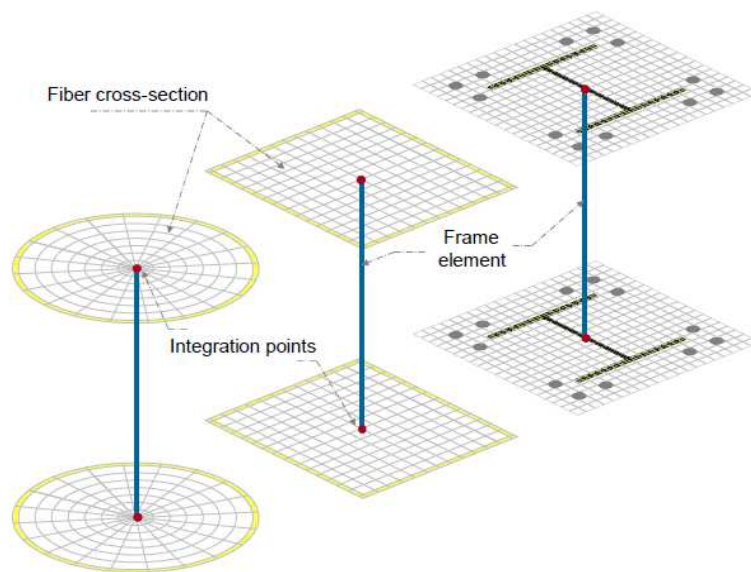


Figure 2.10: A single frame element with ends coupled to fiber cross-sections (Perea & Leon 2008)

Two issues with using fiber sections in *OpenSees* which were encountered was that having fibers be too large could change the resulting output by a significant amount, especially in circular sections. The other problem was that if the fibers are too small then the amount of fibers becomes so large that it slows down the analysis or may even have the analysis run out of memory and not run at all. In order to remedy both of these problems a variable in the input parameters for the model was created which provides a limiting fiber dimension for the web members and end rods in the analysis. The fiber sizes in the chords are slightly larger to reduce the chance the analysis would run out memory; the results of the analysis were not observed to change significantly if these larger fiber sizes were used. Unfortunately, a precise way to determine the most efficient fiber size has not been implemented; therefore a trial-and-error method must be employed by the user. For different buildings, sometimes it is required to vary the fiber size in order to determine a size to use which is small enough to not affect the results, but large enough so the analysis still has enough memory to run.

Using fiber sections and the specified steel material, elements are made for the chords, web members, and end rods using *OpenSees's* *element dispBeamColumn* command which creates displacement-based nonlinear beam-columns which is based on the iterative displacement formulation to solve for element behavior (PEER 2013b). Description of their sections and other information is given in the following subsections. Details of the model are illustrated in Figure 2.11 and Figure 2.12.

Nodes are Represented by *

Zero-Length Elements Connecting Web Members and End Rods to Chords are Represented by o

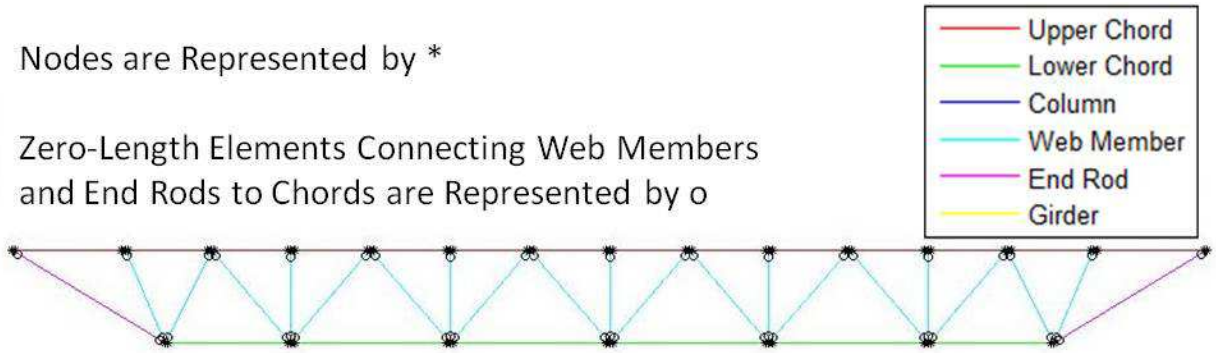


Figure 2.11: Location of nodes and zero-length elements in a joist

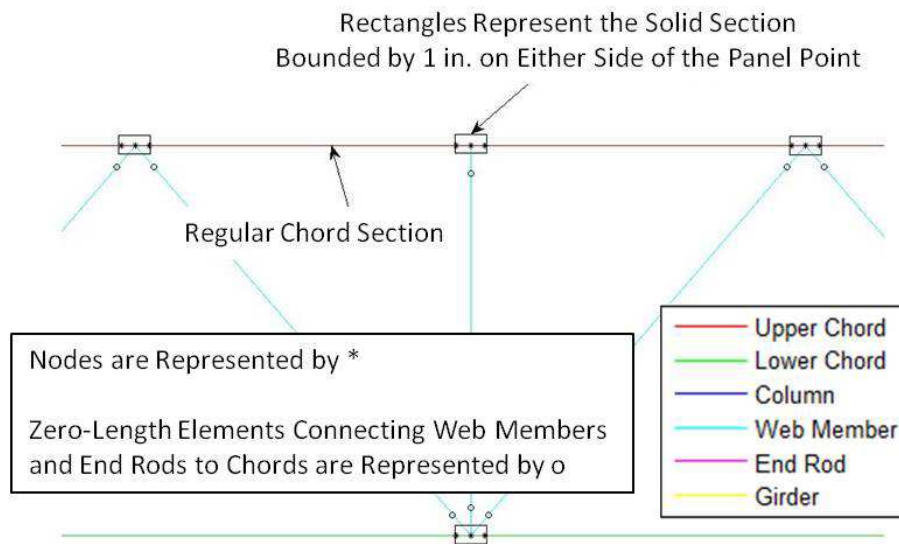


Figure 2.12: A closer look at the positions of nodes and zero-length elements in a joist

2.5.1.1 Upper (Top) Chord

The upper (top) chord is continuous across the entire span of an individual joist. Modeling a continuous chord is simple in *OpenSees*, because the program assumes that any two elements meeting at a node are rigidly connected. Despite being continuous, the upper chord is modeled with a number of discrete sections with these rigid connections. At panel points the sections become relatively solid due to the connection of the two angles through welds and either the web member or end rod, so extra nodes are placed 1 in. on either side of the panel points, as

seen in Figure 2.12. Between these two nodes and the panel point node the section between the two angles is completely solid (Figure 2.15) while the rest of the upper chord sections have the space between the two angle sections (Figure 2.14).

Aside from knowing how the elements are connected to each other, the main things needed to model any nonlinear element in *OpenSees* are the geometric transformations of the elements, the material used in the fibers of the elements, the fiber make-up of the element's sections, the number of sections being evaluated within the element, and the size and dimensional properties of the sections themselves.

Geometric transformations are needed to orient the local coordinate system within the global three-dimensional coordinate system. To describe the local coordinate system in *OpenSees*, a vector must be specified in global coordinates. This vector must be located in the local x-z plane with the local x-axis along the length of the element (PEER 2013b). To do this simply, we can describe the vector as the local z-axis itself. The upper chord elements are always connected from left to right; therefore, as seen in Figure 2.13, the local x-axis is the same as the global x-axis. For ease of modeling, the author assigned the local z-axis on the global x-z plane, defining the local and global z-axes would be in the same direction. This means the vector to use for the geometric transformation is $[0 \ 0 \ 1]$.

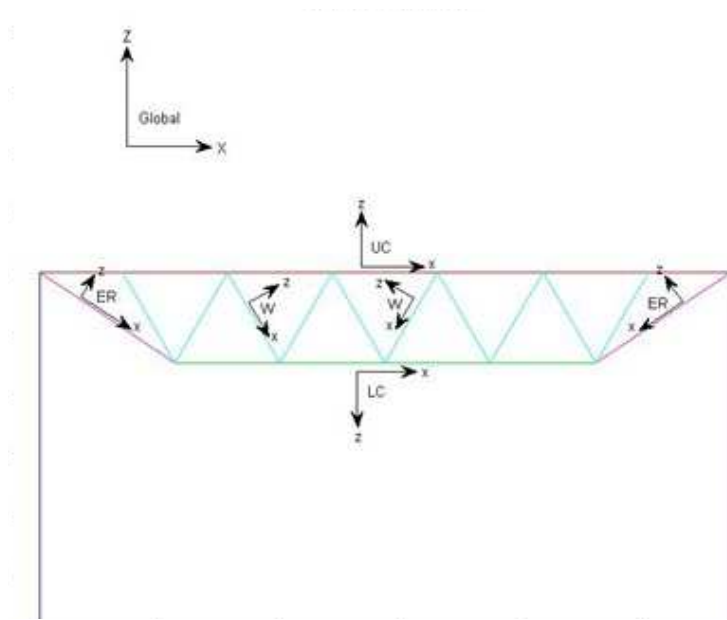


Figure 2.13: Global and local coordinate systems

Now that the direction is defined it is possible to define the section of the upper chord itself. As described in earlier sections, many OWSJs use back-to-back angle sections as the upper chord (Buckley *et al.* 2008), so this is what the modeling accommodates for. The spacing between the two angles must be equal to the diameter of the end rod and the crimped web members. The angles are then divided into fibers, each of which has the typical steel material characteristics described earlier. These section arrangements are used in the regular upper chord elements seen in Figure 2.12 and are evaluated at 3 integration points within these elements (one at each end and one in the center) to determine the behavior of the element. Figure 2.14 shows an upper chord section of two back-to-back L2x2x0.148 angles in its local coordinate system with fiber dimensions no more than 0.075 in. along with 12 points of interest within the upper chord section. Note also that this upper chord section has a spacing large enough to accommodate an end rod with a 0.938 in. diameter.

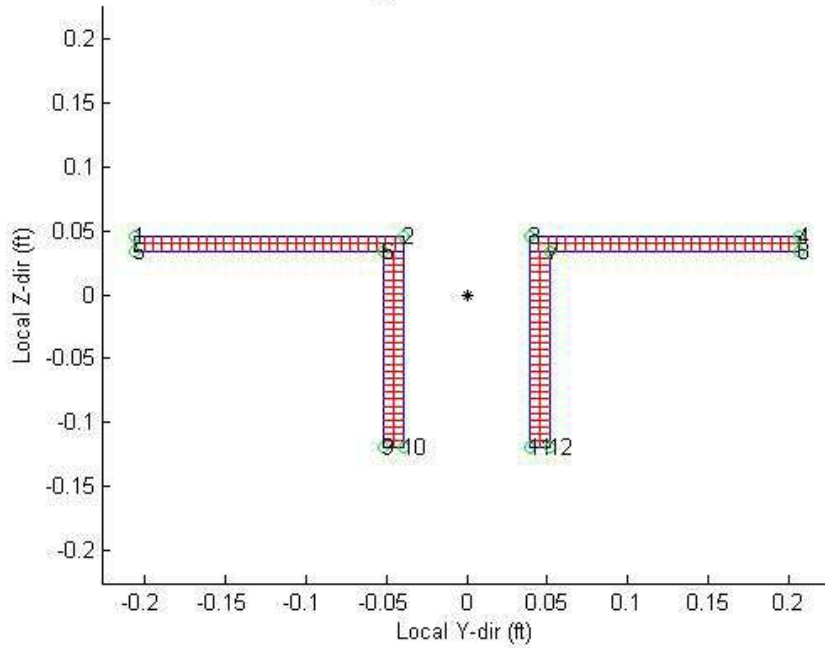


Figure 2.14: Typical upper (top) chord section

As mentioned earlier, around the panel points a different section is used for upper chord members in order to simulate the effect of the web member or end rod occupying the space between the angle sections. These very short elements (see Figure 2.12) resemble two back-to-back chords with the space between filled in. Figure 2.15 illustrates the solid sections around the panel points to accompany the typical upper chord sections shown in Figure 2.14.

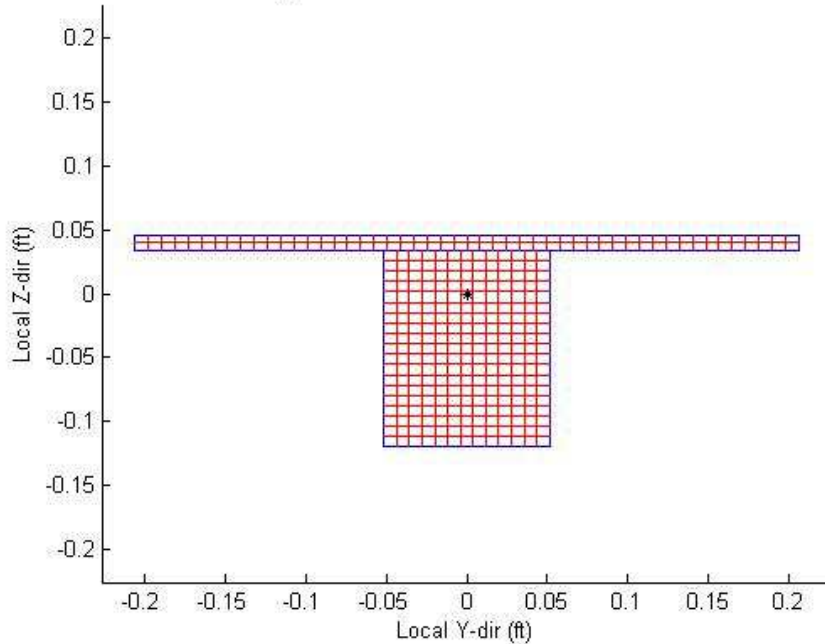


Figure 2.15: Upper (top) chord section around panel points

2.5.1.2 Lower (Bottom) Chord

The lower (bottom) chords are similar to the upper chords in the manner that they are continuous throughout the span of the joist and have discrete (rigidly connected) solid sections surrounding the panel points as seen in Figure 2.12.

The lower chord elements are also similar to upper chord elements because they are always applied in a way so that the local x-axis corresponds to the global x-axis. Unlike the upper chord, the lower chord elements are defined so that the positive local z-direction is in the opposite direction of the positive global z-direction as seen in Figure 2.13. Accordingly, the geometric transformation vector, which described the positive local z-direction in global coordinate terms, is $[0 \ 0 \ -1]$.

The lower chord is like the upper chord in the sense that it is practically always composed of back-to-back angles as its section (Buckley *et al.* 2008). However, there are other lower chord sections that could be used (double rod, etc...), but the back-to-back angle is by far the most

commonly used lower chord and is therefore the only one considered in this study. Once again, the back-to-back angle is discretized into fibers with the properties of the typical steel material. These regular sections, which are much longer than the solid lower chord sections (see Figure 2.12), are evaluated at 4 integration points in order to determine the behavior of each element. Figure 2.16 shows a lower chord section of two back-to-back L1.5x1.5x0.170 angles in its local coordinate system with fiber dimensions no more than 0.06 in. 12 points of interest within the lower chord section are also identified. It can also be noted that this lower chord section has a spacing large enough to accommodate and end rod with a 0.938 in. diameter.

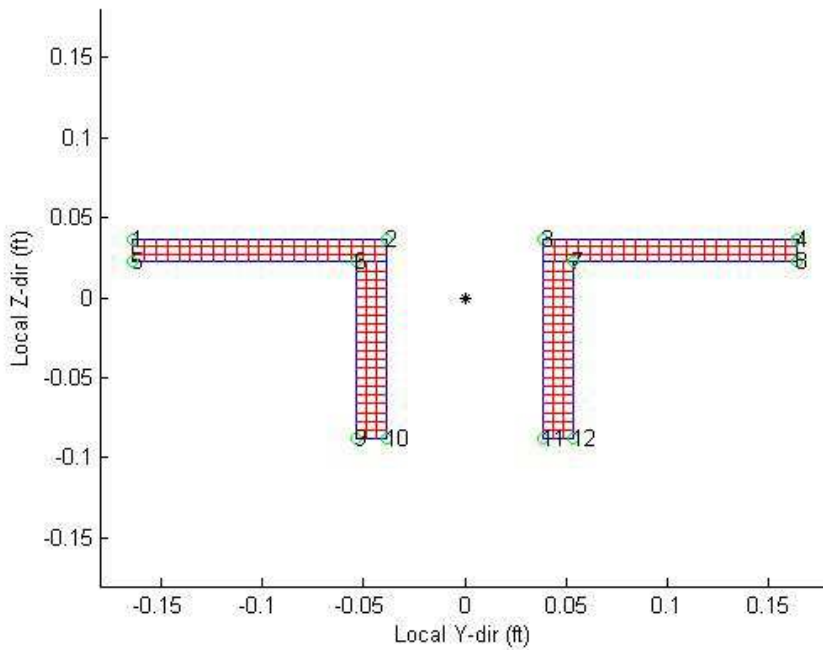


Figure 2.16: Typical lower (bottom) chord section

As mentioned earlier in this section, like the upper chord the lower chord has 1 in. elements on either side of its panel points which represent the two back-to-back angles being connected together due to the presence of the web member or end rod welded to each angle. This solid section is evaluated at only two sections (both ends) of the short, solid element. This short solid part of the lower chord is illustrated in Figure 2.17.

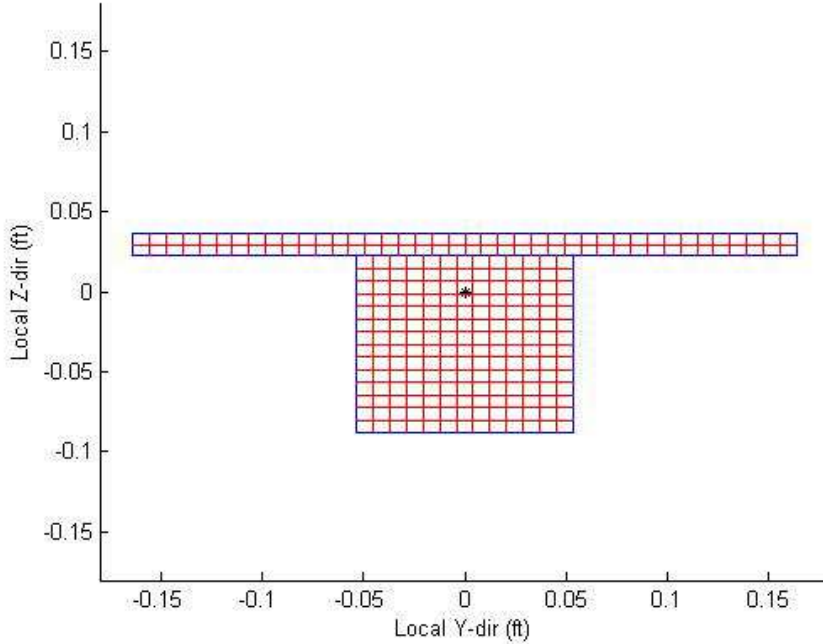


Figure 2.17: Lower (bottom) chord section around panel points

2.5.1.3 End Rods

The end rods are modeled as a single element that extend from the end of the upper chord to the end of the lower chord on each side of the joist. The end of these single elements are connected by welds and therefore not necessarily rigidly connected. To account for the behavior of these connections a zero-length element connecting the end of the chord to the end of the end rod is used to represent the weld material. This zero-length element will be discussed further in a later section.

The geometric transformation vector used to describe the end rods depends on which end rod we are discussing. The end rods are always arranged such that the initial node is on the upper chord and the final node is on the lower chord, which means the positive local x-axis is always in a downward angled direction (see Figure 2.13). If we define the angle θ_{ER} as the angle between the upper chord and the end rod, the geometric transformation vector for the left end rod in

Figure 2.13 is $[\sin(\theta_{ER}) \ 0 \ \cos(\theta_{ER})]$, while the right end rod's geometric transformation vector is $[-\sin(\theta_{ER}) \ 0 \ \cos(\theta_{ER})]$.

As the name end rod implies, these elements will always have circular sections (i.e. they are rods) of a specified diameter (Buckley *et al.* 2008). The end rods on both sides of the joist always have the same section. There is a command in *OpenSees* which allows fiber sections to be defined in a circular manner. In this case the limiting fiber dimension is prescribed by the radial dimension (fibers along a line from the center to the outside) and the number of circular fibers (fibers split up by the concentric circles) is established to match the number of radial fibers. All the fibers in the section use the stress-strain relationship for the rod steel buckling material that was presented earlier. Figure 2.18 shows an end rod section with a diameter of 0.938 in. in its local coordinate system, with fiber dimensions no more than 0.05 in. Four fibers of interest are identified for discussion later. The end rod element is evaluated at 5 integration points along the length of the element in order to predict the behavior of the end rods.

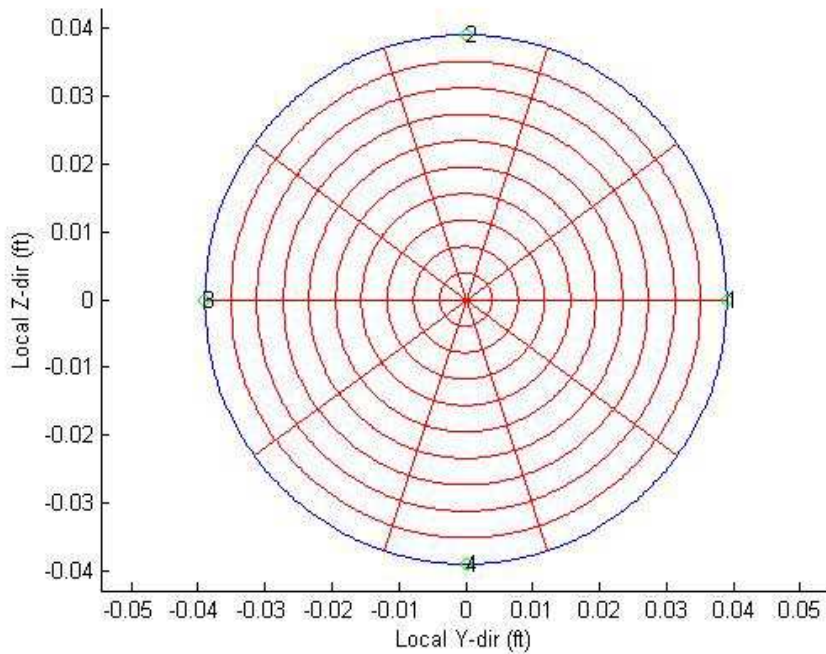


Figure 2.18: End rod section

2.5.1.4 Web Member

Like the end rods, the web members are connected to the chords by welds. These connections are modeled as semi-rigid zero-length elements; these zero-length elements will be discussed in a later section. Also like the end rods, the web member's geometric transformations also depend on how the element itself is defined, *i.e.* whether local nodes i and j define the member from upper left to lower right (\backslash) or from the upper right to lower left ($/$) in Figure 2.13. This allows the geometric transformation vector for the web members going from upper left to lower right (\backslash) to be $[\sin(\theta_w) \ 0 \ \cos(\theta_w)]$, while the geometric transformation vector is $[-\sin(\theta_w) \ 0 \ \cos(\theta_w)]$ for a web member going from upper right to lower left ($/$). In this case, θ_w is the angle between the upper chord and the web member.

Vertical web members are also commonly present in those OWSJs that use rotated angle sections as web members. Although not shown in Figure 2.13, the geometric transformation is easy to determine for the vertical members. The local x-axis is directly down (negative global z-axis), and in order to keep the local z-axis in the global x-z plane we can assign the local z-axis to be in the positive global x-axis. This provides a geometric transformation of $[1 \ 0 \ 0]$ for vertical web members.

Unlike the other three nonlinear elements, there are multiple possible web member section types that can be presented in the model. The two section types that are considered for web members in this analysis are angle sections and rod sections (Buckley *et al.* 2008). In addition, individual web members in a single joist may have different size/section characteristics. In the model, this means that separate values for each web member's dimensions, connection strength, and buckling material must be computed and implemented (Canam 2005).

The first and most common web member section type is the rotated angle member (Buckley *et al.* 2008). This is generally an angle section with equal length legs, which is rotated as shown in Figure 2.19. To generate fibers for this shape of web member, the *patch quad* fiber command is used in *OpenSees* to divide the section into fibers with the specific steel angle buckling material characteristics for each web member depending on its section size.

In real joists, these web members are crimped at the ends, as shown in Figure 2.3 and Figure 2.20, so that they may fit inside the spacing of the upper and lower chords (Yost *et al.* 2004, Buckley *et al.* 2008). Note that although the crimped sections appear to have sharp angles at the location of their bending this is for modelling purposes only. In reality the bends are more rounded. In order to implement the crimped section into the model the web member's nonlinear elements are assigned to have 6 integration points along the length of each web member. Of these 6 integration points, the first two on each end are assigned a crimped angle section such as the one seen in Figure 2.20, while the center two points are assigned uncrimped angle sections such as the one seen in Figure 2.19. This configuration of crimped and uncrimped sections is used to assume that in reality the crimped section extends 0.5 in. past the chord confinement, then a 2 in. transition from crimped to uncrimped occurs. The changing of section geometry also accounts for the internal moment caused by the eccentricity between the centroids of the two sections. Figure 2.19 & Figure 2.20 show an L1x1x0.109 angle web member section with fiber dimensions no more than 0.05" along with 6 points of interest in their local coordinate system. It is important to note that both an uncrimped and crimped web member section with the appropriate angle buckling material is computed for each web member in the joist due to their ability to be different section sizes.

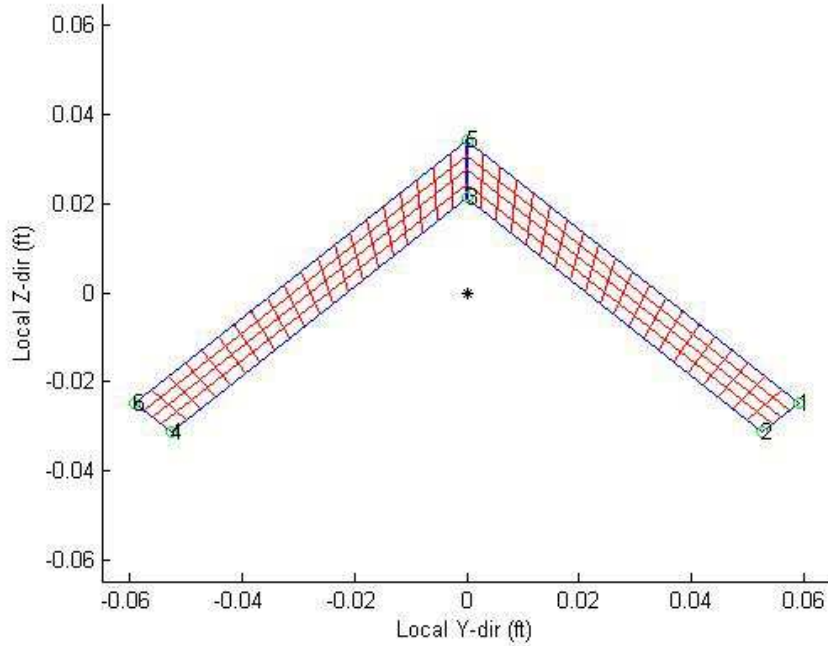


Figure 2.19: Uncrimped, rotated angle web member section

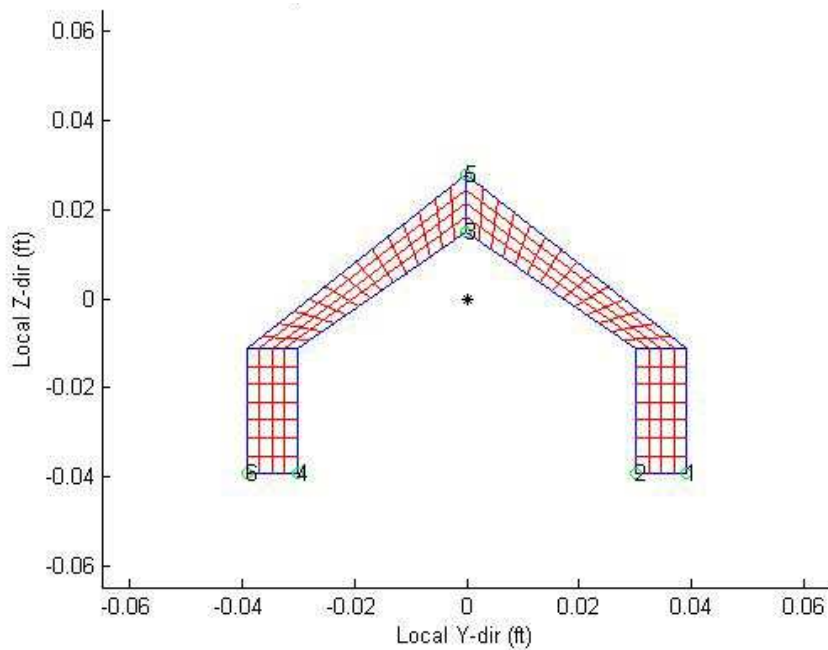


Figure 2.20: Crimped, rotated web member angle section

Web members may also be rod sections (Buckley *et al.* 2008). The process of modeling a rod web member is the same as that used to model the end rod. Figure 2.21 shows a rod web member section in its local coordinate system with fiber dimensions no more than 0.05". As with

previous figures, the numbers indicate 4 points of interest within the web member section. Like the angle web member section, the rod web member section and buckling material are also calculated for each web member within the joist because they may change size depending on their strength requirement.

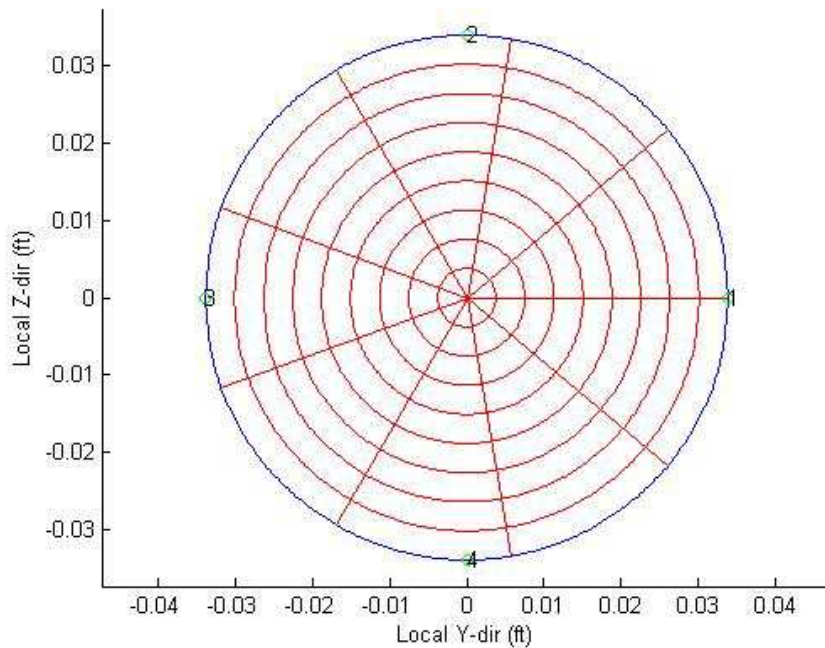


Figure 2.21: Rod web member section

2.5.2 Elastic Elements for Columns, Girders and Lateral Bridging

Due to the investigation being focused about the behavior of the OWSJ roof rather than the inelastic behavior of the columns, girders, and lateral bridging, these members are modeled as elastic elements. This decision implies that neither material nor section nonlinearities are taken into consideration for these three element types. However, they still do require a geometric transformation vector in order to identify the local coordinate system.

The command *element elasticBeamColumn*, which creates the elastic elements in *OpenSees*, requires the area, polar moment of inertia, and moments of inertia in the local y- and z-directions. In terms of material properties, the *element elasticBeamColumn* command requires

the input of material properties for Young's modulus, taken as 29000 ksi, and the shear modulus which can be calculated using the Poisson's ratio of the material, which was taken as 0.3. These properties define the material well enough so that the relation between stress and strain is constant throughout the analysis.

Like the nonlinear elements, elastic elements require a geometric transformation vector in the local x-z plane (the local z-axis) that defines how the local coordinate system is oriented in the global coordinate system. For columns, the local x-direction is always in the negative global z-direction and the local z-direction is defined in the global y-direction (into the page in Figure 2.13) resulting in a column geometric transformation vector of $[0 \ 1 \ 0]$. The local x-direction for the girders is always in the positive global y-direction, and the local z-direction is defined in the global z-direction, so the girder's geometric transformation vector is $[0 \ 0 \ 1]$.

The geometric transformation vectors for the bridging elements depend on which type of bridging is being used. If horizontal bridging is used, then the orientation of the bridging is identical to the girders with a geometric transformation vector of $[0 \ 0 \ 1]$. If diagonal bridging is being used then it is a little more complicated. For both the diagonal bridging members (upper-to-lower chord, lower-to-upper chord), the local x-direction always has a component in the positive global y-direction. Because we would like the local z-direction to always have a component in the positive global z-direction we can determine the geometric transformation vectors to be $[0 \ \sin(\beta) \ \cos(\beta)]$ for the elements going from upper-to-lower chord and $[0 \ -\sin(\beta) \ \cos(\beta)]$ for the elements going from lower-to-upper chord, given that β is the angle between the global y-axis and the bridging element.

2.5.3 *Zero-Length Elements for Welded and Bolted Connections*

As mentioned in earlier sections, OWSJ connections are made by either bolting or welding the two elements together producing semi-rigid connections (SJI 2005). Semi-rigid connections, as the name suggests, are not fully rigid and can therefore allow some rotation between the connected members. However, a semi-rigid connection does provide some resistance to rotation, such that it is not quite pinned either. The modeled connections must be able to account for the predicted rigidity of these connections, as well as the possible failure of the connections.

We can model the connections using zero-length elements (ZLEs) in the *OpenSees* model. A ZLE is capable of defining a connection's resistance to both rotation and displacement, with respect to a local coordinate system. The local coordinate system of a ZLE corresponds to the local coordinate system of the web member or end rod for welded connections, and to the local coordinate system of the upper chord for the joist to girder connection. The local coordinate systems of the ZLEs allow them to have specific force-displacement and moment-rotation relationships in each of the three main local axes in order to represent the different failure modes of the connections (*ex.* shear, axial, torsion, etc...).

In the OWSJ structure model, three different ZLEs are implemented. The first ZLE type describes the connection of the web members or end rods to the chords. The second ZLE type describes the connection of the ends of the joists to either the tops of columns or to girders. The final type of ZLE describes the connection of the bridging to the chords. The following subsections will describe how the moment-rotation and force-displacement curves for each type of ZLE are derived. Once these relations are made, *OpenSees* can use them as the properties for the appropriate ZLE.

2.5.3.1 Welded Connections between Web/End Rods and Chords (ZLE Type 1)

The placement of the ZLEs which connect the web members and end rods to the chords can be seen in Figure 2.11 and Figure 2.12 where they are represented by circles on the web members and end rods. A zero-length element is used to simulate welds by connecting each end of each web member and each end rod to a chord; this means that even though there are some locations where two (or even three) web members approach a single node on a chord, one ZLE is used to attach each web member individually (two or three total) (Figure 2.22a) as opposed to rigidly attaching the two web members together and then using a single ZLE to attach that to the chord (Figure 2.22b). This allows the web members to displace and rotate independently of each other.

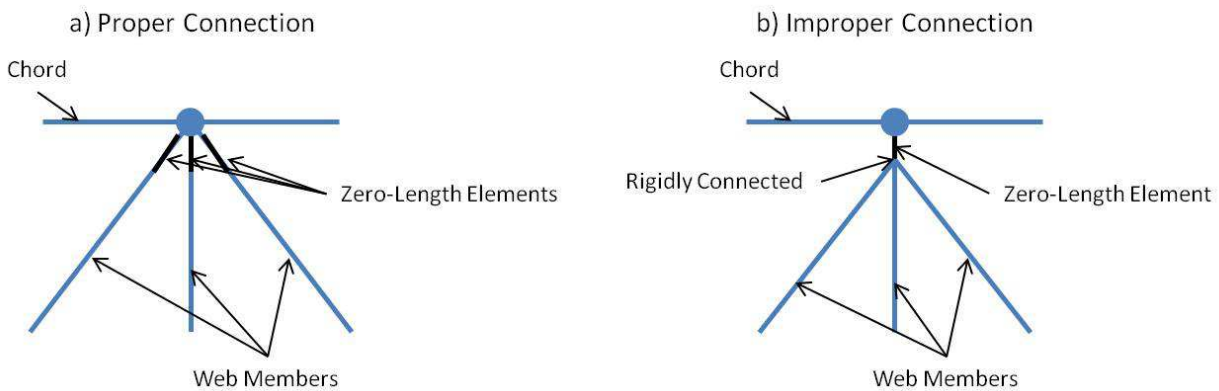


Figure 2.22: ZLE connections between web members and chords

There are three options for modeling the moment-rotation and force-displacement relationships in these connection ZLEs. The first case under consideration occurs if the connections are rigid. Practically speaking, in this case, the ZLE is defined with a linear relation for both the moment-rotation and force-displacement. Because the rigid assumption restricts the connection from rotating or displacing we assign the slope of the linear relation to an extremely high value of 9.9×10^{13} lb-ft/rad or lb/ft. If the connections are assumed to be pinned, the

moment-rotation and force-displacement relationships can once again be described as linear. However, this time we want free rotation, but still no displacement, so we can make the slope of the moment-rotation line extremely low at 10^{-13} lb-ft/rad while the slope of the force-displacement line remains extremely high at 9.9×10^{13} lb/ft.

The third and more interesting case is modeled to represent the welded connections as semi-rigid. This is the connection model used in all analyses for this study. The first step in determining the relationships for a semi-rigid welded connection was to find a model which described weld strength with respect to displacement. Kwan *et al.* (2010) discusses an experimentally tested and validated weld model by Lesik & Kennedy (1990), which AISC (2011) also uses, describing the force-displacement relationship of welds as a function of their angle of loading relative to the length of the weld (θ) to be:

$$F = 0.60F_{EXX}A_w(1.0 + 0.5\sin^{1.5}\theta)f(\rho) \quad (2.12)$$

In these equations, F is the force in the weld segment and ρ is the ratio of deformation in the direction under investigation to ultimate deformation (Δ/Δ_u). Lesik & Kennedy (1990) demonstrate that the necessary parameters to substitute into Equation (2.12) can be easily determined: d is the thickness of the as-built weld which is based on the size of the web member section and taken from charts provided by a well-known joist manufacturing company, and A_w is the area of the failure surface of the weld which can be taken as weld thickness, d , by weld length, L , divided by $\sqrt{2}$. Δ_u is the deformation at the ultimate load and Δ_f is the fracture deformation, which can be computed from

$$\Delta_u = 0.209d(\theta + 2)^{-0.32}, \Delta_f = 1.087d(\theta + 6)^{-0.65} \quad (2.13)$$

The angle of loading relative to the length of the weld, θ , is taken as 0° for axial forces in the web member and weld and 90° for shear forces in the web member. The term $f(\rho)$ is calculated by Lesik & Kennedy (1990) as:

$$f(\rho) = 8.234\rho \quad \text{if } 0 < \rho \leq 0.0325 \quad (2.14)$$

$$f(\rho) = -13.29\rho + 457.32\rho^{\frac{1}{2}} - 3385.9\rho^{\frac{1}{3}} + 9054.29\rho^{\frac{1}{4}} - 9952.13\rho^{\frac{1}{5}} + 3840.71\rho^{\frac{1}{6}} \quad \text{if else} \quad (2.15)$$

F_{EXX} , the weld electrode strength, is determined by pairing a 70 ksi electrode (E70XX) with base steel greater than Grade 36. If the base steel is Grade 36, then a 60 ksi electrode is used (E60XX), as recommended by the AISC (2011).

This leaves the final value to determine as the length of the weld. The length depends on the geometry of the connected elements. Figure 2.23 shows a couple weld configurations, depending on the orientation of the angle sections and whether crimping is applied (Yost *et al.* 2006). Knowing where the welds are located between the web members and chords, and by assuming that the single angle web members are always crimped, trigonometry can be used to determine the length of each individual weld (see Figure 2.24). The lengths of the welds vary depending on the orientation of the web member section and the angle between the web members and the chords. This means that the connection strength will differ between the connection to upper and lower chords with different angle leg sizes because of a change in weld length. Weld connections on end rods and rod sections are assumed to have just two welds on either side of the rod as seen in Figure 2.25c. Because it is impractical to assume that the welds extend along the web members or end rods all the way to the edge of the chords, the weld length considered for each individual weld in the calculations is actually reduced from its full length.

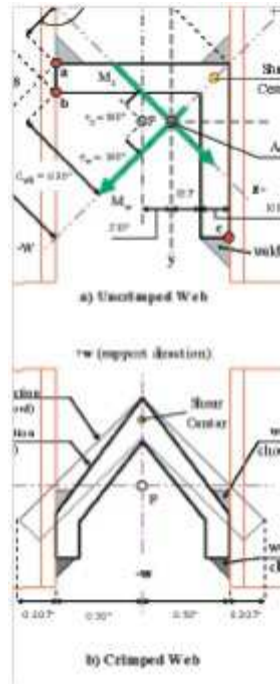


Figure 2.23: Welding of single angle web members to chords (Yost *et al.* 2006)

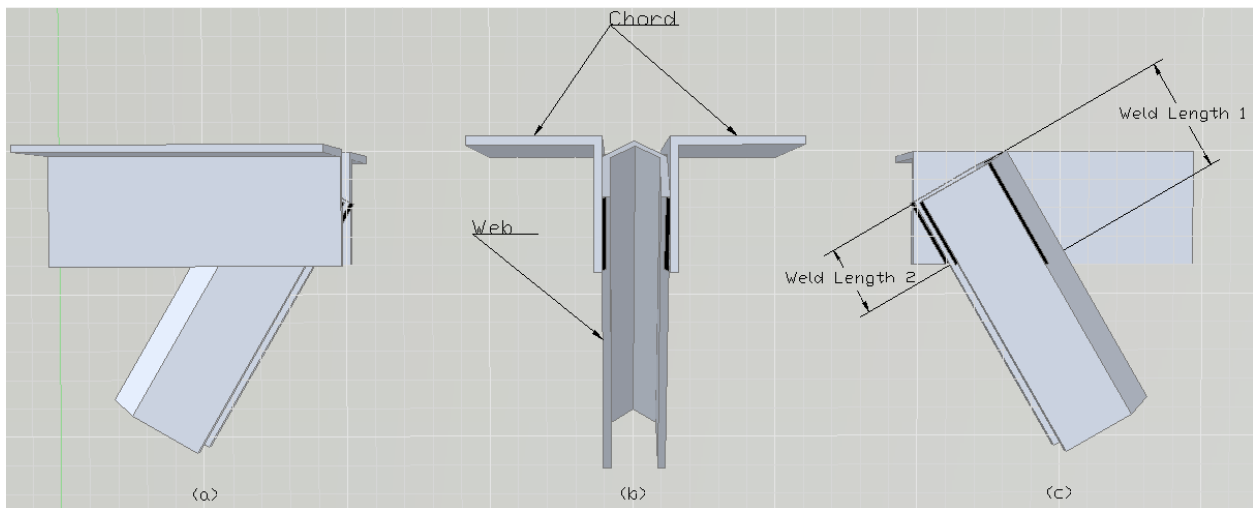


Figure 2.24: Crimped single angle web connection to chord, a) side view, b) view looking down chord, c) weld position

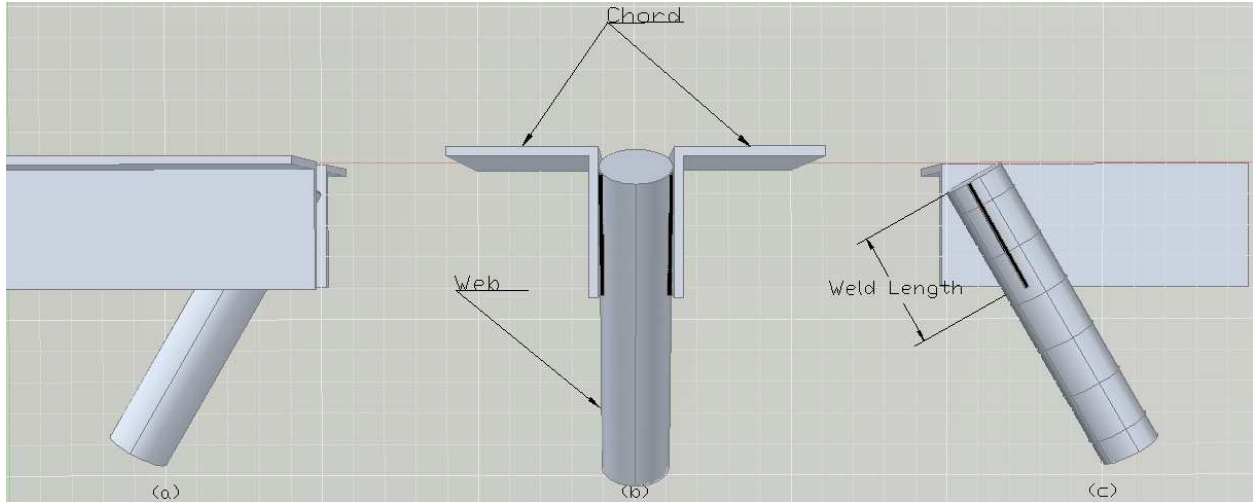


Figure 2.25: Rod Web or end rod connection to chord, a) side view, b) view looking down chord, c) weld position

The force-displacement relationships for each connection (like the one shown in Figure 2.26) can be determined using the Lesik & Kennedy (1990) model with a weld length, L , equal to the sum of weld lengths of all the welds at that connection (*i.e.* in Figure 2.24 $L = 2x[\text{Weld Length 1}] + 2x[\text{Weld Length 2}]$, in Figure 2.25 $L = 2x[\text{Weld Length}]$).

Each individual weld's weld length is then used separately in order to determine the moment-rotation relationship. The analysis is done by using the elastic method of analysis as recommended by AISC (2011), Section 8. Each weld is split into 100 parts and a section analysis is performed to determine the capacity of the weld section to resist increasing deformations. As the rotation occurs about the center of the weld group, the sections of each weld experience different loading angles and different deformations depending on where the section is located relative to the center of the weld group. The different deformations and loading angles are used with the Lesik & Kennedy (1990) model described above to determine the amount of force resisted by that section of the weld. These forces are then multiplied by their respective distances

between the welds and the center of the weld group to determine the moment that is resisted by each individual weld section. These individual moment resistances are combined to determine the total moment resistance of the group of welds at that connection. Once a deformation in a weld section surpasses the fracture deformation, Δ_f , set by the Lesik & Kennedy (1990) model, that section is assigned no resistance.

Recall that each web member within a single joist may have different section properties and weld sizes. It is for this reason that it is essential to calculate specific force-displacement relationships for both axial (local x) and shear forces (shear is used in both non-axial directions) and moment-rotation curves at the upper and lower chord connections for each web member and end rod within an OWSJ. Figure 2.26 and Figure 2.27 show the relationships for force-displacement and moment-rotation respectively for a crimped L1x1x0.109 angle section web member, like the one in Figure 2.23b and Figure 2.24, connecting to back-to-back L2x2x0.148 angles at the upper chord and back-to-back L1.5x1.5x0.170 angles at the lower chord. The post peak response in the force-displacement curve shows the eventual weld fracture of the material under axial and shear loads in Figure 2.26. The curves end at the point where the weld reaches the fracture deformation causing the connection to have a force capacity of 0 lbs for larger displacements. In the moment-rotation relationship, after the fracture of multiple weld segments occurs the weld loses moment strength extremely quickly until it reaches a moment capacity of 0 lb-ft. In the model, this point of 0 lb-ft is assumed to be reached immediately after the point where the beginning of this moment loss propagation occurs.

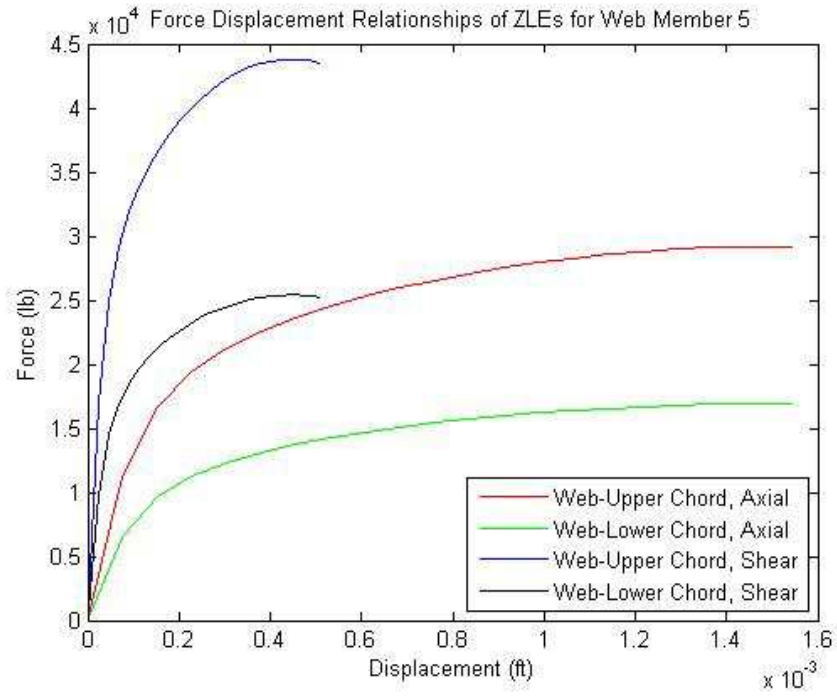


Figure 2.26: Force-displacement relationships for a web-chord connection

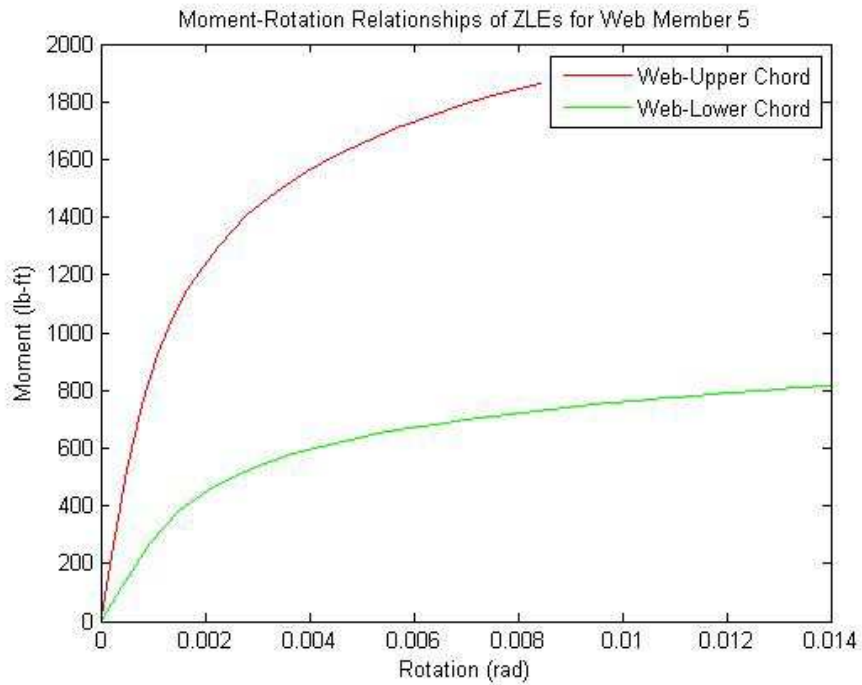


Figure 2.27: Moment-rotation relationships for a web-chord connection

Once the moment-rotation and force-displacement relationships are determined for each of the semi-rigid ZLEs in the OWSJ, they are input into *OpenSees* through the *uniaxialMaterial ElasticMultiLinear* command. Similar to how the command was used to describe the steel materials, we assumed the relationships are identical in the negative direction, and the relationships needed to be discretized to make the modeling easier.

2.5.3.2 Bolted Connections between Joist and Columns or Girders (ZLE Type 2)

The connections between the joist and columns or girders employ two $\frac{1}{2}$ " ASTM A307 bolts (SJI 2005). In the models, these connections are represented as semi-rigid, using the procedures described below to determine their nonlinear properties. An alternative to using two $\frac{1}{2}$ " ASTM A307 bolts which is also recommended for use by the SJI (2005) is using two 1" long 0.125" fillet welds.

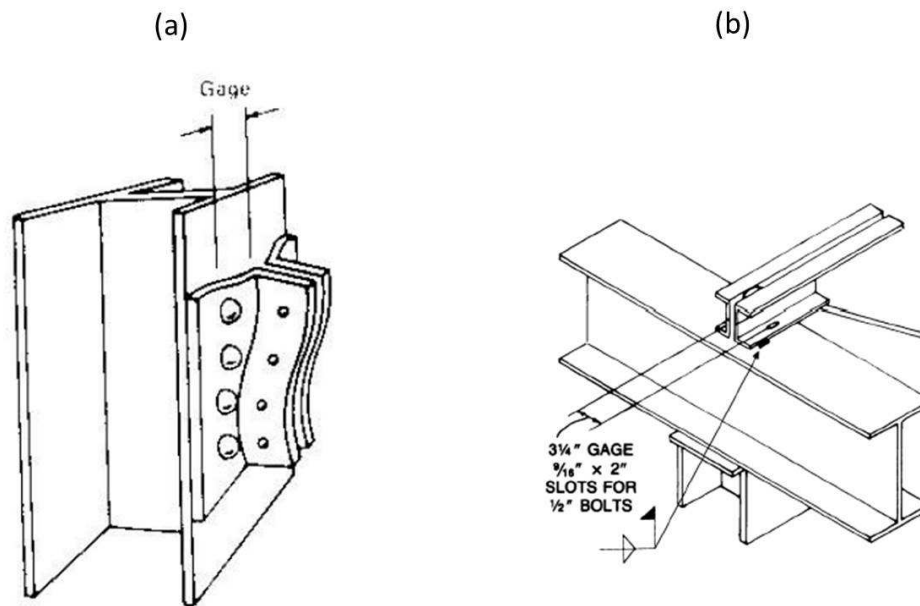


Figure 2.28: Comparison between a) double web angle connection (Green *et al.* 2005) and b) OWSJ-girder connection (SJI 2005)

For the semi-rigid properties in the column/girder – joist ZLEs, the moment-rotation relationship was determined by assuming the connection reacts the same way as a double web angle connection for connecting beams to columns. This assumption can be verified by observing that a double web angle connection on a W-section column (Figure 2.28a) closely resembles the connection between the bearing angles connected to the chord of an OWSJ and a W-section Girder (Figure 2.28b). However, assuming these connections are identical may also lead to the connections being stiffer in rotation in the model than in reality due to no consideration being given to the flexibility of the web of the girder. Chan & Chui (2000) provide guidelines to model this type of connection using a polynomial model and coefficients provided by Frye & Morris (1975). Taking moments in kip-in, rotation in radians, dimension d in inches, flange thickness, t , in inches, and gage length, g , in inches the following equation for rotation, θ , as a function of moment, M , can be made:

$$\theta_c = C_1(KM) + C_2(KM)^3 + C_3(KM)^5 \quad (2.16)$$

where $C_1 = 3.66 \times 10^{-4}$, $C_2 = 1.15 \times 10^{-6}$, $C_3 = 4.57 \times 10^{-8}$, $K = d^{2.4} t^{-1.81} g^{0.15}$. In our case, g is the distance between the two bolts on the two angles including the spacing between the angles, determined by using the AISC Steel Construction Manual (2011) and relating the appropriate gage length of each angle to the leg size, as seen in Figure 2.28a. Also the dimension d is the length of the angle touching the connecting member (column or girder in our case). So in our calculations d is taken as either half the depth of the column, or if a girder is present then it is taken as half the width of the girder. The model response is identical in the positive and negative directions.

The issue with the model represented by Equation (2.16) is that it does not predict fracture, so technically the model goes on until an infinite rotation. For simplicity, we assumed

the model will continue along a slope equal to the tangent at 0.2 rad for higher rotations; it is unlikely the connection will experience that much rotation at this connection.

In *OpenSees*, the bolted connections are represented with ZLE type 2 that mimics the response of Equation (2.22) using the *uniaxialMaterial ElasticMultiLinear* command. The model produces a moment-rotation relationship like that shown in Figure 2.29 (which is for a specific connection between an upper chord and a girder).

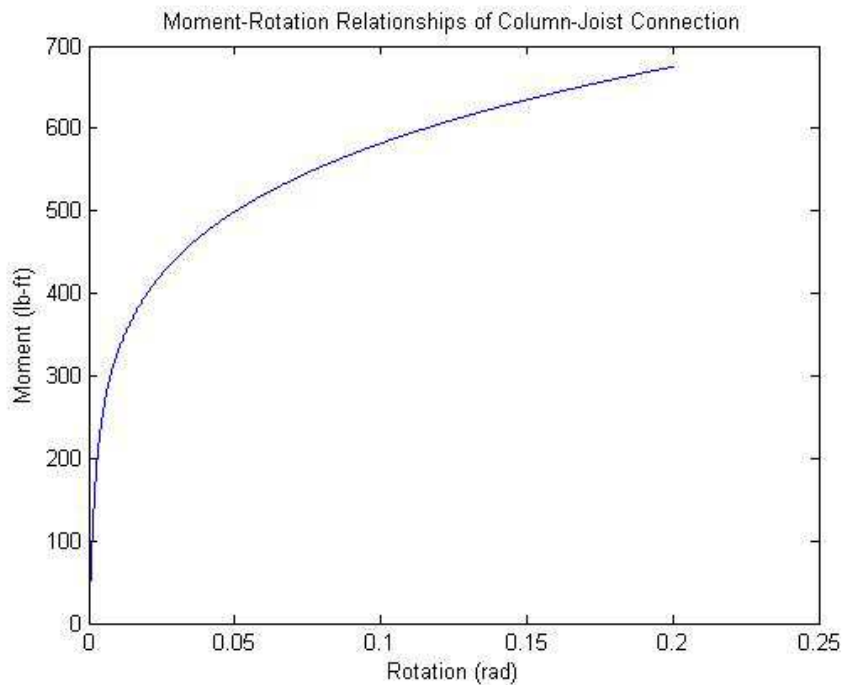


Figure 2.29: Moment-rotation relationship for a column-joist connection

The next step is to determine force-displacement relationships defining the axial and shear response of the bolted connections. In order to develop these models, ASTM A307-12 was referenced for additional data about ½” A307 bolts including the effective stress area of 0.1419 in² and an ultimate tensile strength of 8500 lb. A307 bolts in general must be able to resist at least 60 ksi and an elongation of 18% on a 2 inch bolt (which corresponds to about 0.36 in. of displacement). AISC (2011) provides nominal values for the bolts in tension of 45 ksi and in

shear of 24 ksi. Using this information, the following assumptions can be made to determine the force-displacement relationship: the bolts are 2 inches long and have a strain hardening ratio of 0.003, slipping is ignored in shear, prying is ignored in tension, and the failure of the connection in shear or axial directions only occurs due to the failure of the bolts.

In the two shear directions of the connection the yield stress is already known from AISC (2011), so the yield strength can be calculated by multiplying the yield stress by the area of the two bolts (0.2838 in^2), resulting in a shear yield strength of 6811.2 lb. The same procedure can be performed to find the tensile yield strength of the connection of 12771 lb. The elastic modulus of the connection in tension can then be back-calculated using the tensile yield strength, ultimate tensile strength of the bolts, ultimate tensile elongation, and the assumption of a 0.003 strain hardening rate. This same elastic modulus is used for shear directions as well.

The results allow us to express the behavior as curved using the *uniaxialMaterial Steel02* (Giuffr -Menegotto-Pinto Model with Isotropic Strain Hardening) which is already included in *OpenSees* and only requires input for the yield strength of steel, initial elastic modulus determined through the back-calculation explained above, strain hardening ratio, and a couple of parameters to describe the transition from elastic to plastic. This information is included for both the shear and tensile (normal) directions; the resulting behavior resembles the curves shown in Figure 2.30.

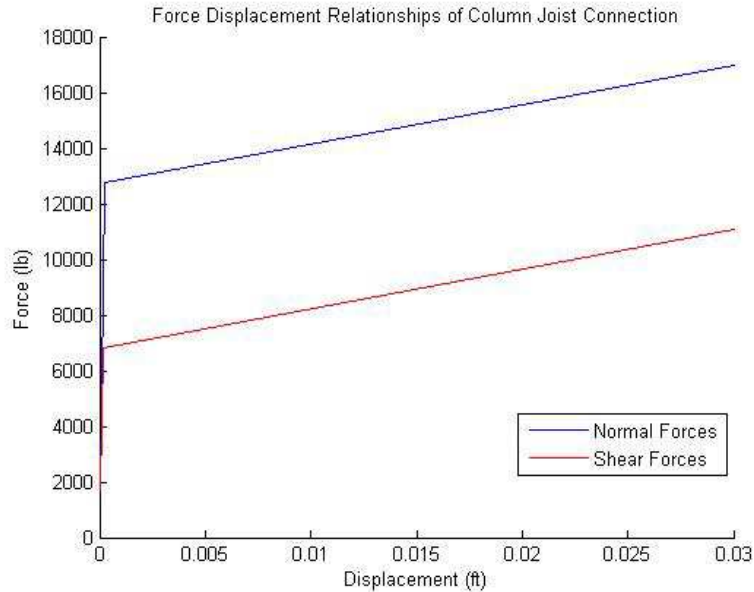


Figure 2.30: Approximate force-displacement relationships for a column-joist connection in response to shear and axial (normal) forces

2.5.3.3 Connections between Bridging and Joist Chords (ZLE Type 3)

The connections between the bridging and the chords are also represented by zero-length elements. Vulcraft (2007) states that bridging must be connected to the joist chords by “positive mechanical means”. The properties of the ZLEs used in these connections are always considered to be completely rigid. Because we are not concerned with how the bridging or bridging – chord connections behave under the applied load we can simply make the connection a rigid connection. This means that the force-displacement curves in all directions are modeled as a linear function with an extremely high slope of 9.9×10^{13} lb/ft to resist relative displacement, and the moment-rotation curves in all directions are also modeled as linear with the high slope of 9.9×10^{13} lb-ft/rad to resist relative rotation.

2.6 Displacement Controlled “Pushdown” Analysis

In order to trace the behavior of the OWSJ roof structure under various roof snow loads a pushdown analysis is used. The main idea behind a pushdown analysis is to increase the load on

the roof in a pre-defined pattern until the loads cause a failure of the building. This process, along with the data that is provided from the analysis, will be explained in further detail in later sections. The pre-defined load patterns are explained in the following section.

2.6.1 Loading

2.6.1.1 Dead Loads

There are 3 types of vertical (in direction of gravity) loading that are applied to the model; the self-weight of the members, the additional dead load (DL), and the roof snow load (RSL). The former two are discussed in this section while the latter is discussed in the following two sections. The self-weight of the members is calculated by determining the product of the cross-sectional area of the specific element and the density of steel, typically taken as 490 lb/ft³ (Geis 2011). This specific distributed load is then applied in the negative global z-direction on the respective element using the *OpenSees* command *eleLoad -ele [element designation] -type -beamUniform*. The *eleLoad* command requires the load input to be in terms of the local coordinate system.

Additional dead load (DL) is also applied to the model in order to account for roof loads such as the roof drainage system, roof decking, and roofing itself. This additional dead load is inputted into the model and can be varied depending on the type of roof under consideration. The additional dead load is applied only on the upper chords in the model based on the tributary area (*i.e.* the building does not use decking to distribute the loads) and is again applied through the *OpenSees* command *eleLoad -ele [element designation] -type -beamUniform* which applies distributed loads on elements. A diagram of the distribution of the area distributed dead load, DL, over a 1 bay by 1 bay structure is shown in Figure 2.31.

2.6.1.2 Uniform Roof Snow Load

The magnitude of the roof snow load (RSL) will vary in the analysis and can be considered in either a uniform or drifted load pattern depending on the analysis of interest. When the roof snow load is a uniformly distributed load over an area, it is distributed to the upper chords of the structure through tributary area (again, decking is not modeled to distribute the loads), the same way that the additional dead load is distributed and as can be seen in Figure 2.31. When a pushdown analysis is being run the additional dead load is applied in full while the roof snow load is varied depending on the induced displacement. This means that there is a constant dead load applied to the roof throughout the pushdown analysis while the snow load applied varies. The pattern of the roof snow load during a pushdown analysis is in the same pattern that the loads are in when it is fully applied, meaning that the distributed RSL on the upper chords of the interior joists are always double the distributed RSL on the upper chords of the exterior joists, such as the pattern in Figure 2.31.

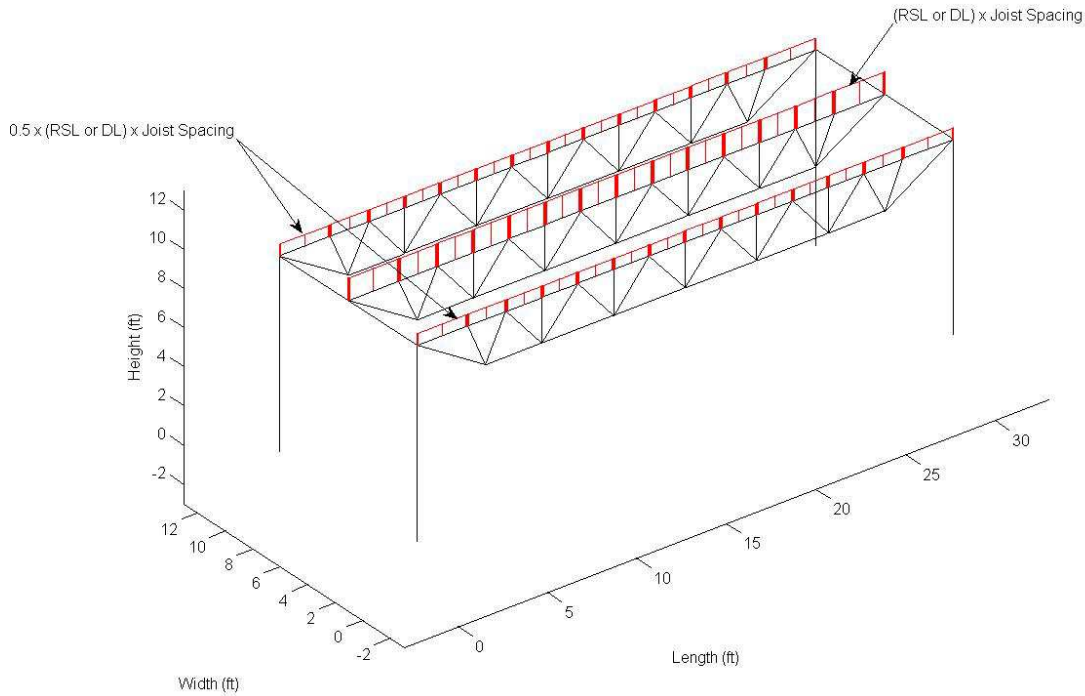


Figure 2.31: Uniform load pattern on a 1 bay x 1 bay structure

2.6.1.3 Drifted Snow Load

In addition to running a pushdown load in the uniform roof snow load pattern that is shown above, the code can also accommodate pushdown loads in a drifted load pattern. The drifted load pattern is assumed to follow the shape defined by ASCE 7-10, Section 7.8, assuming that the drifts are only formed in the windward direction against a parapet; all roofs are assumed to be flat so other drifting equations do not apply. Although the ASCE 7-10 drift model does not take into account factors such as local wind speed it does take into account key parameters such as the height of the parapet or obstruction and the upwind length of the roof (*aka* the snow fetch). It has also been observed that the ASCE 7 equations provide a snow drift which is conservative compared to more sophisticated drift models (Cocca & O'Rourke 2008). In the *OpenSees* model, drifts can be implemented to drift in any direction on the roof and can vary in size depending on

the specified design ground snow load (p_g) and exposure factor (C_e) of the site, the building's thermal factor (C_t) and importance factor (I_s), and parapet height

According to ASCE 7-10, drift loads for design purposes are computed as follows. The first step is to use the previously mentioned factors to determine the design base snow load on the roof (p_f):

$$p_f = 0.7C_eC_tI_s p_g, \text{ but not less than } I_s p_g \text{ if } p_g \leq 20 \text{ psf, or } 20I_s \text{ if } p_g > 20 \text{ psf} \quad (2.17)$$

Note that the drifted snow pattern requires the design base snow load. For uses other than designing the building or determining the shape of the snow drift the minimum roof snow load requirements are ignored for the base snow load.

The height of the uniform base snow load on the roof, h_b , can then be computed using the following snow density equation provided by ASCE 7-10:

$$h_b = \frac{p_f}{\gamma}, \text{ where } \gamma = 0.13p_g + 14 \text{ (but not greater than } 30 \text{ pcf)} \quad (2.18)$$

The available height to which the drift can grow is the difference between the height of the parapet and h_b ; this value is designated h_c . In order to determine the possible height to which the drift can grow, the length of the roof downwind from the drift, l_u , and the ground snow load, p_g , is used with Fig. 7-9 in ASCE 7-10 (found in Appendix B) to determine the maximum possible height of the drift, h_d . However, because the drift is formed due to windward drifting against a parapet the maximum height is reduced to $0.75h_d$. This maximum drift height is then used with the following equations from ASCE 7-10 to determine the length of the drift, w :

$$\text{if } (0.75h_d) \leq h_c \rightarrow w = 4(0.75h_d) \quad (2.19)$$

$$\text{if } (0.75h_d) > h_c \rightarrow w = 4 \frac{(0.75h_d)^2}{h_c} \text{ (but } \leq 8h_c), \text{ the value of } h_d \text{ is now } h_c \quad (2.20)$$

The assumed shape of the drifted snow is shown in Figure 2.32.

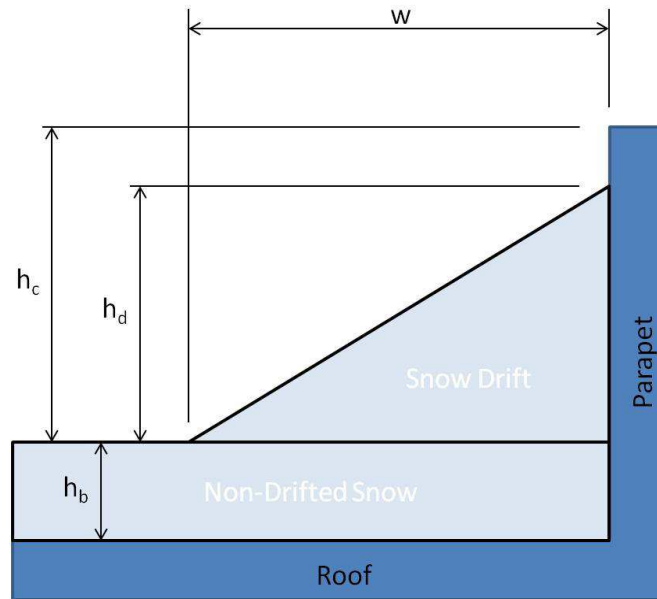


Figure 2.32: Heights and lengths in snow drift as described by ASCE 7-10

This drift is converted to a load by multiplying the drift height by the snow density found earlier (γ). Again, considering the joists' tributary width, this load is directly applied to the upper chord members in the appropriate pattern by having a uniform load applied to each upper chord element which is equal to the actual sloped drift pattern's value at the midpoint of the element. Applying the loads as a series of uniform loads as opposed to a sloped distributed load is reasonable due to the short lengths of the elements along the upper chord. The model allows for the drifted load pushdown to be applied in three ways; (1) the drifted load pattern is applied to the building, but no base load pattern is applied (Figure 2.33); (2) the drifted load pattern is applied to the building and a constant base load equal to the design load, p_f , is applied but does not increase during the pushdown analysis (Figure 2.34); and (3) both the drifted load and base load increase during the pushdown load together in a pattern that corresponds to the design load that should be applied to the building (Figure 2.35). Case (3) is used in the drifted analyses of this study.

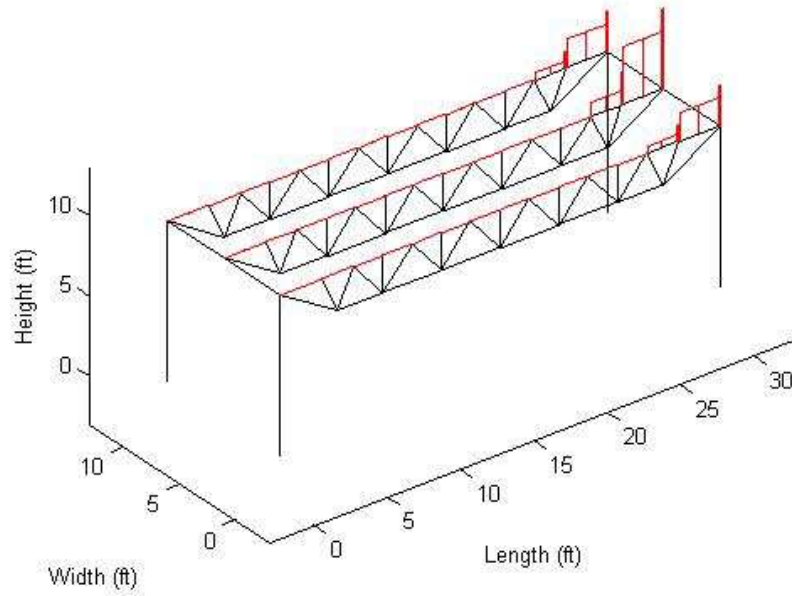


Figure 2.33: Increasing drifted load with no base load pattern (case 1) on a 1 bay x 1 bay structure

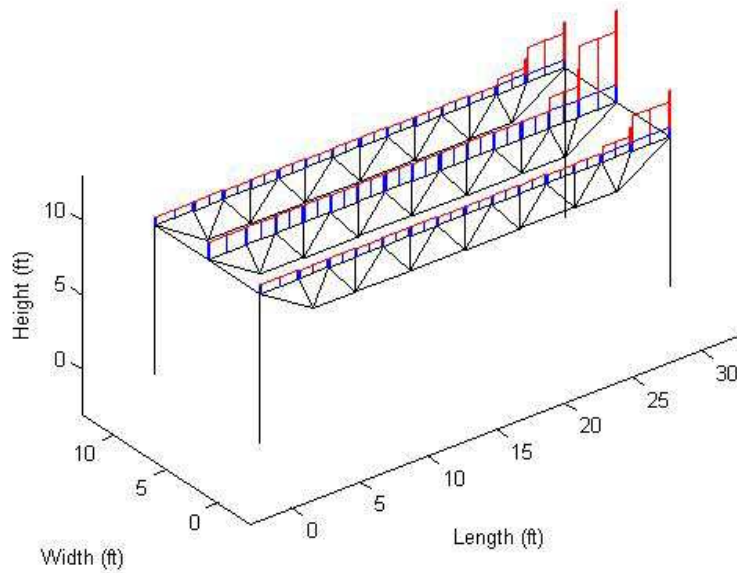


Figure 2.34: Increasing drifted load (red) with a constant base load pattern (blue) (case 2) on a 1 bay x 1 bay structure

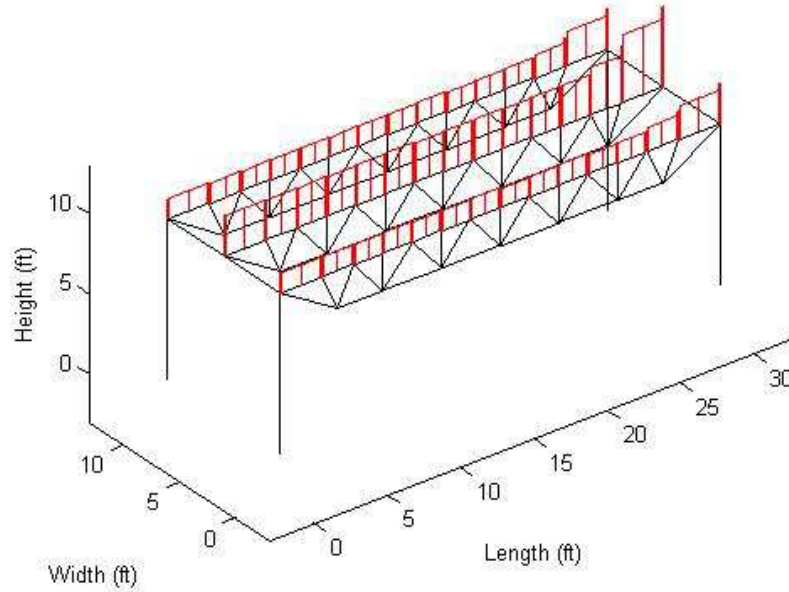


Figure 2.35: Increasing drifted load and base load pattern (case 3) on a 1 bay x 1 bay structure

2.6.2 Pushdown Analysis Details

The first part of the pushdown analysis which applies the self-weight, additional dead load, and a constant base roof snow load if that type of drifted analysis is chosen, is a load controlled static analysis in 10 steps. This means that these loads are applied in 10 equal load increments to the structure until the full load is reached. Once the self-weight, dead load, and base loads are applied to the structure a pushdown pattern load is then applied.

The main part of the pushdown analysis is a displacement-controlled analysis, which is used to apply an induced displacement to whichever node of interest was determined (Figure 2.36) in the downward (negative global z-) direction. The analysis then determines the load required (in the predetermined distribution) to achieve this displacement and records all the necessary data for that displacement increment, including the distributions of stresses and strains within each element of the structure. The analysis then increments to the next induced displacement and the process is repeated (PEER 2013b). It is important to use a displacement

increment size which will capture enough data without increasing the analysis time too much. After some experimenting with the model, the author applied an initial displacement increment of -0.001 ft. If the size needs to be adjusted to accommodate a higher or lower displacement increment then the integrator will vary the increment size between -0.0001 ft. and -0.004 ft.

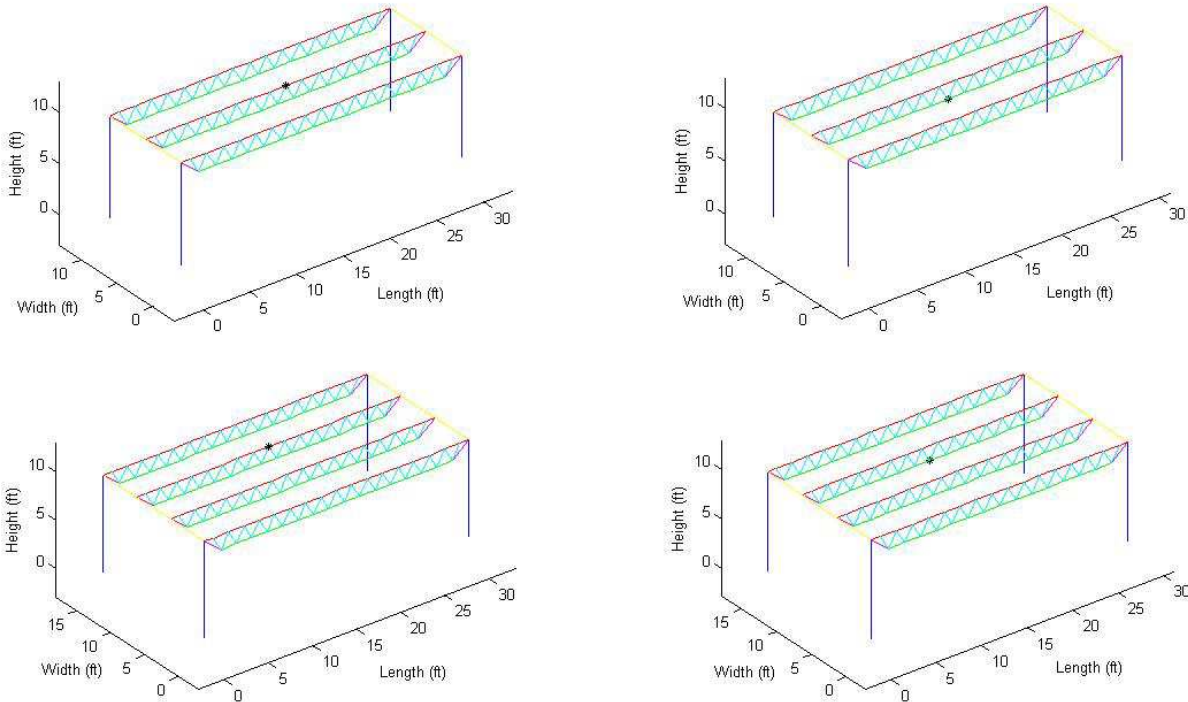


Figure 2.36: Positions of the node of interest, represented by a star, to use in a pushdown analysis

As explained in Section 2.6.1, there are a variety of load patterns to choose from. The magnitude of the loads in the pattern load does not matter, only the relationships between them matter. This is due to the displacement control integrators ability to modify the magnitude of the load pattern to match a desired displacement. For the OWSJ structures being analyzed under the uniform pattern load, linear distributed loads of magnitude 1 (unit doesn't matter) are applied to the upper chord elements of the inner joists, and a linear distributed load of magnitude 0.5 are applied to the upper chord elements of the exterior joists. These patterns vary depending on the type of loading under investigation (uniform, drifted with no base load, drifted with a constant

base load, or drifted with a consistent base load), all of which can be found in Section 2.6.1 of this document.

2.6.3 Convergence Algorithm

The pushdown analysis also implements a convergence algorithm to ensure that the solution to the system of equations achieves an appropriately accurate solution. The convergence algorithm consists of a series of tests of the error in the solution, each of which is less stringent than the test before. This procedure ensures that an analysis which fails the most accurate test continues with the analysis because it still passes a less accurate, yet still within reasonable limits, convergence test. Once the analysis reaches a point where convergence isn't reached even with the least accurate of the acceptable tests in the algorithm, then the analysis ends. The algorithm follows the pattern described below:

- Starts using the Normal Displacement Increment test (*test NormDispIncr*) with a tolerance of $1.0e-06$ and a maximum of 10 iterations. The displacement increment test uses a solution vector taken from the system of equations formed by the integrator to determine a displacement, and then compares the calculated displacement with the actual displacement to determine whether convergence is achieved (PEER 2013b).
- If the previous test does not converge it analyzes again using *test NormDispIncr* with a tolerance of $1.0e-06$ and a maximum of 10 iterations.
- If the previous test does not converge it analyzes again using *test NormDispIncr* with a tolerance of $1.0e-06$ and a maximum of 100 iterations.
- If the previous test does not converge it analyzes again using *test NormDispIncr* with a tolerance of $1.0e-05$ (*i.e.* allowing slightly higher error) and a maximum of 10 iterations.

- If the previous test does not converge it analyzes again using *test NormDispIncr* with a tolerance of 1.0e-05 and a maximum of 100 iterations.
- If the previous test does not converge it analyzes again using *test NormDispIncr* with a tolerance of 1.0e-04 and a maximum of 10 iterations.
- If the previous test does not converge it analyzes again using *test NormDispIncr* with a tolerance of 1.0e-04 and a maximum of 100 iterations.
- If the final test does not converge then the analysis ends and the structure is considered to have failed.

2.6.4 Parallel Processing

Due to the large number of nodes, members, fibers, and zero-length elements present in the buildings and roof systems we wish to model, the single processor *OpenSees* system is not capable of building the structure or analyzing it due to a lack of memory within the program. For this reason the parallel processor version of *OpenSees* known as *OpenSeesMP* was used to analyze large buildings.

To run *OpenSeesMP*, a building is modeled using a tcl code split up among a specified number of files. Each of these files is written to create approximately the same amount of elements, along with the associated nodes and load. By dividing the tcl code into separate files, *OpenSeesMP* will designate a single processor to run through an individual file and split the required memory among multiple processors. The code then tells all the processors to wait until all the building files are complete, at which time an analysis may be run on any single processor, which analyzes the structure created by all the processors combined.

There are some complications in running the parallel-built structural model on a single processor. The first is that the pushdown load pattern used must be assigned on different

processors. More specifically, the processor which created the specific element to which a load pattern is being assigned must also be the processor which assigns the load pattern for that element. The second consideration which must be done is that the numberer used in the analysis is *ParallelRCM* and the solver is *ParallelProfileSPD*. These must be used in order for the load applied in the analysis to affect the entire structure and not just the part of the structure built by the processor being used. Aside from these changes, any other files needed to be run may only be written once and shared amongst the processors being used, as illustrated by Figure 2.37.

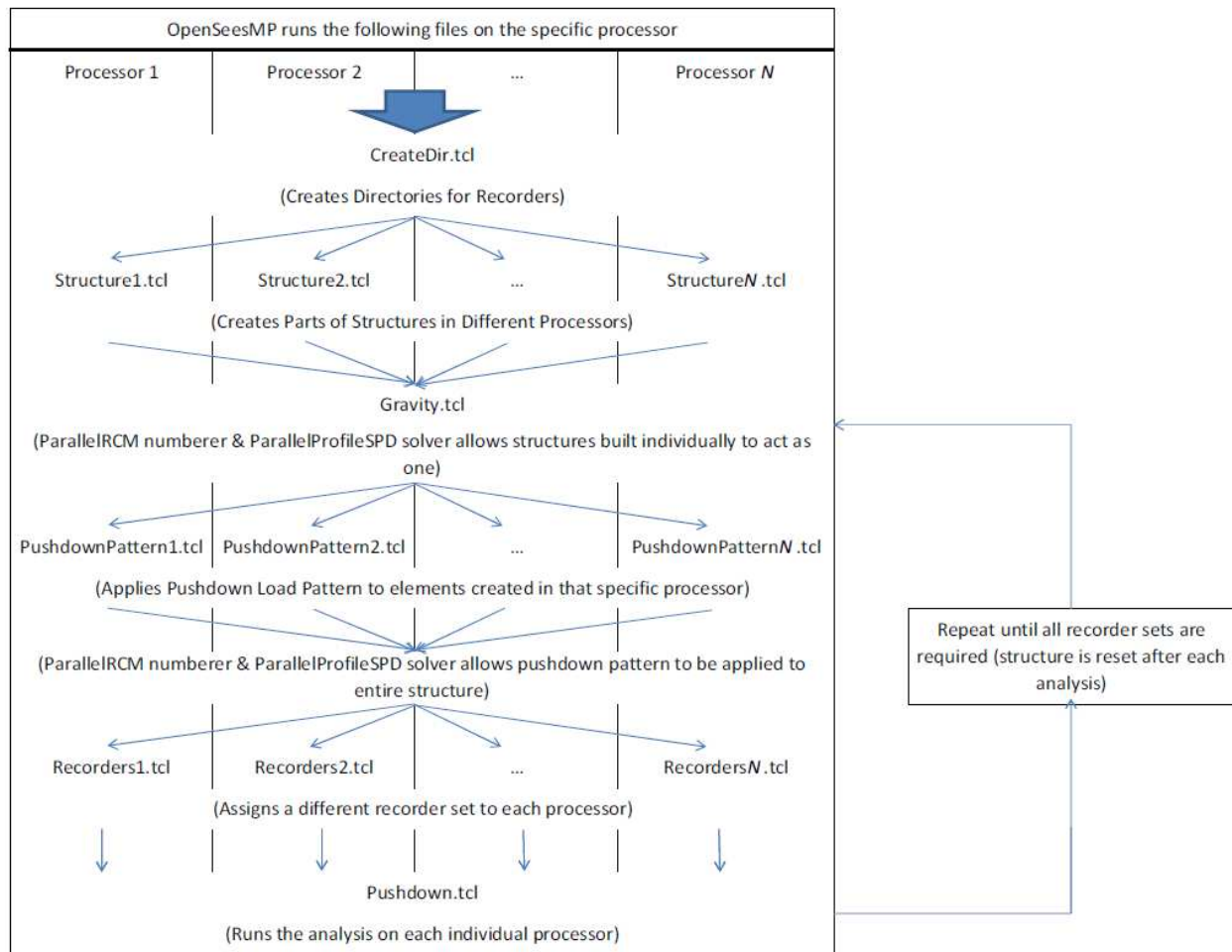


Figure 2.37: Procedure followed by processors

OpenSees uses recorder files to dictate what aspects of the structural analysis and response the analyst wants to save. Although *OpenSees* can run the model on multiple

processors, if three processors are used in *OpenSeesMP* and only one recorder file is used it will record those same recorders three times. Instead, three different recorder files are created, which can be accessed by different processors at the same time. This parallel processing of recorders speeds up the total analysis time when multiple sets of recorders are required.

2.6.5 Output

The main output from the pushdown analysis is the pushdown curve itself which plots the downward displacement of the node of interest along the x-axis and the roof load (in lb/ft or psf) for a uniform snow load pattern, as seen in Figure 2.38, or equivalent uniform roof load (in lb of lb/ft) for drifted load patterns along the y-axis. The equivalent uniform roof load represents the uniform roof load if all the snow on the roof, including the snow in the drift, is distributed uniformly over the entire roof. This pushdown curve allows the user to determine the exact failure load and displacement associated with the load pattern of interest.

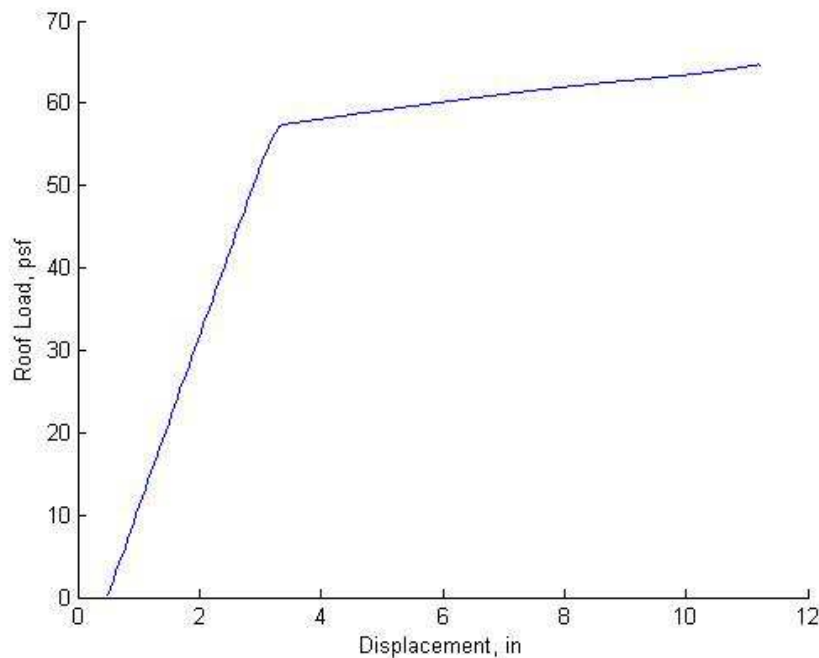


Figure 2.38: Pushdown curve

Recorders are also implemented to ensure that other data, besides just the roof load and displacement, are saved to disk. The data recorded includes displacements and rotations of nodes, local forces and moments of elements, stresses and strains of fibers of interest at the center section of the nonlinear elements, and the forces and moments recorded by the ZLEs. Unfortunately recording all these recorders at once often exceeds the upper limit on the number of recorded values defined in *OpenSees* for recording values at one time. As a result, the recorders are split into 11 different sets to be recorded separately. This is where using multiple processors at once helps to reduce total analysis time. Instead of running the analysis 11 different times in order to record all the desired values, the 11 can be split amongst the processors so the analysis needs to be run less. A good way to show how much time this saves is by observing that using two processors will almost cut the total analysis time in half.

The values recorded from the analyses allow the structure to be analyzed so the behavior and cause of failure of the structure can be known. Two separate MATLAB scripts were written in order to post-process the output data; one analyzes the data recorded while the other performs a Monte Carlo simulation on the structure to determine the reliability of the structure in specific areas.

2.6.5.1 Analyze.m

The MATLAB script *Analyze.m* uses the data recorded for a single joist and produces plots, examples of which are shown in a later chapter, which can be used to determine the behavior of the joist and why the structure failed. The first plot produced is the pushdown curve (Figure 2.38), which can be used as a comparison for the rest of the plots to identify the loads and displacements at which certain critical events occur. Following that, plots which produce the maximum or minimum stress values within all the nonlinear elements recorded is plotted along

the span of the joist. The option to then view the stress progression for all the fibers of specific nonlinear elements can be seen as a plot of stress on the y-axis against displacement of the control node along the x-axis. Comparing these plots to the known material properties should yield some insight into the behavior within the elements of the joist.

The zero-length element forces may also be looked at in the same way that section stresses are observed. The ability to see how the forces are resisted by the connections throughout the analysis and their comparison to the known ZLE properties in each direction allows the user to determine whether failure occurred in the connections.

The final plots that can be produced show the deformed shape of the joist and which elements within the joists are in tension or compression. This plot is made at multiple steps throughout the analysis so that the progressive shape change can be observed and the change of forces within an element can also be noticed.

2.6.5.2 *MonteCarlo.m*

The MATLAB script *MonteCarlo.m* uses snow load data provided by the Structural Engineers Association of Colorado's snow load committee to predict the reliability of the structure analyzed when subjected to snow records from different cities and towns in Colorado (SEAC 2007). The locations considered in Colorado are Boulder, Copper Mountain, Denver, Keystone, and Lamar. A Monte Carlo simulation is performed by taking a certain number of randomly selected ground snow load values from a distribution of snow loads for a specific site, then converting the ground snow load to roof snow load, using a known ground snow load to roof snow load distribution (O'Rourke 2010), and observing what occurs to the structure at that roof snow load by using the pushdown curve. This process is illustrated in Figure 2.39.

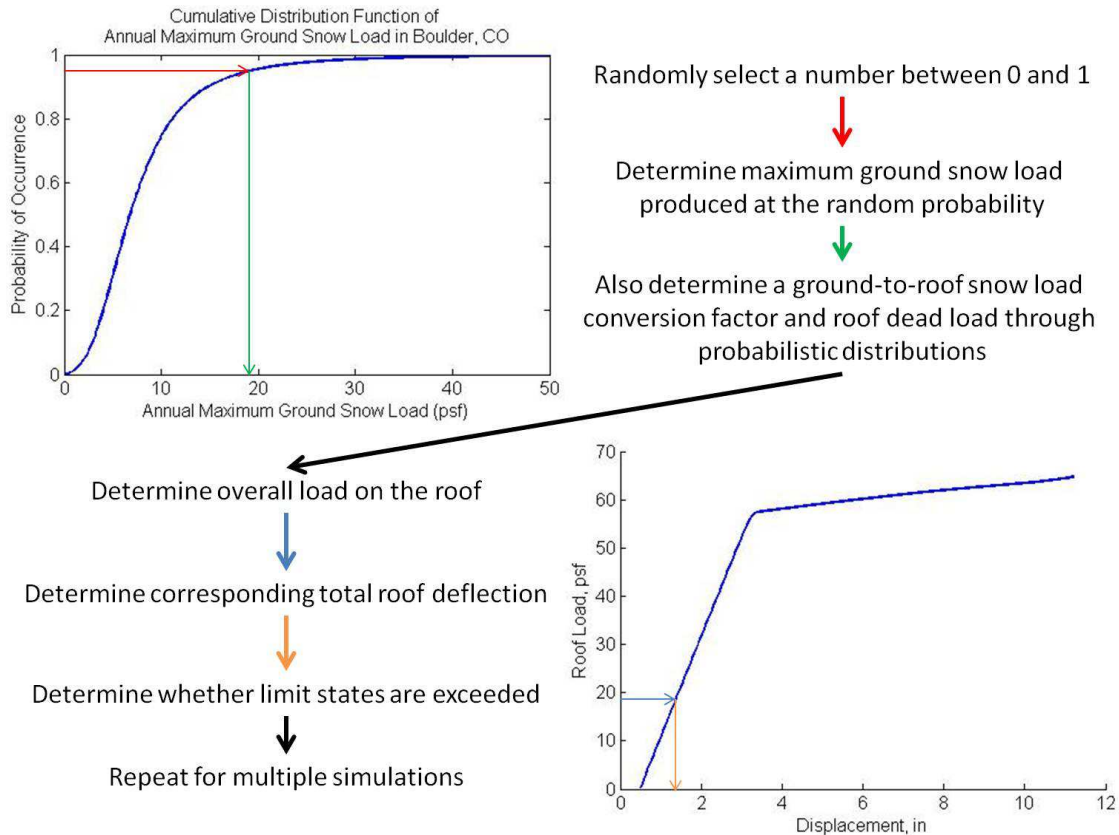


Figure 2.39: Monte Carlo simulation process

The two limits observed in the Monte Carlo simulation are whether the total deflection (*i.e.* including dead loads) exceeds $1/240^{\text{th}}$ of the span (as recommended by the ASCE 7-10 Commentary) and whether the structural fails. The latter limit is exceeded if the randomly produced roof load exceeds the roof load capacity found on the pushdown curve. The number of times each of these limits is exceeded is recorded and divided by the total number of trials run in order to determine the probability of the structure to exceed each limit state.

The annual probability of failure for each limit state is then converted to a 50-year reliability index, β . The reliability index is determined by first converting the annual probability of failure to a probability of failure over 50 years, p_f , Equation (2.27) then converts the probability to a reliability index.

$$\beta = -\Phi^{-1}(p_f) \quad (2.27)$$

where $\phi()$ is the standard normal distribution, meaning a normal distribution with a mean of 0 and a standard deviation of 1 (Melchers 1999). Knowing the reliability index is useful in comparing the observed results to the recommendations set by the ASCE 7-10 commentary (2010), shown in Table 2.1.

Table 2.1: Acceptable reliability (maximum annual probability of failure) and associated reliability indexes (β) for load conditions that do not include earthquake (ASCE 2010)

Basis	Occupancy Category			
	I	II	III	IV
Failure that is not sudden and does not lead to wide-spread progression of damage	$P_F = 1.25 \times 10^{-4}/\text{yr}$ $\beta = 2.5$	$P_F = 3.0 \times 10^{-5}/\text{yr}$ $\beta = 3.0$	$P_F = 1.25 \times 10^{-5}/\text{yr}$ $\beta = 3.25$	$P_F = 5.0 \times 10^{-6}/\text{yr}$ $\beta = 3.5$
Failure that is either sudden or leads to wide-spread progression of damage	$P_F = 3.0 \times 10^{-5}/\text{yr}$ $\beta = 3.0$	$P_F = 5.0 \times 10^{-6}/\text{yr}$ $\beta = 3.5$	$P_F = 2.0 \times 10^{-6}/\text{yr}$ $\beta = 3.75$	$P_F = 7.0 \times 10^{-7}/\text{yr}$ $\beta = 4.0$
Failure that is sudden and results in wide spread progression of damage	$P_F = 5.0 \times 10^{-6}/\text{yr}$ $\beta = 3.5$	$P_F = 7.0 \times 10^{-7}/\text{yr}$ $\beta = 4.0$	$P_F = 2.5 \times 10^{-7}/\text{yr}$ $\beta = 4.25$	$P_F = 1.0 \times 10^{-7}/\text{yr}$ $\beta = 4.5$

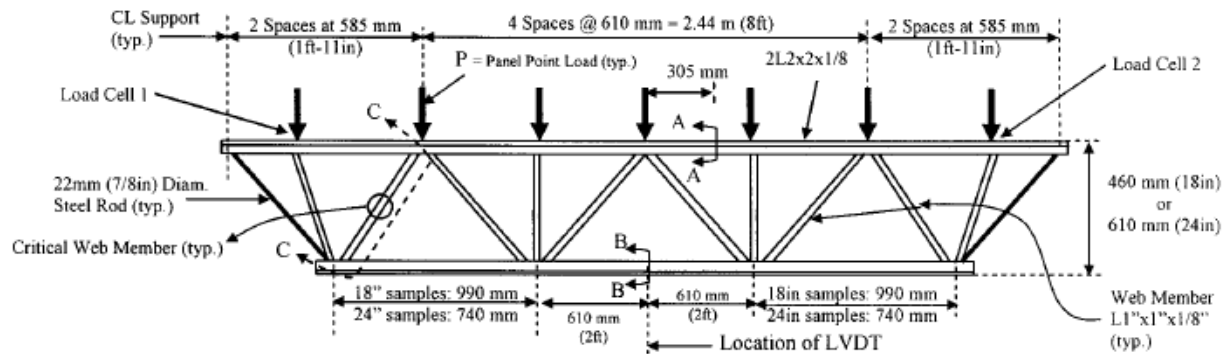
¹The reliability indices are provided for a 50-year service period, while the probabilities of failure have been annualized. The equations presented in Section 2.3.6, Load Combinations for Non-Specified Loads, are based on reliability indices for 50 years because the load combination requirements in 2.3.2 are based on the 50-year maximum loads.

²Commentary to Section 2.5 includes references to publications that describe the historic development of these target reliabilities.

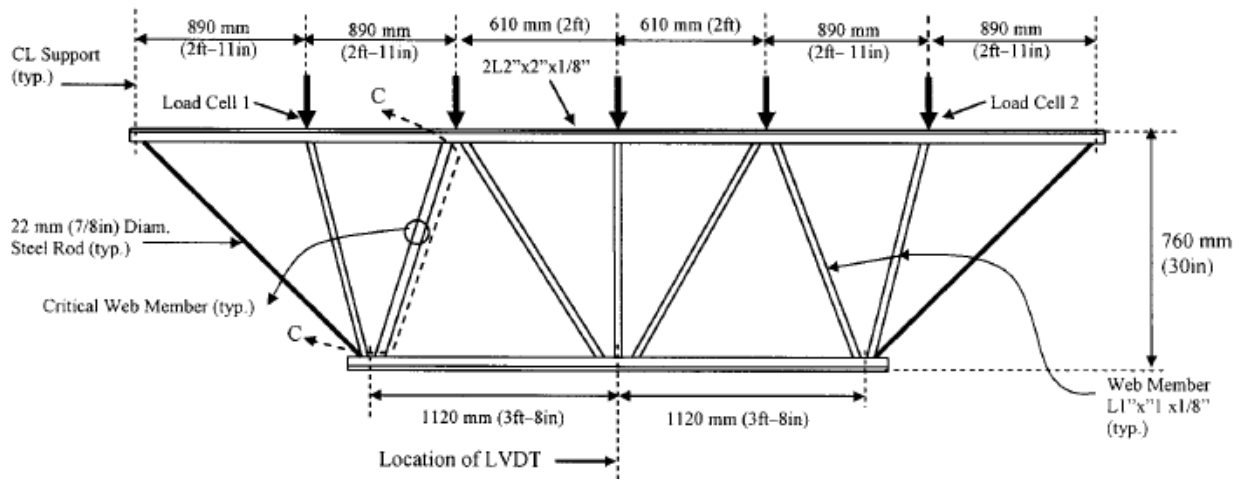
2.7 Validation of the Model

Using the experimental results from Yost *et al.* (2004), three single joists which had a span of 15 ft. 8 in. are analyzed using the model described above and compared to actual, experimental results. Details of the three joists analyzed are shown in Figure 2.40. Each experiment was repeated three times with identical specimens. The *OpenSees* The comparison between the model results and the experimental results were very favorable for all three joists as shown in Figure 2.41. For the 18 in. deep joist, the displacement at failure and the stiffness of the joist were within the range set by experimental while the force at failure was equivalent to 10.82 kN being applied at each panel point, which is within the experimental range. The 24 in. Joist comparison revealed the model stiffness and the displacement at failure to be within the range of the experimental results, but the failure load is about 9% larger than the largest experimental result. In the 30 in. deep joist, the displacement at failure, the joist stiffness, and the failure load

were once again within the experimental range. Both the experimental and model results also failed by the buckling of the critical web member. The common failure mechanism, paired with the extremely similar stiffnesses between the model and experimental results, can lead to the conclusion that this model accurately represents the joist.

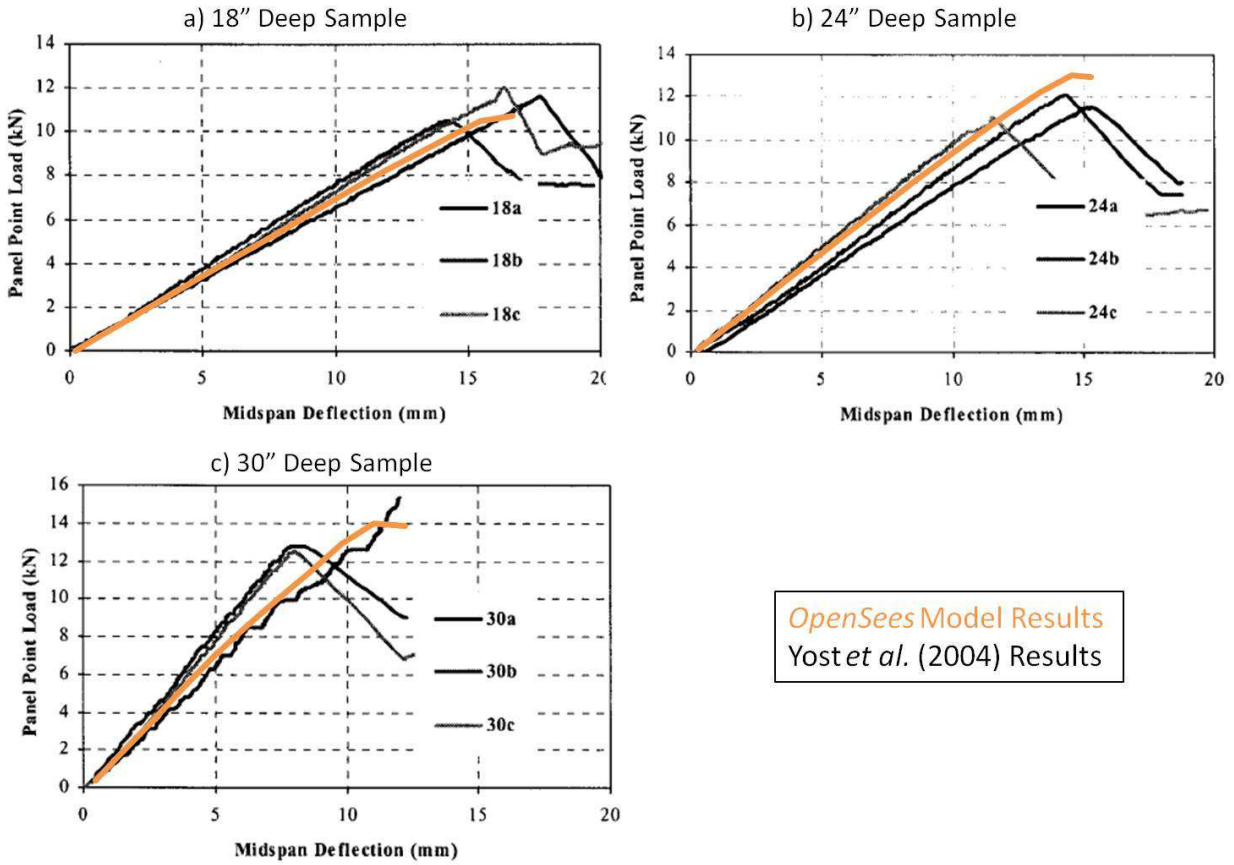


a) Typical 18in and 24in Deep Joist Sample



b) Typical 30in Deep Joist Sample

Figure 2.40: Details of joists used for validation (Yost *et al.* 2004)



OpenSees Model Results
 Yost *et al.* (2004) Results

Figure 2.41: Comparison of Yost *et al.* (2004)'s experimental results to the *OpenSees* model

3 RESPONSE OF OPEN WEB STEEL JOIST STRUCTURES UNDER SNOW LOADS

This chapter studies the behavior of open web steel joist structures with varying building characteristics when subjected to both uniform and drifted snow loads. Trends in the failure points as well as trends in the method of failure for the buildings are the main focus. This chapter is a version of the paper under preparation for submission to the *Journal of Structural Engineering*. The paper is authored by Derek L. Kozak and Abbie B. Liel.

3.1 Introduction

Snow loads have been responsible for a number of roof collapses throughout the years, leading to loss of life and property, and structural damage. For example, in the U.S., during the five-year span from 1974 to 1978, about 55% of roof losses reported to insurance agencies were caused by snow loads; in fact, during the 1977 to 1978 period alone, approximately 200 buildings collapsed due to roof snow loads, causing around \$40 million (1978 US dollars) in damage (O'Rourke *et al.* 1983). More recently, Bolduc (2011) found that over 40% of the 350 structural failures in the U.S. in 2010 were caused by snow loads on roofs.

Modern building codes prescribe snow loads for use in roof design. In the U.S., these snow loads are based on the ground snow load that occurs on average every 50 years, *i.e.* has a 2% probability of occurring annually (ASCE 2010). Snow-induced structural failures in properly designed and constructed buildings generally occur due to three categories of phenomena that can lead snow loads to exceed the design load: overloading of snow, rain-on-snow, and the formation of snow drifts. Here, the term “overloading” refers to situations in which the snow load on the roof exceeds the 50-year design snow load because the location experienced rare, large snowfall (DeGaetano *et al.* 1997). For example, in January, 1996, the northeastern U.S. was affected by a large snowstorm, which saw many buildings fail due to the large amount of

snow. Analyses by DeGaetano *et al.* (1997) found that the snow accumulation during that storm exceeded the 50-year design snow load at many sites, and, indeed, exceeded the 100-year return period snow load at some sites. Likewise, Peraza (2000) attributed many of the roof collapses in New England during the winter of 1993-1994 to loads that overtook design values. Rain-on-snow occurs when rain falls onto a snow layer that is already on the roof and remains trapped. Rain-on-snow increases the density of the snow layer, raising the snow load on the roof, although the depth of the snow may actually decrease (Ogrin & Ortar 2007). Rain-on-snow events occur regularly in regions, such as the northwestern U.S. (McCabe *et al.* 2007), and have been responsible for a number of past roof collapses (O'Rourke & Downey 2001). The third phenomena, snow drifting, causes an increase in snow loads on a localized section of roofs, such that some parts of the roof may be overloaded relative to their design loads (Peraza 2000). Snow drifts can occur with only low velocity winds if the roof has a vertical irregularity, such as a parapet or step (Meløysund *et al.* 2007). Drifting snow is one of the major contributors to snow-related damage, causing millions of dollars in losses each year (O'Rourke & Auren 1997).

Of snow-related roof failures in the U.S., approximately 37% of major snow-induced failures occur in buildings with steel roof systems (Geis *et al.* 2011). Geis (2011) hypothesizes that lightweight steel buildings may be particularly vulnerable to snow loads. This suspicion is supported by previous studies that analyzed the reliability of steel elements and buildings and concluded that the ratio of dead-to-snow load (which is very small for lightweight buildings) is directly related to the reliability of the element or structure (Bennett 1988, Holický 2007, Sadovský & Pálež 2008). In other words, reliability decreases if a building (or component) has a smaller dead-to-snow load ratio. Open web steel joists (OWSJ) are a particularly common type of lightweight roof construction. The potential susceptibility of OWSJ roofs to snow loads, in

particular, is apparent from numerous case studies of buildings having either open web steel joist or steel truss type roofs. Some of the most notable snow-induced collapses of these types of buildings are the Katowice Fair Building (Biegus & Rykaluk 2009) and the Hartford Civic Center Arena (Martin & Delatte 2001, Levy & Salvadori 2002). Other case studies document failure of school gymnasiums, auditoriums or warehouses with lightweight steel roof structures under snow loads (Geis 2011, Tanzer 2011).

This paper analyzes the effects of roof snow loads on open web steel joist roofs. The study is organized around the analysis of 22 OWSJ roof structures, which vary in terms of the ground snow load used in design, design dead-to-snow load ratios, joist spans, joist spacing, and other features. The response of each roof under snow loads is obtained from simulation of the roof structure under snow load, using a model capable of capturing key failure modes of the system. The responses of OWSJ roof buildings with these different characteristics are explored in order to identify which characteristics make roofs more susceptible to snow loads. These responses also indicate which parts or regions of the joists are of concern when the roofs are subjected to snow loads. Roof structures are analyzed under both uniform and drifted snow loads.

3.2 Open Web Steel Joists

3.2.1 Design, Regulation and Uses of Open Web Steel Joists

Open web steel joists (OWSJ) are prefabricated structural elements composed of steel web and chord members. Through truss action, the composite OWSJ behaves as a flexural element that can be used as an alternative to conventional steel (*e.g.* wide flange) sections. Due to their open arrangement of steel components, OWSJs have a high ratio of strength (flexural resistance) to weight. This efficiency is a major reason for the popularity of OWSJs in building

design and construction (Fisher *et al.* 2002, Yost *et al.* 2004, Buckley *et al.* 2008). OWSJs are also relatively simple to design, requiring the designer to calculate the factored uniformly distributed load on each joist and, then, choose a joist that satisfies the required resistance criteria from tables prepared by the Steel Joist Institute (SJI). The use of load tables reduces design time and facilitates the selection of the most efficient joist for the design (Fisher *et al.* 2002). Custom joists for non-uniform loads may also be requested from joist manufacturers (SJI 2005).

SJI design load tables are developed for different types of joists. The three most common types are: K-Series joists, which are for medium to long spans with factored uniform loads of less than 825 lbs/ft.; LH-Series joists, which are for longer spans or loads greater than 825 lbs/ft.; and DLH-Series joists, which are for long span deep joists (Fisher *et al.* 2002, Yost *et al.* 2004, SJI 2005). The SJI joist designation describes the type of joist, along with the joist depth and a measure of its relative strength. For example, a 22K9 joist refers to a 22 in. deep K-Series joist with a relative strength of 9, indicating is stronger than a 22K8 joist, but weaker than a 22K10 joist with the same span (SJI 2005). Although there can be differences in the arrangement and sizes of the components within OWSJs depending on the fabricator, all manufacturers who wish to be certified by the SJI must comply with SJI standards. To comply, fabricators must prove, through some form of analysis, that their joists meet the load capacities provided by the SJI for the relevant joist designation (Canam 2005, SJI 2005).

As a result of their relative efficiency and simplicity, OWSJ-supported roofs are found in a large number and wide variety of buildings in the United States. In particular, OWSJs are commonly used for industrial plants, offices, commercial shops, malls, academic facilities, civic and institutional structures, and recreational facilities (Fisher *et al.* 2002). Figure 3.1 shows some examples of OWSJs in these types of buildings.

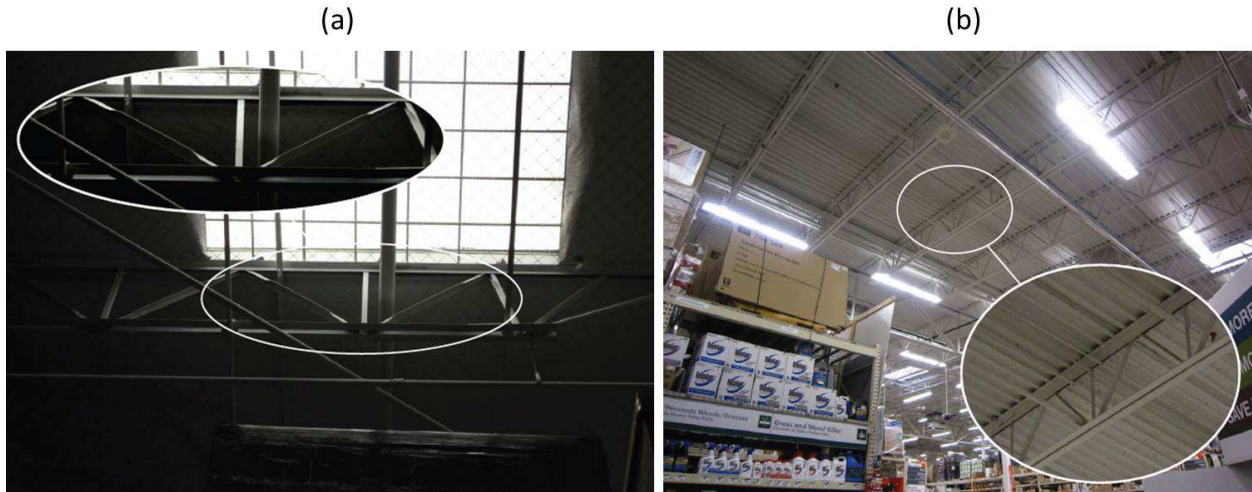


Figure 3.1: Examples of OWSJ roofs (Geis 2011)

3.2.2 Components of Open Web Steel Joists

Figure 3.2 illustrates the four different components that comprise an OWSJ: the top chord, bottom chord, web members, and end web members. The locations where top or bottom chords intersect with web members are known as “panel points”.

The top and bottom chords usually consist of two back-to-back angle sections, which are continuous throughout the entire span of the joist. The chords are fabricated with spacing between the angles so that the web members and end web members are attached to both angles, fitting within this space. The top chord of an OWSJ is in compression under uniform loading. Due to the presence of steel roof or floor decking connected to the top chord at regular, relatively small intervals, the top chord is typically considered as continuously laterally braced (Buckley *et al.* 2008). The bottom chord is under tension when a uniform downward load is applied (Buckley *et al.* 2008). The bottom chord is also braced laterally by angle bridging sections that connect the joist (in the out of plane direction) to the adjacent joist(s); the specifications of the location and size of the bracings are defined by the SJI and discussed later. Some joists have additional

horizontal end chord members that extend to a column or wall to provide lateral resistance in the in-plane direction.

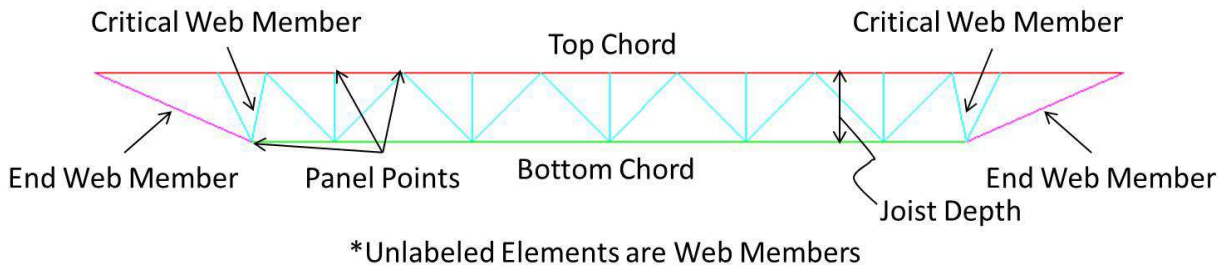


Figure 3.2: Arrangement of the components within an OWSJ

Web members can be composed of various sections, with the most common being rods for end web members and either rods or single angles for interior web members (Buckley *et al.* 2008). The term “critical” web member refers to the web member with the largest required compressive resistance, due to its position in the joist. When the web members are single angles, they are non-continuous along the joist, meaning separate angle sections are used for each web member spanning between a pair of panel points. However, rod web members may be continuous along the joist, meaning a single long rod is bent at each panel point creating all of the web members in the joist (Canam 2005). If the web members are non-continuous, the individual web member section sizes may be tuned to the load requirements reflecting the member’s position and orientation in the joist, further enhancing the efficiency of the system.

At the panel points, web members and chords are generally attached to each other through shop welds. These welds connect the web members to the interior spacing between the angles comprising the top and bottom chords (SJI 2005). Single angle web members need to be crimped so that the angle sections can fit in the space where the connection is made. As a result of this crimping, the centroids of the uncrimped and crimped sections are unaligned, creating an

eccentricity in the line of loading in the uncrimped section. This eccentricity creates a moment in the member when axial loads are present (Buckley *et al.* 2008).

In the U.S., OWSJs are designed and prefabricated by a number of companies, including Vulcraft, Canam and Valley Joist. The specific sizes of the sections used in the chords and web members depend on the manufacturer and many of the design details concerning the arrangement and size of the OWSJ's components are proprietary. This study obtained design details for OWSJs from a well-known OWSJ manufacturing company, but the joist specifications and the company's name are kept confidential.

3.2.3 OWSJ Roof Systems

In a roof system, OWSJs are generally supported by girders that may be larger OWSJs, wide flange sections, or another type of structural element. The SJI (2005) describes specific requirements for welded or bolted connections between the top chord and the supporting girders. For example, K-Series joists may be connected using two 1/8 in. fillet welds, which are each 1 in. long, or by two 1/2 in. ASTM-A307 bolts. This study assumes connections between the joists and the supporting girders are bolted.

The SJI also sets requirements for the minimum size and spacing of the bridging elements, which provide lateral (out-of-plane) support along the span of a joist. Bridging is typically angle sections of various sizes, which can be arranged either horizontally or diagonally (SJI 2005). Horizontal bridging is usually long, continuous members that connect multiple joists, top chord-to-top chord or bottom chord-to-bottom chord. Diagonal bridging spans from the bottom chord of one joist to the top chord of the adjacent joist forming an X pattern between adjacent joists (Fisher *et al.* 2002, Buckley *et al.* 2008). Both types of bridging are required to be

attached to the chords of the OWSJs by “positive mechanical means,” which can be satisfied by bolts or welds (SJI 2005).

3.3 Buildings Considered in This Study

OWSJ roofs have widely varying characteristics. The purpose of the building could dictate the size and shape of the roof; the location affects the loads for which the roof is designed; building use may constrain column placement and joist or girder span lengths. All else being equal, the depth and type of joist may vary at the discretion of the design team. This study examines buildings with varying characteristics to explore their response under uniform and drifted snow loading.

3.3.1 Basic Building

All buildings considered are variations on the so-called “basic building”. This building is of average size, with typical features identified through observation of local structures in Boulder, CO. The basic building, shown in Figure 3.3, is a 330 ft. by 120 ft. single story structure. The joists are aligned with the long direction of the building in 11 bays, and span 30 ft. between girders. In the short direction, the girders span 3 bays of 40 ft. each. The joists are spaced at 10 ft. intervals along the girders. The roof of the building is 30 ft. high.

The building is designed for Boulder, CO according to ASCE 7-10 and the Boulder Revised Code for the following roof loads: (1) a roof live load (LL) of 20 psf (ASCE 2010); (2) a roof dead load (DL) of 9 psf representing a metal decking covered with composition roofing (Boise Cascade 2009); (3) the dead load self-weight of the OWSJs (SJI 2005); and (4) a ground snow load (SL) of 30 psf (City of Boulder 2013). The building is in Risk Category II, as defined by ASCE 7-10, indicating standard occupancy. Additionally, the building is assumed to be in a partially exposed location (exposure category B) and to have the thermal characteristics of a

building that is not intentionally kept cold. These characteristics are typical of buildings that are neither heavily sheltered nor highly exposed, are heated, and have typical amounts of insulation. Using the ASCE 7-10 standard to convert the ground snow load to roof snow load, the design roof snow load was determined to be 21 psf. The load combination of $1.2DL + 1.6SL + 1.0LL$ governs (ASCE 2010).

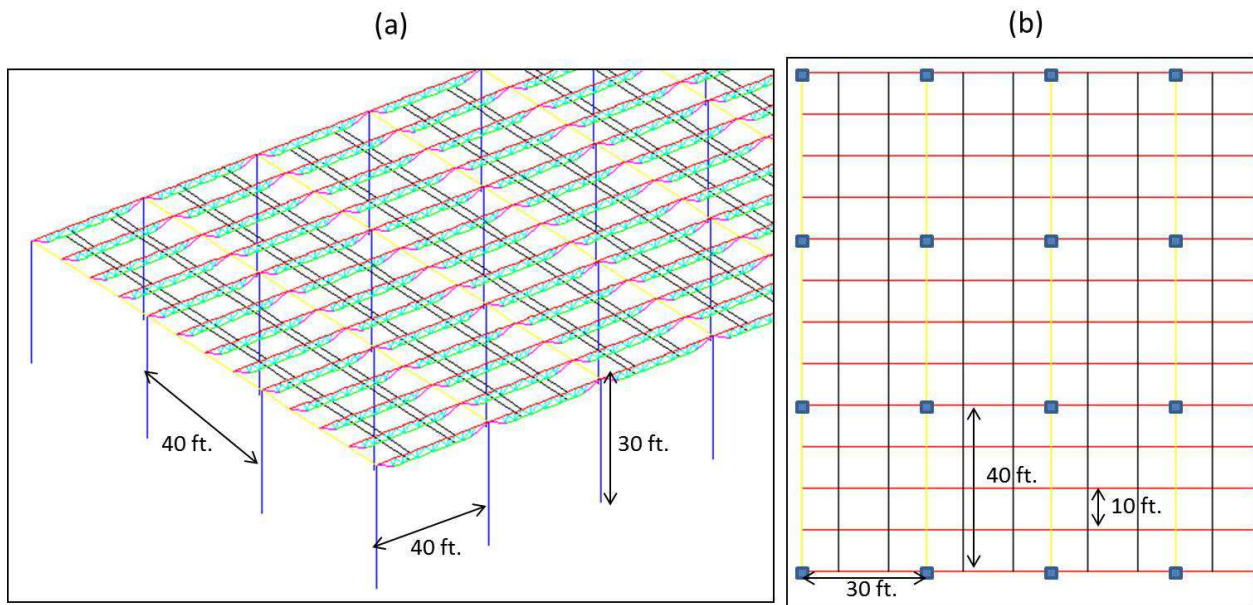


Figure 3.3: a) 3D view of a portion of the basic building, b) plan view of a portion of the basic building with girders in yellow, joists in red, bridging in black and columns in blue

These loads resulted in the selection of W14x82 girders and 22K9 OWSJs, with HSS 6x6x3/8 columns. Lateral support is provided to the joists through two rows of L2x2x1/8 horizontal bridging per joist. The 22K9 joist weighs 11.3 lbs/ft. and has a safe factored uniformly distributed load of 745 lbs/ft. (SJI 2005), which is sufficient to withstand the design loads. It is worth noting that a number of joists of different depths satisfy the design criteria; the 22K9 joist was chosen because 22 in. is close to the median of the possible joist depths. This building has a ratio of unfactored design dead-to-snow loads (D/S) of 0.487, providing a measure of its

lightweight nature. The building, like all other buildings in this study, is not designed explicitly for serviceability.

The building has a completely flat roof without parapets or other protuberances. As a result, it is designed for uniformly distributed snow loads only and therefore drifted snow loads are not required to be considered (ASCE 2010). Other considerations such as partial roof loading and rain-on-snow are also ignored in the basic building design.

A second basic building is designed with all the characteristics of the first basic building, except that a 3.5 ft. parapet is now present along the perimeter of the building roof. When there is a parapet, drifts may accumulate because the parapet collects snow on its windward side; we do not consider leeward drifts that may occur on the downwind side of the parapet at the other end of the building because it is assumed the building is far enough from other roofs and sources of snow that could lead to the formation of leeward drifts. The size and shape of the design drift was determined according to ASCE 7-10 equations, which leads to a triangular shaped drift whose shape is based on the parapet height, design ground snow load, and downwind length of roof from the parapet (known as the snow fetch). When designed for these drifts, the basic building has 24LH09 joists and W21x62 girders. As recommended by SJI (2005), these joist sizes were determined by designing for the largest distributed snow load found on the roof, which occurs at the peak of the snow drift, assuming this load is present across the entire joist, and then selecting the appropriate joist from the uniform load tables. In actual designs, for buildings where snow drifts are a large concern, the joist manufacturers usually create unique joists designed specifically to meet the customer's requirements (SJI 2005).

The basic buildings are identified as Bldg. BU for analyses with uniform snow loads and Bldgs. BD1 and BD2 for analyses with drifted snow loads.

3.3.2 *Building Variations*

The basic buildings' properties are varied in order to produce 17 additional buildings to be analyzed under uniform snow loads (Table 3.1) and 2 additional buildings to be analyzed under drifted snow loads (Table 3.2). All of the building variations are designed to resist the same dead and live loads, with the same assumptions about building exposure and thermal characteristics, and assuming the same column sections and building height. However, due to variations in the building location and properties, the roof OWSJ, girder, and bridging are redesigned for each case according to requirements of ASCE 7 (2010) and SJI (2005).

As shown in Table 3.1, Bldgs. U1-U4 are located in different parts of the state of Colorado. The design ground snow load changes when different locations are considered, requiring redesign of the joist, girder, and bridging sections. Bldg. U1 is located in Lamar, CO, which is in eastern Colorado, away from the mountains, and has a design ground snow load of 15 psf (SEAC 2007). In this case, the roof snow load is also equal to 15 psf because the minimum load of the risk factor (taken as 1.0) times the design ground snow load governs. Bldg. U2 is designed for Denver, CO with a design ground snow load of 25 psf (City of Denver 2011) and a design roof snow load of 20 psf. Keystone, CO, where Bldg. U3 is located, is a ski community in Summit County, which requires a design ground snow load of 75 psf (Summit County 2013), leading to a design roof snow load of 52.5 psf. Finally, Bldg. U4 is designed for Copper Mountain, CO, also a Summit County ski area, which has a design ground snow load of 90 psf (Summit County 2013) corresponding to a design roof snow load of 63 psf. Two rows of L2x2x1/8 horizontal bridging per joist are provided for Bldgs. U1 and U2. Two rows and one row per joist of L2.5x2.5x5/32 horizontal bridging members are provided in Bldgs. U3 and U4, respectively.

Table 3.1: Buildings subjected to uniform snow loads (i.e. having no parapet)

Bldg. No.	Site	D/S	Building Length (ft.)	Building Width (ft.)	Joist	Girder	Variation from Basic Building
BU	Boulder, CO	0.487	330	120	22K9	W14x82	Basic Building
U1	Lamar, CO	0.670	330	120	22K7	W12x79	Reduced Ground Snow Load (15 psf)
U2	Denver, CO	0.511	330	120	22K9	W24x55	Reduced Ground Snow Load (25 psf)
U3	Keystone, CO	0.215	330	120	24LH09	W27x84	Increased Ground Snow Load (75 psf)
U4	Copper Mountain, CO	0.186	330	120	24LH11	W27x94	Increased Ground Snow Load (90 psf)
U5	Boulder, CO	0.463	340	120	20K3	W16x50	Reduced Joist Span (20 ft.)
U6	Boulder, CO	0.516	360	120	24LH07	W18x86	Increased Joist Span (40 ft.)
U7	Boulder, CO	0.487	330	120	22K9	W18x46	Reduced Girder Span (30 ft.)
U8	Boulder, CO	0.487	330	120	22K9	W27x94	Increased Girder Span (60 ft.)
U9	Boulder, CO	0.508	330	120	22K4	W18x60	Reduced Joist Spacing (5 ft.)
U10	Boulder, CO	0.479	330	120	22K7	W12x79	Reduced Joist Spacing (8 ft.)
U11	Boulder, CO	0.489	330	120	18K10	W14x82	Reduced Joist Depth (18 in.)
U12	Boulder, CO	0.492	330	120	20K10	W14x82	Reduced Joist Depth (20 in.)
U13	Boulder, CO	0.488	330	120	24K8	W14x82	Increased Joist Depth (24 in.)
U14	Boulder, CO	0.485	330	120	26K7	W14x82	Increased Joist Depth (26 in.)
U15	Boulder, CO	0.487	330	120	28K6	W14x82	Increased Joist Depth (28 in.)
U16	Boulder, CO	0.803	330	120	28K12	W24x62	Increased D/S Ratio (0.803)
U17	Boulder, CO	1.268	330	120	20LH06	W24x68	Increased D/S Ratio (1.268)

The next set of variations (Bldgs. U5 and U6) includes buildings with different joist spans for Boulder, CO. Bldg. U5 decreases the joist span from the basic building's 30 ft. to 20ft., which requires the size of the building to be changed such that there are 17 bays of 20 ft. span 20K3 joists in one direction, resulting in a footprint of 340 ft. by 120 ft. Bldg. U6 increased the joist span to 40 ft. This is accomplished with a building with 9 bays of 40 ft. span 24LH07 joists in one direction and a footprint of 360 ft. by 120 ft. Similarly, Bldgs. U7 and U8 have different girder spans from the basic building. Bldg. U7 reduces the girder span to 30 ft., which increases the number of bays in the short direction to four, and can be satisfied by lighter girder sections. Bldg. U8 uses 60 ft. span W27x94 girders, which decreases to two the number of bays in the short direction.

Variation of the joist spacing occurs in Bldgs. U9 and U10. Bldg. U9 uses a smaller joist spacing of 5 ft., such that weaker joists satisfy the design. Due to changes in joist spacing, the horizontal bridging requirements are also altered to two rows of L1x1x7/64 horizontal bridging

per joist. Bldg. U10 also has a joist spacing smaller than the basic building of 8 ft., allowing the use of 22K7 joists and two rows of L1.75x1.75x7/64 horizontal bridging per joist.

Since it is possible to use a large variety of joists with different depths to accommodate the same loads using the SJI's load tables, Bldgs. U11-U15 vary the depth of the joist being used from the 22 in. deep joists typically selected for the other building designs. The different depth joists listed in Table 3.1 for Bldgs. U11 – U15 are selected to be as close as possible to the 22K9 basic building joists in terms of weight (11.3 lbs/ft.) and resistance (745 lbs/ft.) (SJI 2005). The weight of the redesigned joists varies from 10.9 lbs/ft. (26K7) to 12.2 (20K10) and the safe factored load ranges from 715 lbs/ft. (18K10; 28K6) to 799 lbs/ ft. (20K10) (SJI 2005).

Bldgs. U16 and U17 have different design dead-to-snow load ratios. This variation is achieved by altering the design roof dead load. Bldg. U16 considers a larger roof dead load of 15 psf, and the design dead load for Bldg. U17 is even greater at 25 psf. The joists selected for Bldgs. U16 and U17 were designed such that the ratio of SJI load table capacity to design load is between 1.11 and 1.13. Keeping the ratios of design load to indicated capacity permits a direct comparison with the basic building.

Table 3.2: Buildings subjected to drifted snow loads

Bldg. No.	Design Dead/Snow	Building Length (ft.)	Building Width (ft.)	Joist	Wind Direction	Parapet Height (ft.)	Variation from Basic Building
BD1	0.537	330	120	24LH09	→	3.5	Basic Building (3.5 ft. Parapet Height) →
BD2	0.537	330	120	24LH09	↓	3.5	Basic Building (3.5 ft. Parapet Height) ↓
D1	0.506	330	120	20LH06	→	2	Reduced Parapet Height (2 ft.) →
D2	0.506	330	120	20LH06	↓	2	Reduced Parapet Height (2 ft.) ↓

For analyses with drifted snow loads, a slightly different set of parameters are varied, as shown in Table 3.2. The primary building design characteristic explored is the parapet height. The parapet height dictates the shape of the drift according to equations from ASCE 7-10, changing both the drifted loads considered in the design and the distribution of snow in the drift

snow analysis. Parapet heights of 2 ft. and 3.5 ft. are considered. The drifted snow cases also vary the wind direction assumed in the analysis in order to investigate the effects on the roof given prevailing winds in two different directions. The analysis of buildings under snow loads is examined in more detail in Section 3.4.3.

3.4 Nonlinear Models of OWSJ Supported Roof Buildings

3.4.1 Properties of Nonlinear Models

Nonlinear models for all the buildings described were created with the *OpenSees* software (PEER 2013a). The developed models are intended to be capable of representing failure mechanisms in the OWSJs that have been observed in case studies of failed buildings (*e.g.* Lavon & Stivaros 2005, Biegus & Rykaluk 2009, Holický & Sykora 2009) and other literature on the behavior of OWSJs (*e.g.* Yost *et al.* 2004, Buckley *et al.* 2008). Each component in the OWSJ roof structure was modeled with either (1) elastic elements, (2) nonlinear elements, or (3) zero-length elements depending on the expected behavior.

The elements designated as elastic elements are those that are not part of the OWSJ itself, including the girders, bridging, and columns. These components are assumed to remain linear elastic to reduce computational expense, since case studies have shown that failures of OWSJ roofs typically occur in the joist. An elastic modulus of 29000 ksi is used for the steel sections in this study.

As mentioned previously, the section properties of chord and web members within the OWSJs were obtained from a well-known OWSJ manufacturer. In *OpenSees*, the chord and web member elements are modeled as nonlinear, displacement-based beam-columns discretized into fiber sections. A fiber modeling approach is employed because it can (1) represent complicated cross-sections that vary along the length of the member and (2) incorporate nonlinear stress-

strain behavior in the fibers of the cross-sections (Perea & Leon 2008). In a fiber element, a member's cross-section is divided into fibers as illustrated in Figure 3.4. Each fiber is assigned a stress-strain relationship. During the analysis, the stress-strain response of each fiber is tracked and the behavior over the length of the frame element is determined using finite element interpolation functions that satisfy compatibility and equilibrium of the element (Perea & Leon 2008).

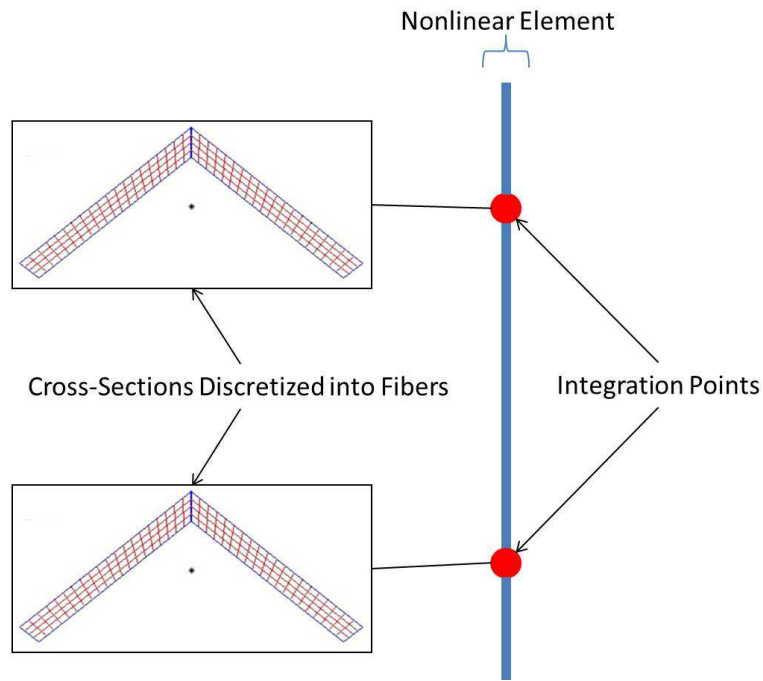


Figure 3.4: Illustration of a nonlinear beam-column element discretized into fiber sections

The stress-strain relationships of the grade 50 steel used for the nonlinear elements are defined based on the Dodd & Restrepo-Posada (1995) steel model, which takes into account steel properties beyond the linear range, such as the yield plateau region and a strain hardening region. This model was determined to be the most useful despite it being initially created for rebar. In this model, any strain past the strain at ultimate stress is considered to be a material failure, *i.e.* fracture. The material failure is represented by a negative slope which decreases from the

ultimate stress to zero stress for strains larger than the strain at ultimate stress. In the *OpenSees* model, a general multilinear backbone is defined to capture the key points on the Dodd & Restrepo-Posada curve, as illustrated in Figure 3.5.

The top and bottom chords are assumed not to buckle and the same stress-strain relationship defines compressive and tensile behavior (labeled the typical material in Figure 3.5). Web members, however, may buckle (Yost *et al.* 2004). Buckling is considered following Elnashai & Elghazouli (1993)'s recommendations. In this approach, the strain at which buckling occurs is computed and, for strains occurring beyond this point, the compressive stress resistance of the fiber is reduced, as shown in Figure 3.5. Equations from the AISC Steel Construction Manual (2011) are employed to calculate the strain at which local torsional or flexural-torsional buckling occurs, depending on the characteristics (section, length, etc.) of the web member. These calculations assume an effective length factor of 0.7 (corresponding to semi-rigid connections), which is supported by comparison of models and experimental studies (Yost *et al.* 2004).

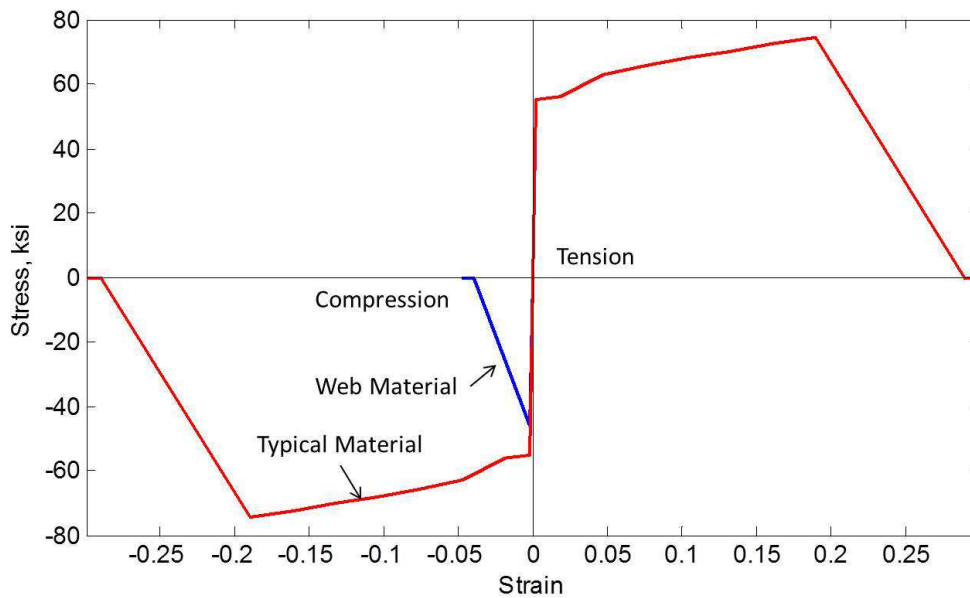


Figure 3.5: Nonlinear steel materials for chords and web members

If composed of single angles, the interior web members present an additional modeling challenge because crimping produces variable section properties along the length of the member. At the end integration points, where the web member is crimped for connection with the chords, the crimped shape is represented in fiber sections, while integration points away from the chords are assigned the regular angle shape sections, as demonstrated in Figure 3.6. Chords and end web members maintain constant cross-sections at all integration points.

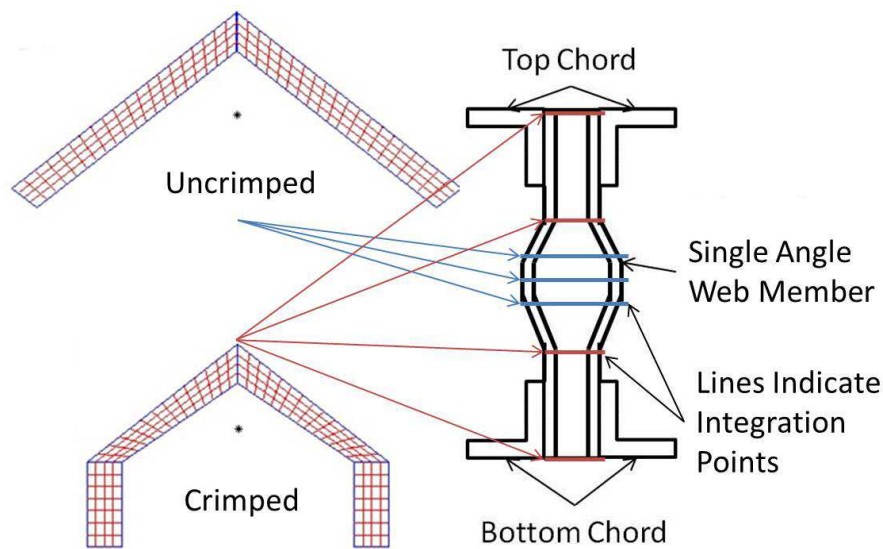


Figure 3.6: Crimped and uncrimped sections defined for web members, shown from the perspective of a cross-section of an OWSJ

The third type of element, the zero length elements, is used to model the connections between chords and web members, and between the top chord of the joist and the girder. The failure of the welds between the chords and web members or of the bolts between the top chord and the girder are common OWSJ failure mechanisms (Buckley *et al.* 2008). The bolted girder-joist connections are modeled to simulate the semi-rigid connection and possible failure due bolt shear or fracture. The shear and tensile properties of the bolted connection were determined

based on (Chan & Chui 2000, SJI 2005, ASTM 2012) and models of the force-displacement and moment-rotation relationships are assigned to zero length springs defined in the appropriate direction at the connection point. Welds between the web members and chords have an assumed strength corresponding to E70XX electrodes. The force-displacement relationships of these connections are modeled using the Lesik & Kennedy (1990) weld material model. The moment-rotation relationships are developed based on calculations using the elastic method, as recommended by the AISC (2011), and the Lesik & Kennedy (1990) model for weld force and displacement, with the weld lengths determined from the connection geometry. Lesik & Kennedy (1990)'s model also predicts a weld failure point, beyond which the weld section is assumed to have fractured and cannot resist any additional load.

3.4.2 Pushdown Analysis

Nonlinear models for each building are analyzed through a pushdown analysis in which the displacement of a designated control node in the downward direction is incrementally increased until failure of the building is reached. For each displacement increment, the analysis determines the amplitude of the pre-defined load pattern required to induce this level of displacement and fiber stress-strain responses, nodal displacements, and other behavioral characteristics are recorded. The resulting "pushdown curve" relates the applied roof load to the maximum (downward) displacement of the roof over the entire displacement range. The control node is located at the center of the roof (in plan).

In this study, the load is arranged in one of two patterns: (1) a uniformly distributed snow load over the entire roof and (2) a drifted load. In the uniform load case, the roof load presented in the pushdown curves is the magnitude of uniform roof load in psf, which consists of the roof's

dead, live, and snow loads. More details about the drifted load analysis are provided in Section 3.4.3.

Example pushdown results for the uniform load distribution case are illustrated in Figure 3.7. The last point plotted on the pushdown curve indicates the final converged step in the analysis. The analysis is unable to find a solution after this point because of the precipitous failure of one or more fibers or elements in the structure. The analysis utilizes a robust convergence algorithm that tries multiple solution algorithms and step sizes to find the solution. In addition, the error tolerated in the solution is gradually relaxed to see if a solution can be reached. Should the model fail the first convergence test, the model is run through more convergence tests, each of which has less strict convergence criteria than the previous one. Failure finally occurs once the model fails to pass a convergence test with the most relaxed criteria (corresponding to maximum acceptable error).

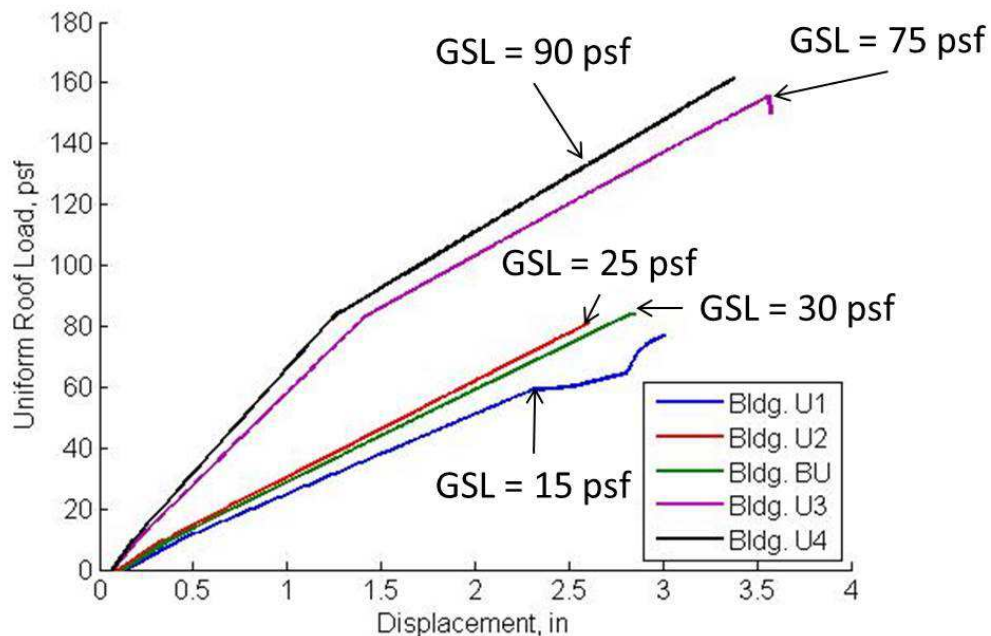


Figure 3.7: Pushdown curves for roofs with varying design ground snow loads

3.4.3 Specific Features of Analysis under Drifted Snow Loads

Due to the nature of drifting, the analysis of drifted snow loads is slightly more complicated than the uniform snow load case. The drifted snow analysis is performed for two directions of wind for each building variation, such that the wind acts either (a) parallel to the joists (denoted \rightarrow) or (b) orthogonal to the joists (denoted \downarrow). The arrows indicate the direction of the wind with reference to Figure 3.3b, such that \rightarrow indicates the wind is parallel to the joists and the snow drift forms against the right edge in the plan view, and \downarrow indicates the wind is acting orthogonal to the joists and the snow drift forms against the building's lower edge in the plan view. These two different wind directions are analyzed separately and, therefore assigned distinct building identifiers in Table 3.2, despite having identical structural characteristics. Although the design for snow drifts with wind in both directions produces the same structure in this case, this is not always true and the roof design often varies due to a difference in multiple factors described below which affect the size and shape of the drift

In the analysis, drifts are assumed to develop in the shape of the idealized distribution defined in ASCE 7-10. The shape of the drift is idealized based on the assumed wind direction, the building's parapet height, the roof size and other factors. As the pushdown load on the roof increases, the base snow load and the drifted snow load increase in the same drifted snow pattern as the snow drift which the roof is designed for from ASCE 7-10.

An obstruction, such as a penthouse, parapet or adjacent roof must be present for drifts to form. This study investigated the effect of the height of the parapet that is present along the perimeter of the buildings. The change in parapet height varies the shape of the drift, which, in turn, affects how the snow is distributed over the joists. According to the drifted shapes assumed in this study, larger parapet heights create taller and longer snow drifts.

The pushdown analysis results for the drifted load cases are plotted with respect to an equivalent uniform roof load. This equivalent roof load is computed for comparison purposes by taking the total load acting on the roof (consisting of snow, dead, and live load) and dividing it uniformly across the area of the roof (even though the modeled load is not uniform). The equivalent roof snow load represents the snow that must be present on the roof for its accompanying drift to be formed (*i.e.* the snow that is blown into the drift).

3.4.4 Model Validation

The models developed in *OpenSees* are validated by comparing model pushdown results with pushdown results from physical experiments on OWSJs performed by Yost *et al.* (2004). Note that the model was not calibrated to match these results so this is a pure comparison of results. Yost *et al.* (2004) tested three different joists of varying depth and configuration (with three specimens each). Figure 3.8 shows good agreement between the modeled pushdown results for the Yost *et al.* joists and the experimental results. In particular, the stiffnesses of the modeled joists and the displacements at ultimate load matched well with the test data. The modeled ultimate loads were at most 9% higher than the experimental results. The models are also able to reproduce the failure mechanism of the joists observed in the experiment: buckling of the critical web member.

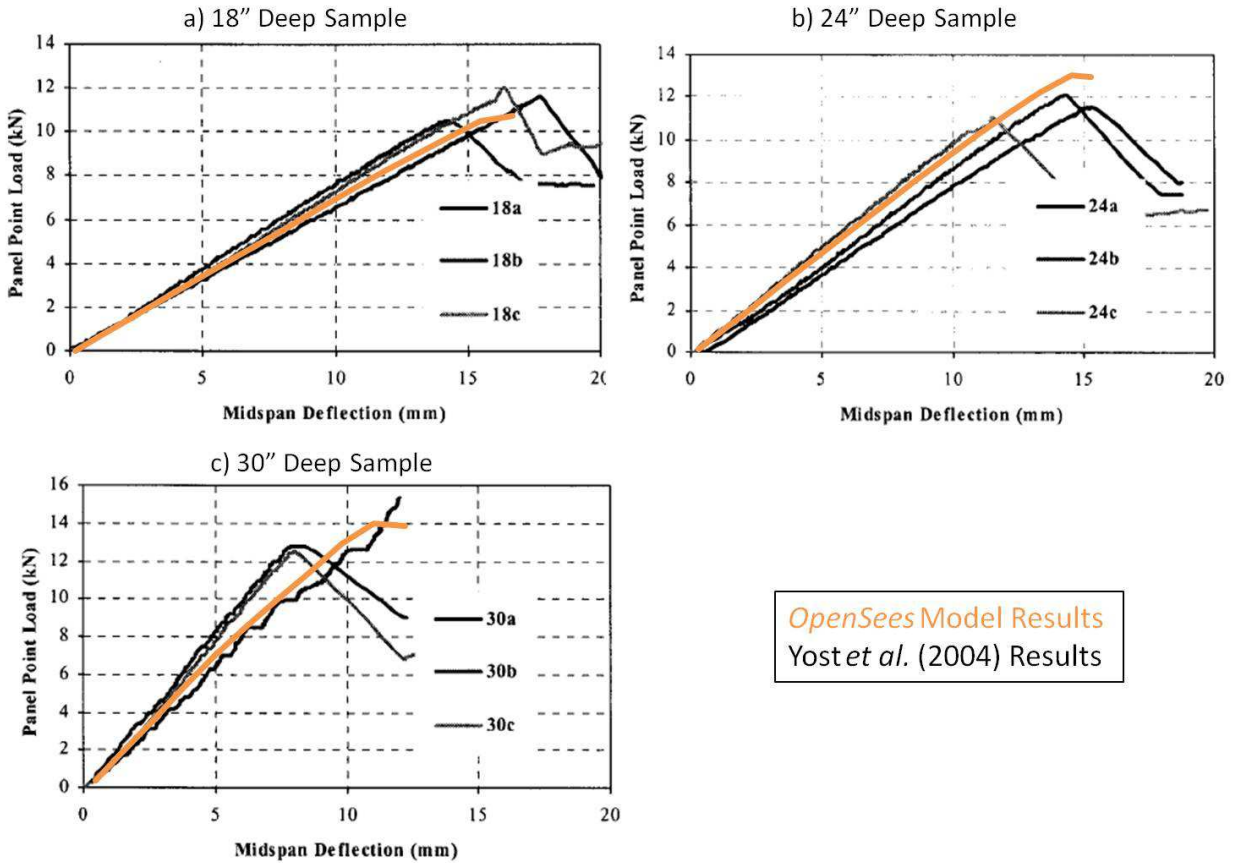


Figure 3.8: Comparison of model results with experimental results from Yost *et al.* 2004

3.5 Response of OWSJ Supported Roofs to Snow Loads

3.5.1 Overview

This section describes the observed responses of the OWSJ roofs, with the discussion presented in three parts. Section 3.5.2 illustrates the failure modes observed in the joists of the various buildings. Then, Sections 3.5.3 and 3.5.4 explore the sensitivity of the response and behavior of the buildings to different design characteristics, with Section 3.5.3 examining the results of the buildings subjected to uniform roof snow loads and Section 3.5.4 examining the results of buildings subjected to drifted roof snow loads.

Table 3.3 summarizes the responses of the different roof structures, providing the basis for the subsequent discussion. Before proceeding, some general observations can be made about

the overstrength of the joists. As documented in the final column of Table 3.3, the SJI-reported joist capacity exceeds the required design strength from factored loads by a factor of around 1.1 to 1.2. This overstrength is due to the discrete nature of the design process in which there is rarely a joist available with a capacity that exactly matches the required load. In addition, we observe that the roofs are consistently stronger than the SJI reported joist capacity, reflecting inherent overstrength stemming from differences between nominal and expected strengths found in the SJI load tables (and perhaps conservatism in the load tables). When combined, these two sources of overstrength produce a factor of safety on the order of 1.3. The reasonable levels of inherent overstrength observed in the results also further support the validation of the appropriateness of the models.

Table 3.3: Summary of pushdown results for OWSJ supported roofs

Bldg. No.	Design Characteristic of Interest	Maximum Roof Displacement at Failure (in.)	Roof Load at Failure (psf)	Ratio of Roof Load at Failure to SJI Load Carrying Capacity (Inherent Overstrength)	Ratio of SJI Load Carrying Capacity to Design Factored Load (Design Overstrength)
BU	Basic Building	2.85	83.9	1.13	1.13
BD1	Basic Building (3.5 ft. Parapet Height) →	0.97	44.9	0.61 (Relative to Top of Drift)	1.05 (Relative to Top of Drift)
BD2	Basic Building (3.5 ft. Parapet Height) ↓	3.90	101.0	0.84 (Relative to Critical Joist)	1.05 (Relative to Top of Drift)
U1	Reduced Ground Snow Load (15 psf)	3.01	77.1	1.25	1.11
U2	Reduced Ground Snow Load (25 psf)	2.61	81.3	1.09	1.16
U3	Increased Ground Snow Load (75 psf)	3.56	155.6	1.11	1.19
U4	Increased Ground Snow Load (90 psf)	3.38	161.6	1.04	1.16
U5	Reduced Joist Span (20 ft.)	2.04	122.0	1.57	1.19
U6	Increased Joist Span (40 ft.)	4.20	82.0	1.11	1.11
U7	Reduced Girder Span (30 ft.)	2.56	79.5	1.07	1.13
U8	Increased Girder Span (60 ft.)	5.78	85.5	1.15	1.13
U9	Reduced Joist Spacing (5 ft.)	2.06	79.8	0.88	1.37
U10	Reduced Joist Spacing (8 ft.)	2.99	94.3	1.22	1.17
U11	Reduced Joist Depth (18 in.)	3.21	80.7	1.13	1.09
U12	Reduced Joist Depth (20 in.)	3.17	91.1	1.14	1.21
U13	Increased Joist Depth (24 in.)	2.94	91.1	1.21	1.14
U14	Increased Joist Depth (26 in.)	2.69	88.9	1.20	1.12
U15	Increased Joist Depth (28 in.)	2.02	72.1	1.02	1.09
U16	Increased D/S Ratio (0.803)	2.02	84.87	1.03	1.12
U17	Increased D/S Ratio (1.268)	4.98	139.1	1.46	1.11
D1	Reduced Parapet Height (2 ft.) →	4.27	128.8	1.87 (Relative to Top of Drift)	1.06 (Relative to Top of Drift)
D2	Reduced Parapet Height (2 ft.) ↓	2.70	68.8	0.72 (Relative to Critical Joist)	1.06 (Relative to Top of Drift)

3.5.2 Observed Failure Mechanisms in Modeled OWSJs

Table 3.4 summarizes the five different types of failure modes observed for the different structures, most of which were brittle in nature.







The first failure mode listed in Table 3.4 involves the shear failure of the top chord occurred at the end-most section in the joist. Although OWSJs are typically idealized as being simply supported, in fact the bolted connection between the girder and the joist provides some resistance against rotation. This bending resistance and the interaction with the joists in the adjacent spans introduces a negative bending moment in the ends of the joist, whereas the middle of the joist is in positive bending. The rapid transition between the regions of negative and positive moment creates a large shear force, which, at the ends of the joist is resisted primarily by the top chord. The bending moment diagram for this portion of the joist is shown in Figure 3.9. Although this failure mode is observed in a number of the analyzed buildings, this type of failure has not been observed in experiments (*e.g.* Yost *et al.* 2004, Buckley *et al.* 2008). However, the experiments consider only one simply supported joist without the girder connection, which alters the bending moment diagram. Physical experiments also consider the moment caused by the eccentricity between the joist-girder connection and the end rod while the *OpenSees* model does not. Although shear forces at the ends of simply supported joists are also quite high, they are likely not large enough to cause failure of the top chord. This theory is confirmed by isolating a single joist from a roof model that, when modeled as the full building, fails in shear; in the single joist model, the negative moment is not present and the failure is governed by other mechanisms. This observation illustrates the potential significance of considering the interaction in the roof system rather than a single joist.

Failure of a welded connection between the web member and the bottom chord also occurred in multiple building models. The connection failure, as described in an earlier section, represents the loss of ability of a weld to carry loads in the axial, shear or moment direction. In our models, the observed welds failed in the direction corresponding to the axial component of

the web member. Failures of welded connections between a web member and a chord are commonly observed in experimental tests (Buckley *et al.* 2008).

Another commonly observed failure mode among the studied buildings is the local buckling of a section between two panel points along the top chord. This failure occurs in the top chord when it is under high amounts of compression and the section begins to move out of the plane of the joist due to the global bending of the roof. This failure mechanism has been observed in case studies (Biegus & Rykaluk 2009) and experimental tests (Buckley *et al.* 2008) in the past.

Table 3.4: Failure modes for OWSJ supported roofs

Bldg. No.	Failure Mode	Location ^c
BU, U1, U2, U5, U9, U11, U12	Shear Failure in End Section of Top Chord	
U3, U13, U14, U15, U16	Welded Connection Failure	
U7, U8, U10, BD2 ^a , D2 ^a	Top Chord Local Buckling at Joist Midspan	
U4, U17, BD1 ^b	Buckling of Critical Web Member	
U6	Buckling of Another (Non-Critical) Web Member	
BD1	Flexural Failure in End Section of Top Chord	

^a In these buildings, this failure occurred in the joist that is under the heaviest load of the drift.

^b In this building, the buckling only occurred in those critical web members that lay beneath the drift

^c Due to the uniform loading, in many cases multiple joists experienced the same failure mode simultaneously.

As described above, the buckling of web members is a common failure mechanism in OWSJs (Yost *et al.* 2004, Buckley *et al.* 2008). In our study, buckling is observed when fibers in the web member (critical or non-critical) exceed the pre-determined buckling strain and rapidly lose strength and stiffness, distributing load to nearby fibers. This leads to progressive failure of the structure.

Finally, a flexural failure of an outer top chord member is observed in one building. This flexural failure occurs under a drifted snow load which causes excessive bending in the end-most

top chord element. When the snow drift is large enough, the bending moment within the chord element becomes large enough for the chord to fail.

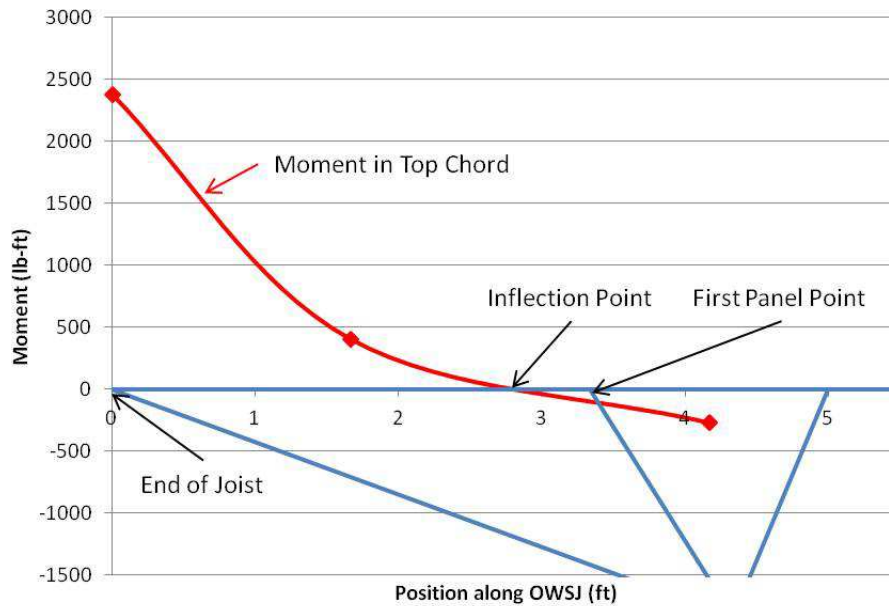


Figure 3.9: Bending moment diagram in the top chord at the end of a joist, positive values on the plot indicate negative bending (*i.e.* tension at the top)

3.5.3 Uniform Snow Load Pushdown Results

3.5.3.1 Effect of Design Snow Loads

The uniform snow load pushdown curves for the buildings with varying design snow loads are plotted in Figure 3.7, showing the increased strength and stiffness in buildings designed for larger loads. In Figure 3.10, the same results are presented, but the load has been normalized by the design load in the SJI load tables. Of particular interest is the observation that the failures all occur at around the same normalized load value, showing consistent inherent overstrength in the different building models. However, referring back to Table 3.4, there are significant differences in failure modes among the different joists. Specifically, the roofs designed for lower snow loads tend to experience shear failure of the top chord, the roofs designed for higher exhibit

web member buckling and or connection failures. In fact, the stronger, heavier joists exhibit some nonlinearities in their response as well.

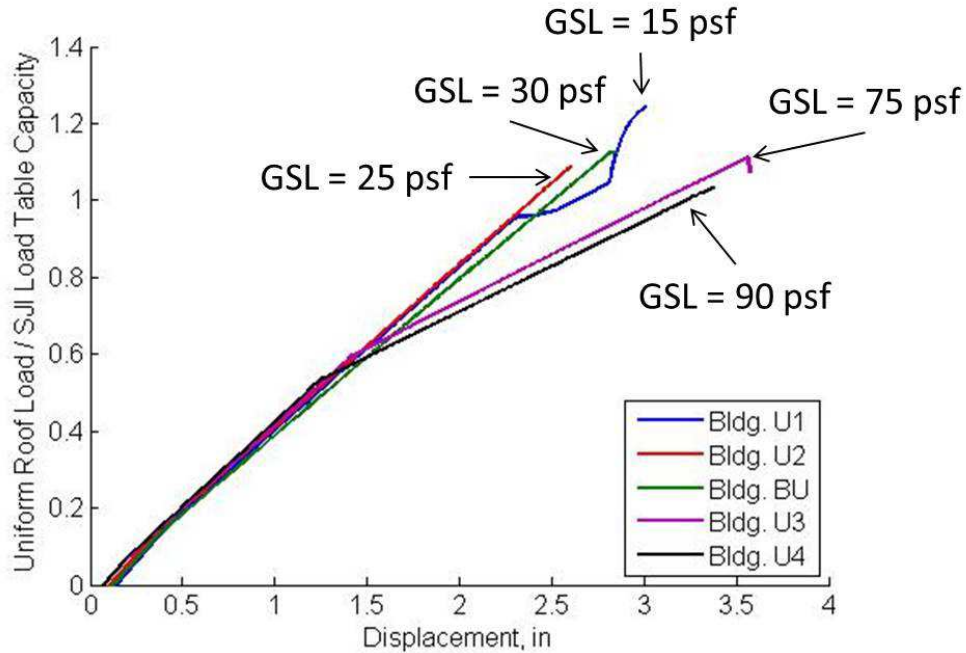


Figure 3.10: Normalized pushdown curves for roofs with varying design ground snow loads

3.5.3.2 Effect of Joist Span

The pushdown curves obtained for the three buildings with varied joist spacing, analyzed under uniform loads, are shown in Figure 3.11, with the normalized curves shown in Figure 3.12. The main trend that can be observed is that the building stiffness decreases as the joist span increases, producing larger roof deflections at the same load level. Although unsurprising, this result has important implications for serviceability failures of the structure that may be associated with excessive deflection. In terms of strength, the results show a trend in which the longer spans are able to resist smaller loads despite the SJI load table's capacities for these joists remaining roughly the same. This seems to be due to the change in failure mode with increasing span length. Shear failure of the top chord dominates at short spans, but web buckling controls at longer spans. Web buckling dominating at longer spans is likely due to the use of deeper joists to

achieve the same load capacity in the longer span joists. Joist depth is explored in more detail in Section 3.5.3.5.

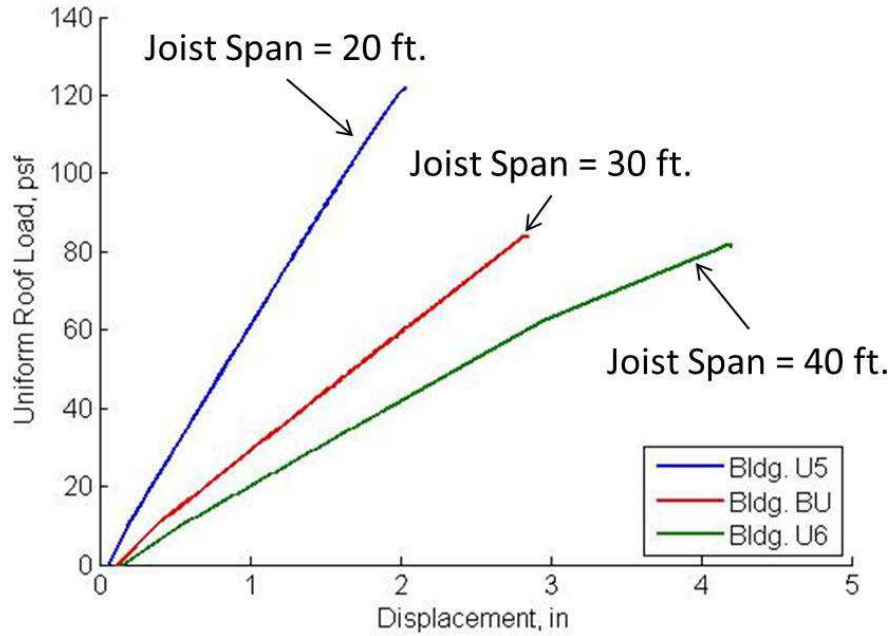


Figure 3.11: Pushdown curves for roofs with varying joist spans

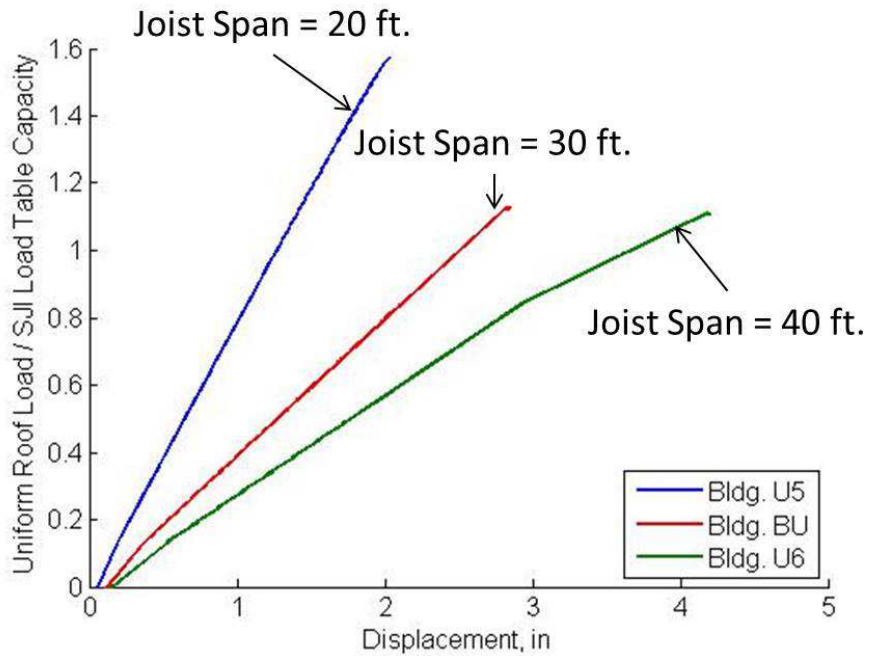


Figure 3.12: Normalized pushdown curves for roofs with varying joist spans

3.5.3.3 Effect of Girder Span

Figure 3.13 and Figure 3.14 illustrate the effect of the variation of girder span on pushdown performance. As with the joist span, the first trend observed is that of the building's stiffness decreases as the girder span increases. The relationship between girder span length and deflections depends on the relative increase of the moment of inertia, I , in the design, relative to the increase in design length of the beam. Girders were designed with the lightest section that satisfied load requirements. Since the girders themselves are assumed to remain elastic in the analysis, the alteration in girder span leads to little impact on the load-bearing capacity of the roof.

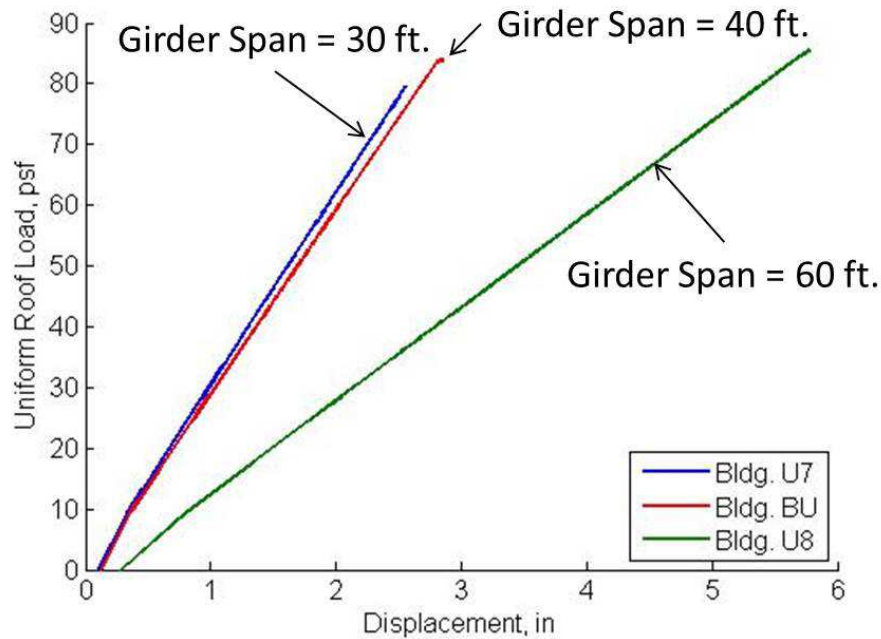


Figure 3.13: Pushdown curves for roofs with varying girder spans

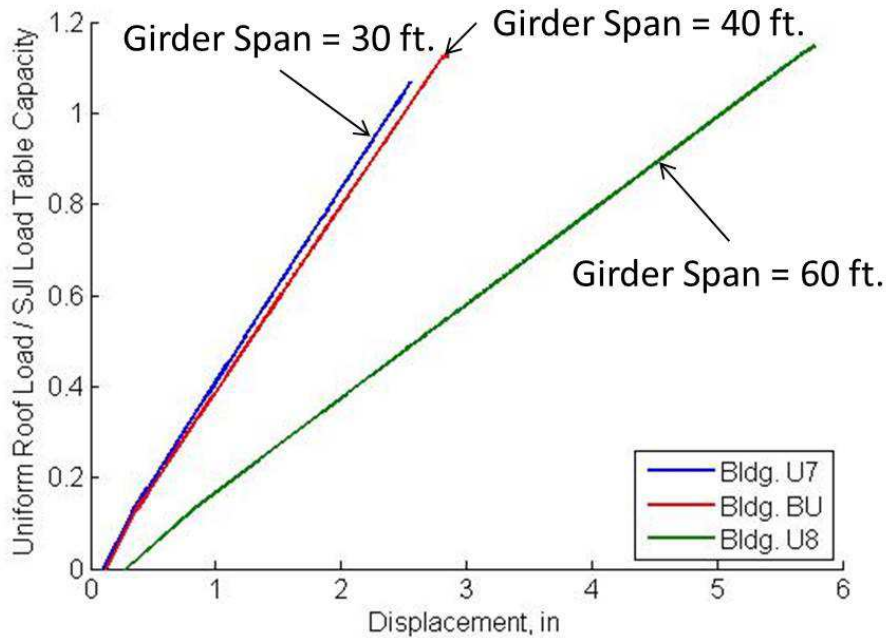


Figure 3.14: Normalized pushdown curves for roofs with varying girder spans

3.5.3.4 Effect of Joist Spacing

Joist spacing does not have a significant influence on the roof performance when the pushdown curves are normalized to the SJI load table values, as shown in Figure 3.16. The buildings also experience similar failure modes. However, when the pushdown curves are not normalized, as shown in Figure 3.15 there is a clear trend of increasing building stiffness as the joist spacing decreases. The worst-performing of these three buildings is Bldg. U9, which doesn't even reach its SJI capacity load due to the increased stiffness of the building causing larger joist interaction effects than usual creating a lower failure load for the building.

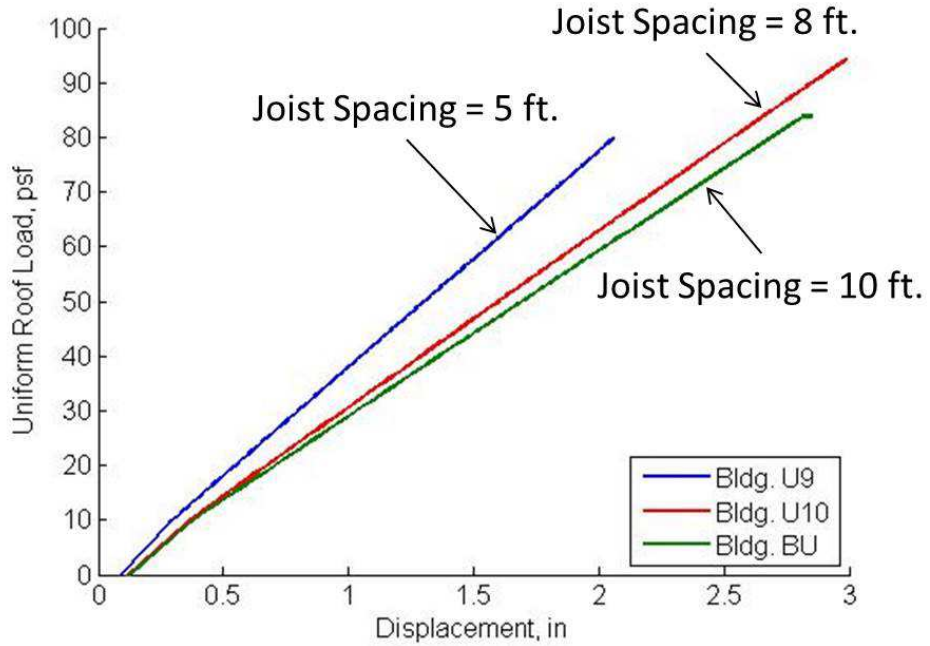


Figure 3.15: Pushdown curves for roofs with varying joist spacing

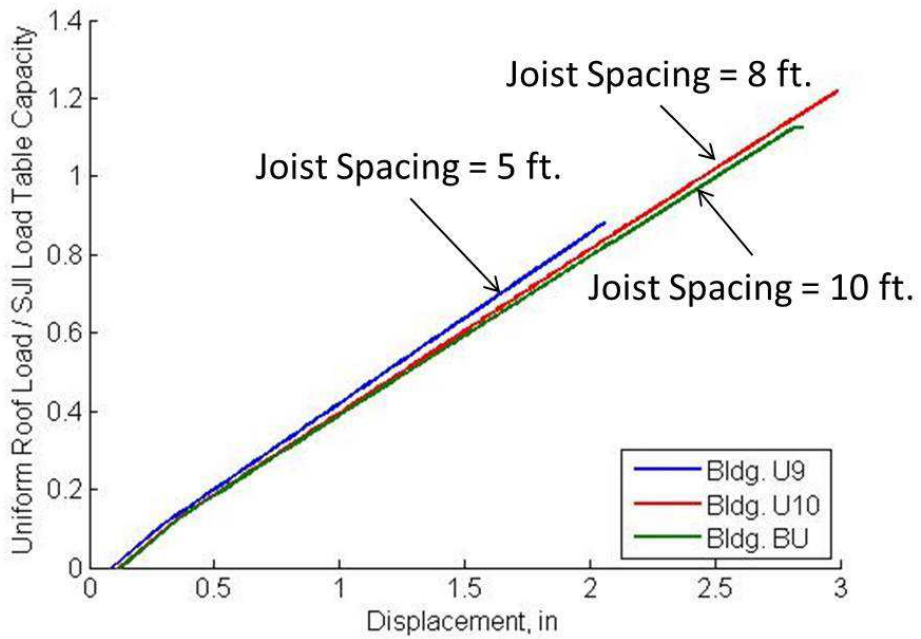


Figure 3.16: Normalized pushdown curves for roofs with varying joist spacing

3.5.3.5 Effect of Joist Depth

Figure 3.17 and Figure 3.18 illustrate the effect of the variation of joist depth on pushdown response. The most apparent trend observed during the variation of joist depth is the increase in building stiffness as the joist depth increases, which corresponds to a decrease in the displacement at which failure occurs (Figure 3.17). In addition, the results show a transition in failure mechanisms with joist depth, wherein the shallower joists seem to fail due to shear failure and the deeper joists fail in the connections. This transition occurs because the web members are oriented closer to perpendicular in the deeper joists, which increases the axial loads in the web members and the connections. As shown in Figure 3.18, the mid-depth joists exhibit the highest (normalized) strength. The deeper the joist, the greater the axial loads are in the welded connections (relative to the applied load), causing the connections to fail under lower overall loads. On the other hand, the shallower joists, experience the shear type failure at lower loads.

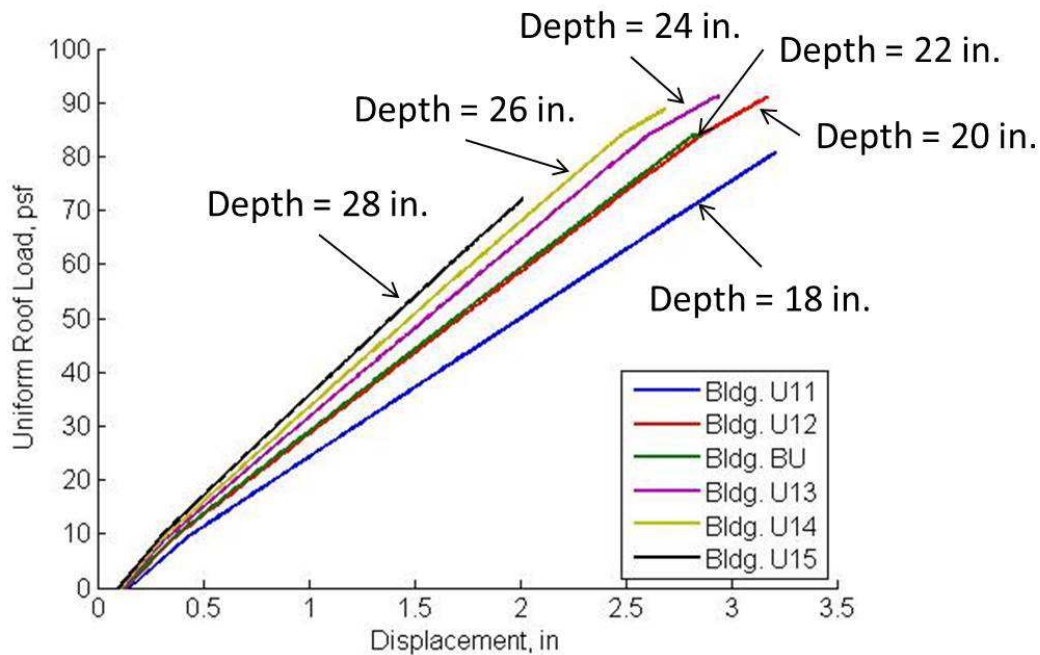


Figure 3.17: Pushdown curves for roofs with varying joist depth

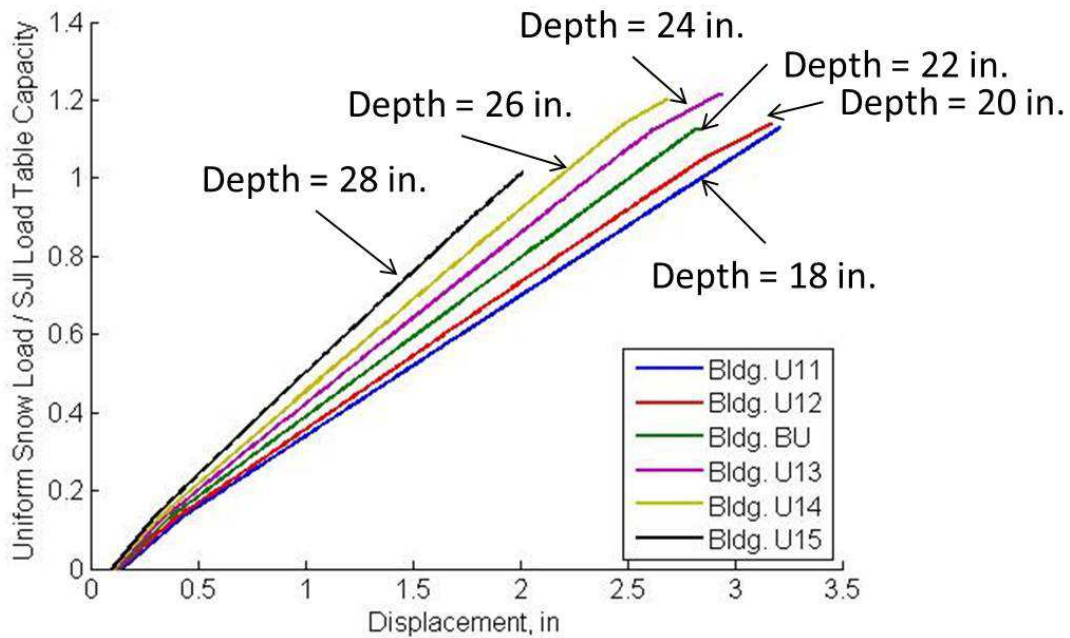


Figure 3.18: Normalized pushdown curves for roofs with varying joist depth

3.5.3.6 Effect of Design Dead-to-Snow Load Ratio

The pushdown curves obtained for Bldgs. BU, U16, and U17, which vary the design dead-to-snow load ratios (D/S), are found in Figure 3.19. The normalized pushdown curves are presented in Figure 3.20. The most clearly defined trend is that the roofs designed for larger D/S ratios tend to be stronger. This trend in strength stems from the way the investigation of D/S is constructed, in which larger D/S ratios are obtained by increasing the dead load. When the results are normalized (Figure 3.20), these differences are reduced, although the building with the largest D/S ratio still has the largest overstrength relative to its SJI defined capacity due to it being an LH-Series joist which would likely have a larger inherent overstrength to compensate for the large loads and spans they're used for. Overall, it seems that many of the key behavior aspects (stiffness, maximum deflection, failure mechanism) have no clear trend and depend more on other properties of the selected joist than on the D/S ratio.

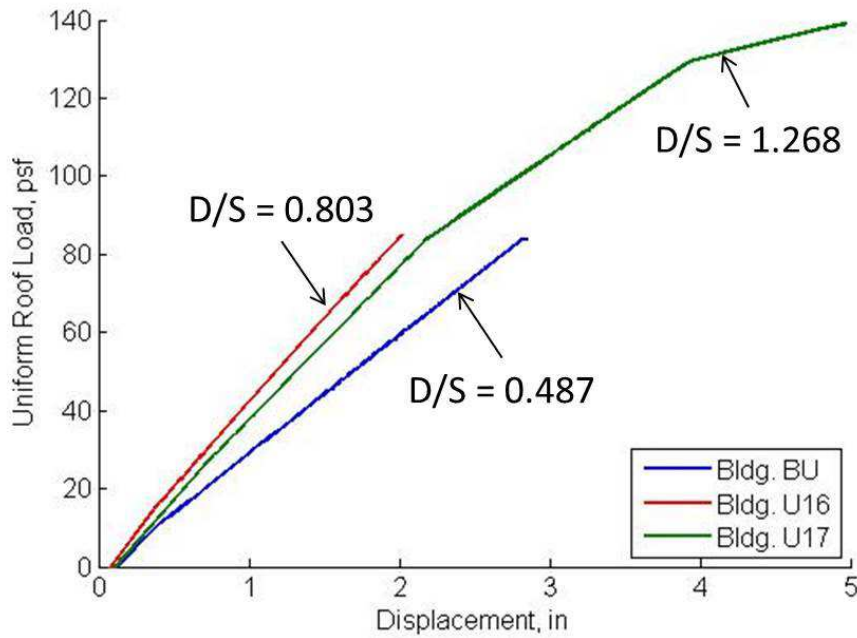


Figure 3.19: Pushdown curves for roofs with varying design dead-to-snow load ratios

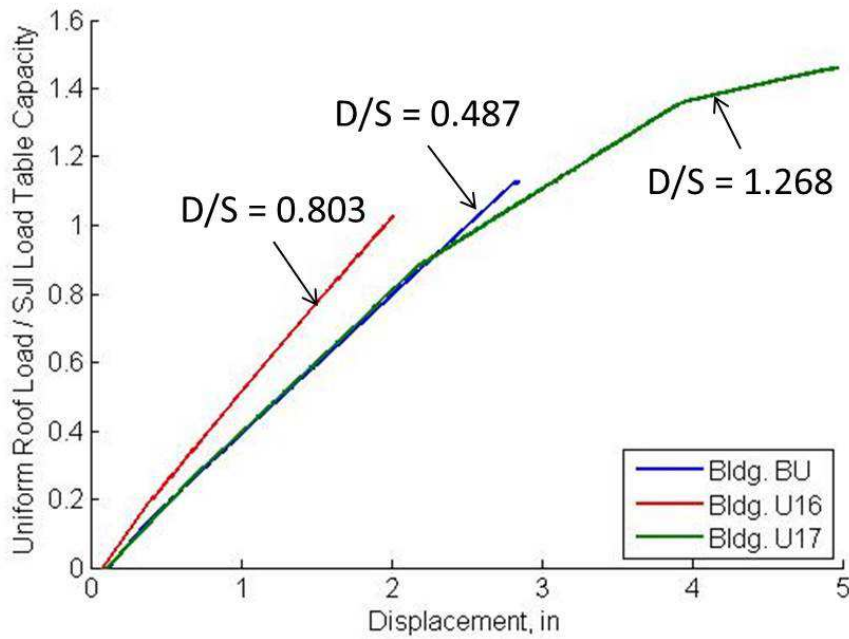


Figure 3.20: Normalized pushdown curves for roofs with varying design dead-to-snow load ratios

3.5.4 Drifted Snow Load Pushdown Results

3.5.4.1 Effect of Parapet Height

Parapet heights of 2 ft. (Bldgs. 19 and 20) and 3.5 ft. (Bldgs. 21 and 22) are examined in this section and pertinent values from the pushdown analyses are presented in Table 3.3 and illustrated in Figure 3.21 – Figure 3.24. Bldgs. D1 and BD1 illustrate the effects of parapet height when the wind direction is parallel to the joists. The design of the two buildings is slightly different due to the difference in parapet height. Due to the assumed wind direction, in this case, the drifting creates a non-uniform loading on joist spans on the windward side of the building. The results indicate that the roof with the smaller parapet height appears relatively stronger than the building with the higher parapet height. This is because the drift generated with a larger parapet height is larger, taller, and longer making it less concentrated over a single OWSJ panel. Due to the larger drift being less concentrated it also results in larger deflections under the same equivalent uniform roof loads. Notice also that Bldg. 19 exhibits significantly nonlinear behavior. This occurs because the more concentrated drift creates a load imbalance over a small section of the building which allows some connections in the localized area to become nonlinear while most of the rest of the building is still in the linear range and is able to carry the load.

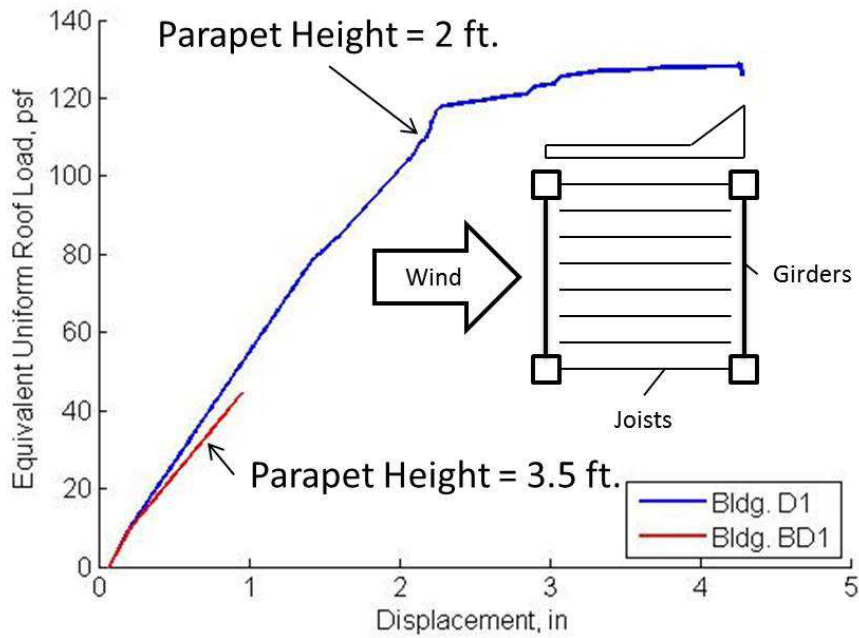


Figure 3.21: Pushdown curves for roofs with varying parapet heights for the assumed wind direction shown

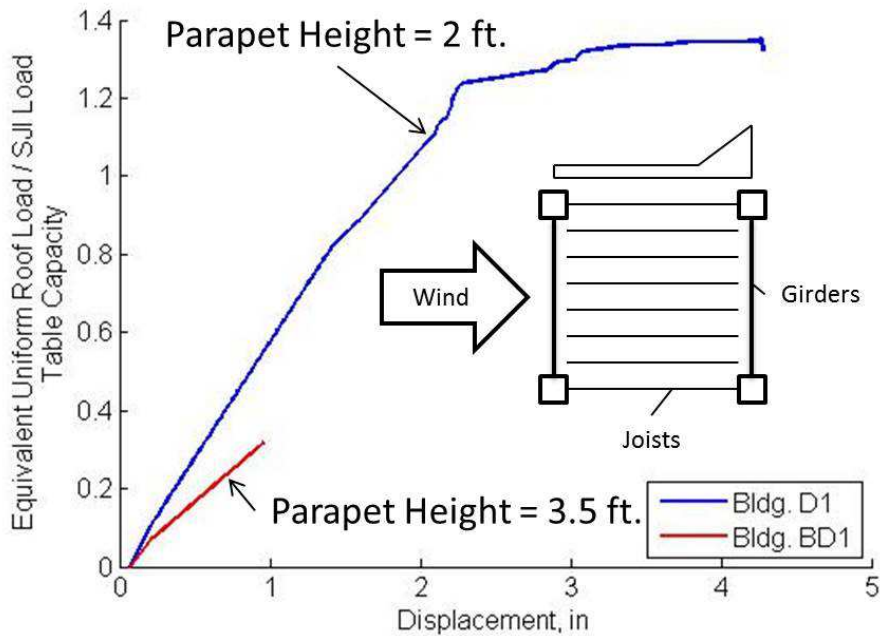


Figure 3.22: Normalized pushdown curves for roofs with varying parapet heights for the assumed wind direction shown

Figure 3.23 and Figure 3.24 shows the same type of result but for the case with the wind blowing in the orthogonal direction. In this case, the drifts are forming in such a way that they are producing a fairly uniform load on the joists parallel to and closest to the parapet (in the windward direction). The equivalent uniform load capacities observed for Bldgs. D2 and BD2 appear very low. However much of the roof load is concentrated on a couple of joists. If we consider the equivalent uniform load acting on only the critical joist, the values are 68.6 psf and 117.4 psf for the critical joists in Bldgs. D2 and BD2 respectively. These values are less than the ultimate loads obtained from the uniform load case of 95.2 psf for Bldg. D2 and 140 psf for Bldg. BD2 determined from the SJI load tables (2005). This discrepancy results from the imbalanced load on the roof causing some torsion in the joists, which initiates the local buckling of the top chord at lower than expected loads. For the same reason, the building with the 2 ft. parapets (Bldg. D2) fails under lower loads, because more uneven loading is present due to the more concentrated drift causing a larger imbalance and local buckling to be initiated earlier.

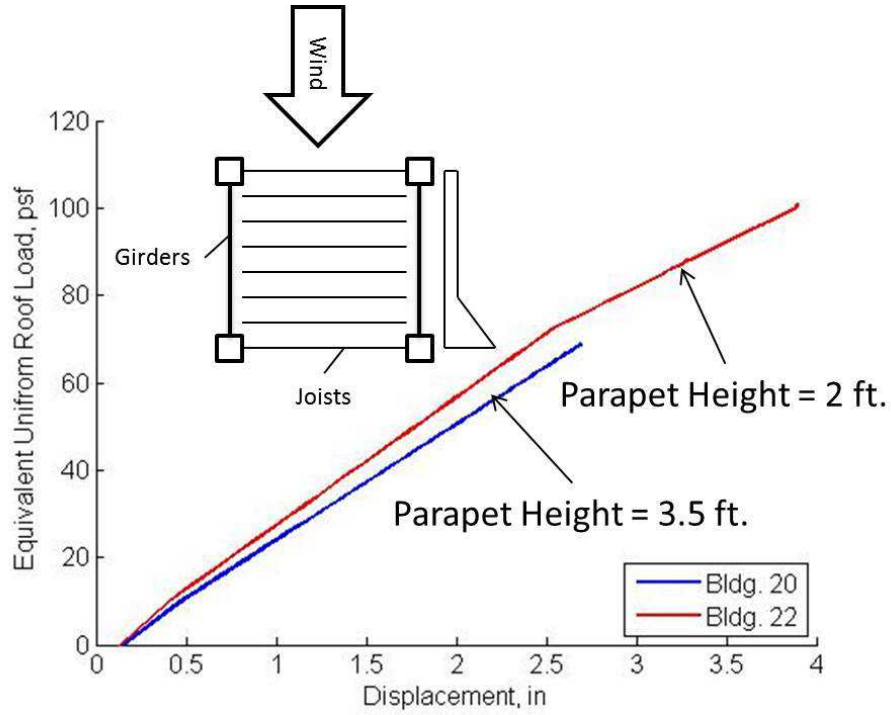


Figure 3.23: Pushdown curves for buildings with varying parapet heights; wind is acting orthogonal to the joists

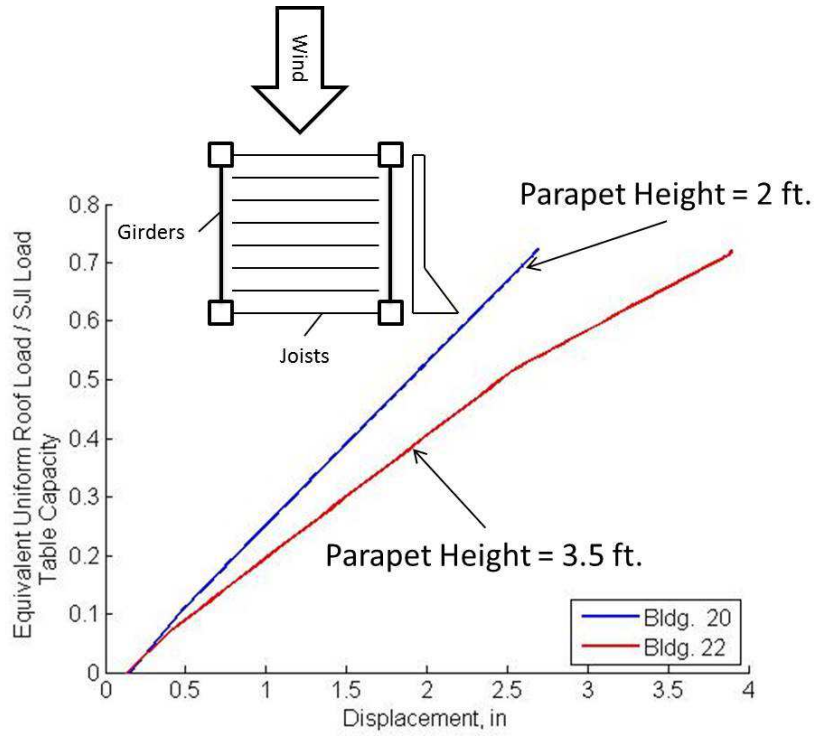


Figure 3.24: Normalized pushdown curves for buildings with varying parapet heights; wind is acting orthogonal to the joists

3.6 Conclusions

The author analyzed the effect of roof loads on 22 buildings by developing nonlinear models capable of capturing the nonlinear response of the structure and the interaction between the different joists in a roof structure. For buildings which are exposed to uniform roof snow loads it was observed that the majority of properly designed buildings will fail at loads which are between 1.03 to 1.25 times the stated capacities of the SJI's load tables. Observations concerning buildings subjected to uniform roof snow loads include the buildings with shorter joist spans achieving a higher load capacity due to the increased stiffness which accompanies this building trait. As well the stiffness of the building is increased when the girder span is decreased, the joist spacing is increased, or the joist depth is increased. This increase in stiffness is a major cause of the roof deflections at failure increasing as the girder span increases or the joist depth decreases. It was also observed that the design dead-to-snow load ratio has little effect on the behavior of the building when compared to other building characteristics.

Buildings were also subjected to drifted snow loads with interesting conclusions being drawn. The ratio of determined capacity load at the top of the drift to SJI load table capacity for buildings with drifts due to wind parallel to the joists varied from 0.61 to 1.87 which highlights the need for OWSJs under drifted loads to be specifically designed by the joist manufacturer for drifted loads as opposed to designing for peak drift load. The ratio of determined capacity acting on the critical joist to SJI load table capacity for buildings with drifts due to wind orthogonal to the joists varied less being only between 0.72 and 0.84. The pushdown analyses under drifted snow loads also showed that when the wind direction is parallel to the joists the behavior of the building becomes nonlinear. Under uniform loads, the components of the OWSJ are highly

optimized; so many elements are stressed to the same level (relative to their capacity). In the non-uniform case, the uneven distribution stresses means that some redistribution of loads can occur even after a single element or connection has failed. These results demonstrate the wide variety of results that can be achieved when buildings are subjected to drifted loads. This highlights the importance of understanding the behavior of snow drifts in order to help make buildings safer. The results may be highly sensitive to the assumed drift distribution.

The key failure mechanisms determined from the analyses included the local buckling of various parts of the top chord, shear failure along the top chord, connection failure between the bottom chord and the critical web member, buckling of web members, and the flexural failure of a top chord element under a drift. Of these mechanisms the shear failure along the top chord is the most concerning due to it not being identified in previous studies, which focused on the response of single simply supported OWSJs.

3.7 Failure Methods

This section is not included in the paper “Response of Open Web Steel Joists under Snow Loads,” but is included here to provide an in-depth look at how the failure methods of the different joists were identified. The post-processing of recorded nodal and element data from the *OpenSees* analysis allow plots to be made which present the stresses in certain fibers within the chords, web members, or end web members, as well as the zero length springs representing the connections. Observations from these results can assist in identifying how the joist, and therefore the structure, failed. The five failure methods observed in the joists in the study are: (1) buckling of a web member, (2) connection failure, (3) shear failure of a chord section, (4) flexural failure of a chord section, and (4) local buckling of a chord element. Each failure method encountered is discussed in the following sections.

3.7.1 *Buckling of a Web Member*

As explained previously, the buckling of web members is a common failure method for OWSJs (Yost *et al.* 2004). This failure method is incorporated into the *OpenSees* model by modifying the material properties of the web members such that they experience rapid strength and stiffness degradation after a buckling strain is reached. The buckling strain was calculated separately for each unique rod or web element in the structure from AISC (2011) equations that describe the flexural and flexural-torsional buckling modes. The lowest buckling strain is calculated and implemented into the model for the specific web member.

To determine whether web buckling failures occurred, the post-processing plot which describes the stress progression of the fibers of interest against the downward displacement of the control node is compared to the buckling strain for each web member calculated by the AISC (2011) equations. Once a fiber within a web member, most likely within the critical web member, reaches the buckling strain and stress the member may be capable of deflecting a little more due to stress redistribution, but will fail shortly after, once all fibers in the section reach the buckling limit. This means that once a fiber within a web member reaches the buckling strain and its accompanying buckling stress the excessive load is redistributed due to the fiber's inability to carry any higher stress. This failure of one fiber propagates to the failure of the entire web member which leads to the inability of the joist and structure to carry higher loads which causes structural failure.

Bldg. U4 illustrates this failure mode. According to the AISC (2011) calculations, the dominant buckling mode of the critical web member is flexural buckling in the plane of the joist. The calculations indicate that buckling occurs when a fiber in the element is stressed in compression at 41 ksi (5.91×10^6 psf). The stress progression of the critical web member is shown

in Figure 3.25 and demonstrates the redistribution of the stresses and strains once fibers 3 and 5 reach the buckling strain and stress, then, as the building continues to deflect, the failure of the member occurs once the entire section reaches the buckling stress and strain.

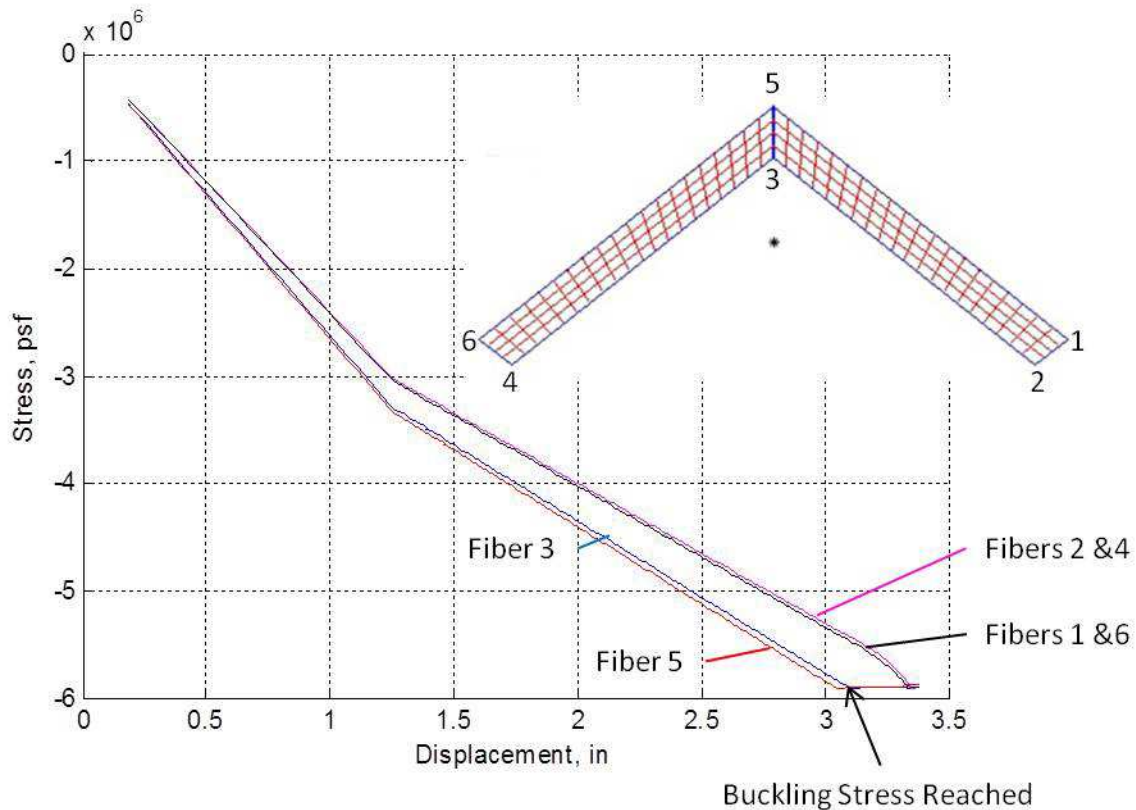


Figure 3.25: Example of a failure due to web buckling, showing stresses in the critical web member of Bldg. U4. Plot shows stress in fibers in web member against the downward displacement of the control node during the analysis

3.7.2 Connection Failure

The failure of a welded connection between a web member and a chord is also commonly observed (Buckley *et al.* 2008). This failure mode is accounted for through the zero-length elements at the connections, which describe the moment-rotation and force-displacement behavior in various directions given the connection's specific weld geometry.

A connection failure is identified by observing the force or moment progression within the connections as the control node's downward displacement increases and comparing the values to the expected and modeled behavior of the connection. Failure of the connection, and subsequently the joist and structure, occurs when the maximum force or moment designated to the connection is achieved. Once the maximum force or moment in a connection is reached it cannot resist any more force or moment causing the resistance to drop to zero and the connection to fail. The maximum force or moment that a connection can achieve is described through a plot which shows the force-displacement (Figure 3.26 shows an example, not included in the figure is the decline of the relationship to zero) or moment-rotation behavior in various directions.

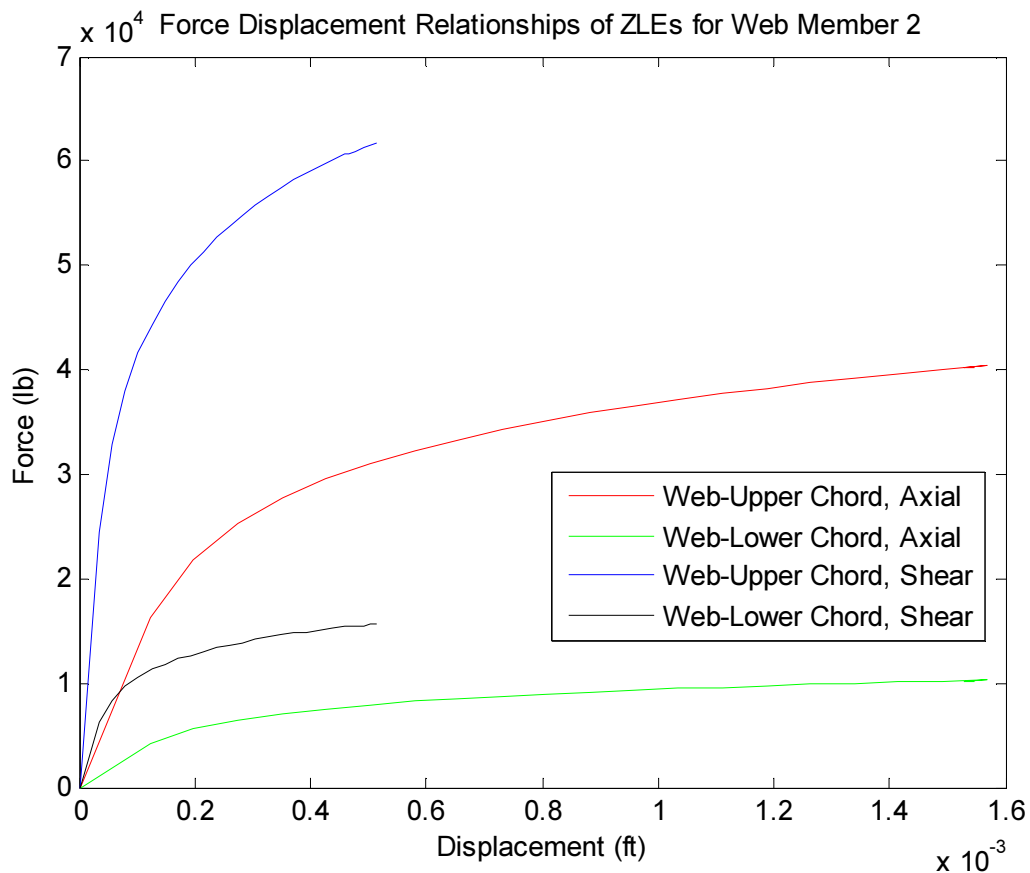


Figure 3.26: Example of modeled force-displacement relationships describing the connection between the web and the top and bottom chords for the critical web member in Bldg. U15. Plot shows the force capacity of the connection under different displacements of the control node

Bldg. U15 provides an example of a connection failure. The progression of the axial force in the connection between the critical web member and the bottom (lower) chord of Bldg. U15 is shown in Figure 3.27 and can be seen to reach a certain axial load before dropping steeply to a force resistance of 0. Through comparison with the appropriate axial force-displacement relationship shown in Figure 3.26, which shows that the maximum force that the web member to bottom (lower) chord can take axially is just over 10,000 lbs., it can be seen that the connection fails at the predicted point, indicating that this is the reason for the failure. Due to this connection's inability to resist axial loads the load through the critical web member cannot be resisted causing an inability for the joist to resist higher loads.

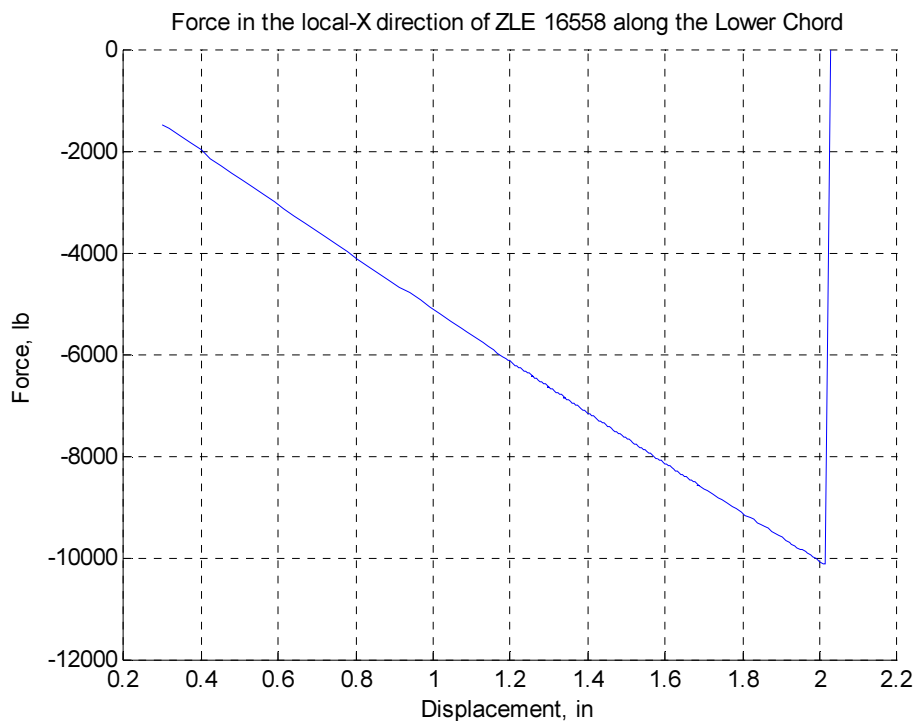


Figure 3.27: Example of an axial force progression through a welded connection between the critical web member and bottom chord of Bldg. U15 leading to loss of load carrying capacity. Plot shows the axial stress in the connection against the downward displacement of the control node

3.7.3 Flexural Failure of a Chord Section

This type of failure only occurs to top chord elements underneath a snow drift. Due to the extreme load concentrated over a single chord section, the bending in that particular section becomes extremely large. The flexural failure of a top chord section occurs due to the neutral axis which the particular top chord section is bending about rising into the top chord itself. Due to some fibers of the top chord being in tension the stresses in the compression fibers increase to large values. This causes an extremely large bending action to take place. Once the bending becomes too large the fibers in compression begin to fail due to a localized buckling failure at the tops of the top chord. This local buckling initiated by large flexural loads barely initiates before the section as a whole loses compression resistance and results in the failure of the OWSJ and the structure.

This failure method is observed by plotting the stress progress in the fibers of a top chord section under pushdown. Bldg. BD1 demonstrates this failure method happening in the section of the top chord that is directly beneath a snow drift. As seen in Figure 3.28, the fibers at the bottom of the section are in tension (positive sign convention) while the fibers at the top are in compression. As the roof deflection increases, the compression applied to the top fibers due to excessive bending increases. Failure finally occurs at a point where the moment is large enough to create a sufficiently large compression in the top fibers which initiates their failure. The failure can be observed in Figure 3.28 through the flat lines at the end of the stress progression in compression for fibers 1-8. Once this failure is initiated the analysis fails convergence and the building fails shortly after.

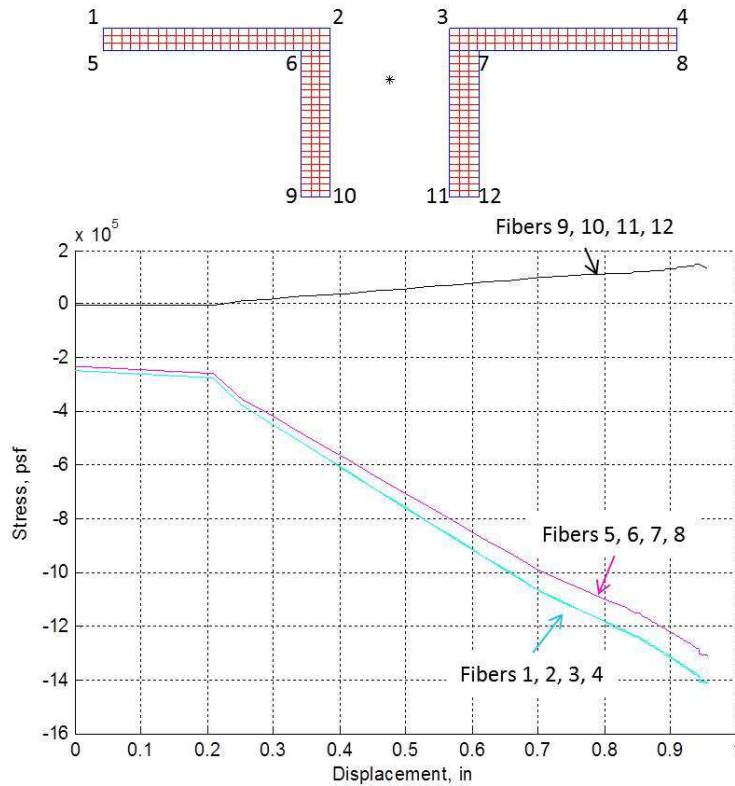


Figure 3.28: Example of a flexural failure in a top chord section of Bldg. BD1. Plot shows the stress progression of the fibers in a top chord against the maximum downward deflection in the roof

3.7.4 Local Buckling of a Chord Element

Similar to the flexural failure of a chord section, the local buckling of a chord element occurs due to excessive compression stresses in the extreme fibers of a top chord section. Unlike the flexural failure, these excessive compressive stresses are not caused by a large bending moment; instead they are caused by the large compressive force within the top chord itself. It is identified through the divergence of the stresses of fibers that are located in the same plane in the global z-axis of the structure, and therefore have similar stresses (*i.e.* fibers 1, 2, 3, and 4 in Figure 3.29) for the majority of the analysis. This divergence of stresses at different sides of the section (*i.e.* the left and right sides, or fiber 1 and 4 in Figure 3.29) indicates that the sides are moving in different directions (one is increasing in tension while the other in compression)

caused by the chord bending in the joist's out-of-plane direction. At a certain point, the analysis does not converge which indicates the failure. However, if the analysis were to continue, the fibers would reach an asymptote in the plot that defines local out-of-plane buckling. The buckling is brought on by the joists being out-of-plumb due to the bending of the horizontal bridging and girders. Once this occurs the load still acts in the downward (plumb) direction causing some torsion in the joist which is resisted by the bridging at some points, but causes small out-of-plane forces on other points of the top chord.

Bldg. U7 fails due to local buckling of the top chord. Figure 3.29 shows the response with many of the fibers grouped together for the majority of the analysis until a certain point is reached when the fibers in the center of the top chord element (between two panel points) begin to diverge. It can be seen that symmetric fibers located on different sides of the section (1 vs. 4, 5 vs. 8, 10 vs. 12, etc...) diverge in different directions and the difference between their stresses becomes larger at an increasing rate demonstrating the approach towards the asymptote which defines local buckling of the section.

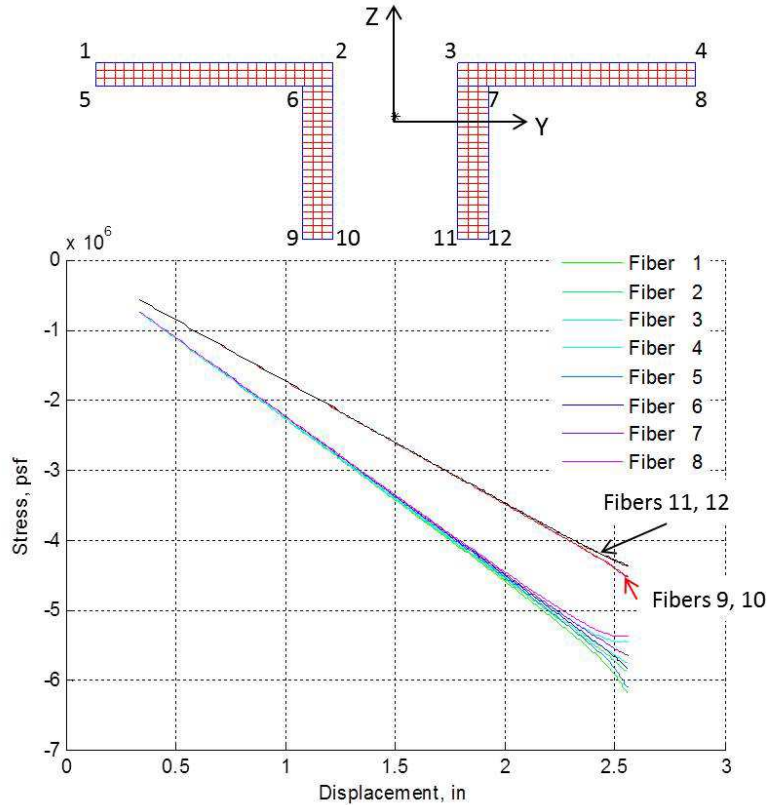


Figure 3.29: Example of local buckling of a top chord element in Bldg. U7. Plot shows the stress in the fibers of the chord section against the downward displacement of the control node

3.7.5 Shear Failure of a Chord Section

Shear failure of a chord section was also observed to occur in the OWSJs studied here. This failure mode was identified by recognizing that the outer-most top chord section (*i.e.* the section between the joist-girder connection and the first panel point) experienced negative bending while the inner chord element adjacent to it (*i.e.* between the first and second panel point) was experiencing positive bending. The negative bending moment in the outer-most part of the chord is due to the semi-rigid nature of the connections between the top chords and girders. The connection resists some bending and creates bending moments across the top chord similar to ones produced by a continuous beam over multiple supports. It can be identified that the inflection point of the bending (*i.e.* the point where there is no bending present, only axial

loads) and the location of maximum slope in the bending moment diagram are located within the outer-most chord section. The position of the bending moment's maximum slope is also known to be the point of maximum shear (due to $dM/dx = V$). Once the shear stress within the section reaches a certain point failure occurs at the point of maximum change in moment leading to failure of both the OWSJ and structure.

Shear failure of the top chord is not recorded in physical experiments of OWSJs; however, this is likely due to these studies only experimenting on a single, simply supported OWSJ instead of on an entire building. In the entire building, the interaction between the other members in the structure and the non-pinned connection between the joist and girders allow forces and moments to be transferred from joist to joist. Another reason why this method may not be encountered in experiments is due to a counteracting moment being formed due to the joist-girder connection and the end web member not intersecting. This eccentricity causes the bearing force on the joist at the support and the tensile force in the end web member to form a moment which would reduce the negative moment found at the ends of the joists. This failure method highlights the importance of considering more than just the joist in future physical experiments. Inclusion of connections to girders or developing tests in a way that can include the interaction between OWSJs is also very important in order to understand the overall behavior of a building and should be thoroughly studied in the future.

An example of identifying a shear failure is found in Bldg. U1. Using the stress distributions within the fiber sections to calculate moments for the outer-most and first inner chord section, as well as the recorded moment at the chord-to-girder connection allowed a bending moment diagram to be formed. The bending moment diagram, shown in Figure 3.30, clearly shows the point of maximum moment change, and therefore maximum shear, produced

within the outer-most top chord section under the loading at failure for Bldg. U1. Due to the steep slope of the bending moment curve produced, this point is taken to be the point of shear failure.

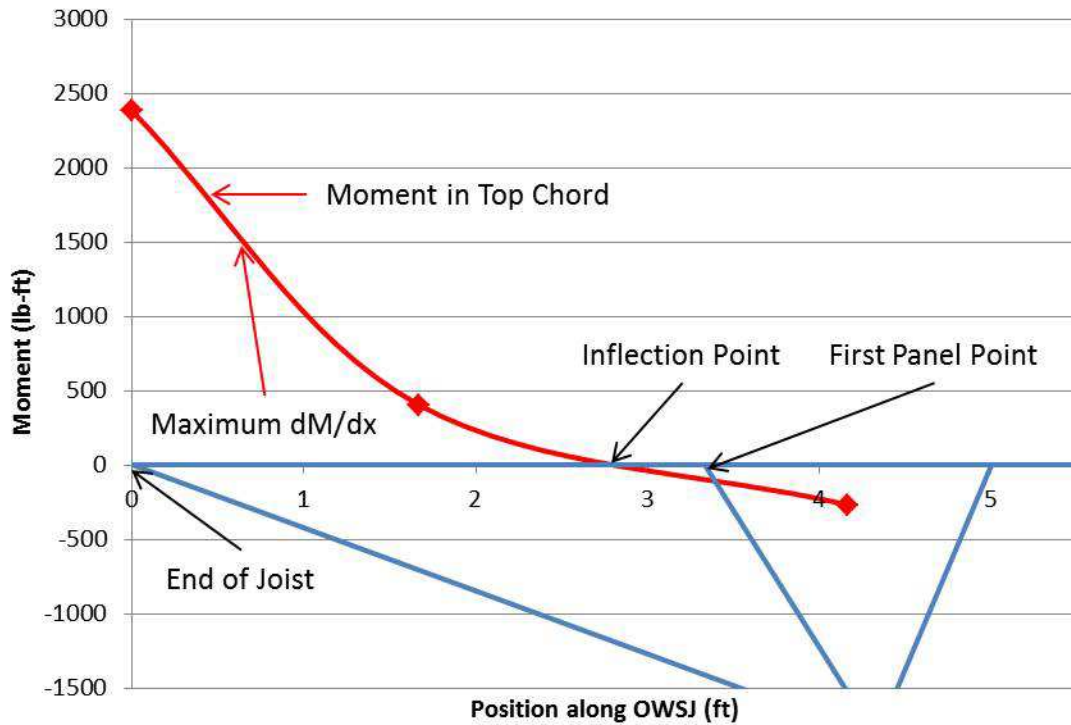


Figure 3.30: Bending moment diagram for the top chord of a Bldg. U1 OWSJ at failure

4 RELIABILITY ANALYSIS OF OPEN WEB STEEL JOIST ROOF STRUCTURES UNDER SNOW LOADS

This chapter is a version of the paper under preparation for publication in *Structural Safety*. The paper is authored by Derek L. Kozak and Abbie B. Liel. This chapter studies the reliability of the structures presented in Chapter 3 through Monte Carlo simulation. The results are compared to Monte Carlo simulations of comparable simply supported W-section beams, as well as with recommended limits from ASCE 7-10.

4.1 Introduction

Roof snow loads prescribed by modern building codes and standards for design are based on probabilistic estimations of ground snow loads (Gulvanessian 2004). In particular, ASCE 7-10 snow load criteria and related state snow load maps (*e.g.*, the Structural Engineering Association of Colorado's map of design ground snow loads for the state) take a map of 50-year recurrence interval snow loads (corresponding to a 2% annual probability of exceedance) as the basis for design ground snow loads (ASCE 2010, SEAC 2007). Once the ground snow load is determined, a design uniform roof snow load is obtained by multiplying the ground snow load by a ground-to-roof conversion factor that depends on the building's risk category, the roof's exposure and slope, and the building's thermal conditions (*e.g.* insulation). In ASCE 7-10, this factor varies between approximately 0.3 and 1.3. The effects of partial and drifting snow loads are also considered. A roof is then designed according to a governing load combination. In places where there are high snow loads, the load combination of 1.2 times the roof dead load, 1.6 times the roof snow load, and 1.0 times the roof live load typically governs roof design (ASCE 2010). Including the roof live load in design with snow is not typically performed in design, however it is considered in all buildings for this analysis providing consistency in the designs.

The load factors for snow design, *i.e.* the 1.6 factor in ASCE 7-10, and similar values in other modern documents, like the Eurocode (Holický *et al.* 2005), are based on structural reliability theory and analysis (Ellingwood *et al.* 1980, Gulvanessian 2004). These factors are intended to ensure that a structure designed according to the provisions achieves a targeted safety index (also known as the reliability index, β) (Ellingwood *et al.* 1980; Bennett 1988) or, equivalently, an acceptably low annual probability of failure (ASCE 2010). The commentary for ASCE 7-10 states the target safety indices to be achieved by buildings designed according to that standard, which depend on the building's occupancy and the consequences of failure. For typical buildings (Risk Category II) and failure that is not sudden and does not lead to progressive damage, the desired safety index is 3.0 over the 50 year lifespan of the structure, which corresponds to an annual probability of failure of 3.0×10^{-5} . A safety index of 3.5 is targeted for buildings in which the failure is sudden (ASCE 2010).

It is an open question, however, whether these target safety levels are actually achieved for real roofs whose design is governed by snow loads. A number of studies have shown that, in some cases, the reliability of actual buildings under snow loads is lower than the code-defined goals. Holický (2007) and Sadvský & Pálež (2008), for example, found that lightweight structures designed according to the Eurocode have safety indices in the range of 2.5 to 3.5 under snow loads, undershooting the Eurocode target reliability level of 3.8. Takahashi & Ellingwood (2005) investigated structures designed according to the Japanese Building Code (JBC) and determined that the reliability index of steel elements under snow loads typically range between 1.0 and 2.5. These authors then compared these results to the ASCE 7 target reliability index of 3.0, suggesting that the JBC is non-conservative. In the United States, reliability analyses of lightweight steel structures and elements have quantified safety indices between 1.35 for

extremely lightweight structures (ratio of design dead to design snow load ratio of 0.2) and 2.75 for moderately lightweight structures (dead-to-snow ratio of 0.67), compared to intended safety indices of 3.0 (Ellingwood *et al.* 1980, Bennett 1988).

As illustrated by Figure 4.1, the reliability of a roof structure depends on the distribution of resistance (*i.e.* the uncertain capacity of the roof) and the distribution of the load (*i.e.* the uncertain demand on the roof over the 50-year life span of the structure). On the capacity side, a number of researchers have suggested that the gap between the achieved and targeted reliability is due to inadequate load factors and faulty ground-to-roof snow load conversion factors used in design, especially for lightweight (low dead load) structures (Bennett 1988, Takahashi & Ellingwood 2004, Holický 2007, Sadovský & Páleš 2008, Holický & Sykora 2009).

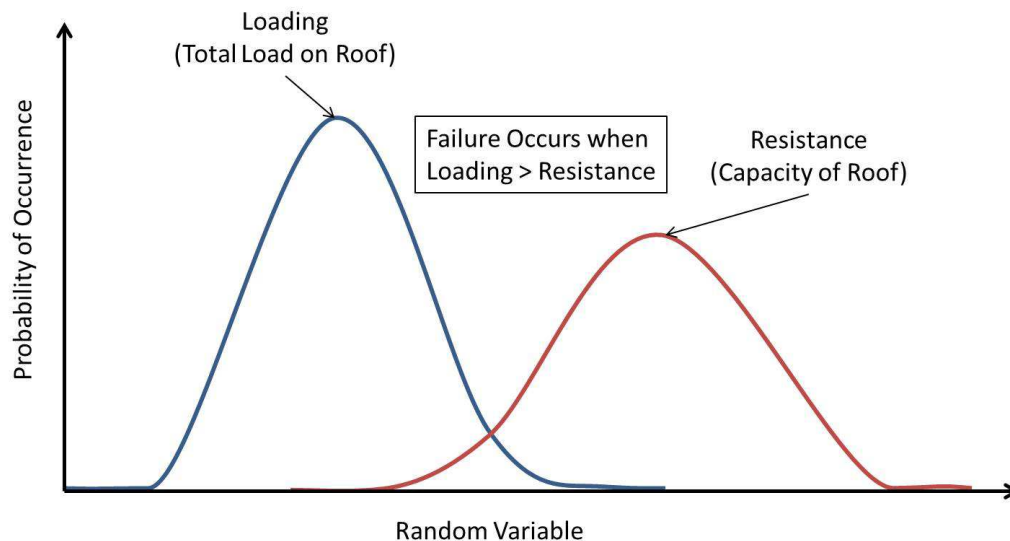


Figure 4.1: Illustration of distributions of loading and resistance impacting computation of structural reliability

The distribution of roof snow loads depends on the variability in ground snow loads at a particular site and the ground-to-roof snow load conversion factor. There are a large number of uncertainties associated with the determination of the ground snow load distribution. In ASCE 7, design ground snow loads are based on historically recorded snow depth data, which are fitted to

a lognormal distribution representing maximum annual snow depth at each site where such data is available (ASCE 2010, DePaolo 2013). This distribution provides the basis for computation of a design snow depth that has a 2% annual probability of exceedance, which is then converted to a ground snow load using an exponential equation fitted based on regression analysis (Tobiasson & Greatorex 1996). Due to ease of measurement, most historical records report only snow depth rather than load. As a result, the ground snow load distribution at a site of interest depends on available recorded data, uncertainties in interpolation between sites where data has been recorded (SEAC 2007), uncertainties and variability in the depth-to-load relationship (DePaolo 2013), and uncertainties in the appropriate shape of the probability distribution to represent the ground snow load (DePaolo 2013, Tobiasson *et al.* 2000). Note that there is a relationship between the load and resistance effects on the reliability assessment; if a different probability distribution is used to represent the ground snow load, this may change the 50-year snow load used in design, influencing the resistance as well as the loading in the calculations.

This study quantifies the reliability of buildings with properly designed roofs under snow loads for various sites in Colorado using structural reliability analysis. The analysis focuses on open web steel joist (OWSJ) roofs, which are lightweight steel truss systems. The vulnerability of OWSJs and truss roofs to snow loads has been observed in a number of notable cases, including the deadly collapse of the Katowice Fair Building (Biegus & Rykaluk 2009), the high profile Hartford Civic Center Arena (Martin & Delatte 2001, Levy & Salvadori 2002), and multiple high school gymnasiums and auditoriums (Geis 2011, Tanzer 2011), as well as warehouses and other structures (Peraza 2000, Lavon & Stivaros 2005, Geis 2011). These failures can have costly impacts on building owners and endanger building occupants (Geis *et al.* 2012, Strobel & Liel 2013). Results for the OWSJ roof structures can be compared to the ASCE

7-10 reliability index targets and against the reliability indices obtained for roof systems composed of simply supported wide flange steel (W-section) beams that are designed to carry similar loads to single OWSJs. This study builds on previous reliability studies, including Takahashi & Ellingwood (2005), Holický (2007), and Sadovský & Páleš (2008), but incorporates nonlinear models of the roof structure to capture response of the roofs up to collapse with detailed probabilistic modeling of the snow load hazard at different locations in the state of Colorado.

4.2 OWSJ Supported Roof Structures

4.2.1 Configuration and Design

Open web steel joists are prefabricated structural elements, composed of steel web and chord members that are arranged in a truss formation, resisting gravity (downward) roof loads through the truss's composite flexural action. OWSJ roof structures are typically arranged such that the joists are supported by wide flange girders or stronger joist systems oriented in the orthogonal direction.

The primary components of the OWSJ itself are the top and bottom chords, and the interconnecting web members, shown in Figure 4.2. Top and bottom chords are typically composed of two continuous back-to-back angle sections that span the entire length of the joist. The end web members are typically rod sections, while the interior web members may be either rods or single angle sections (Buckley *et al.* 2008). Under a uniform load, the top chord is in compression and the bottom chord is in tension (Buckley *et al.* 2008). Global buckling of the chords is generally not of concern due to the connection of roof or floor decking to the top chord at regular short intervals. Both chords are also braced laterally by angle sections or “bridging” between adjacent joists in the out-of-plane direction. The magnitude and direction (*i.e.*, tension

or compression) of the force in a web member depends on the position and orientation of the web member within a joist. For this reason, a highly optimized design may utilize different sections for web members at each position within a joist, particularly if web members are angles.

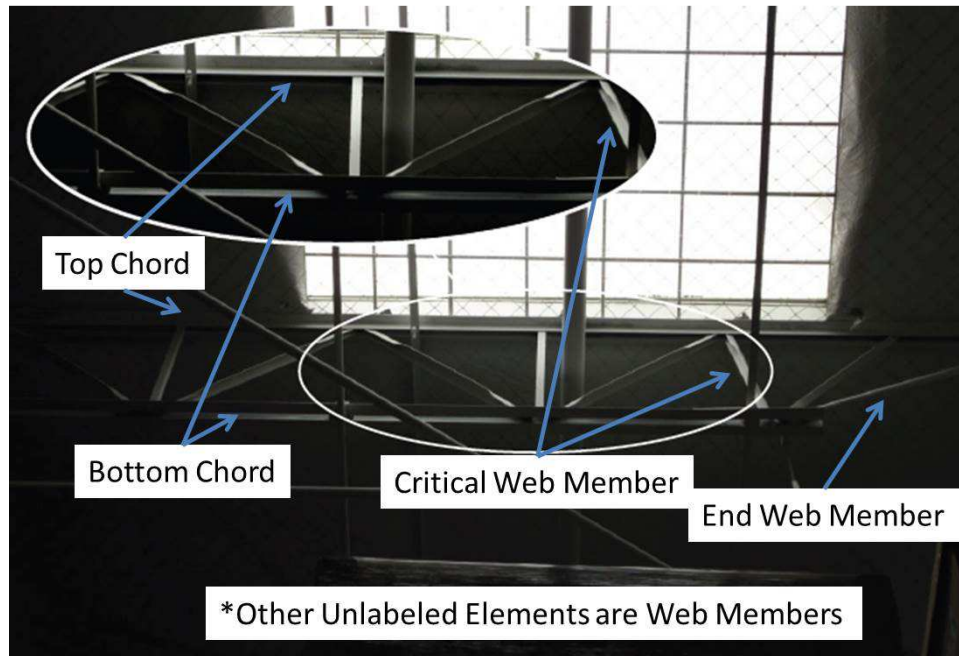


Figure 4.2: Arrangement of the components within an OWSJ (Adapted from Geis 2011)

Web members connect with top and bottom chords at so-called “panel points”. The connections between web and chord members within the joist are typically welded (Yost *et al.* 2006), and the web member lies between the two angles comprising the top or bottom chord. If angled web members are used, the angle must be crimped at the ends to fit in this connection. This crimping creates a variation in the centroid of the web member along its length, which in turn creates an internal moment within the member (Buckley *et al.* 2008). Bolts or welds can be used to connect the joist to the supporting girder (SJI 2005).

The design of OWSJs is proprietary and the U.S. has a number of manufacturers, including Vulcraft, Canam, and Valley Joist. Each joist manufacturer may use different sizes for web and chord members and these design details are proprietary. However, all designs must meet

the requirements set out by the Steel Joist Institute in order to be a certified member of the Steel Joist Institute (SJI 2005). Specifically, the SJI load tables dictate the required uniformly distributed load that a specific designation of OWSJ should be able to withstand. The SJI joist designation describes the joist type, depth, and relative strength. For example, a 22K9 joist is a 22 in. deep K-Series joist with a relative strength of 9, meaning it is stronger than a 22K8 joist, but weaker than a 22K10 joist with the same span (SJI 2005). SJI (2005) also imposes requirements for bridging and connections. The SJI load tables also provide guidance for designing buildings under serviceability requirements as well by listing the maximum unfactored distributed load for each joist such that a deflection of $1/360^{\text{th}}$ or $1/240^{\text{th}}$ of the joist span is not exceeded (SJI 2005).

OWSJ roofs are commonly found in retail, industrial and other forms of construction, such as schools and recreational facilities (Fisher *et al.* 2002, Geis 2011). The popularity of OWSJs in construction can be attributed to the simplicity of the load table based design procedure and the efficiency of the OWSJ system. OWSJs have a highly optimized design and a large bending to weight ratio, due to the mostly hollow web configuration and strategically placed web members (Fisher *et al.* 2002, Yost *et al.* 2004, SJI 2005, Buckley *et al.* 2008).

4.2.2 Representative Buildings Considered in Assessment

4.2.2.1 Overview

This reliability assessment is based on 22 buildings with OWSJ supported roofs that are designed with different characteristics and for different locations in the state of Colorado. All of the buildings are hypothetical, in that they are designed for the purpose of this study, but realistic in the sense that they are designed according to governing provisions (ASCE 2010, SJI 2005) and have characteristics consistent with surveys of real construction (Geis 2011). In the

discussion that follows, we describe first the design and characteristics of the so-called “basic building”. The rest of the buildings are variations on the basic building, in which a single design characteristic is altered to investigate its influence on the structural reliability.

4.2.2.2 *Basic Building*

The basic building is a single story structure with a 30 ft. roof height, encompassing a plan footprint of 300 ft. by 120 ft. As shown in Figure 4.3, the roof structure is laid out with 3 bays of 40 ft. long girders in the short direction and 11 bays of 30 ft. long OWSJs in the other direction, which are supported by the girders. The OWSJs are spaced at 10 ft. on center. These dimensions are typical of OWSJ roof construction.

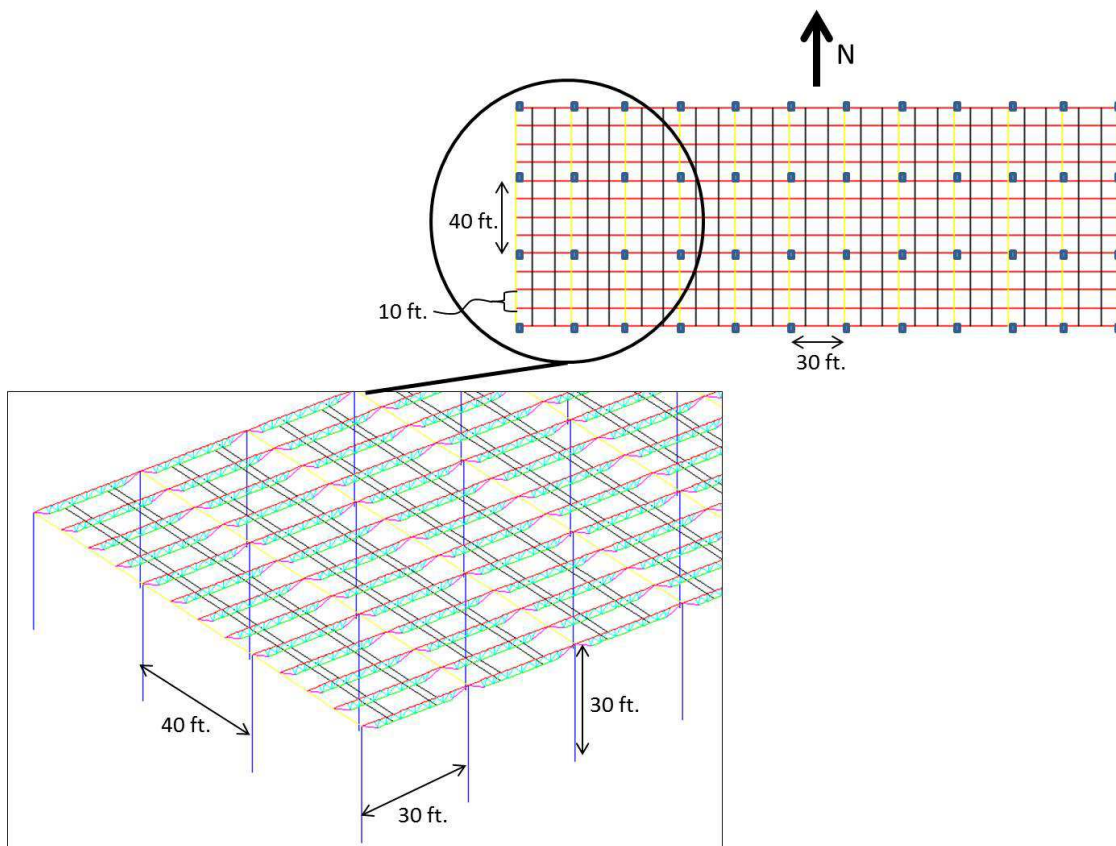


Figure 4.3: Plan view of the basic building with girders in yellow, joists in red, and bridging in black, a 3D view of a portion of the building accompanying

The roof of the basic building is designed for Boulder, CO to withstand the following loads: (1) a roof dead load of 9 psf representing a metal decking covered with composition roofing (Boise Cascade 2009); (2) the dead load corresponding to the self-weight of the roof structure; (3) a roof live load of 20 psf (ASCE 2010); and (4) a ground snow load of 30 psf, from the Boulder Revised Code (City of Boulder 2013). The building is in Risk Category II, indicating standard occupancy. The ground snow load is converted to a roof snow load based on the building's thermal characteristics according to the ASCE 7-10 standard (ASCE 2010). The basic building is assumed to be partially exposed (exposure B), with the thermal characteristics of a building that is not intentionally kept cold. These characteristics are typical of buildings that are not heavily sheltered or highly exposed and are heated with typical amounts of insulation. Based on these assumptions, the uniform design roof snow load is 21 psf.

The first basic building, which is identified in this study as Bldg. BU, has no parapet or other roof protuberances, so the roof design is based on the uniform snow load, in addition to the already mentioned live and dead loads, according to ASCE 7-10 load combinations. A roof design of 22K9 joists supported by W12x82 girders satisfies the design loads. In addition, two rows (per joist) of L2x2x1/8 angles for bridging are provided. Columns are HSS 6x6x3/8 sections. Lateral loads are assumed to be resisted by bridging shown in the north-south direction of Figure 4.3. Serviceability is not directly considered in the design. However, 22K9 joists do end up satisfying a serviceability requirement of deflections not exceeding $1/240^{\text{th}}$ of the joist span purely by coincidence and not by design.

A second basic building is designed, with the same location, building size, shape, and distribution of joists and girders. However, this building has parapets along the perimeter of the roof, and must be designed for drifted as well as uniform snow loads. The design drifted snow

load is determined from ASCE 7-10, assuming a 3.5 ft. parapet and that there are no buildings with higher roofs in the direct vicinity. Because there are no higher roofs in the vicinity, the design can neglect leeward snow drifts and consider only the windward snow drifts against a parapet. Since the SJI load tables are developed for uniform loads, in the case of non-uniform drifted loads the SJI (2005) recommends determining the maximum distributed load in the drift and selecting a joist that has a uniform load capacity larger than that value, although, in reality, this drifted load is not present across the entire span. Two wind directions are considered in this study which accounts for snow drift formation: (1) when the wind is parallel to the joists (\rightarrow , or west-to-east direction in plan) and (2) when the wind is orthogonal to the joists (\downarrow , or north-to-south direction in plan). These two different wind directions are analyzed separately and therefore labeled separately as basic buildings BD1 and BD2, respectively, despite having identical structural characteristics. Bldgs. BD1 and BD2 are designed with 24LH07 joists and W21x62 girders. It should be noted that although this design process is suggested by the SJI, it is also possible, and more common, to request joist manufacturers to design and create custom OWSJs which account for specific design loads, including a drifted snow distribution (SJI 2005).

4.2.2.3 Building Variations

Table 4.1 lists the 17 buildings considered in the reliability assessment of buildings under uniform snow loads. Each building is a modification of Bldg. BU, and for each revised set of design characteristics, the roof's OWSJ, girder, and bridging are redesigned.

The assessment considers the effect of six building design characteristics: (1) design ground snow load (GSL), (2) joist span length, (3) girder span length, (4) joist spacing, (5) joist depth and (6) ratio of design dead-to- snow loads. The first five characteristics vary substantially in roof design of different structures. The design dead-to-snow load ratio is varied to investigate

the effects of lightweight OWSJ buildings, compared to less lightweight structures. In Table 4.1, Bldgs. U1, U2, U3, and U4 are located in different communities in Colorado, leading to different design ground snow loads. In Bldgs. U5 and U6, the joist span is varied from the 30 ft. span of Bldg. BU; note that this span variation also leads to slight changes in the building footprint, as reported in Table 4.1. Similarly, Bldgs. U7 and U8 have different girder spans than Bldg. BU. The next design variable considered, in Bldgs. U9 and U10, is the joist spacing. Altering the joist spacing also changes the loads on the joists, affecting the load pattern on the girders. Bldgs. U11-U15 explore the impact of different joist depths. For this variable, the design loads and building configuration are unaltered, so these joists represent alternative solutions to the same design loads. Finally, to investigate the impact of relative variations in design dead-to-snow load ratios (D/S), the basic building is redesigned for Boulder, CO with different dead load assumptions (represented physically by different roofing systems) in Bldgs. U16 and U17. Bldg. BU is designed for a roof snow load of 21 psf and a roof dead load of 9 psf, providing a D/S of 0.48. Bldg. U16 has the same design roof snow load, but a larger roof dead load of 15 psf for a D/S = 0.80. Similarly, Bldg. U17 is designed with 25 psf of roof dead load yielding a D/S of 1.26. For the D/S investigation, care was taken to ensure the selected joists have consistent levels of overstrength between 1.11 and 1.13 in terms of the ratio of provided to required capacity.

Table 4.1: Buildings subjected to uniform snow loads

Bldg. No.	Location	D/S	Building Length (ft.)	Building Width (ft.)	Joist	Girder	Variation from Basic Building
BU	Boulder, CO	0.48	330	120	22K9	W14x82	Basic Building
B1	Lamar, CO	0.67	330	120	22K7	W12x79	15 psf Design GSL (SEAC 2007)
B2	Denver, CO	0.51	330	120	22K9	W24x55	25 psf Design GSL (City of Denver 2011)
B3	Keystone, CO	0.21	330	120	24LH09	W27x84	75 psf Design GSL (Summit County 2013)
B4	Copper Mountain, CO	0.18	330	120	24LH11	W27x94	90 psf Design GSL (Summit County 2013)
B5	Boulder, CO	0.46	340	120	20K3	W16x50	20 ft. Joist Span
B6	Boulder, CO	0.51	360	120	24LH07	W18x86	40 ft. Joist Span
B7	Boulder, CO	0.48	330	120	22K9	W18x46	30 ft. Girder Span
B8	Boulder, CO	0.48	330	120	22K9	W27x94	60 ft. Girder Span
B9	Boulder, CO	0.47	330	120	22K4	W18x60	5 ft. Joist Spacing
B10	Boulder, CO	0.48	330	120	22K7	W12x79	8 ft. Joist Spacing
B11	Boulder, CO	0.48	330	120	18K10	W14x82	18 in. Joist Depth
B12	Boulder, CO	0.49	330	120	20K10	W14x82	20 in. Joist Depth
B13	Boulder, CO	0.48	330	120	24K8	W14x82	24 in. Joist Depth
B14	Boulder, CO	0.48	330	120	26K7	W14x82	26 in. Joist Depth
B15	Boulder, CO	0.48	330	120	28K6	W14x82	28 in. Joist Depth
B16	Boulder, CO	0.80	330	120	28K12	W24x62	0.80 D/S Ratio
B17	Boulder, CO	1.26	330	120	20LH06	W24x68	1.26 D/S Ratio

Table 4.2 lists the buildings investigated under drifted snow loads. Two different parapet heights are considered in the design and analysis of the buildings: 2ft. (Bldgs. D1 and D2) and 3.5 ft. (Bldgs. BD1 and BD2). Each parapet height is then analyzed considering separately two different wind directions: west to east, denoted \rightarrow , and north to south, denoted \downarrow (where the directions refer to Figure 4.3). Drifts are assumed to develop on the windward side of the parapet, along the downwind edge of the parapet only. The analysis also assumes that the drifts form the idealized triangular shape described in ASCE 7 (2010).

Table 4.2: Buildings subjected to drifted snow loads

Bldg. No.	Design Dead/Snow Loads	Building Length (ft.)	Building Width (ft.)	Joist	Wind Direction	Parapet Height (ft.)	Variation from Basic Building
BD1	0.552	330	120	24LH07	→	3.5	Basic Building
BD2	0.552	330	120	24LH07	↓	3.5	Basic Building
D1	0.542	330	120	20LH06	→	2	2 ft. Parapet Height
D2	0.542	330	120	20LH06	↓	2	2 ft. Parapet Height

4.2.3 Nonlinear Response under Snow Loads

4.2.3.1 Modeling Approach

The response of each of the different OWSJ roof structures under snow loads is simulated using a nonlinear model created in *OpenSees* (see Chapter 2). To facilitate the modeling, the dimensional details of specified OWSJs were provided by a well-known manufacturer, but neither the name of the manufacturer nor the detailed joist specifications are reported here to maintain confidentiality.

The models employ (1) nonlinear displacement-based beam-columns to represent the web and chord components within the OWSJs, (2) zero-length spring elements to simulate the connections at the panel points in the OWSJs, and the connections between the joists and girders, and (3) elastic steel elements to describe the girders, columns, and bridging. The nonlinear beam-column elements are composed of fiber sections; each fiber section is assigned an assumed stress-strain response and finite element interpolation equations are used to describe the behavior between the fiber sections and maintain compatibility requirements (Perea & Leon 2008). In these models, the fiber geometries at each section is arranged to mimic the shape of the section of interest. In the case of the crimped web members, different fiber geometries are assigned to the crimped (ends) and un-crimped (middle) sections. The nonlinear stress-strain response of each fiber is based on the Dodd & Restrepo-Posada (1995) material model; this model captures

steel response from small deformations until fracture occurs. In addition, the stress-strain material response of the web members in compression is modified to capture buckling. Specifically, AISC (2011) buckling equations are used to determine the stress and strain at which buckling occurs. After this point, the buckled fiber's load carrying capacity is assumed to decay following the recommendations of Elnashai & Elghazouli (1993).

The model also tracks the response and failure of the connections between components of the OWSJ and between the joist and the girder, which are represented by nonlinear zero-length spring elements. The weld connection properties depend on the weld geometry and are modeled using the Lesik & Kennedy (1990) weld material model for E70XX electrodes. In this study, all models assume two ½" A307 bolts are provided to connect the joist and the girder. The springs representing the bolted joist-to-girder connections are modeled to follow bolt shear and pullout equations (Chan & Chui 2000, SJI 2005, ASTM 2012). These models take into account many of the nonlinearities present in the connections which are otherwise neglected in analyses by joist manufacturers who generally assume pinned connections (Yost *et al.* 2004, Canam 2005). More details are provided in Chapter 2.

Although model validation is difficult due to the lack of laboratory tests or previous analytical studies, the authors modeled three joists that have been tested experimentally by Yost *et al.* (2004) to examine the capabilities of the developed models. Analytical results showed good agreement with the tests, in terms of the load and deflection at failure. In addition, in all three cases, the joist model correctly predicted the failure mode observed experimentally.

4.2.3.2 Pushdown Analysis and Results

The response of each building roof model is analyzed through a displacement-controlled “pushdown” procedure. In pushdown, a load distribution, which can define a uniform or drifted

snow pattern, is applied to the roof. The magnitude of the load is statically increased, maintaining the same load distribution, until a specified deflection of the control node is reached. The control node is located at the center of the middle-most joist in the structure. The specified deflection is then increased and the load adjusted accordingly, repeating the analysis at successive deformation levels until the model fails to converge due to a sudden decrease in load capacity that represents the failure of one or more elements within the model. Due to the highly optimized features of the joist design, failure of one element does tend to lead to the loss of load bearing capacity in the entire joist, as observed in experimental studies, for example, by Yost *et al.* (2004). In addition, since all the joists in the roof are identical, failure of one joist precipitates a progressive failure that will likely follow as described by Takahashi & Ellingwood (2004).

Pushdown results are presented by plotting the control node displacement on the x-axis versus the amplitude of the load present at that displacement on the y-axis, as illustrated in Figure 4.4. In the uniform load analysis, the load represents the sum of the dead, live and snow loads applied to the roof. In the drifted load analyses, the drifted snow load is converted to an equivalent uniform snow load by taking the total drifted snow load on the roof and dividing it by the roof area. The plotted load represents the sum of the dead, live, and equivalent snow loads applied to the roof. The pushdown curve can then be used to determine the capacity of the building and deflection of the roof under different load levels.

Results of the pushdown analyses for buildings subjected to uniform and drifted snow loads are provided in Figure 4.4 and Figure 4.5, respectively. Consider first Figure 4.4. The pushover response for the basic building, Bldg. BU, indicates that it failed at a uniform roof load of 83.9 psf and a displacement of 2.85 in. This load is 1.13 times the design factored load of 74.5 psf, indicating a capacity of 74.9 psf for live load and snow load beyond the 9 psf roof load.

Figure 4.4a illustrates the pushdown curves for roofs with different design ground snow loads. Unsurprisingly, the buildings designed for snowier locations are also stronger and stiffer. Also, in the stronger roofs, nonlinearity in the behavior appears due to the larger loads applied to the joists causing some connections and materials to reach nonlinear ranges. The pushdown curves for buildings with different joist spans are shown in Figure 4.4b. The roofs with larger joist spans are more flexible, deflecting more before failure occurs. Note also that the shortest joist span building appears significantly stronger, despite the same design loads. This variation in strength comes from the predominant failure mode in the shorter joist: web member buckling rather than top chord shear failure. The variation of girder span, the results of which are presented in Figure 4.4c, has little impact on the failure load because the roof load carrying capacity is controlled by the joist, not the girder. However, girder span and flexibility does have the predicted influence on roof deflection. Next, the effects of joist spacing on the pushdown results are shown in Figure 4.4d. As the joist spacing increases, the stiffness of the structure also increases. Figure 4.4e illustrates the impact of joist depth, which increases the stiffness, but does not significantly alter the load carrying capacity. Due to the change in the configuration of the joist components, changing joist depth (for the same design load) also brings about a different failure mode. The deepest joists (Bldgs. U13, U14, and U15) failed at the welded connection between the critical web member and the chord, whereas the shallower joists experienced other types of failures. The final building variation, the variation of the design dead-to-snow load ratios (D/S), results in the pushdown curves seen in Figure 4.4f. There is no direct trend in stiffness due to the varying joist depths and required capacities used for these joists. However, as expected, the joist capacity increases as the D/S ratio increases. This is observed through Bldg. BU (D/S = 0.49) has a total

roof load capacity of 83.9 psf, Bldg. U16 ($D/S = 0.80$) has a total roof load capacity of 84.9 psf, and Bldg. U17 ($D/S = 1.27$) has a total roof load capacity of 139.1 psf.

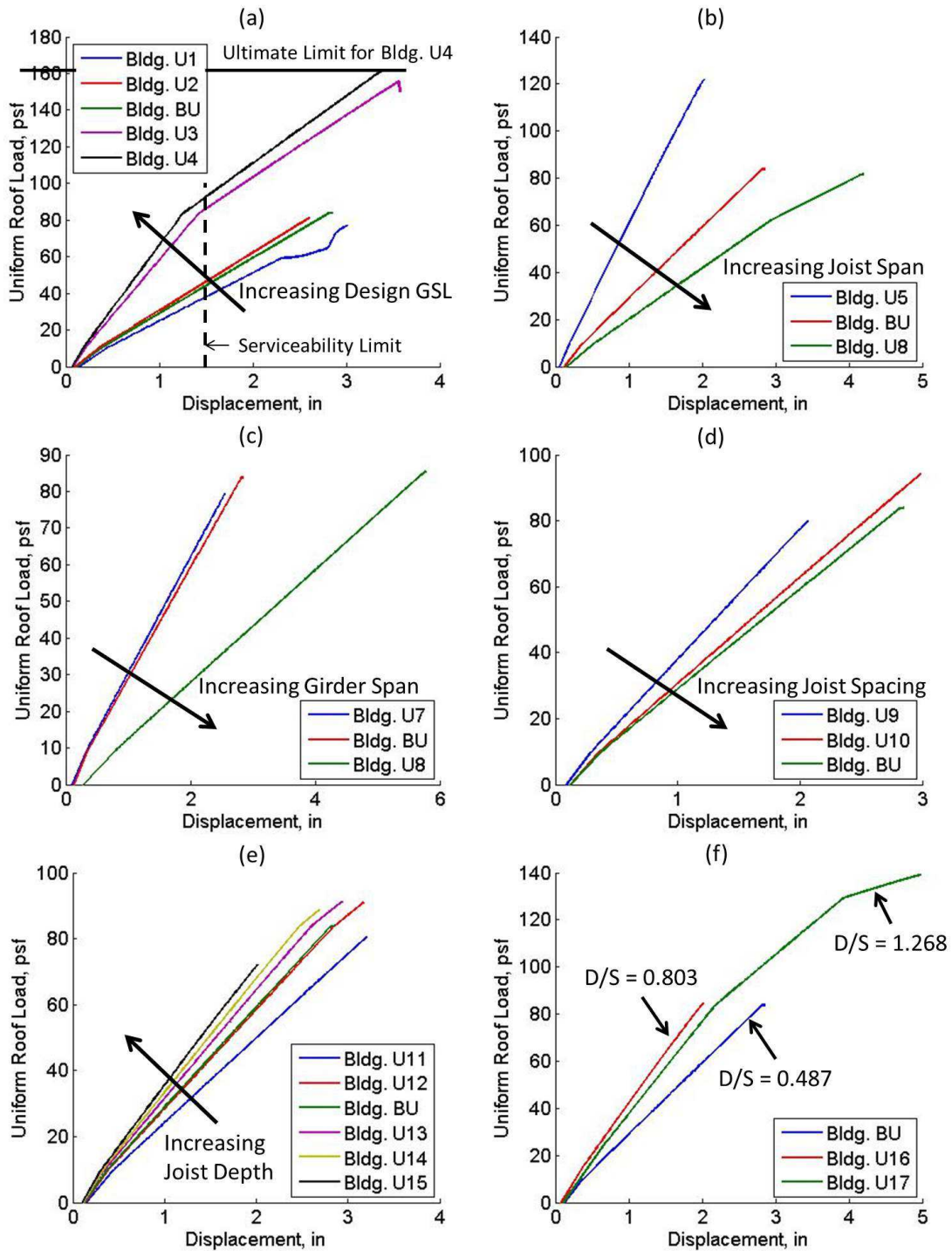


Figure 4.4: Pushdown curves for roofs under a uniform snow load with varying a) design ground snow load (including examples of limit states), b) joist span, c) girder span, d) joist spacing, e) joist depth, and f) design dead-to-snow load ratio

Figure 4.5 explores the effect of snow drifting on roof structures with two different parapet heights. The roofs with higher parapets are designed for a larger drifted load. As mentioned previously, the analysis considered the effect of wind acting in two different directions: (1) west-to-east, *i.e.* parallel to the joists, as shown in Figure 4.5a; and (2) north-to-south, *i.e.* orthogonal to the joists, as shown in Figure 4.5b. In the first case, the drifting develops a non-uniform distribution of snow on each joist as shown by the line drawing. In the second case, the drifting leads to non-uniform distributions of snow between the joists, whereby the joists situated on the downwind side of the building are more heavily loaded (but the load on each joist is uniform). In Figure 4.5a, the parapet height has an important influence due to the highly concentrated load on a particular joist. In Figure 4.5b, we notice that buildings with shorter parapets resist higher loads. Recall however, that this load is an equivalent uniform load, and the roof load is normalized over the entire roof. When looking at the critical joists alone, results show that the building with the shorter parapet fails under a uniform 68.6 psf load, while the critical joist of the building with the higher parapet fails under a uniform 117.4 psf load. These values are lower than expected; SJI load tables state they should be at least 95.2 psf and 140.0 psf, respectively. These premature failures occur due to the unbalanced load on the building causing some twisting in the joists leading to local buckling of the top chord.

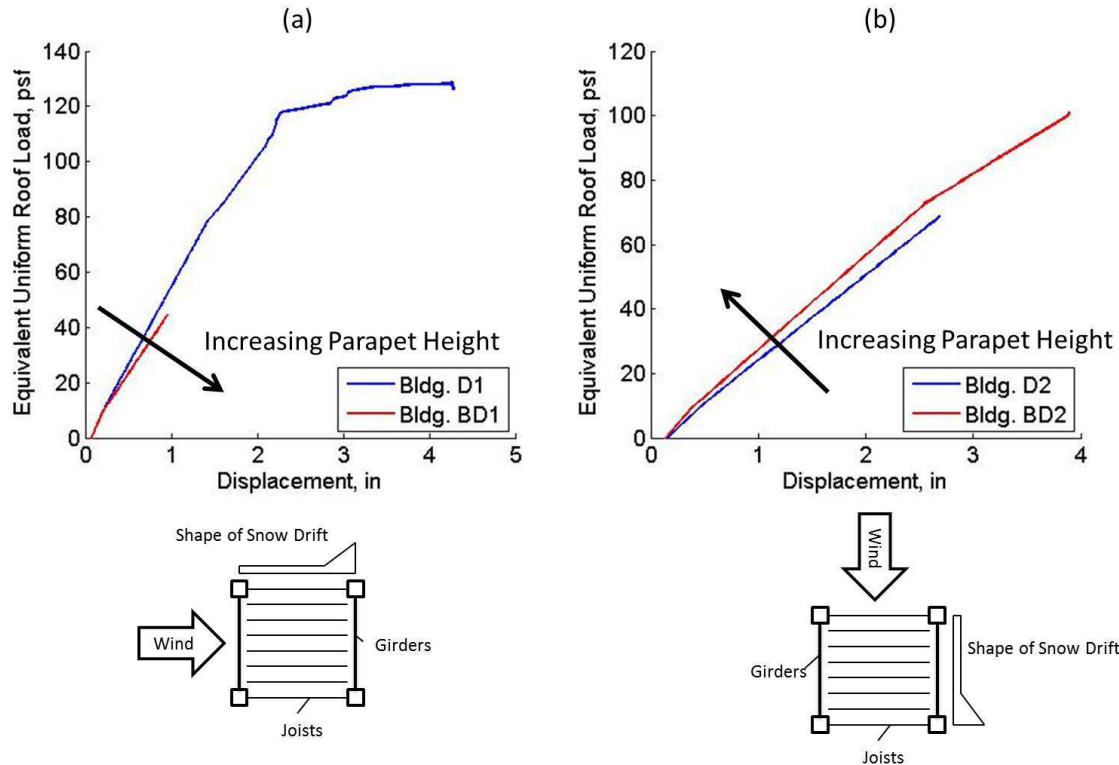


Figure 4.5: Pushdown curves for roofs under a drifted snow load with varying a) parapet height with wind assumed to act parallel to joists, & b) parapet height with wind assumed to act orthogonal to joists

4.3 Roof Structures Supported by Wide Flange Steel Sections

4.3.1 Configuration, Design and Representative Buildings

In the next part of the study, each of the roof structures was redesigned, replacing the OWSJs with conventional wide flange (W-section) steel beams. The rest of the roof design used the same loading and configuration assumptions as before. The W-sections are treated as simply supported by the girders in the design. The required W-sections for each of the roof structures designed for uniform loads are listed in Table 4.3. These sections satisfy design bending moment and shear requirements from ASCE 7 (2010) and AISC (2011). Serviceability design was not considered in the design for consistency with the OWSJ study. The W-sections are selected based on the lightest section that meets the required strength limits. Note that the change in

girder span (represented by Bldgs. U7 & U8) does not affect the design of the W-section and is not considered here. Also note that the joist depth variation (represented by Bldgs. U11-U15) is not considered in this part of the study due to a variation in W-section depth not being considered.

Table 4.4 lists the wide flange steel beam supported roof structures analyzed under drifted loads. These buildings, which have two different parapet heights, are designed by determining the maximum moment and shear produced at any point along the member when subjected to the appropriate drifted load from ASCE 7-10 equations. The W-section is then designed to resist this maximum moment and shear. Since the west-to-east wind direction produces an uneven load distribution on the wide flange section, it represents the more interesting case to consider.

Table 4.3: Re-designed roof structures with W-section steel beams subjected to uniform snow loads

Bldg. No.	W-section Replacing OWSJ	Variation
WBU	W12x16	Basic Building
WU1	W12x14	15 psf Design GSL (SEAC 2007)
WU2	W12x16	25 psf Design GSL (City of Denver 2011)
WU3	W16x26	75 psf Design GSL (Summit County 2013)
WU4	W16x26	90 psf Design GSL (Summit County 2013)
WU5	W8x10	20 ft. Joist (W-section) Span
WU6	W16x26	40 ft. Joist (W-section) Span
WU9	W10x12	5 ft. Joist (W-section) Spacing
WU10	W12x14	8 ft. Joist (W-section) Spacing
WU16	W12x19	0.84 D/S Ratio
WU17	W14x22	1.31 D/S Ratio

Table 4.4: Re-designed roof structures with W-section steel beams subjected to drifted snow loads

Bldg. No.	W-section	Variation
WBD1	W14x22	Basic Building
WD1	W12x19	2 ft. Parapet Height

4.3.2 Response of Wide Flange Section Steel Sections

Unlike the OWSJ reliability assessment, which employed a complex nonlinear model of the OWSJ to simulate structural response, the W-section reliability assessment uses linear equations to compute the strength demand on the section and the deflection under the applied load on a single span. This analysis assumes the beams are simply supported by the girders and neglects the interaction between the W-section, girders, and any lateral bracing provided. Exceedance of the capacity of the W-section is taken to signify failure of the roof.

4.4 Structural Reliability Assessment under Snow Loads

4.4.1 Reliability Assessment Methods and Metrics

This study assesses the reliability of buildings with OWSJ and wide flange steel section (W-section) roof structures with varying characteristics. The desired outcome of such an assessment is the reliability index, β , which is an interpretation of the probability of a certain limit state being exceeded in a structure of interest. Higher β s indicate buildings that are more reliable and, hence, less likely to experience a damaging limit state. Mathematically, the β computed for a particular structure and limit state is related to the probability of exceedance for that same limit state, p_f , as follows:

$$\beta = -\Phi^{-1}(p_f) \quad (4.1)$$

where $\Phi(\cdot)$ is the cumulative standard normal distribution (Melchers 1999). The study computes reliability indices for the OWSJ roof structures for both serviceability and ultimate limit states, as detailed in Table 4.5. The study only observes the ultimate limit state reliability indices for W-sections due to them not being designed for serviceability. Serviceability is considered only for OWSJ roof structures because it was determined that the majority of the buildings indirectly satisfy serviceability requirements during the strength design. For the

serviceability limit state, the deflection demand from the applied load is compared to allowable deflection limits. For the ultimate limit state, if the load demand exceeds the capacity, the roof or roof element is considered to have failed.

Table 4.5: Definition of limit states of interest.

Limit State	Description	Metrics
Ultimate	Load applied to structure exceeds failure capacity of OWSJ structure or exceeds flexural or shear capacity of W-section members	β^{ult}, p_f^{ult}
Serviceability	Maximum deflection of roof exceeds acceptable deflection limits, defined as 1/240 th of the joist span length.	β^{serv}, p_f^{serv}

The reliability assessment considers uncertainty in both the strength (resistance) of the roof structure and in the loading, stemming from dead, live or snow loading, on the roof. The random variables representing the loading on the roof structure are listed in Table 4.6. The ground-to-roof snow load conversion factor and the dead load are assumed to be normally distributed based on the limited number of available measurements of loads on real roofs. The live load is not distributed and considered as constant in all simulations. The ground snow load distributions represent the annual maximum ground snow load, based on available historical data. This study uses the historical best-fit probability distribution for the sites of interest as determined by SEAC (2007). The ground snow load distributions for Lamar, CO and Boulder, CO are fitted to Log-Logistic distributions, for Denver, CO to a Log-Pearson type III distribution, for Keystone, CO to a Generalized Extreme Value distribution, and for Copper Mountain, CO to a Generalized Logistic Distribution, as plotted in Figure 4.6.

Table 4.7 describes the random variables representing the resistance of the roof structure. The reliability assessment for the OWSJ roof structures treat structural response and capacity as deterministic, based on the pushdown response of each structure as simulated in *OpenSees*. For the steel wide-flange beam roof systems, uncertainty in the elastic modulus, yield strength and section modulus, are considered.

Table 4.6: Random variables considered in reliability assessment of OWSJ and W-section roof structures (loading)

Variable	Distribution	Mean	C.O.V.	Source
Ground Snow Load (GSL)	Depends on site of interest	Varies (see Figure 4.6)	Varies (see Figure 4.6)	SEAC (2007)
Dead Load (DL)	Normal	$1.05DL$	0.05	Ellingwood <i>et al.</i> (1980)
Ground-to-Roof Snow Load Conversion (CF)	Normal	0.55	0.5	O'Rourke (2010)

Table 4.7: Random variables considered in reliability assessment of OWSJ and W-section roof structures (resistance)

Variable	Distribution	Mean	C.O.V.	Source
<i>OWSJ Supported Roof Structures</i>				
Pushdown Response	Deterministic, based on <i>OpenSees</i> Analysis			
<i>W-section Supported Roof Structures</i>				
Elastic modulus (E)	Normal	$0.99E$	0.076	Hess <i>et al.</i> (2002)
Yield strength (F_y)	Lognormal	$1.05F_y$	0.11	Takahashi & Ellingwood (2005)
Section Modulus (Z)	Normal	$1.01Z$	0.05	Takahashi & Ellingwood (2005)

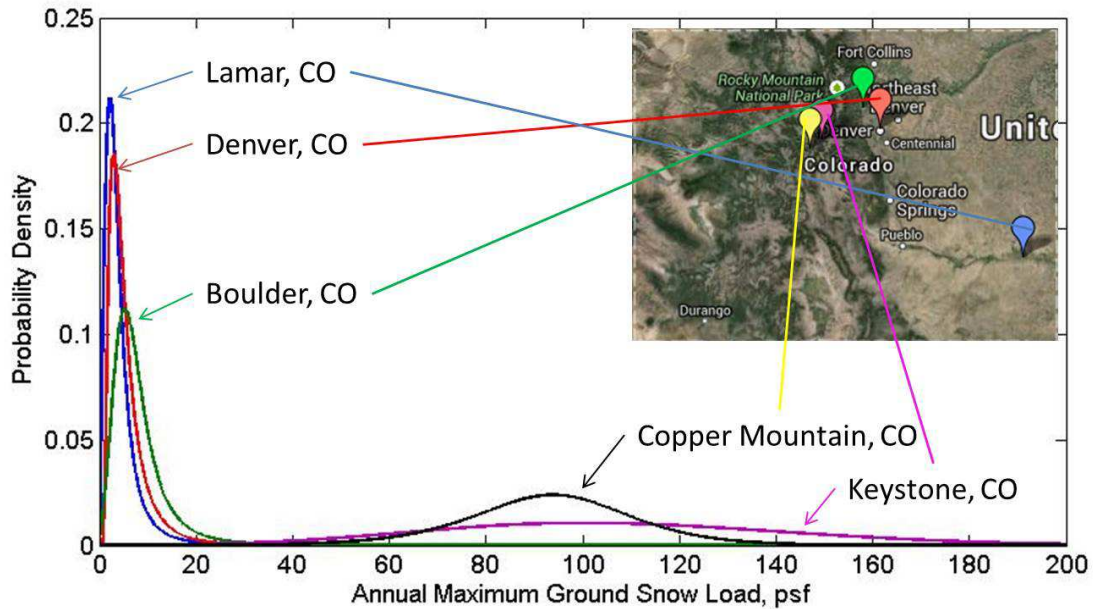


Figure 4.6: Distribution of annual maximum ground snow loads for various sites in Colorado (Map from Google)

The reliability assessment is performed using the Monte Carlo simulation approach (Melchers 1999). For each of N Monte Carlo simulations, realizations of each of the random variables listed in Table 4.6 and Table 4.7 are generated according to the defined probability

distributions using a random number generator. In the random number generation process, the different random variables are assumed to be uncorrelated. Then, the demand (load) on the structure and the capacity (resistance) of the structure is computed based on the generated set of random variable realization. In each Monte Carlo simulation, the roof load is computed as the sum of the randomly generated roof dead load, the instantaneous roof live loads, and the roof snow load. The snow load on the roof is based on the randomly generated values of the ground snow load and the ground-to-roof conversion factor. The instantaneous live load is taken as deterministic with a value of 14.3 psf based on Paz (1994). Once the load on the roof is computed in a given Monte Carlo simulation, the analysis determines whether either the ultimate or serviceability limit states have been exceeded. For the OWSJ roof structures, the ultimate (structural failure) limit state is identified as occurring if the load exceeds the maximum load obtained from pushdown analysis. The serviceability limit state is violated if the deflection observed from the pushdown analysis under the sampled roof loading value exceeds $1/240^{\text{th}}$ of the joist span (illustrated in Figure 4.4a). In the wide-flange steel beams, the ultimate limit state is exceeded in a given Monte Carlo simulation if the roof load exceeds the member capacities calculated from equations from AISC (2011):

$$M_{cap} = Z F_y \quad (4.2)$$

$$V_{cap} = 0.6 F_y d t_w \quad (4.3)$$

In Equations (4.2) & (4.3), Z and F_y are as defined in Table 4.7, and d and t_w are the depth and web thickness of the wide-flange section, respectively.

This process of generating realizations of the key random variables and determining whether one of the limit states of interest is violated is repeated in N simulations. The probability of exceeding a particular limit state is then computed by counting the number of simulations in

which a particular limit state was exceeded, divided by the total number of simulations (Melchers 1999). In this study, since the ground snow load distribution defines the annual maximum snow load, the computed probability corresponds to an annual probability of failure. Once obtained, the probability of failure can be converted to a reliability index using Equation (4.1). Note, however, that Equation (4.1) requires that the probability of exceedance and the reliability index be defined for the same time period. However, the target reliability index, expressed for example in design standards like ASCE 7-10, is typically based on a 50-year period, the assumed life span of a typical building, whereas the probability computed is on an annual basis. To convert the annual probability of exceedance, p_o , to the 50-year probability of exceedance, p_f , the Poisson distribution is used with $t = 50$ years (Melchers 1999):

$$p_f = 1 - e^{-p_o t} \quad (4.4)$$

Before the analysis, the anticipated probability of failure can be used to determine the number of Monte Carlo simulations required to carry out the reliability assessment, where smaller failure probabilities require a larger number of simulations. For typical buildings, *i.e.* not special or high occupancy with either sudden or progressive failure occurring, the target reliability indices defined by ASCE (2010) are on the order of $\beta = 3.5$, which corresponds to an annual failure probability, p_o , of 5.0×10^{-6} . Accordingly, the minimum number of Monte Carlo simulations to predict this probability of failure with 95% confidence level is found to be $N \approx 600,000$ from

$$N > \frac{-\ln(1-C)}{p_o} \quad (4.5)$$

where p_o is the annual probability failure, C is the confidence level and N is the required number of simulations (Melchers 1999). Using this process, and assuming that the β for OWSJ buildings is on the order of 4.0, 4,280,000 simulations were performed. W-section β s are

assumed to be on the order of 3.5, leading to 600,000 simulations being performed. Using these values in other equations which determine the number of simulations to use (Shooman 1968) shows that this number of simulations provides an error no greater than 113% with 95% confidence for both OWSJs and W-sections.

According to the ASCE 7-10 commentary the target reliability values for structural reliability are 3.5 for the OWSJ buildings and 3.0 for the W-sections. This is due to both being analyzed under Risk Category II, but the failure of an OWSJ building is sudden and causes progressive damage while the failure of a W-section is assumed to not be sudden.

4.4.2 Reliability Assessment for OWSJ Supported Roof Structures

The structural results obtained in previous sections are incorporated into the Monte Carlo based reliability assessment to evaluate the annual probability of exceedance and reliability indices for limit states related to ultimate failure and serviceability. The outcome of the reliability assessment for the OWSJ supported roof structures are shown in Table 4.8 and Table 4.9.

The average reliability index for the buildings subjected to uniform loads is 1.99. Overall, it is observed that the reliability indices for the ultimate limit state are lower than the target value of 3.5. Also, for the ultimate limit state with uniform snow loads the results can be deemed to be not overwhelmingly low by observing that the average return period for the failure of a building is about 3900 years which is much longer than the lifespan of most buildings. However, drifted snow load cases are shown to be significantly less reliable with an average index of 1.75.

As expected, the reliability indices for the serviceability limit state are much lower than those for the ultimate limit state with an average index of 0.05 which corresponds to about a 50% chance of exceeding the limit state in 50 years. Although these reliability indices are quite small,

it is of less concern due to the less catastrophic nature which comes with serviceability failure as compared to structural failure.

Table 4.8: Reliability assessments for OWSJ supported roof structures under uniform snow loads

Bldg. No.	Structural Failure (Ultimate Limit State)		Serviceability Limit State	
	p_f^{ult}	β^{ult}	p_f^{serv}	β^{serv}
BU	4.08×10^{-4}	2.05	9.96×10^{-3}	0.27
U1	4.02×10^{-4}	2.06	9.10×10^{-3}	0.34
U2	7.27×10^{-5}	2.69	2.37×10^{-3}	1.22
U3	2.44×10^{-2}	-0.54	3.60×10^{-1}	-5.54
U4	3.71×10^{-4}	2.09	1.36×10^{-1}	-3.05
U5	9.18×10^{-5}	2.61	1.75×10^{-3}	1.38
U6	4.55×10^{-4}	2.00	1.47×10^{-2}	-0.05
U7	5.14×10^{-4}	1.95	7.26×10^{-3}	0.51
U8	3.96×10^{-4}	2.06	1.00	-INF ^a
U9	5.39×10^{-4}	1.93	2.32×10^{-3}	1.23
U10	2.63×10^{-4}	2.22	7.19×10^{-3}	0.52
U11	5.14×10^{-4}	1.95	3.38×10^{-2}	-0.90
U12	2.94×10^{-4}	2.18	1.11×10^{-2}	0.18
U13	2.94×10^{-4}	2.18	5.93×10^{-3}	0.65
U14	3.27×10^{-4}	2.14	4.33×10^{-3}	0.86
U15	7.87×10^{-4}	1.77	3.05×10^{-3}	1.07
U16	5.50×10^{-4}	1.92	2.41×10^{-3}	1.21
U17	9.11×10^{-5}	2.61	1.95×10^{-2}	-0.31
Max	2.44×10^{-2}	2.69	1.00	1.38
Min	7.27×10^{-5}	-0.54	1.75×10^{-3}	-INF
Average	1.71×10^{-3}	1.99	9.06×10^{-2}	-0.02

^a The combined self-weight of the structure and instantaneous live load, both of which are constant in the Monte Carlo analysis, exceeds the allowable deflection defining serviceability limit state alone. This means the structure always fails in serviceability leading to a reliability index of -infinity.

Table 4.9: Reliability assessments for OWSJ supported roof structures under drifted snow loads

Bldg. No.	Structural Failure (Ultimate Limit State)		Serviceability Limit State	
	p_f^{ult}	β^{ult}	p_f^{serv}	β^{serv}
BD1	9.18×10^{-3}	0.34	9.18×10^{-3}	0.34
BD2	2.06×10^{-4}	2.32	1.44×10^{-2}	-0.03
D1	7.29×10^{-5}	2.68	4.48×10^{-4}	2.01
D2	1.02×10^{-3}	1.65	3.29×10^{-2}	-0.87
Max	9.18×10^{-3}	2.68	3.29×10^{-2}	2.01
Min	7.29×10^{-5}	0.34	4.48×10^{-4}	-0.87
Average	2.62×10^{-3}	1.75	1.42×10^{-2}	0.36

The reliability assessments allow for some trends to be identified in the reliability of the OWSJ roof structures as building characteristics vary, which are summarized in Table 4.10. Of particular interest are the buildings with varying design ground snow loads. The ultimate limit state reliability indices are relatively constant, except for Bldg. U3. Bldg. U3 is designed for Keystone. Here, there is an insufficient snow load design value. The insufficient snow design for

Keystone can be observed by noting that the suggested 50-yr design ground snow load is 75 psf, while the distribution used in the simulations indicated that this value should be 186 psf. The reason for this inconsistency is likely due to the 50-yr design ground snow load being for the developed part of Keystone while the distribution is recorded at a different location very close to Keystone, yet further in the mountains. The increase of β^{ult} as D/S increases is also significant in this study to emphasize the fact that lightweight structures are less reliable under snow loads than non-lightweight structures.

Overall, out of the buildings considered in this study the largest change in β^{ult} is observed when buildings with varying parapet heights were subjected to drift with wind in the west-east direction (Bldgs. D1 and BD1). This change in parapet height of only 1.5 ft. causes the reliability index for the ultimate limit to decrease from 2.68 to 0.32. This change demonstrates the importance of understanding the behavior of snow drifts on buildings. The β^{ult} changes in all other trends were fairly minimal with values close to each other as compared to the drifting buildings. The largest change in β^{serv} is associated with the variation of girder spans (Bldgs. U7, BU, and U8). This trend demonstrates the need for caution when designing extremely long girders to avoid serviceability issues.

Table 4.10: Trends observed from reliability indices of OWSJ buildings, where \uparrow signifies increase, \downarrow signifies decrease, -- signifies no significant change

Building Characteristic	Change in β^{ult}	Change in β^{serv}
As Design GSL increases	-- except Bldg. U3	\downarrow
As Joist Span increases	\downarrow	\downarrow
As Girder Span increases	--	\downarrow
As Joist Spacing increases	\uparrow	\downarrow
As Joist Depth increases	--	\downarrow
As D/S increases	\uparrow	\uparrow then \downarrow
As Parapet Height (Wind \rightarrow) increases	\downarrow	\downarrow
As Parapet Height (Wind \downarrow) increases	\uparrow	\uparrow

4.4.3 Reliability Assessment for Wide Flange Roof Structures

The results of the reliability assessments for the W-section equivalent members to the OWSJ buildings are presented in Table 4.11 and

Table 4.12. It can be observed that once again the resulting reliability indices for the ultimate limit state in W-sections is less than the recommended value of 3.5 set by the ASCE 7-10 commentary. The β^{ult} values are fairly similar to the results obtained from the OWSJ buildings being only slightly smaller at an average reliability index of 1.83. Like the OWSJ buildings, the reliability indices seem small compared to the ASCE (2010) recommendations; however they are not overwhelmingly low, as observed through the average return period of over 2700 years, which is longer than the life span of many buildings. These values are also within the range of reliability index results for steel sections, 1.47-2.75, obtained by Bennett (1988).

The drifted reliability indices are larger on average than the results obtained for W-sections under uniform snow loads. This is likely due to the design snow drift having a larger difference between actual load and design load than the uniform snow load. This is caused by the 1.6 design load factor in design producing much larger design snow loads at the top of the drift in drifted load analyses than in uniform load analyses. Due to the maximum moment being in the drift, this increase in difference between actual and designed load leads to an increase in reliability. For example, in Boulder the uniform design roof snow load is 21 psf which increases to 33.6 psf when the load factor is applied, an increase of 12.6 psf. However, the top of the drift in W-section WBD1 is subjected to 62.7 psf and designed for 100.2 psf, an increase of 37.54 psf. In this case the uniform snow load will exceed 33.6 psf more frequently than a drifted load, which varies height and length with every simulation according to the roof snow load, will exceed its limit, allowing the drifted snow load scenario to be more reliable.

As explained earlier, the W-sections are not designed for serviceability requirements and serviceability reliability indices are not provided. However, it should be noted that if serviceability was required in the design of the members that it would govern the design. Due to serviceability governing the design the members would be stronger and an increase in their ultimate state reliability index would increase. This can be observed through the results for W-section WBU when designed for serviceability which results in the use of a W16x26 member and a β^{ult} of 3.09.

Table 4.11: Reliability assessments for W-section supported roof structures under uniform snow loads

Bldg. No.	Structural Failure (Ultimate Limit State)	
	p_f^{ult}	β^{ult}
WBU	7.50×10^{-4}	1.79
WU1	7.55×10^{-4}	1.79
WU2	1.32×10^{-4}	2.48
WU3	1.73×10^{-2}	-0.20
WU4	1.04×10^{-3}	1.64
WU5	6.40×10^{-4}	1.86
WU6	2.93×10^{-4}	2.18
WU9	2.82×10^{-4}	2.20
WU10	4.78×10^{-4}	1.98
WU16	4.48×10^{-4}	2.01
WU17	1.67×10^{-4}	2.40
Max	1.73×10^{-2}	2.48
Min	1.32×10^{-4}	-0.20
Average	2.03×10^{-3}	1.83

Table 4.12: Reliability assessments for W-section

Bldg. No.	Structural Failure (Ultimate Limit State)	
	p_f^{ult}	β^{ult}
WBD1	9.00×10^{-5}	2.61
WD1	2.98×10^{-4}	2.18
Max	2.98×10^{-4}	2.61
Min	9.00×10^{-5}	2.18
Average	1.94×10^{-4}	2.40

Like the results for the OWSJ buildings, the observation of the reliability indices indicates some significant trends, reported in Table 4.13. It can be noted that the W-section results for W-section WU3 are also skewed due to the inconsistent design snow load for Keystone, CO. Again, like in the OWSJ buildings, the reliability of the W-sections increases as

the D/S ratio increases. This provides further evidence to lightweight structures being less reliable.

The largest differences in reliability index are observed when the design ground snow load and design dead-to-snow load ratios vary. By increasing the design ground snow load the reliability index varies between values ranging from 1.64 to 2.48 (the extreme outlier of W-section WU3 is ignored). Although this range of indices is large, there is no pattern as to how they are arranged. Unlike the design ground snow load variation, the design dead-to-snow load ratio (D/S) has a clear pattern, which shows that the reliability increases as D/S increases. For this reason it can be concluded that the design dead-to-snow load ratio is the most important factor to consider when examining the reliability of W-sections.

Table 4.13: Trends observed from reliability indices of W-sections, where \uparrow signifies increase, \downarrow signifies decrease, -- signifies no significant change

Building Characteristic	Change in Structural Failure β
As GSL increases	Slight \downarrow , except Bldg. WU3
As Joist Span increases	\uparrow
As Girder Span increases	--
As Joist Spacing increases	\downarrow
As Joist Depth increases	--
As D/S increases	\uparrow
As Parapet Height (Wind \rightarrow) increases	\uparrow

4.5 Discussion

4.5.1 Overview

This section discusses the trends determined through the Monte Carlo simulations of OWSJ buildings and W-sections in more detail. Focus is put on the comparison of trends between the two building/member types.

Something that should be considered when observing these results is that some of the difference between the responses may be due to the difference in Monte Carlo simulation technique. What is meant by this is that some portion of the difference may be accounted for due to the OWSJ buildings having a deterministic, constant capacity while the capacity of the W-

sections vary. This slight difference causes the W-sections to be less reliable than they would be if they were deterministic as well. For example, by analyzing W-section WBU with a deterministic capacity (*i.e.* the yield strength, section modulus, and elastic modulus do not vary) the reliability index for the ultimate limit state increase slightly from 1.79 to 1.83.

Another factor that could account for some portion of the difference between the OWSJ buildings and the W-sections could be due to W-sections not being affected by their interaction with other joists and are simply supported while OWSJs are considered as a whole building. When a Monte Carlo simulation is performed for a single simply supported 22K9 OWSJ (used in Bldg. BU), the capacity of the joist increases by 27% such that not a single structural failure occurs in 4,280,000 simulations. This indicates the large amount of impact that the interactions between joists in a building and the semi-rigid connections used at the ends of the joists have.

During the analysis of the buildings subjected to drifted snow loads it is also important to recall that the snow drift shape is based on ASCE 7-10 equations. These equations are considered to be conservative compared to actual snow drift shapes and other, more accurate snow drift models which consider more factors (Cocca & O'Rourke 2008).

4.5.2 Variation of Design Ground Snow Loads

As seen in Figure 4.7, the reliability indices for the ultimate limit state in OWSJ buildings and W-section beams are extremely similar. The trends for both types of buildings seem to show that the indices remain fairly consistent with values never deviating too far from each other and with no clear pattern emerging. The only buildings that do deviate from the rest of the buildings are the ones designed for Keystone, CO (75 psf). The reasoning for why they are so different is explained earlier and deals with inconsistent design snow loads compared to the actual snow load.

The serviceability reliability indices for OWSJ buildings seems to follow the same pattern as the ultimate limit state reliability indices, including the large dip in value at the Keystone site. The major difference identified is that the Copper Mountain, CO site (90 psf) also provides very low reliability in serviceability rather than reverting back to the reliability levels seen in the three low snow load buildings. This is due to an increased uniform load on each individual joist causing increased deflections. This leads to the conclusion that the reliability in serviceability decreases as the design ground snow load increases.

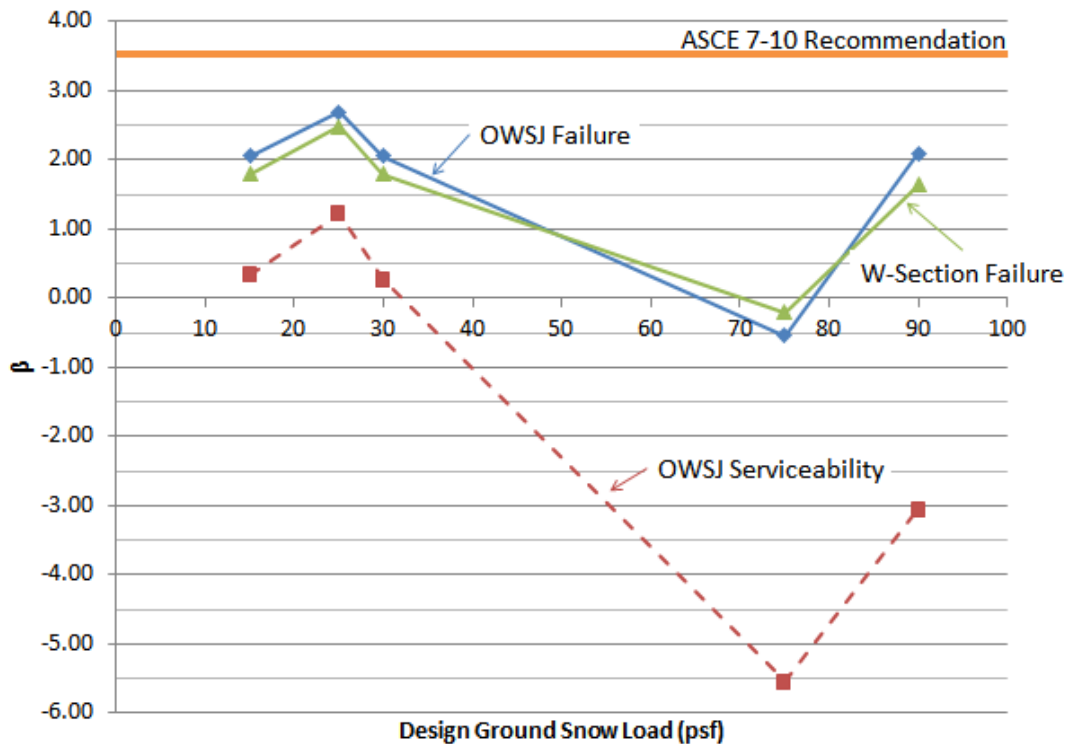


Figure 4.7: Trends in OWSJ and W-section reliability indices with varying design ground snow loads

4.5.3 Variation of Joist Span

The resulting reliability indices for the ultimate limit state from varying the joist span in OWSJ buildings and W-section joists are shown in Figure 4.8. Once again, the results for the two building types are grouped closely together. A major difference between the two sets of results is

the fact that the reliability in OWSJ buildings decreases as the joist span increases while the opposite occurs in W-sections. At a certain point the trends cross, leading to the observation that at shorter joist spans the OWSJ buildings are more reliable while at longer joist spans the W-sections are more reliable. This is due to the observed decrease in OWSJ capacity as the joist span increases and some design overstrength in the 40 ft. span W-section.

The serviceability reliability indices for OWSJ buildings decrease as the joist span increases. This is due to the additional deflection that occurs in longer spans under the same load. This is an interesting result given that all buildings involved in the varying of joist span would pass the SJI (2005) requirements for serviceability design.

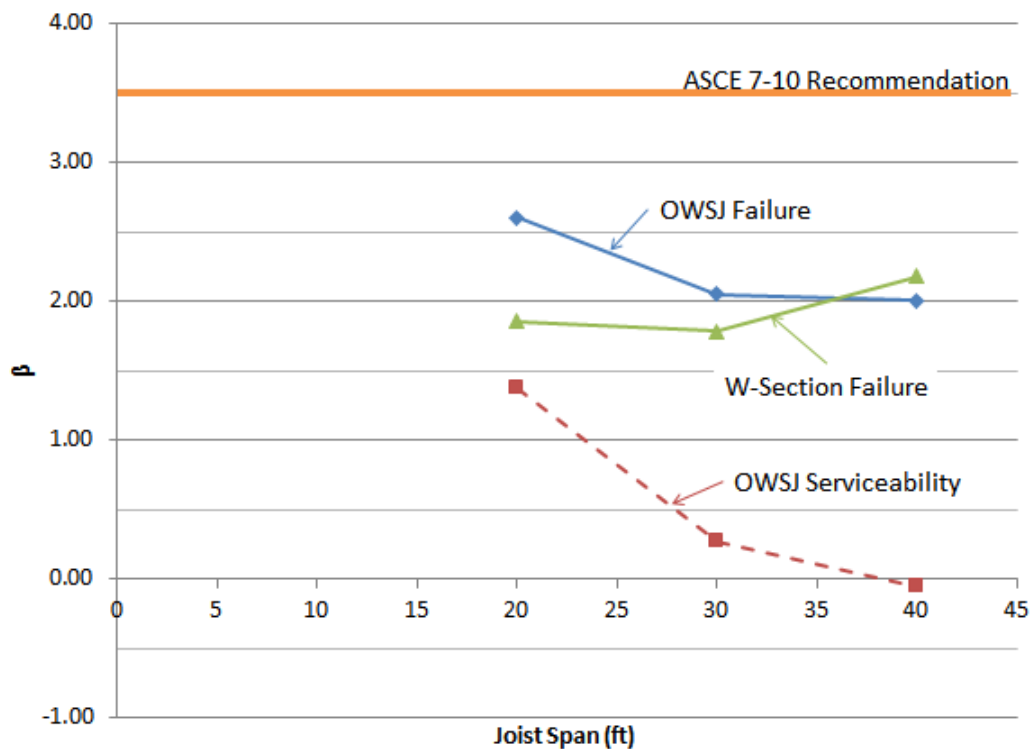


Figure 4.8: Trends in OWSJ and W-section reliability indices with varying joist spans

4.5.4 Variation of Girder Span

There is no significant change in the reliability indices for the ultimate limit state in OWSJ buildings, as seen in Figure 4.9. Recall that there were no specific W-sections for the

variation of girder span, the points presented in Figure 4.9 all reference W-section WBU which would satisfy the requirements of all three girder spans and are included in the figure for comparison purposes. The results for the ultimate limit state of both building types are extremely similar whose differences could be exaggerated due to reasons explained in Section 4.5.1. Despite the results being similar to each other they do not come close to ASCE (2010)'s recommended reliability index of 3.5.

The interesting trend found in these results is the serviceability reliability indices. As stated earlier, the probability of the roof exceeding serviceability limits becomes 100% with a 60 ft. girder span. This provides a reliability index of $-\infty$, demonstrating the extreme effects that girder span can have on the serviceability of a roof. It should also be noted in that the girders, like all other members in the buildings, were not designed for serviceability. If serviceability was accounted for in the design then serviceability would govern the design of the 40 ft. and 60 ft. span girders. This would have likely had a significant difference in the building's behavior and serviceability reliability.

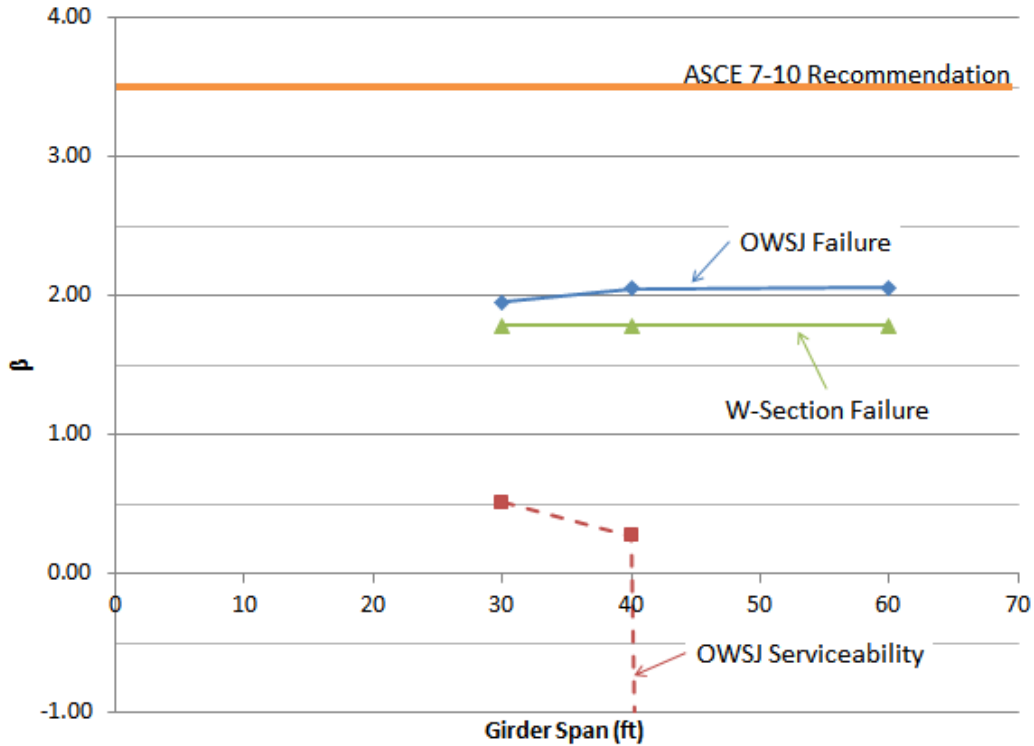


Figure 4.9: Trends in OWSJ and W-section reliability indices with varying girder spans

4.5.5 Variation of Joist Spacing

The variation of Bldgs. U9, U10, and BU, along with W-sections WU9, WU10, and WBU produce the reliability indices presented in Figure 4.10. When comparing the trends for the ultimate limit state reliability indices of the OWSJ buildings and W-sections it can be seen that the W-section reliability consistently decreases as the joist spacing increases. It initially seems as if the trend for the OWSJ buildings increases and decreases. However, if we observe that the building with a joist spacing of 8 ft. (Bldg. U10) has more capacity due to its combined large design and inherent joist overstrength relative to the other two buildings, it can be reasoned that the reliability of that building is slightly higher than appropriate for comparison. Taking this into account, the OWSJ buildings can be observed to become slightly more reliable as the joist spacing increases. These trends can be used to determine that with shorter joist spacing the W-section is more reliable, but the OWSJ is more reliable in buildings with wider joist spacing. This

trend can be explained through the increased effects the joist interactions have with each other as the joist spacing decreases. This is what causes the reliability increase in the OWSJs, but is not present in the W-section reliability causing it to have a different trend.

The serviceability reliability indices for the OWSJ buildings are also interesting as a clear trend of a decrease in reliability as joist spacing increases can be observed. This can be explained through the decrease in load on joists with shorter joist spacing when compared to a building of the same size with longer joist spacing. These decreased loads on individual joists make the building stiffer by splitting the load up on more joists causing them to deflect less. The increase in stiffness allows for less deflection and a higher serviceability reliability, which decreases as the joist spacing increases and the building stiffness decreases.

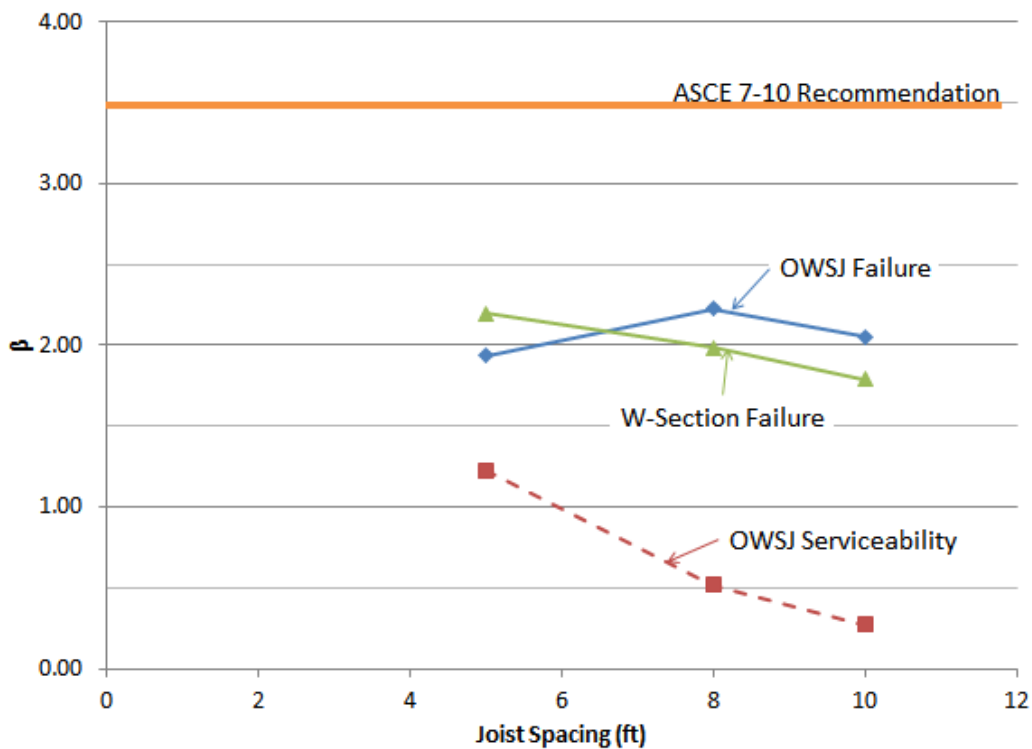


Figure 4.10: Trends in OWSJ and W-section reliability indices with varying joist spacing

4.5.6 Variation of Joist Depth

Figure 4.11 presents the reliability indices for OWSJ buildings that vary the depth of the joist. Recall that the depth of W-section joists were not varied, instead the results for W-section WBU is presented on the figure as a point with a depth of 12 in. (it's a W12x16 section). The ultimate limit state reliability indices for the OWSJ buildings are once again smaller than the recommended value (ASCE 2010); however the results are all within the same range of about 2.0. In addition to the trend being that the indices do not vary significantly, it can be observed that the index for the W-section considered is also within the same range.

Unlike the ultimate limit state reliability trend, the serviceability reliability clearly increases as the OWSJ depth increases. This is due to the increase in stiffness in the building caused by the increased stiffness of deeper joists compared to shallow joists. Under further investigation it is observed that all the OWSJ roofs satisfied serviceability design except for Bldg. U11 (depth of 18 in.). It is interesting to observe that all buildings which satisfied serviceability remained larger than $\beta^{\text{serv}} = 0.0$; however, the building which fails serviceability design experiences a negative reliability index. Despite Bldg. U11 not satisfying serviceability design requirements, the trend of increasing serviceability reliability as the joist depth increases can still be observed in the buildings which do conform to SJI (2005) serviceability design.

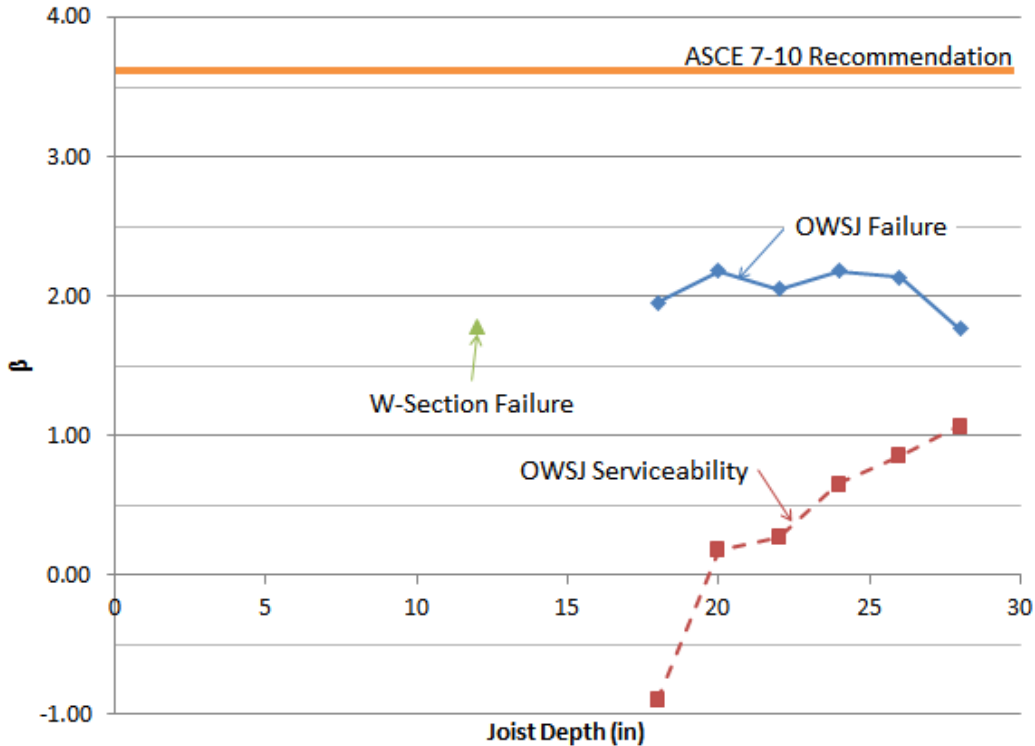


Figure 4.11: Trends in OWSJ and W-section reliability indices with varying joist depths

4.5.7 Variation of Design Dead-to-Snow Load Ratios

The resulting reliability indices for buildings with varying design dead-to-snow load ratios are presented in Figure 4.12. The reliability indices for the ultimate limit state in both the OWSJ buildings and W-sections once again do not reach the recommended value of 3.5 (ASCE 2010). The comparisons between the ultimate limit state reliabilities for the two building types are observed to be comparable with values similar to each other. Although the W-section results seem slightly lower than the OWSJ building values, this difference may be due to one of the reasons presented in Section 4.5.1. The trends for ultimate limit reliability are also the same with the reliability increasing as the D/S ratio increases (*i.e.* when becoming less lightweight). The bend in the ultimate limit reliability for the OWSJ buildings can be explained as being low due to the relatively low actual capacity-to-SJI load table capacity ratio (inherent overstrength) Bldg. U16 (D/S = 0.80) has. The low inherent overstrength value makes the reliability index lower than

it would be if it had similar inherent overstrength than the other two buildings. Taking this into account is why the trend is considered to be generally increasing as D/S increases.

The lack of a trend in the serviceability reliability for OWSJ buildings can be attributed to the selection of buildings being focused more on providing comparable SJI load table capacity-to-design capacity ratios than on providing comparable joist depths. As discussed earlier, the depth of the joist plays a major role in the stiffness, and therefore the serviceability reliability, of a building. The same conclusions reached when analyzing serviceability under varying joist depths are reached here with the shallowest joist (Bldg. U17, D/S = 1.27) having the least reliable results and the deepest joist (Bldg. U16, D/S = 0.80) having the most reliable results.

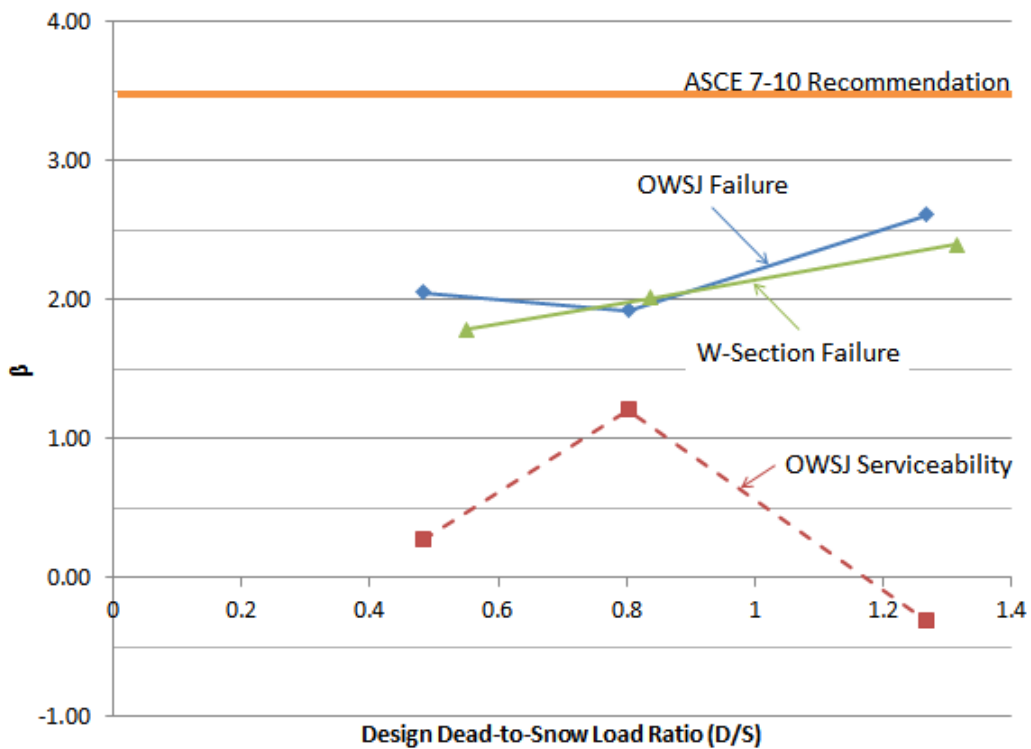


Figure 4.12: Trends in OWSJ and W-section reliability indices with varying design dead-to-snow load ratios

4.5.8 Variation of Parapet Height

The reliability indices for OWSJ buildings and W-sections subjected to drifts parallel to the joist (\rightarrow or west-east in plan) are presented in Figure 4.13. The reliability indices for the ultimate limit state with a parapet height of 2 ft. is shown to produce a relatively small difference between the reliability of the OWSJ building and the W-section. However, the ultimate limit reliability trends are opposite when a 3.5 ft. parapet is included in the data, with the reliability of OWSJ buildings decreasing dramatically while the reliability of the W-sections increases. This may be attributed to the different methods used to design each member. The OWSJ is designed using the tables to resist the load at the top of the snow drift. Although this process seems conservative in nature, the different loading pattern may cause unexpected moments at points along the joist other than at midspan, which is where the maximum moment under uniform loading occurs. The new point of maximum moment or shear in the OWSJ may not have sufficient capacity to properly resist the stresses causing an early failure. The W-sections are designed by considering the maximum shear and moment along the entire length of the beam and because the section remains the same throughout the span (*i.e.* the moment and shear capacity does not vary at any point along the member) an appropriate section was selected to resist the maximum applied loads. This difference in design could explain the difference in reliability trends between the two types of elements.

The serviceability reliability of OWSJ buildings also decreases as the parapet height increases. An interesting point in Figure 4.13 to discuss is that the reliability index for both the ultimate limit state and the serviceability are the same for Bldg. BD1 (parapet height = 3.5 ft.). This is caused by observing that the building fails before it deflects 1.5 in. ($1/240^{\text{th}}$ of the joist span). Due to this, the only loads which will cause a displacement which exceeds serviceability

limits are those which also exceed the capacity of the building, creating identical probabilities of failure and reliability indices for both limit states.

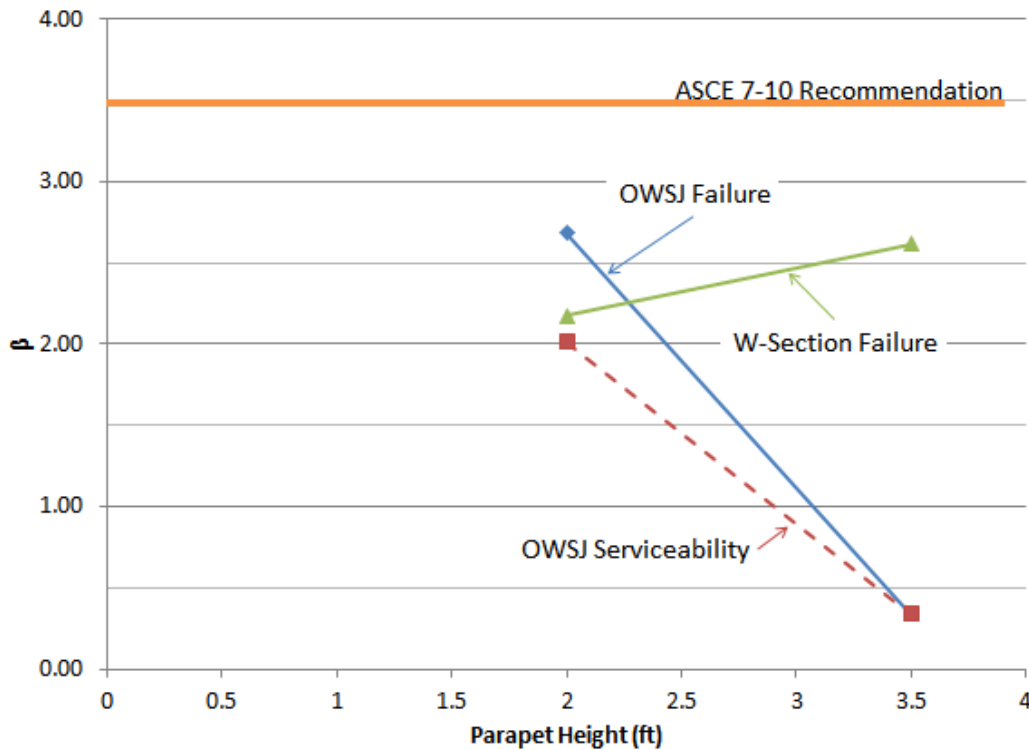


Figure 4.13: Trends in OWSJ and W-section reliability indices with varying parapet heights and wind blowing parallel to the joists (\rightarrow)

OWSJ buildings whose parapet height are varied and have a wind direction orthogonal to the joists (\downarrow or north-south in plan) produce the reliability indices presented in Figure 4.14. The trend observed for reliability for both ultimate and serviceability limits can be seen to increase as the parapet height increases. This difference can be attributed to the shape of the drift that each parapet creates. The 2 ft. parapet height building (Bldg. D2) produces a more concentrated drift load, which affects fewer joists than the more distributed drift caused by a 3.5 ft. parapet height. The 2 ft. parapet height drift overloads the control joist earlier due to its concentration, while the 3.5 ft. parapet height drift allows the load to be distributed among more joists creating less impact on any single joist. Also, the 2 ft. parapet height drift provides a more unbalanced load on

the roof when compared to the more distributed 3.5 ft. parapet height drift. The unbalanced load causes the girders and bridging to twist the joist which accelerates the top chord buckling. The larger load imbalance in the 2 ft. parapet height and its corresponding twisting of the joist allows for buckling to occur under smaller equivalent uniform loads. The joists used in Bldg. D2 (2 ft. parapet height) are also weaker OWSJs.

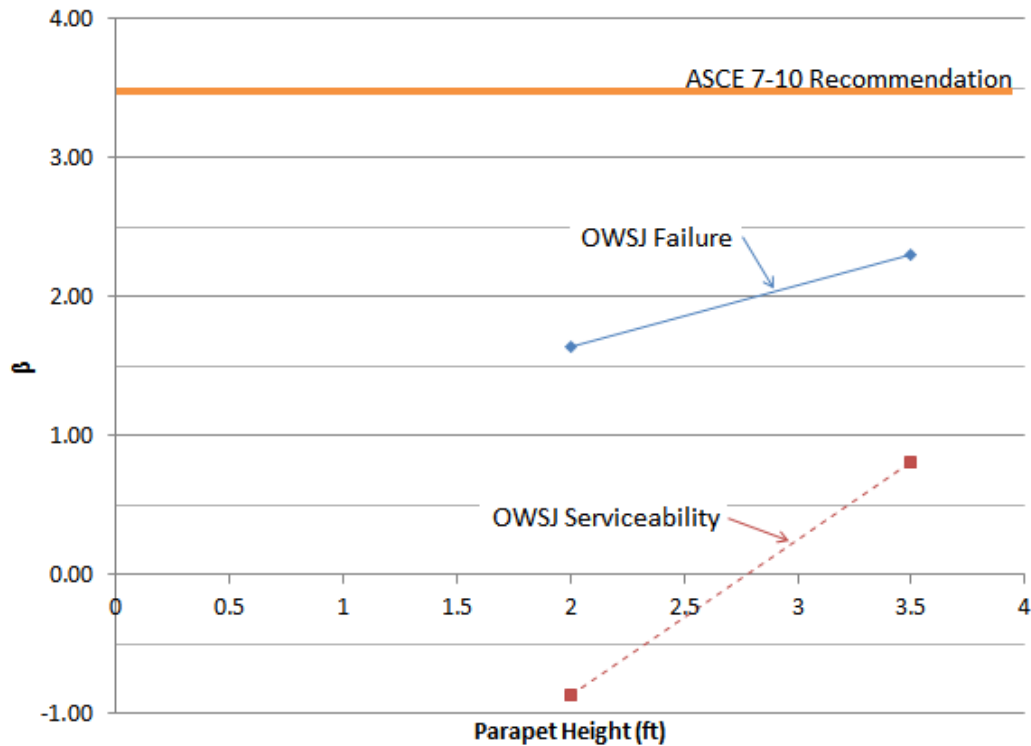


Figure 4.14: Trends in OWSJ and W-section reliability indices with varying parapet heights and wind blowing orthogonal to the joists (↓)

4.6 Conclusions

Through Monte Carlo simulations of various open web steel joist buildings and W-section joists some general conclusions were achieved concerning building characteristics and their reliability. The most prevalent conclusion is the inability for all OWSJ buildings and W-sections to achieve a reliability index similar to recommendations by the ASCE (2010). This

conclusion demonstrates the non-conservative nature of the ASCE 7-10 snow load design codes in a risk-based assessment.

The OWSJ buildings with varying parapet heights observed large variations in reliability. This conclusion highlights the importance of reconsidering the design process for OWSJs subjected to non-uniform loads. A possible alternative is the more commonly used in design method of having joist manufacturers design custom OWSJs for specific loads. There are also other building characteristics that led to significant changes in reliability. These characteristics include the joist span, joist spacing, and design dead-to-snow load ratio. There is little-to-no significant change in the reliability of buildings with varying design ground snow load, girder span, and joist depth. Regarding the serviceability limit state, it was concluded that the girder span has an extremely large effect of the probability of the roof exceeding $1/240^{\text{th}}$ of the joist span, and joist depth also plays a large role in serviceability reliability. Future studies should consider serviceability design of both the OWSJ roofs and W-sections in order to observe any differences in the trends observed in this study.

In both the OWSJ building and W-section analyses it is observed that the design dead-to-snow load ratio has a significant effect on the reliability of the building or member. The results match the initial hypothesis that more lightweight buildings and members (smaller design dead-to-snow load ratio) are less reliable than non-lightweight structures when subjected to snow loads.

5 EFFECT OF CONSTRUCTION ERRORS ON THE RISKS OF SNOW-INDUCED FAILURE OF ROOFS SUPPORTED BY OPEN WEB STEEL JOISTS

This chapter is a study of common construction errors and the effects they have on open web steel joist roof structures. It is a version of the conference paper with the same name as this chapter which was submitted and presented at the 11th International Conference on Structural Safety and Reliability (ICOSSAR) held from June 16th to June 20th, 2013 at Columbia University in New York, NY. The paper was written by Derek L. Kozak and Abbie B. Liel.

5.1 Abstract

The cause of the structural failures due to snow loads on lightweight steel roofs range from being overloaded due to drifted or extremely dense snow, to errors made in construction and design. Open web steel joist structures, which have a low dead load to snow load ratio, may be particularly vulnerable to snow-induced roof failure. This paper investigates the effects of construction errors on the reliability of these types of structures by describing common types of construction errors observed in properly designed OWSJ supported lightweight steel roofs, and quantifying the impact of construction errors such as weakened welds in the joists, joists being installed in incorrect positions, and joists being out-of-plumb on the overall structure's risk of ultimate or serviceability failure under extreme snow loads.

5.2 Introduction

The structural collapse of a roof due to snow loads can lead to costly repairs, injuries, and even death of building occupants. Bolduc (2011) showed that over 40% of the structural failures occurring in North America during 2010 were associated with roofs collapsed by snow. Metal or steel roof systems may be particularly vulnerable to snow-induced collapse. Geis *et al.* (2011) examined patterns in snow-induced building failures between 1979 and 2009, showing that the

1,029 incidents identified in the United States caused nineteen fatalities, 146 injuries, and up to \$200 million in building damages. Moreover, 53% of the incidents involved metal or steel constructed buildings. The study also reported that warehouses and factories were among the most affected building types. Numerous collapses of steel roofs have also been recorded in the northeastern United States during the winters of 1993-94 and 1995-96 (Peraza 2000), and during the January 1996 storm (DeGaetano *et al.* 1997).

Several studies have identified a common trend indicating the vulnerability of open web steel joist and truss supported roofs. Case studies show that a major contributor to snow-induced open web steel joist and truss supported roof failures are errors in the design, fabrication, or erection of the structure (Holicky & Sykora 2009). The general term “construction error” will be used in this paper to describe fabrication and construction errors; design errors are not directly considered here. The effects of these construction errors on open web steel joist and truss supported roofs has caused collapses of structures such as schools (Tanzer 2011), as well as other heavily occupied buildings such as the Hartford Civic Center Coliseum (Martin & Delatte 2001), the Katowice Fair Building (Biegus & Rykaluk 2008), and department stores (Lavon & Stivaros 2005) under snow loads.

This paper investigates some of these construction errors and the behavior of an open web steel joist (OWSJ) supported roof structure subjected to snow loads when construction errors are present. Comparisons will be made between (1) properly designed and constructed OWSJ structures and (2) OWSJ structures with construction errors, in order to quantify the risk of these construction errors under snow loads present in Denver, Colorado.

5.3 Open Web Steel Joists

5.3.1 Uses of OWSJs

Open web steel joists are prefabricated structural elements that utilize the truss action of web and chord elements, such that the composite OWSJ reacts as a single flexural element to support a roof or floor system. OWSJs are prefabricated. All fabricators working with the Steel Joist Institute (SJI) must specify OWSJs that conform to SJI load tables. These tables state the allowable uniformly distributed load which can be safely resisted by a particular joist type with a defined span length. The SJI load tables are meant for the design of uniformly applied gravity loads, but manufacturers can also provide joists designed to resist non-uniform loads. The SJI offers load tables for many different joist types, the three most common being: K-Series for medium to long spans and a uniform load per foot of less than 550 lbs/ft., LH-Series for longer spans and a uniform load per foot greater than 550 lbs/ft., and DLH-Series for deep, long span joists (Fisher *et al.* 2002, Yost *et al.* 2004). Joists are denoted by specific numbers which indicate the joist depth, joist series, and relative strength. For example, 18K10 refers to a K-series joist with a depth of 18 in. and a relative strength of 10 (implying the joist is stronger than joists with smaller relative strength values).

OWSJs are often preferred over conventional wide flange sections when designing and constructing long span roofs due to their economy, and the simplicity of the design process. OWSJs use less steel in their truss-like web system as compared to the solid steel wide flange section with the same load resistance characteristics. This high bending resistance to weight ratio makes OWSJs an efficient and desirable structural member in steel building construction and design (Fisher *et al.* 2002, Yost *et al.* 2004, Buckley *et al.* 2008). In addition, the load table-based design process can reduce design time and make the structure more cost efficient by

facilitating selection of the joist that resists the required load in the most efficient manner (Fisher *et al.* 2002).

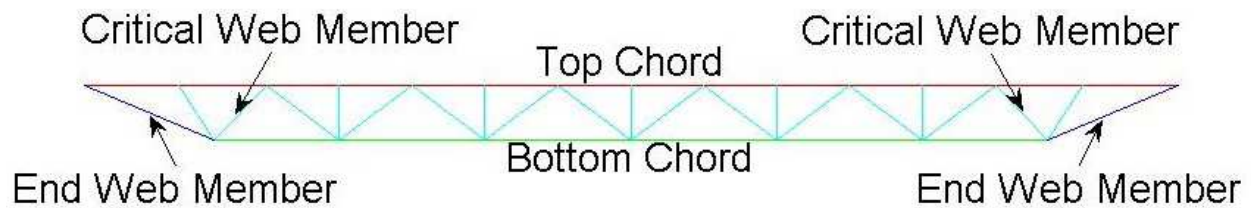
OWSJs' desirability is made apparent by the wide variety of steel buildings for which these structural members are popular. These structures include many buildings which can accommodate large human occupancies or expensive merchandise such as warehouses, industrial plants, offices, commercial shops and malls, schools and other academic facilities, civic and institutional structures, and recreational facilities (Fisher *et al.* 2002). The combination of the large capacity of these buildings with regards to both people and merchandise, along with their susceptibility to snow loads, makes understanding the behavior of these structures critical.

5.3.2 Components of OWSJs

There are four main components of OWSJs: top chord, bottom chord, web members, and end web members, as depicted in Figure 5.1. The top chord is typically under compression when gravity loads are applied and consists of back-to-back angle sections, spaced so that web members can fit between them, and are continuous over the span length of the joist. The top chord is typically continuously laterally braced by the roof or floor decking that the joist supports. The bottom chord is fabricated from two back-to-back angle sections with spacing for web members (Buckley *et al.* 2008). The bottom chord is in tension when loaded and is only laterally braced by angle sections acting as bridging between the joists at certain points. The location of bridging is determined through tables provided by the SJI (Fisher *et al.* 2002, Buckley *et al.* 2008).

Chord members intersect with the diagonally-oriented web members at "panel points". The web members and end web members may be in tension or compression depending on their orientation and position along the joist. For K-Series joists, the end web members are generally

rods, while the interior web members can be fabricated as rods, single angles, or crimped single angles (Buckley *et al.* 2008). When the web members are angle sections, the webs are non-continuous, meaning separate web elements are used between each panel point. However, rod web members are typically composed of one long rod that is bent at every panel point (Canam 2005). If the web members are angles, they must be crimped at the ends for connection with chord members. This crimping causes the centroid of the member to be eccentric to the line of loading, creating a moment in the section (Buckley *et al.* 2008).



*Unlabeled Elements are Web Members
Figure 5.1: Arrangement of the components within an OWSJ

Two types of connections are commonly found in OWSJs. Welds are used to connect the web members and bridging to the chords while bolts are generally used to connect the top chords to the girders that typically support the joists (SJI 2005).

OWSJs are prefabricated by a number of different companies. Owing to the proprietary nature of this process, most of these companies keep design details confidential.

5.3.3 OWSJ Design for Denver, CO

The structure used in this study is a 90 ft. by 120 ft. single story building which has 3 bays of 40 ft. span wide flange section girders in one direction, as shown in Figure 5.2. The roof is supported by 30-ft. K-series OWSJs in the orthogonal direction, which are spaced at 10 ft. intervals along the girders. The roof is 30 ft. high with HSS 6X6X3/8 columns. The structure is designed according to ASCE 7-10.

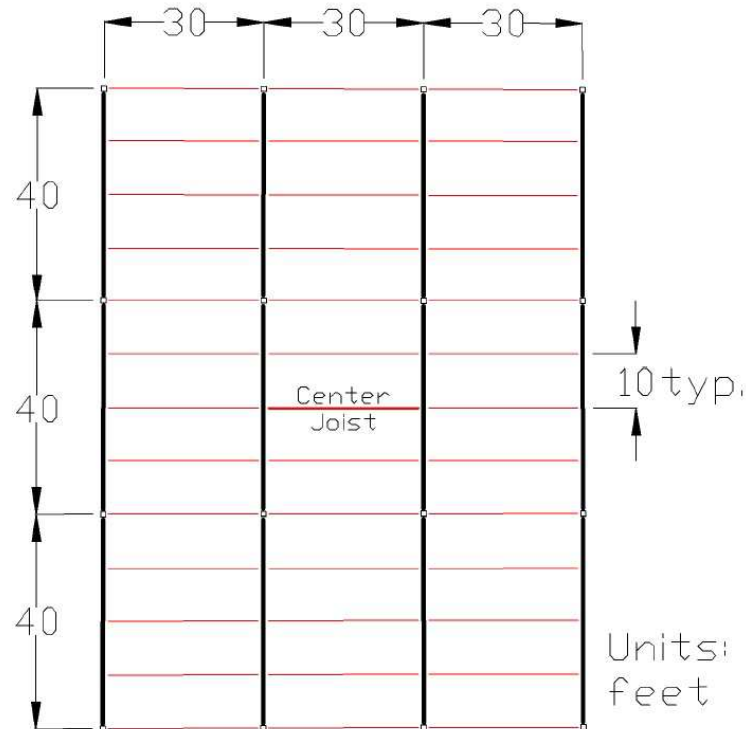


Figure 5.2: Plan view of the structure showing the location of OWSJs (red) and girders (black)

The following loads were considered to design the roof for Denver, CO: (1) a roof live load of 20 psf; (2) a roof dead load of 9 psf, based on data from Boise Cascade (2009) for a metal deck covered in composition roofing; (3) the self-weight of the joist from the SJI's load tables (2005); and (4) a ground snow load of 25 psf, from the City of Denver's Amendments to the Building Code (2011). Using ASCE 7-10 standards for determining roof loads from ground snow load, the design roof snow load is 20 psf. These calculations are based on a structure that is partially exposed (exposure category B), risk category II, and thermal characteristics of a building not kept intentionally cold. The design was performed by uniformly applying the loads on the entire roof.

Using LRFD design and the SJI's load tables (2005), two joists of different depths were found to satisfy the design conditions:

- 18K10, which has a depth of 18 in., a self-weight of 11.7 lbs/ft., and a safe factored uniformly distributed load of 715 lbs/ft..
- 28K6, which has a depth of 26 in., a self-weight of 11.4 lbs/ft., and a safe factored uniformly distributed load of 715 lbs/ft..

The designed girder sections are W18x65. Two rows of L2x2x1/8 sections are used to satisfy SJI (2005) horizontal bridging requirements.

The sizes of chord and web elements and configuration of these elements for both of these joists was determined through a contact with a well-known OWSJ manufacturing company. In order to maintain confidentiality, neither the component sizes nor the name of the company is included in this paper.

5.4 Construction Errors

5.4.1 Possible Construction Errors

The authors collected and reviewed publications in conference proceedings and academic journals on roof failures, as well as a wide variety of roof failure case studies. A large number of the causes for failure of the roofs involved an error in the design, fabrication, or erection of the structure and its components. The identified construction errors can be generally categorized into six types: improper erection, misplacement of members, improper manufacturing of elements, welding errors, handling and construction damage, and deficient materials.

Improper erection of the structure is a major concern due to it resulting in a significant deviation from the appropriate design for the structure. These deviations could include the erection of a structure with incorrect spacing between joists, or installing the joists hanging slightly out-of-plumb (Green *et al.* 2007). Both of these errors create unanticipated stresses in the joist members that were not considered in the design. Other erection errors can include cutting or

altering the joists in contradiction to recommendations by the SJI to leave joists unaltered (Green *et al.* 2007). In other cases, the error may be due to simply not following the construction and erection drawings, for example, leading to installing a member backwards (Geis 2011) or neglecting to install elements such as bridging in the structure (Biegus & Rykaluk 2008).

The misplacement of members occurs if joists are inadvertently swapped in the construction process. Structural failure may occur when a weaker member is substituted into a position where it is not capable of carrying the design loads. This initial failure can then lead to progressive collapse of the entire roof (Lavon & Stivaros 2005, Geis 2011). Misplacement of members can be avoided by reviewing construction drawings and comparing them with the erected structure and appropriately tagging joists (Ratay 2000). However, should the tags fall off or are placed on improper joists, many of the joists look similar to the naked eye. In fact, members used in different joists are generally very similar and may only vary in thickness by dimension on the order of $1/25^{\text{th}}$ of an inch. The probability of a joist losing its tag or joists being placed in the wrong locations occurring is low, but it has occurred in the past (Geis 2011).

Improper manufacturing of elements involves the use of prefabricated or built-up sections which do not necessarily violate the construction or erection drawings, but which incurred errors during the fabrication process. In these types of errors, wrong types or sizes of components are used due to misunderstandings between designers and fabricators (Lavon & Stivaros 2005). These errors often leave the fabricator's facility unnoticed and are erected in the structure due to erectors assuming the fabricators' work is correct (Martin & Delatte 2001, Small & Swanson 2006).

The most common source of structural failure in properly designed structures concerns the connections between all elements (Ratay 2000). In particular, welds may be faulty and have

irregularities or discontinuities such as insufficient weld length, porosity in the weld, cracks in the weld, lack of penetration, or lack of fusion with the base metal (Feld 1968, Ratay 2000, Martin & Delatte 2001, Velhulst *et al.* 2009, Tanzer 2011). These errors are difficult to detect visually. This type of error can occur in any structural system, but the large number of welds involved in OWSJs, trusses, and space trusses along with the common use of these systems, has led to major failures in the past (Martin & Delatte 2001, Tanzer 2011).

Handling and construction damage may be encountered if OWSJs are handled or erected by methods not recommended by the SJI. Handling damage can result in the bending of components or in the crumpling of chord or web members where straps are attached in order to lift and move the joists. Construction damage varies from small dents due to a machine or element contacting another element, to components such as the chords being accidentally cut while drilling is taking place nearby. These errors are generally detectable by a visual inspection, as recommended by the SJI, before the joists are erected (Green 2007, Green *et al.* 2007).

The final construction error identified is the use of a deficient material in construction, which could have a variety of consequences. For OWSJs, the most relevant material deficiencies are insufficient yield and ultimate strength in steel (Tanzer 2011) and base steel that is inappropriate for welding and therefore contributing to weak welds (Feld 1968).

Many of these errors can be avoided by inspecting the structure prior to every step of the construction, in order to verify that the design is followed and that there is no visible damage to the elements and OWSJs. The SJI recommends, but does not require an inspector on site (Martin & Delatte 2001, Green 2007, Green *et al.* 2007, Holicky & Sykora 2009).

5.4.2 Construction Errors Considered in this Study

This study analyzes three of these types of construction errors. First, because the variation in as-built weld properties can be vast and this variation has such a large effect on the structural performance of a joist, weld deficiencies are analyzed. Second, the misplacement of a joist can have a significant impact on the structure, so analyses included a single joist in the structure that differed from the rest of the joists. The third and final construction error investigated concerns the improper erection of the structure, represented by a single joist that is slightly out-of-plumb.

5.5 Numerical Model of OWSJs

5.5.1 Properties of Nonlinear Models

Nonlinear models of the buildings shown in Figure 5.2 were created in the software *OpenSees*. The developed model is capable of representing the major failure mechanisms identified through literature review of case studies of building failures and other studies of OWSJs. Material nonlinearities were implemented in the model for the chords and web members of the joists through the use of nonlinear beam-column (fiber) elements. Steel material nonlinear properties for the grade 50 steel are similar to those proposed by Dodd & Restrepo-Posada (1995), which take into account steel properties beyond the yield point by defining a yield plateau region followed by a strain-hardening region. The Dodd-Restrepo model is based on experimental results and considers any strain past the strain at ultimate stress to be a failure of the material. In order to implement this material in *OpenSees*, the post-peak behavior was taken as a linear reduction from the ultimate stress to zero to represent fiber fracture. The geometry of the nonlinear elements is captured through the use of fiber sections that represent the shape of chord members and end web rods along their entire length. In the case of crimped angle web

sections, meaning the legs of the angle are bent inwards in order to fit between the chord members, the model represents the crimped shape near the panel points and the uncrimped shape in the middle of the member. The columns, girders, and bridging are modeled as elastic beam-columns.

Other failure mechanisms considered in the model are buckling of the end and interior web members (Yost *et al.* 2004). The buckling of the web members is accounted for using equations from the AISC Steel Construction Manual (2011) to calculate the strains at which local torsional and flexural-torsional buckling occurs in angle and rod sections. These calculations assume a semi-rigid effective length factor of 0.70, which is supported by comparison of models and experimental studies. These buckling strains are specific to each web member and are used to modify the steel material used for the individual web member's fibers so that the material strength decreases after the buckling strain is reached following recommendations by Elnashai & Elghazouli (1993), in lieu of continuing on the path defined by the Dodd-Restrepo model. The bottom and top chords are assumed not to buckle because the former is in tension and the latter is braced by the presence of the roof system.

The failures of welded or bolted connections (Buckley *et al.* 2008) are accounted for through the use of zero-length elements, which are modeled at every connection between elements. Bolted connections are located where the chords of the joists meet the girders. The SJI requires that K-Series joist ends be connected by two ½" A307 bolts (SJI 2005). The shear and tensile properties for the connection details were determined and applied as force-displacement and moment-rotation curves in the appropriate directions in the zero length springs. Welds constructed using E70XX welding electrodes are assumed to connect the grade 50 steel web members with the chords. The Lesik & Kennedy (1990) weld material model is employed to

determine the force-displacement properties of the welds. The moment-rotation properties were based on the weld lengths required by the connection geometry and the elastic method as recommended by the AISC (2011). These models represent nonlinear behavior at the welded and bolted joints. Failure displacements and rotations are also calculated and implemented within the spring properties to represent weld fracture.

5.5.2 Implementation of Construction Errors

The modeled building was modified to accommodate the three construction errors described above. Table 5.1 lists the structures analyzed in this study. All three errors under investigation are applied to only the center joist in the structure (Figure 5.2), while the other joists are modeled without construction errors.

Table 5.1: List of buildings under investigation designed for Denver, CO (25 psf of design ground snow load)

Bldg. No.	As-designed OWSJ	Error in center joist
1	18K10	No Error
2	18K10	Weld Length Reduced 65%
3	18K10	Misplaced Joist: 18K7
4	18K10	Out-of-Plumb 1"
5	18K10	Out-of-Plumb 2"
6	28K6	No Error
7	28K6	Weld Length Reduced 35%
8	28K6	Misplaced Joist: 28K12
9	28K6	Out-of-Plumb 1"
10	28K6	Out-of-Plumb 2"

The weak weld construction error is implemented by assigning the welds for the critical web members (the location of which is shown in Figure 5.1) reduced weld lengths. The shorter welds reduce the rotation capacity and ultimate forces and moments that the connection can withstand. The weld reduction is different for the two structures to ensure that weld failure governs the building failure. The structure with 18K10 joists reduces the weld lengths in the critical web connections by 65%, while the weld lengths in the 28K6 structure are reduced by 35%.

The misplacement of joists is represented by the replacement of the center joist of the structure with another joist that looks similar to the properly designed joist. For the structure with 18K10 joists, the erroneous joist is an 18K7 joist. The 18K7 joist differs only 1/25 in. in chord thickness from the 18K10, but can only resist 502 lb/ft. (SJI 2005), which is 213 lb/ft. less than an 18K10 joist. The misplaced joist for the 28K6 structure is a 28K12 joist, which can resist 110 lb/ft. more than a properly designed 28K6 joist with 825 lb/ft. of resistance.

The out-of-plumb joists are executed in the model by defining the model geometry such that the top and bottom chords are not aligned with each other. Out-of-plumbness at 1 in. and 2 in. is considered.

5.5.3 Pushdown Analysis

The models are analyzed using a pushdown load, under which the downward load on the roof is increased in a pre-defined pattern until one or more elements in the joist fails due to one of the mechanisms described above. The analysis is displacement controlled with the control node at the center of the structure in plan. The displacements and corresponding loads are recorded and plotted against each other in order to form the pushdown curve, which relates loads to displacements. During this analysis, the response of key nodes and elements is recorded to determine how the structure is failing. In this study, only uniform loads were considered in the pushdown analysis; however, drifted loads or other load patterns may be examined in future studies.

The models were validated by comparing results from an analytically derived pushdown curve to pushdown results from physical experiments on OWSJs performed by Yost *et al.* (2004). The models of three experimental specimens matched the pushdown curves of the experimental results well. The stiffness of the model joists were within the range of stiffness

determined through experimental results. The comparison of the ultimate load and displacement at ultimate load were also favorable with the modeled ultimate loads being only slightly higher than the experimental results and the displacements being within the range of experimental results. In addition, both the model and experimental joists failed in the same mechanism: buckling of the critical web member. Another point of comparison for the models is through comparison with the design loads for each joist defined in the SJI load tables. The modeled failure load for the joists used in this study exceeds the design loads provided in the SJI's load tables by over 250 plf for the 18K10 joist, as expected.

5.5.4 Pushdown Analysis Results

The results from the pushdown analyses of all ten building are presented in Figs. 3 & 4. On these figures, the roof load includes the load on the roof applied in excess of the dead load; the displacement represents the downward displacement of the control node (at center of the center joist). Due to the reported roof load being in excess of the dead load, the curve has a non-zero displacement under no load which corresponds to the displacement of the control node under dead loads only.

Figure 5.3 provides the basis for comparison of *Bldgs. 1-5*, which all use the joist 18K10 as the base joist. The error-free building, *Bldg. 1*, fails at the point indicated on Figure 5.3 due to buckling of the critical web members in the majority of joists. *Bldg. 2* fails at a lower load than *Bldg. 1* because of the weakened weld connection between the critical web member and the bottom chord. *Bldg. 3* is unique because it is the only building out of the ten to exhibit significant ductility. Since the center joist of *Bldg. 3* is weaker than the surrounding joists, loads are redistributed from the center joist to others, until a load causing localized buckling at the mid-span of the top chord of the center joist is reached. The different joist is also the reason why

Bldg. 3 is less stiff than the other buildings. The buildings with out-of-plumb joists, *Bldgs. 4 & 5*, fail under different loads, but due to the same failure mechanism. The out-of-plumb joist creates torsion within the entire OWSJ, which adds a significant bending moment out of the plane of the joist to the web members. These members are designed to solely account for axial loads, causing them to buckle. This failure mechanism affects all the web members, but those designed originally for tension are affected the most due to their relatively low moments of inertia.

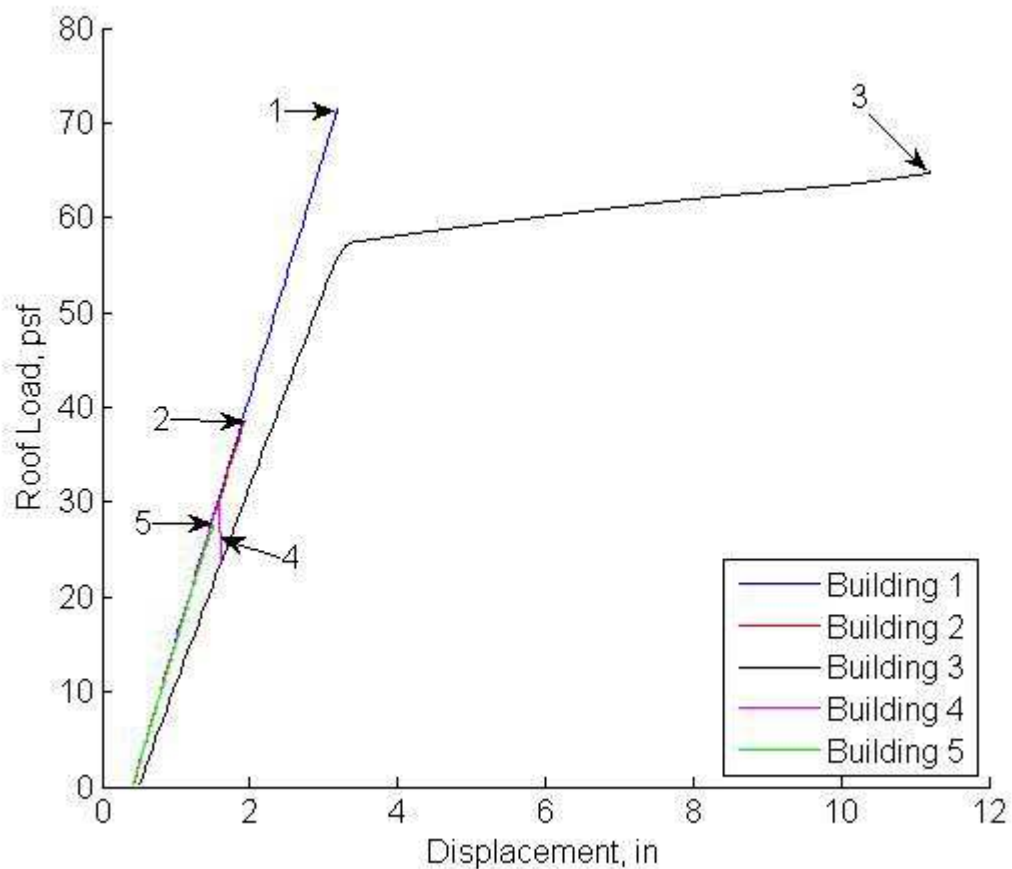


Figure 5.3: Pushdown results for buildings 1-5

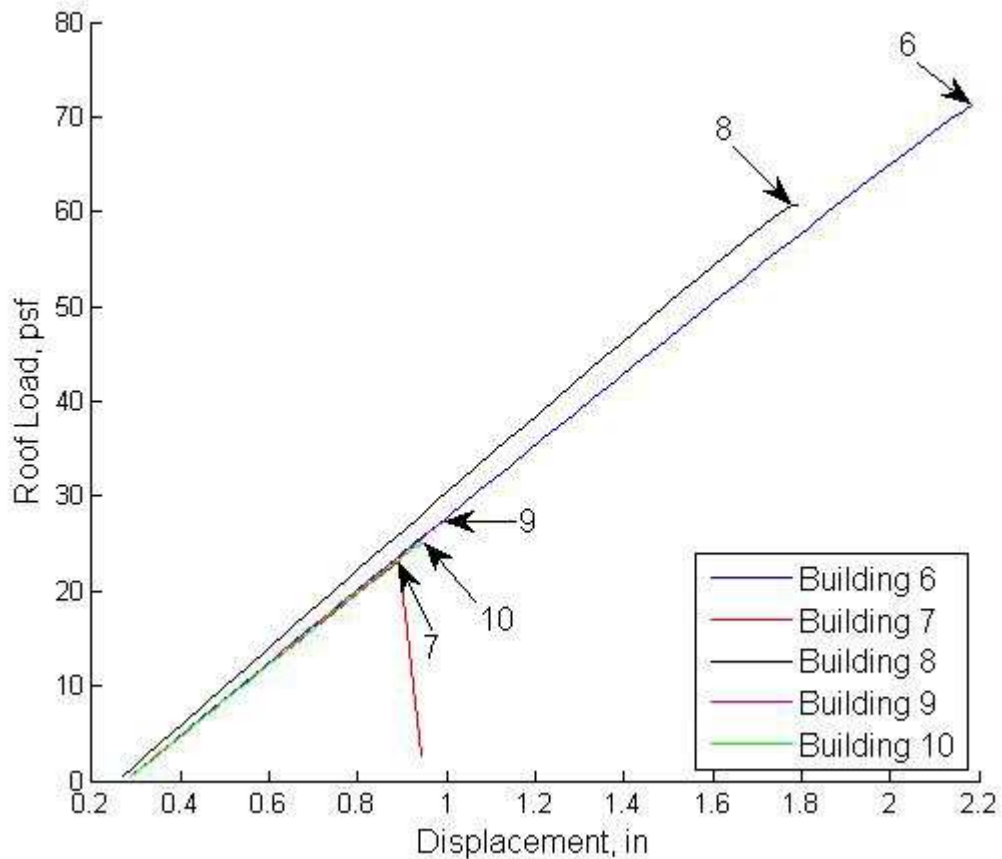


Figure 5.4: Pushdown results for buildings 6-10

Figure 5.4 presents the pushdown curves for *Bldgs. 6-10*, all of which have a 28K6 joist as their base joist. The error-free building, *Bldg. 6*, fails due to the fracture of the connection between the critical web members and the bottom chord. This failure mechanism is also encountered in *Bldg. 7*, but occurs at a lower load due to the weakened weld in that building. *Bldg. 8* demonstrates what happens when the center joist is stronger than the surrounding joists. Due to the joist misplacement, the stiffness of the building increases. However, failure still occurs at about the same load as the error-free building because the joists adjacent to the center joist have the original joist strength. As with *Bldgs. 4 & 5*, *Bldgs. 9 & 10* fail by web member buckling resulting from global torsion of the OWSJ.

5.6 Reliability Analysis

5.6.1 Methodology

Using the pushdown results, a reliability analysis can be performed to assess the risk of the roof failure under snow loads for Denver, CO. The model assumes the dead load and a roof live load of 14.3 psf (based on recommendations from Paz, 1994) is present on the roof at any given time. Different realizations of snow load are applied on top of the dead and live load. These snow loads represent the probability density function (PDF) for snow load in Denver and are applied to the model through Monte Carlo simulation. The PDF for Denver's ground snow load, shown in Figure 5.5, was obtained through 121 years of recordings of snow depth and snow water equivalence at the Stapleton Airport in northeast Denver (SEAC 2007). The history of ground snow load data at the site was fitted to a Log-Pearson III distribution with a mean annual maximum ground snow load of 5.77 psf with standard deviation of 4.54 psf. For simplicity, the ASCE 7-10 equations are used to translate ground to roof snow loads, taking the thermal, exposure, and importance factors equal to unity:

$$SL_{roof} = 0.7SL_{ground} \quad (5.1)$$

In the reliability analysis, 100,000 randomly selected annual maximum roof snow loads representing Figure 5.5 and Equation (5.1) are considered. The limit states under investigation are: (1) total roof load surpassing the ultimate strength of the building, and (2) the downward deflection under total load exceeding 1/240 of the span length (1.5" in. this case). The pushdown curves are used to determine whether these limit states have been reached. These limit states were chosen because they represent failure of the structure which would be dangerous and costly (*i.e.* limit state 1), as well as serviceability failure of the structure which is not as dangerous, but

could still be costly to building owners (*i.e.* limit state 2). The deflection limits in (2) are defined by ASCE 7-10 in the commentary (appendix C).

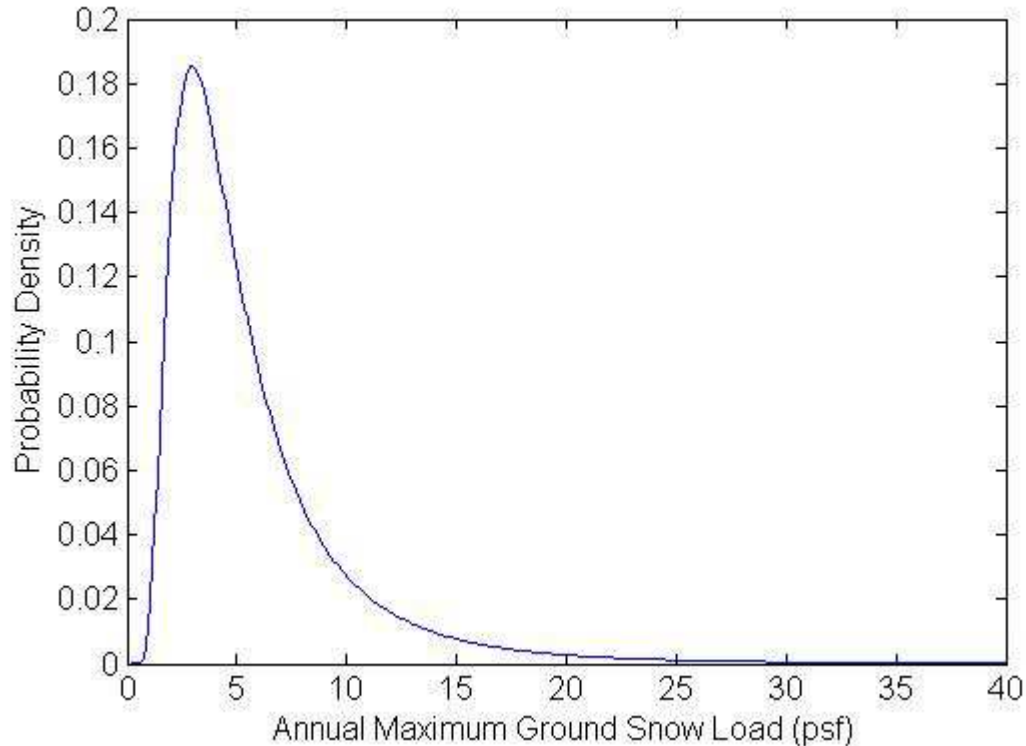


Figure 5.5: Probability density function for the ground snow load of Denver, Colorado

5.6.2 Reliability Results

The results of the reliability analysis for all ten buildings are presented in Table 5.2. For *Bldgs. 1-5*, which use an 18K10 base OWSJ, the safest building in terms of structural failure is *Bldg. 1* (*i.e.* the building with the lowest probability of limit state 1 occurrence), which is to be expected because it is free of construction errors. In Denver, CO this building will only fail once in about 11,111 years. For this discussion, suppose we judge an acceptable probability of structural failure by two conditions: (1) a safety index of 3.5 over 50 years, as recommended by the ASCE 7-10 commentary, which corresponds to an annual probability of failure of 5×10^{-6} (one failure in 200000 years), and (2) a safety index of 2.5 over 50 years which corresponds to an

annual probability of failure of 1.25×10^{-4} (one failure in 8000 years). Results show that the error-free *Bldg. 1* is well within acceptable limits for a safety index of 2.5, but not within the limits for a safety index of 3.5. However, the serviceability limit will be violated about once every 60 years. Exceeding the serviceability limit state may cause visually apparent deformations, general architecture damage, or other damage to non-structural components (ASCE 2010).

Table 5.2: Results of reliability analysis

Building No.	Probability of limit state occurring annually	
	Structural failure	$\Delta_{Tot} > L/240$
1	0.00009	0.01650
2	0.00291	0.01670
3	0.00018	0.10731
4	0.01213	0.01676
5	0.02066	0.02066
6	0.00009	0.00094
7	0.06778	0.06778
8	0.00009	0.00054
9	0.02273	0.02273
10	0.03996	0.03996

Bldg. 3, which has an under-designed joist, also has a low probability of structural failure and has the closest results to those from *Bldg. 1* despite not satisfying the limits of either safety index (about 1 collapse in 5556 years). This relatively high level of reliability can be attributed to the center joist's ability to redistribute load while remaining intact. Interestingly, the under-designed joist has a more significant impact on serviceability than strength. *Bldg. 3* has a high probability of exceeding the serviceability limit state (about once every 9 years). This building has lower stiffness than the others, leading to higher displacements at any load relative to the other nine buildings under investigation.

Of the remaining construction errors, the 18K10 base OWSJ buildings is least affected by weakened welds. *Bldg. 2* produces a failure rate of about once in 344 years which remains relatively close to the results of *Bldg. 1*. On the other hand, *Bldgs. 4 & 5*, which have out-of-

plumb joists, are the buildings with the worst reliability. For *Bldgs. 4 & 5* the probability of collapse corresponds to the buildings failing once every 82 and 48 years, respectively. The probability of exceeding the serviceability limit state is also slightly higher relative to *Bldgs. 1 & 2*, but still less than those from *Bldg. 3*. Despite this last point, the high probability of structural failure and the relatively high probabilities of serviceability failure indicate that *Bldgs. 4 & 5* are the most unreliable of the construction errors considered in the 18K10 joist buildings.

Results from *Bldgs. 6-10* lead to slightly different conclusions. The 28K6 base joist used in these buildings has a smaller bottom chord, leaving less space to weld the web members to the chord and leading to inherently weaker connections. This is observed immediately by recalling that *Bldg. 6*, the base building, fails by a weld failure. The probability of structural failure of the error-free building is outside of the acceptable limits for both safety index values considered, having a probability of structural failure of once in about 11,111 years. However, the deeper joists lead to higher stiffness of *Bldg. 6*, which produces lower probabilities of serviceability limits being exceeded as compared to *Bldg. 1*.

Comparing now the error-free building to those with construction errors, *Bldg. 7*, which has a weakened weld, proves to be the most unreliable building due to the susceptibility to weld failure of this structure. This building produces a probability of structural failure of about once in 15 years, which is dramatically less reliable than *Bldg. 6*. The misplaced joist building, *Bldg. 8*, produces roughly the same results as the error-free building due to their almost identical failure loads. The main difference is that *Bldg. 8* produces smaller displacements throughout the reliability analysis due to its larger stiffness. *Bldgs. 9 & 10*, much like *Bldgs. 4 & 5*, also have high probabilities of experiencing structural failure which are much less than the results from *Bldg. 6* (once in 44 years, and once in 25 years respectively) and high probabilities of exceeding

the serviceability limit. Although *Bldg. 7* is definitely the least reliable building of *Bldgs. 6-10*, the relatively poor performance of *Bldgs. 9 & 10* should not be disregarded.

5.7 Conclusions

This paper sheds light on the potential harm to structures whose roofs are supported by OWSJs with respect to both structural failure and serviceability conditions. The results presented in this paper demonstrate that having an error in the fabrication process such as a weak weld, or errors in the erection of a building such as misplacement of joists or erecting joists out-of-plumb can have negative effects on the reliability of the building. In particular, installing joists that are out-of-plumb in plane greatly decreases the reliability of the structure regardless of the base joist.

These results provide evidence to encourage fabricators and erectors to develop plans to avoid these construction errors. Although these analyses only considered small buildings under uniform snow load, the effects may be even more significant under drifted loads.

6 CONCLUSIONS

6.1 Summary

This thesis discusses the effects which various roof and joist characteristics have on the behavior and reliability of open web steel joist (OWSJ) buildings. The results were obtained through a nonlinear *OpenSees* model of the buildings which included capturing the realistic behavior of welded and bolted connections, as well as for the chord and web elements within the OWSJs.

Chapter 2 details the specific methods used to implement the nonlinear properties of the connections and OWSJ elements into *OpenSees*. The nonlinear properties of connections are represented through zero-length elements. The material and geometric nonlinearities of the OWSJ elements are accounted for through displacement-based beam-columns which use fiber sections. The model is validated as an accurate method of predicting the failure displacement, load, and method through comparison with experimental results achieved by Yost *et al.* (2004). This validation allows the author to have confidence in the results provided by the *OpenSees* model in describing the appropriate behavior of OWSJ buildings.

Chapter 3 of the thesis analyzes the behavior of OWSJ buildings with various building and joist characteristics under both uniform and drifted snow loads. It is concluded from the results of these analyses that the majority of OWSJ buildings will fail at a load 1.03 to 1.25 times larger than the building capacity which is expected from the Steel Joist Institute's (SJI) load tables when subjected to uniform snow loads. Under drifted snow loads with wind parallel to the joists this overstrength ratio changes to being between 0.61 and 1.87 relative to the peak drift load. These differences in overstrength within the OWSJs depending on the loading method highlights the uncertainty involved with OWSJs when subjected to drifted snow loads.

Through observation of the resulting behavior of the OWSJ buildings subjected to uniform snow loads some trends in their behavior are identified. These trends include the increase in the load capacity of buildings with shorter joist spans, and the increase in building stiffness as the girder span decreases, the joist spacing increases, or the OWSJ depth increases. These trends can be used to develop safer OWSJ buildings by avoiding the building characteristics which produce negative effects on the building's behavior.

Other important conclusions gained from the study of the behavior of OWSJ buildings is that the interaction between the joists within the building have a large effect on the failure of the joists. This is concluded by observing that individual simply-supported joists fail well above the capacity provided in the SJI's load tables, however when implemented in buildings the joists fail much closer to the SJI load table values. These joist interactions within buildings also significantly affect the failure method of the joists by introducing failure methods such as having the semi-rigid connections at the ends of the joists cause a shear failure in the top chord. These types of failure methods are not typically observed in single OWSJs providing evidence to the conclusion that joist interaction is an important factor to consider in OWSJ building design.

Chapter 4 studied the reliability of OWSJ buildings in comparison to ASCE 7-10 commentary reliability recommendations and properly designed, simply supported W-sections. The observations provided insight into the trends in reliability for both structural and serviceability failure under OWSJ buildings with varying building characteristics. In general, it is determined that the overall structural reliability of the OWSJ buildings are low compared to the recommended reliability index values provided by the ASCE 7-10 commentary. This leads to concluding that the current design load factors and design ground snow loads may be insufficient and that the ASCE 7-10 snow design may be non-conservative.

The reliability results also provided useful information on which building characteristics affect the reliability of OWSJ buildings. It was determined that significant changes in reliability occur when the joist span, joist spacing, design dead-to-snow load ratio, and parapet height (representing snow drift size) are varied. A couple of interesting points about these conclusions are that lower design dead-to-snow load ratios (also known as lightweight buildings) are shown to be less reliable than buildings with higher design dead-to-snow load ratios. Also, the severe decrease in reliability as the parapet height increases once again highlights the need to investigate the behavior of OWSJs subjected to drifted snow loads in further detail.

Chapter 5 details the effects which construction errors in the fabrication, manufacturing, and erection processes have on the behavior and reliability of OWSJ buildings. It was concluded that the construction errors studied had significant impacts on the behavior and reliability of the buildings, often causing failure at lower loads leading to a severe decrease in reliability. These results provide evidence to the risks involved with construction errors in OWSJ systems and justify the encouragement of fabricators and erectors to be careful in order to avoid these errors.

6.2 Future Work

A main conclusion gathered from this study involved the failure methods of OWSJ buildings and how they varied from the failure methods of single, simply supported OWSJs. Future studies should investigate the specific effects involved with incorporating OWSJs in entire buildings as opposed to studying single OWSJs alone. Studies of these interaction effects could yield results extremely important to decreasing the risk involved in OWSJ buildings by identifying improvements to joist designs which could be made.

Future studies on the subject of open web steel joists subjected to snow loads could focus on variations of the drifted snow load pattern. Although the snow drifts in this study considers

factors such as downwind roof length (snow fetch), snow load, and obstruction (parapet) height, there are still many factors, such as wind speed and elapsed time from snowfall, which can be used to create more accurate snow drift models (Cocca & O'Rourke 2008). The snow drift buildings in this study were identified as having a wide range of behavior and studying these effects under more accurate conditions could yield useful information concerning the design of OWSJs and other members under drifted snow loads.

LIST OF REFERENCES

- American Institute of Steel Construction (AISC). 14th ed. 2011. *AISC Steel Construction Manual*. Chicago, IL: AISC.
- American Society of Civil Engineers (ASCE). 2006. ASCE Standard ASCE/SEI 41-06: Seismic Rehabilitation of Existing Buildings. Reston, VA: ASCE.
- American Society of Civil Engineers (ASCE). 2010. ASCE Standard ASCE/SEI 7-10: Minimum Design Loads for Buildings and Other Structures. Reston, VA: ASCE.
- American Society for Testing and Materials (ASTM). 2012. ASTM A307-12: Standard Specification for Carbon Steel Bolts, Studs, and Threaded Rod 60 000PSI Tensile Strength. West Conshohocken, PA: ASTM International.
- Bennett, R.M. 1988. Snow Load Factors for LRFD. *Journal of Structural Engineering* 114 (10): 2371-2383
- Biegus, A. & Rykaluk, K. 2009. Collapse of Katowice Fair Building. *Engineering Failure Analysis* 16: 1643-1654
- Boise Cascade. 2009. *Weights of Building Materials*. <<http://www.bc.com/wood/ewp/guides-resources/Technical-Notes/General-Technical-Notes.html>>.
- Bolduc, W.T. 2011. When the Roof Collapses. *Structures Congress 2011*: 1827-1838.
- Bruneau, M., Uang, C.-M., & Whittaker, A. 1998. *Ductile Design of Steel Structures*. New York, NY: McGraw-Hill.
- Buckley, E.T., Dinehart, D.W., Green, P.S., Gross, S.P., & Yost, J.R. 2008. Experimental Study of Open Web Steel Joists with Crimped Critical Web Members. *2008 SRCC Annual Stability Conference Proceedings* April, 2008.
- Canam Joists and Steel Deck. 2005. *Joist Catalogue*. Saint-Gedeon, QC: Canam Group.

- Chan, S.L. & Chui, P.P.T. 2000. Non-Linear Static and Cyclic Analysis of Steel Frames with Semi-Rigid Connections. New York, NY: Elsevier.
- City and County of Denver. 2011. *Amendments to the Building Code for the City and County of Denver*. Denver, CO: City and County of Denver.
- City of Boulder, Colorado. 2013. *Boulder Revised Code*. Boulder, CO: City of Boulder.
- Cocca, J. & O'Rourke, M. 2008. Mathematical Simulation of 50-Year Snow Drift Loads. *Structures Congress 2008*: 1-9
- DeGaetano, A.T., Schmidlin, T.W., & Wilks, D.S. 1997. Evaluation of East Coast Snow Loads Following January 1996 Storms. *Journal of Performance of Construction Facilities* May, 1997: 90-94.
- DeGaetano, A.T. & Wilks, D.S. 1999. Mitigating snow-induced roof collapses using climate data and weather forecasts. *Meteorological Applications* 6: 301-312.
- DePaolo, M.R. 2013. A Proposal for a Unified Process to Improve Probabilistic Ground Snow Loads in the United States Using SNODAS Modeled Weather Station Data. MS Thesis, University of Colorado. Boulder, CO.
- Dodd, L.L. & Restrepo-Posada, J.I. 1995. Model for Predicting Cyclic Behavior of Reinforcing Steel. *Journal of Structural Engineering* 121 (3): 433-445.
- Ellingwood, B., Galambos, T.V., MacGregor, J.G., & Cornell, C.A. 1980. *Development of a Probability Based Load Criterion for American National Standard A58*. Washington, DC: National Bureau of Standards.
- Elnashai, A.S. & Elghazouli, A.Y. 1993. Performance of Composite Steel/Concrete Members under Earthquake Loading. Part I: Analytical Model. *Earthquake Engineering and Structural Dynamics* 22: 315-345.

- Feld, J. 1968. *Construction Failure*. New York, NY: John Wiley & Sons, Inc.
- Fisher, J.M., West, M.A., & Van de Pas, J.P. 2002. *Designing with Vulcraft: Steel Joists, Joist Girders and Steel Deck*. Charlotte, NC: Vulcraft, A Division of Nucor Corporation.
- Frye, M.J. & Morris, G.A. 1975. Analysis of flexibly connected steel frames. *Canadian Journal of Civil Engineering* 2 (3): 280-291.
- Geis, J.M. 2011. The Effects of Snow Loading on Lightweight Metal Buildings with Open-Web Steel Joists. MS Thesis, University of Colorado. Boulder, CO.
- Geis, J.M., Strobel, K.M., & Liel, A.B. 2011. Snow Induced Building Failures. *Journal of Performance of Constructed Facilities* 26 (4): 1-12.
- Green, P.S. 2007. Evaluation and Modification of Open-Web Steel Joists and Joist Girders. *2007 Structures Congress* May 2007.
- Green, P., Sputo, T., & Higgins, A. 2005. *Design of All-Bolted Extended Double Angle, Single Angle, and Tee Shear Connections*. A Report Presented to the American Institute of Steel Construction. Jan. 2005.
- Green, P.S., Pugh, C., & Worthley, W. 2007. Safe Handling and Erection of Steel Joists and Joist Girders. *North American Steel Construction Conference 2007 Proceedings* 2007.
- Gulvanessian, H. 2004. System of European Codes and Standards for Construction Work. In *Implementation of Eurocodes, Handbook 1: Basis of Structural Design*, by the Leonardo Da Vinci Pilot Project.
- Hess, P.E., Bruchman, D., Assakkaf, I.A., & Ayyub, B.M. Uncertainties in Material and Geometric Strength and Load Variables. *Naval Engineers Journal* 114 (2) April 2002: 139-166.

- Holický, M. 2007. Safety design of lightweight roofs exposed to snow load. *Engineering Sciences* 58: 51-57.
- Holický, M., Materna, A., Sedlacek, G., Arteaga, A., Sanpaolesi, L., Vrouwenvelder, T., Kovse, I., & Gulvanessian, H. 2005. *Development of Skills Facilitating Implementation of Eurocodes, Handbook 2: Reliability Backgrounds*. Prague, Czech Republic: Leonardo Da Vinci Pilot Project.
- Holický, M. & Sykora, M. 2009. Failures of Roofs under Snow Load: Causes and Reliability Analysis. *Forensic Engineering Congress 2009*: 444-452.
- Kwan, Y.K., Gomez, I.R., Grondin, G.Y., & Kanvinde, A.M. 2010. Strength of welded joints under combined shear and out-of-plane bending. *Canadian Journal of Civil Engineering* 37 (2): 250-261.
- Lavon, B. & Stivaros, P.C. 2005. Structural Steel Framing Failures – What Went Wrong? *ASCE Structures Congress* April, 2005.
- Lesik, D.F. & Kennedy, D.J.L. 1990. Ultimate Strength of Fillet Welded Connections Loaded in Plane. *Canadian Journal of Civil Engineering* 17 (1): 55-67.
- Levy, M. & Salvadori, M. 2002. *Why Buildings Fall Down: How Structures Fail*. New York, NY: W.W. Norton & Company.
- Martin, R. & Delatte, N.J. 2001. Another Look at Hartford Civic Center Coliseum Collapse. *Journal of Performance of Constructed Facilities* February 2001: 31-36.
- McCabe, G.J., Clark, M.P., & Hay, L.E. 2007. Rain-on-Snow Events in the Western United States. *Bulletin of the American Meteorological Society* March 2007: 319-328.
- Melchers, R.E. 1999. *Structural Reliability Analysis and Prediction*. Chinchester, England: John Wiley & Sons.

- Meløysund, V., Lisø, K.R., Hygen, H.O., Høiset, K.V., & Leira, B. 2007. Effects of wind exposure on roof snow loads. *Building and Environment* 42: 3726-3736.
- Ogrin, M. & Ortar, J. 2007. The Importance of Water Accumulation of Snow Cover Measurements in Mountainous Regions of Slovenia. *Acta geographica Slovenia* 47 (1): 47-71
- O'Rourke, M. & Auren, M. 1997. Snow Loads on Gable Roofs. *Journal of Structural Engineering* December, 1997: 1645-1651.
- O'Rourke, M. & Downey, C. 2001. Rain-on-Snow Surcharge for Roof Design. *Journal of Structural Engineering* January, 2001: 74-79.
- O'Rourke, M. 2010. Snow Loads: Guide to the Snow Load Provisions of ASCE 7-10. Reston, VA: ASCE.
- O'Rourke, M., Koch, P., & Redfield, R. 1983. *Analysis of Roof Snow Load Case Studies – Uniform Loads*. Hanover, NH: Cold Regions Research & Engineering Laboratory.
- Paz, M. 1994. International Handbook of Earthquake Engineering; Codes, Problems, and Examples. New York, NY: Chapman & Hall
- PEER. 2013a. *OpenSees (Open System for Earthquake Engineering Simulation)*. <<http://opensees.berkeley.edu/>>.
- PEER. 2013b. *OpenSees Wiki*. <<http://opensees.berkeley.edu/wiki/index.php>>.
- Peraza, D.B. 2000. Snow-Related Roof Collapses – Several Case Studies. Proceedings of the Second *Forensic Congress* May, 2000: 580-589.
- Perea, T. & Leon, R. 2008. Behavior of Composite CFT Beam-Columns Based on Nonlinear Fiber Element Analysis. *Proceedings of the 2008 Composite Construction in Steel and Concrete Conference VI* July, 2008: 237-251.

- Ratay, R.T. 2000. *Forensic Structural Engineering Handbook*. New York, NY: McGraw-Hill.
- Sadovský, Z. & Páleš, D. 2008. Probabilistic Optimization of Partial Safety Factors for the Design of Industrial Buildings. *International Journal of Reliability, Quality and Safety Engineering* 15 (5): 411-424.
- Shooman, M.L. 1968. *Probabilistic Reliability: An Engineering Approach*. New York, NY: McGraw-Hill.
- Steel Joist Institute (SJI). 2005. American National Standard SJI-K-1.1: Standard Specification for Open Web Steel Joists, K-Series. Florence, S.C.: SJI
- Structural Engineers Association of Colorado (SEAC). 2007. *Colorado Ground Snow Loads Map*. Lakewood, CO: SEAC.
- Small, W.W. & Swanson, P.G. 2006. Roof Collapse – A Forensic Analysis Years After. *Forensic Engineering: Proceedings of the Fourth Congress 2006*: 414-422.
- Strobel, K. & Liel, A.B. 2013. Snow Load Damage to Buildings: Physical and Economic Impacts. *Forensic Engineering*, In Press.
- Summit County, Colorado. 2013. *Summit County Building Department Inspection Matrix*. Frisco, CO: Summit County Building Inspection Department.
- Takahashi, T. & Ellingwood, B.R. 2005. Reliability-based assessment of roofs in Japan subjected to extreme snows: incorporation of site-specific data. *Engineering Structures* 27: 89-95.
- Tanzer, A. 2011. High School Gymnasium Roof Truss Support Collapse. *Journal of Failure Analysis and Prevention* 11: 208-214.
- Tobiasson, W. & Greatorex, A. 1996. Database and Methodology for Conducting Site Specific Snow Load Case Studies for the United States. *Proceedings from the Third International Conference on Snow Engineering*: 249-256.

- Tobiasson, W., Buska, J., Grestorex, A, Tirey, J., Fisher, J., & Johnson, S. 2000. Developing ground snow loads for New Hampshire. In *Snow Engineering*, by Hjorth-Hansen, Holand, Løset, & Norem: 313-321.
- Velhulst, S.M., Ahuja, D., & Schober, G.G. 2009. From Concept to Collapse. *Forensic Engineering: Proceedings of the Fifth Congress 2009*: 404-413.
- Vulcraft. 2007. *Steel Joists and Joist Girders*. Florence, SC: Vulcraft Group.
- Yost, J.R., Dinehart, D.W., Gross, S.P., Pote, J.J., & Deeney, J. 2006. Buckling Strength of Single-Angle Compression Members in K-Series Joists. *Engineering Journal*, Second Quarter 2006: 141-152.
- Yost, J.R., Dinehart, D.W., Gross, S.P., Pote, J.J., & Gargan, B. Strength and Design of Open Web Steel Joists with Crimped-End Web Members. *Journal of Structural*

APPENDIX A

This section provides information concerning the open web steel joist bridging guides used for design in the study. The bridging guides are provided by the Steel Joist Institute (SJI) and differ depending on the type of joist (K, LH, or DLH series) and the type of bridging used (horizontal or diagonal).

For K-Series joists Table A.1 provides the number of required rows of bridging per joist for both horizontal and diagonal bridging based on the joist's section number and span. Tables A.2 and A.3 provide the size of the bridging sections to be used for horizontal and diagonal bridging, respectively. The member sizes are based on joist spacing and section number for horizontal bridging and joist spacing and depth for diagonal bridging. The combination of the size of the bridging of the members and the required number of rows of bridging per joist provides all the characteristics required for the bridging to be implemented into the design.

Table A.1: Number of rows of top chord bridging required for K-Series joists (SJI 2005)

U. S. UNITS					
NUMBER OF ROWS OF TOP CHORD BRIDGING**					
Refer to the K-Series Load Table and Specification Section 6 for required bolted diagonal bridging. Distances are Joist Span lengths in feet - See "Definition of Span" preceding the Load Table.					
*Section Number	One Row	Two Rows	Three Rows	Four Rows	Five Rows
#1	Up thru 16	Over 16 thru 24	Over 24 thru 28		
#2	Up thru 17	Over 17 thru 25	Over 25 thru 32		
#3	Up thru 18	Over 18 thru 28	Over 28 thru 38	Over 38 thru 48	
#5	Up thru 19	Over 19 thru 29	Over 29 thru 39	Over 39 thru 50	Over 50 thru 52
#6	Up thru 19	Over 19 thru 29	Over 29 thru 39	Over 39 thru 51	Over 51 thru 56
#7	Up thru 20	Over 20 thru 33	Over 33 thru 45	Over 45 thru 58	Over 58 thru 60
#8	Up thru 20	Over 20 thru 33	Over 33 thru 45	Over 45 thru 58	Over 58 thru 60
#9	Up thru 20	Over 20 thru 33	Over 33 thru 46	Over 46 thru 59	Over 59 thru 60
#10	Up thru 20	Over 20 thru 37	Over 37 thru 51	Over 51 thru 60	
#11	Up thru 20	Over 20 thru 38	Over 38 thru 53	Over 53 thru 60	
#12	Up thru 20	Over 20 thru 39	Over 39 thru 53	Over 53 thru 60	

* Last digit(s) of joist designation shown in Load Table

Table A.2: Bridging member sizes for horizontal bridging for K-Series joists (Vulcraft 2007)

SECTION NUMBER**	BRIDGING MATERIAL SIZE						
	Round Rod	Equal Leg Angles					
	1/2" DIA (13mm) r = .13"	1 x 7/64 (25mm x 3mm) r = .25"	1-1/4 x 7/64 (32mm x 3mm) r = .25"	1-1/2 x 7/64 (38mm x 3mm) r = .30"	1-3/4 x 7/64 (45mm x 3mm) r = .35"	2x 1/8 (51mm x 3mm) r = .40"	2-1/2 x 5/32 (64mm x 4mm) r = .50"
1 thru 9	3'-3" (991mm)	5'-0" (1524mm)	6'-3" (1905mm)	7'-6" (2286mm)	8'-7" (2616mm)	10'-0" (3048mm)	12'-6" (3810mm)
10	3'-0" (914mm)	4'-8" (1422mm)	6'-3" (1905mm)	7'-6" (2286mm)	8'-7" (2616mm)	10'-0" (3048mm)	12'-6" (3810mm)
11 and 12	2'-7" (787mm)	4'-0" (1219mm)	5'-8" (1727mm)	7'-6" (2286mm)	8'-7" (2616mm)	10'-0" (3048mm)	12'-6" (3810mm)

**SECTION NUMBER REFERS TO THE LAST DIGITS OF JOIST DESIGNATION, CONNECTION TO JOIST MUST RESIST 700 POUNDS (3114 N)

Table A.3: Bridging member sizes for diagonal bridging for K-, LH-, and DLH-Series joists (Vulcraft 2007)

Joist Depth	Bridging Angle Size				
	1x7/64 r = .20"	1-1/4x7/64 r = .25"	1-1/2x7/64 r = .30"	1-3/4x7/64 r = .35"	2x1/8 r = .40"
12	6'-6"	8'-3"	9'-11"	11'-7"	
14	6'-6"	8'-3"	9'-11"	11'-7"	
16	6'-6"	8'-2"	9'-10"	11'-6"	
18	6'-6"	8'-2"	9'-10"	11'-6"	
20	6'-5"	8'-2"	9'-10"	11'-6"	
22	6'-4"	8'-1"	9'-10"	11'-6"	
24	6'-4"	8'-1"	9'-9"	11'-5"	
26	6'-3"	8'-0"	9'-9"	11'-5"	
28	6'-2"	8'-0"	9'-8"	11'-5"	
30	6'-2"	7'-11"	9'-8"	11'-4"	
32	6'-1"	7'-10"	9'-7"	11'-4"	13'-0"
36		7'-9"	9'-6"	11'-3"	12'-11"
40		7'-7"	9'-5"	11'-2"	12'-10"
44		7'-5"	9'-3"	11'-0"	12'-9"
48		7'-3"	9'-2"	10'-11"	12'-8"
52			9'-0"	10'-9"	12'-7"
56			8'-10"	10'-8"	12'-5"
60			8'-7"	10'-6"	12'-4"
64			8'-5"	10'-4"	12'-2"
68			8'-2"	10'-2"	12'-0"
72			8'-0"	10'-0"	11'-10"

Similar to K-Series joists, the LH- and DLH-Series joists use tables which dictate the number of rows of bridging per joist and the size of the bridging members. Table A.4 presents the table which indirectly provides the number of rows of bridging per joist. It is indirectly provided because unlike Table A.1 the number of rows of bridging is not explicitly provided, however simple calculations may provide the number of rows of bridging. This is done by determining the maximum spacing of the bridging then determining how many rows of bridging must be provided along the joist span such that this maximum spacing is not violated. For example, if the maximum bridging spacing is 12 ft. along a 30 ft. span joist two rows of bridging must be provided. This is calculated by observing that only one row of bridging would yield a bridging spacing of 15 ft. which is larger than 12 ft. and is unacceptable, but two rows of bridging provides 10 ft. bridging spacing is acceptable.

Table A.4: Bridging spacing for LH- and DLH-Series joists (Vulcraft 2007)

LH-DLH Sect. Number*	Minimum Bolt Diameter**	Max.Spacing of Bridging Lines
02,03,04	3/8"	11'-0"
05,06	3/8"	12'-0"
07,08	3/8"	13'-0"
09,10	3/8"	14'-0"
11,12	3/8"	16'-0"
13,14	1/2"	16'-0"
15,16,17	1/2"	21'-0"
18,19	5/8"	26'-0"

* Last two digits of joist designation.

** Size required due to requirements as indicated for bolted diagonal bridging connections per SJI Specifications Section 104.5(e). Minimum A307 Bolt required for connection.

Knowing the number of rows of bridging per joist, the only remaining information is the size of the bridging members to use for the LH-and DLH-Series joists. The bridging sizes for horizontal bridging is provided in Table A.5 while the sizes for diagonal bridging are the same as the ones used for K-Series joists and are provided in Table A.3.

Table A.5: Bridging member sizes for horizontal bridging for LH- and DLH-Series joists (Vulcraft 2007)

Bridging Angle Size						
Section Numbers**	1x7/64 r =.20"	1-1/4x7/64 r =.25"	1-1/2x7/64 r =.30"	1-3/4x7/64 r =.35"	2x1/8 r =.40"	2-1/2x5/32 r =.50"
02,03,04	4'-7"	6'-3"	7'-6"	8'-9"	10'-0"	12'-4"
05,06	4'-1"	5'-9"	7'-6"	8'-9"	10'-0"	12'-4"
07,08	3'-9"	5'-1"	6'-8"	8'-6"	10'-0"	12'-4"
09,10		4'-6"	6'-0"	7'-8"	10'-0"	12'-4"
11,12		4'-1"	5'-5"	6'-10"	8'-11"	12'-4"
13,14		3'-9"	4'-11"	6'-3"	8'-2"	12'-4"
15,16			4'-3"	5'-5"	7'-1"	11'-0"
17			4'-0"	5'-1"	6'-8"	10'-5"
* Connection to Joist must resist 700 pounds.						
** Refer to last digit(s) of Joist Designation.						

APPENDIX B

This section provides supplemental information concerning ASCE 7-10's snow load design for both uniform and drifted snow loads. The first set of tables presented aids in determining the factors required in Equation (2.17) to determine the uniform design roof snow load.

Table B.1 (ASCE 7-10 Table 1.5-1) describes how the risk category of a building is determined. Using the risk category, an appropriate importance factor, I_s , can be selected from Table B.2 (ASCE 7-10 Table 1.5-2).

Table B.1: Risk category of buildings and other structures for flood, wind, snow, earthquake, and ice loads (ASCE 2010)

Use or Occupancy of Buildings and Structures	Risk Category
Buildings and other structures that represent a low risk to human life in the event of failure	I
All buildings and other structures except those listed in Risk Categories I, III, and IV	II
Buildings and other structures, the failure of which could pose a substantial risk to human life.	III
Buildings and other structures, not included in Risk Category IV, with potential to cause a substantial economic impact and/or mass disruption of day-to-day civilian life in the event of failure.	
Buildings and other structures not included in Risk Category IV (including, but not limited to, facilities that manufacture, process, handle, store, use, or dispose of such substances as hazardous fuels, hazardous chemicals, hazardous waste, or explosives) containing toxic or explosive substances where their quantity exceeds a threshold quantity established by the authority having jurisdiction and is sufficient to pose a threat to the public if released.	
Buildings and other structures designated as essential facilities.	IV
Buildings and other structures, the failure of which could pose a substantial hazard to the community.	
Buildings and other structures (including, but not limited to, facilities that manufacture, process, handle, store, use, or dispose of such substances as hazardous fuels, hazardous chemicals, or hazardous waste) containing sufficient quantities of highly toxic substances where the quantity exceeds a threshold quantity established by the authority having jurisdiction to be dangerous to the public if released and is sufficient to pose a threat to the public if released. ^a	
Buildings and other structures required to maintain the functionality of other Risk Category IV structures.	

^aBuildings and other structures containing toxic, highly toxic, or explosive substances shall be eligible for classification to a lower Risk Category if it can be demonstrated to the satisfaction of the authority having jurisdiction by a hazard assessment as described in Section 1.5.2 that a release of the substances is commensurate with the risk associated with that Risk Category.

Table B.2: Importance factors by risk category of buildings and other structures for snow loads (ASCE 2010)

Risk Category from Table 1.5-1	Snow Importance Factor, I_s
I	0.80
II	1.00
III	1.10
IV	1.20

Figure B.1 provides ASCE 7-10's classification of exposure which is required to determine the exposure factor, C_e , from Table B.3 (ASCE 7-10 Table 7-2).

26.7.3 Exposure Categories

Exposure B: For buildings with a mean roof height of less than or equal to 30 ft (9.1 m), Exposure B shall apply where the ground surface roughness, as defined by Surface Roughness B, prevails in the upwind direction for a distance greater than 1,500 ft (457 m). For buildings with a mean roof height greater than 30 ft (9.1 m), Exposure B shall apply where Surface Roughness B prevails in the upwind direction for a distance greater than 2,600 ft (792 m) or 20 times the height of the building, whichever is greater.

Exposure C: Exposure C shall apply for all cases where Exposures B or D do not apply.

Exposure D: Exposure D shall apply where the ground surface roughness, as defined by Surface Roughness D, prevails in the upwind direction for a distance greater than 5,000 ft (1,524 m) or 20 times the building height, whichever is greater. Exposure D shall also apply where the ground surface roughness immediately upwind of the site is B or C, and the site is within a distance of 600 ft (183 m) or 20 times the building height, whichever is greater, from an Exposure D condition as defined in the previous sentence.

For a site located in the transition zone between exposure categories, the category resulting in the largest wind forces shall be used.

EXCEPTION: An intermediate exposure between the preceding categories is permitted in a transition zone provided that it is determined by a rational analysis method defined in the recognized literature.

Figure B.1: Description of different exposure conditions (ASCE 2010)

Table B.3: Exposure factor, C_e (ASCE 2010)

Terrain Category	Exposure of Roof ^a		
	Fully Exposed	Partially Exposed	Sheltered
B (see Section 26.7)	0.9	1.0	1.2
C (see Section 26.7)	0.9	1.0	1.1
D (see Section 26.7)	0.8	0.9	1.0
Above the treeline in windswept mountainous areas.	0.7	0.8	N/A
In Alaska, in areas where trees do not exist within a 2-mile (3-km) radius of the site.	0.7	0.8	N/A

The terrain category and roof exposure condition chosen shall be representative of the anticipated conditions during the life of the structure. An exposure factor shall be determined for each roof of a structure.

^aDefinitions: Partially Exposed: All roofs except as indicated in the following text. Fully Exposed: Roofs exposed on all sides with no shelter^b afforded by terrain, higher structures, or trees. Roofs that contain several large pieces of mechanical equipment, parapets that extend above the height of the balanced snow load (h_b), or other obstructions are not in this category. Sheltered: Roofs located tight in among conifers that qualify as obstructions.

^bObstructions within a distance of $10h_o$ provide "shelter," where h_o is the height of the obstruction above the roof level. If the only obstructions are a few deciduous trees that are leafless in winter, the "fully exposed" category shall be used. Note that these are heights above the roof. Heights used to establish the Exposure Category in Section 26.7 are heights above the ground.

The thermal factor, C_t , is also required in Equation (2.17). C_t can be determined through

Table B.4 (ASCE 7-10 Table 7-3).

Table B.4: Thermal factor, C_t (ASCE 2010)

Thermal Condition ^a	C_t
All structures except as indicated below	1.0
Structures kept just above freezing and others with cold, ventilated roofs in which the thermal resistance (R-value) between the ventilated space and the heated space exceeds $25 \text{ }^\circ\text{F} \times h \times \text{ft}^2/\text{Btu}$ ($4.4 \text{ K} \times \text{m}^2/\text{W}$).	1.1
Unheated and open air structures	1.2
Structures intentionally kept below freezing	1.3
Continuously heated greenhouses ^b with a roof having a thermal resistance (R-value) less than $2.0 \text{ }^\circ\text{F} \times h \times \text{ft}^2/\text{Btu}$ ($0.4 \text{ K} \times \text{m}^2/\text{W}$)	0.85

^aThese conditions shall be representative of the anticipated conditions during winters for the life of the structure.

^bGreenhouses with a constantly maintained interior temperature of $50 \text{ }^\circ\text{F}$ ($10 \text{ }^\circ\text{C}$) or more at any point 3 ft above the floor level during winters and having either a maintenance attendant on duty at all times or a temperature alarm system to provide warning in the event of a heating failure.

The following figures are used to describe the windward snow drifts considered in the study. Figure B.2 (ASCE 7-10 Figure 7-8) describes the shape of a snow drift using identical variable designations which were used in Equations (2.18) to (2.20). The only difference

between the labels in this figure and the equations used in Chapter 2 is due to Figure B.2 considering a leeward snow drift which is not investigated in this study. The difference between a leeward and windward drift is presented in Figure B.3 (ASCE 7-10 Figure 7-7).

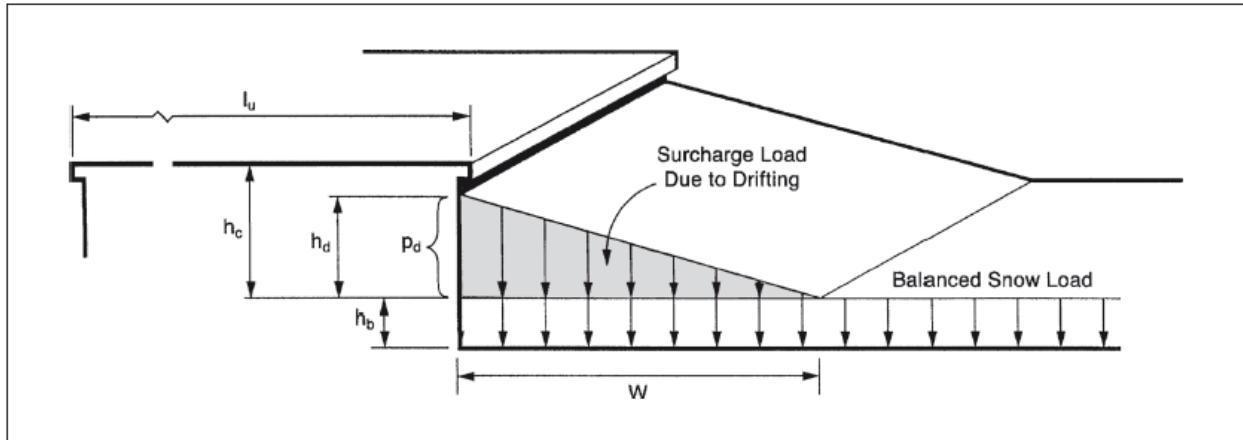


Figure B.2: Configuration of snow drifts on lower roofs (ASCE 2010)

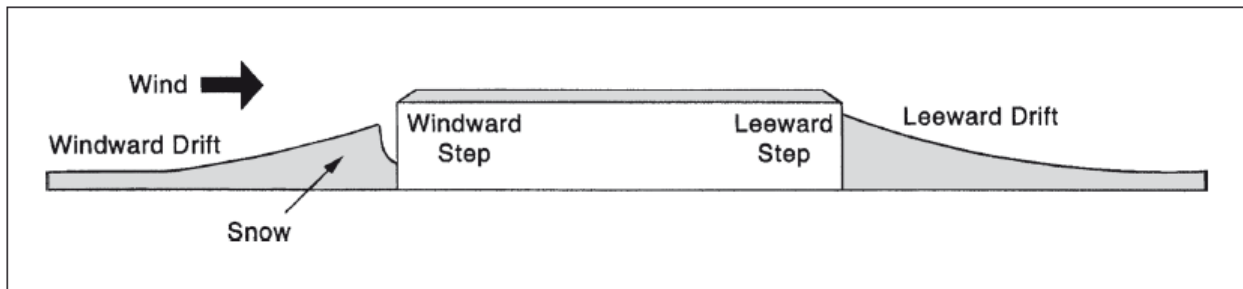


Figure B.3: Drifts formed at windward and leeward steps (ASCE 2010)

The final ASCE 7-10 figure of use for snow design in this study details the relationship between the ground snow load, p_g , the downwind roof length from the snow drift, l_u , and the drift height, h_d . These relations are presented in Figure B4 (ASCE 7-10 Figure 7-9).

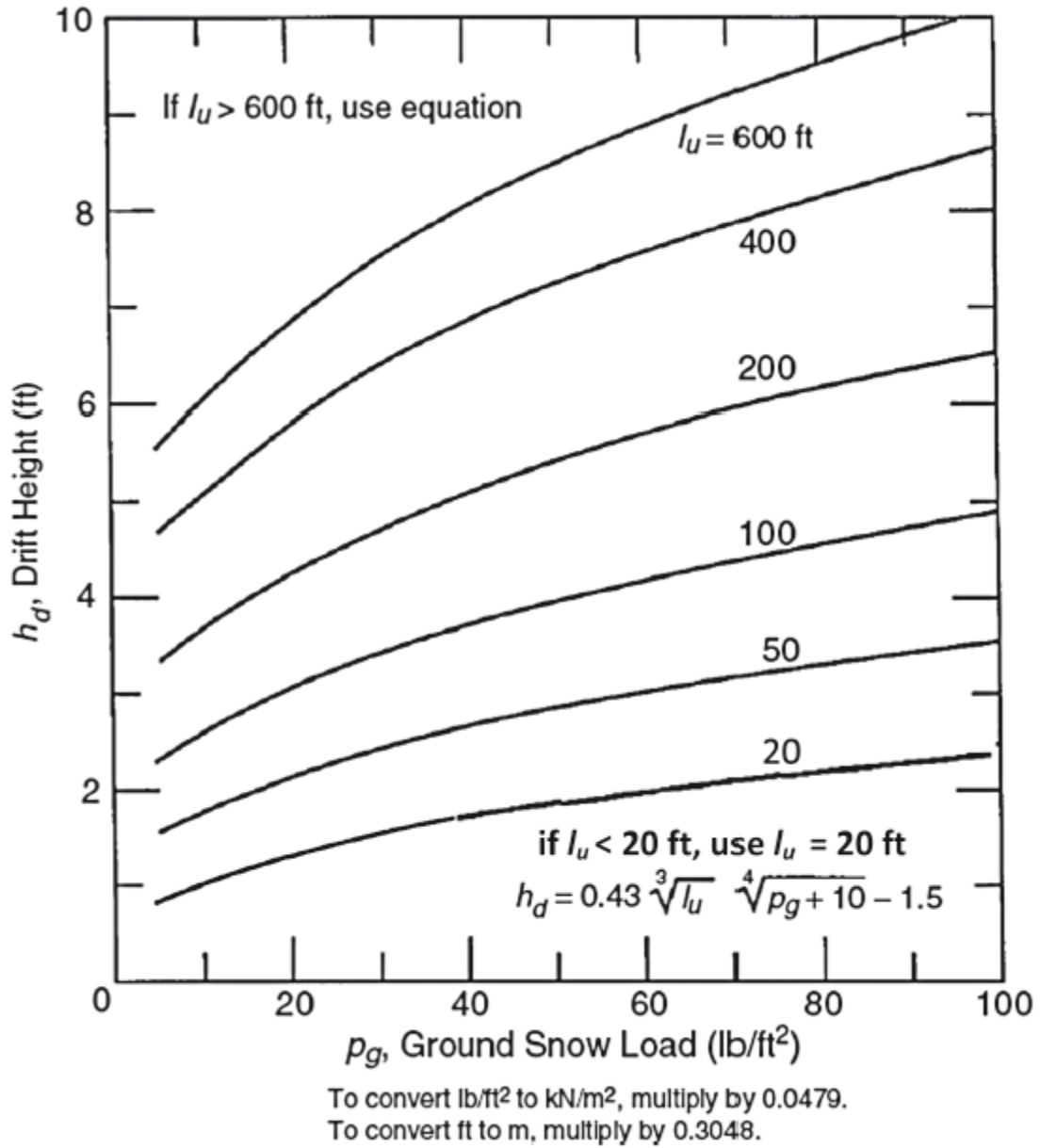


Figure B4: Graph and equation for determining drift height, h_d (ASCE 2010)